FOREWORD

This work was performed by the Southern Research Institute under USAF Contract No. AF 33(616)-6312. The contract was initiated under Project No. 7360, "Chemistry and Physics Materials," Task No. 73603, "Thermodynamics and Heat Transfer," and was administered under the direction of the Directorate of Materials and Processes, Deputy for Technology, Wright-Patterson Air Force Base, Ohio with Mr. Hyman Marcus acting as the project engineer.

This report covers work conducted from 15 March 1959 to 14 November 1960.

ABSTRACT

The heat capacity, thermal expansion, and thermal conductivity were measured for thirteen different refractory materials, including ATJ graphite, tungsten, four nitrides, two borides, a silicate, and four carbides. The temperature range was from 500° F to 5000° F.

The heat capacity was found to vary considerably with temperature and to demonstrate marked inflections at specific temperature ranges.

The thermal expansion parallel with the press direction was found to be in the range of 3×10^{-6} in./in./° F and to vary significantly with the prior thermal history of the specimen. At temperatures within about 1000° F of the melting or deterioration range, the motions of the materials generally increased considerably.

The thermal conductivity perpendicular to the press direction was found to be generally of the same value for materials of the same family, viz., the nitrides or carbides. The prior thermal history had a marked influence on the resulting values.

Considerable information was obtained on the performance of 5000° F furnaces with graphite heaters, high temperature thermocouples, optical pyrometry, and the behavior of specimen materials in these 5000° F environments. All materials except a few failed at considerably below the handbook values for their melting or deterioration temperatures.

PUBLICATION REVIEW

This report has been reviewed and is approved.

FOR THE COMMANDER:

Jules I. Wittebort

JULES I. WITTEBORT
Chief, Thermophysics Branch
Physics Laboratory
Materials Central

TABLE OF CONTENTS

TABLE OF CONTENTS (Continued)

LIST OF ILLUSTRATIONS

LIST OF ILLUSTRATIONS (Continued)

LIST OF ILLUSTRATIONS (Continued)

LIST OF ILLUSTRATIONS (Continued)

LIST OF ILLUSTRATIONS (Continued)

LIST OF ILLUSTRATIONS (Continued)

LIST OF TABLES

LIST OF TABLES (Continued)

LIST OF TABLES (Continued)

THE THERMAL PROPERTIES OF THIRTEEN SOLID MATERIALS TO 5000° F OR THEIR DESTRUCTION TEMPERATURES

INTRODUCTION

This report covers the measurement of the heat capacity, thermal conductivity, and thermal expansion of thirteen solid materials from temperatures ranging from 500° F to 5000° F or to the temperature at which the material deteriorates, whichever is lower. In the course of this work, techniques were developed for reliable furnace operation at temperatures slightly greater than 5000° F. Methods were also developed for measuring the thermal properties of refractory materials at these temperatures. Of considerable interest in this work is the data showing the behavior of some of the refractory materials at these extremely high temperatures. This material behavior not only influenced the thermal property data to a great extent, but also indicated some of the difficulties that might be encountered in structural applications of these materials.

In this report, the equipment that was used in the thermal property measurements is described in considerable detail. The techniques for measuring temperature and the calibration procedures are also described. Properties of the materials are also given where they are available. Chemical analysis of the samples will be made under a subsequent contract and that parameter related to the observed thermophysical properties.

THE 5000° F FURNACES

The furnaces used in the thermal property measurements were designed, built, and operated by Southern Research Institute prior to initiation of work under this contract. During the work, many improvements were incorporated to extend the temperature range and improve

Manuscript released by authors November 1960 for publication as a WADD Technical Report.

the heater life. At the conclusion of the work, four furnaces were available with two of one type capable of operating under pressure or vacuum and two of a second type capable of operating only at atmospheric pressure. The latter are very flexible and permit rapid heater changeout in a few minutes. Details of both types of furnaces are shown in Figures 1 and 2. All furnaces can operate at over 5000° F on heating loads that do not drain excessive heat from the furnace. This condition causes the heater temperature to exceed approximately 5500° F and results in almost complete loss of strength of the graphite so that the heating element breaks.

Three methods of insulating the furnaces were used. First, the graphite heater was surrounded with molybdenum reflection shields to take the major temperature drop. This system was effective with the 15 shields providing about a 150° F drop each; however, the maximum temperature limit of the reflector materials limited the maximum allowable furnace temperature to about 4000° F. Second, the graphite heater was surrounded by a zirconia inner tube with zirconia grog in the inner annulus. This arrangement was excellent to 4500° F; however, at 4800° F and above, the zirconia inner tube melted. A tungsten liner in the zirconia inner tube did not extend the upper temperature limit. Third, the graphite heater was surrounded by a thin wall graphite inner tube with lamp black in the inner annulus. Repeated runs to 5000° F to 5200° F showed no damage to the furnace parts with this arrangement; however, the heat loss was higher by perhaps 10%.

The heater design was rather thoroughly investigated. A simple slotted tube was an effective heater configuration, but provision had to be made to provide for thermal expansion during a run by permitting the electrodes to move. A helical carbon heating element permitted the use of fixed electrodes without introducing serious handling or cost problems. The electrical design of the heater was found to be very important. Using configurations requiring low current and high voltage (150 amps and 70 volts, respectively), the current would rise sharply at 4000° F furnace temperatures suggesting a current bypass in the ionized gas around the heater element. At higher currents and lower voltages (700 amps and 15 volts, respectively), the current bypass was not noted and the furnace temperature increased with input power at a fairly uniform rate to over 5000° F; see Figure 3.

Generally, CS graphite as produced by National Carbon Company was used for the heater element. Different batches were quite different

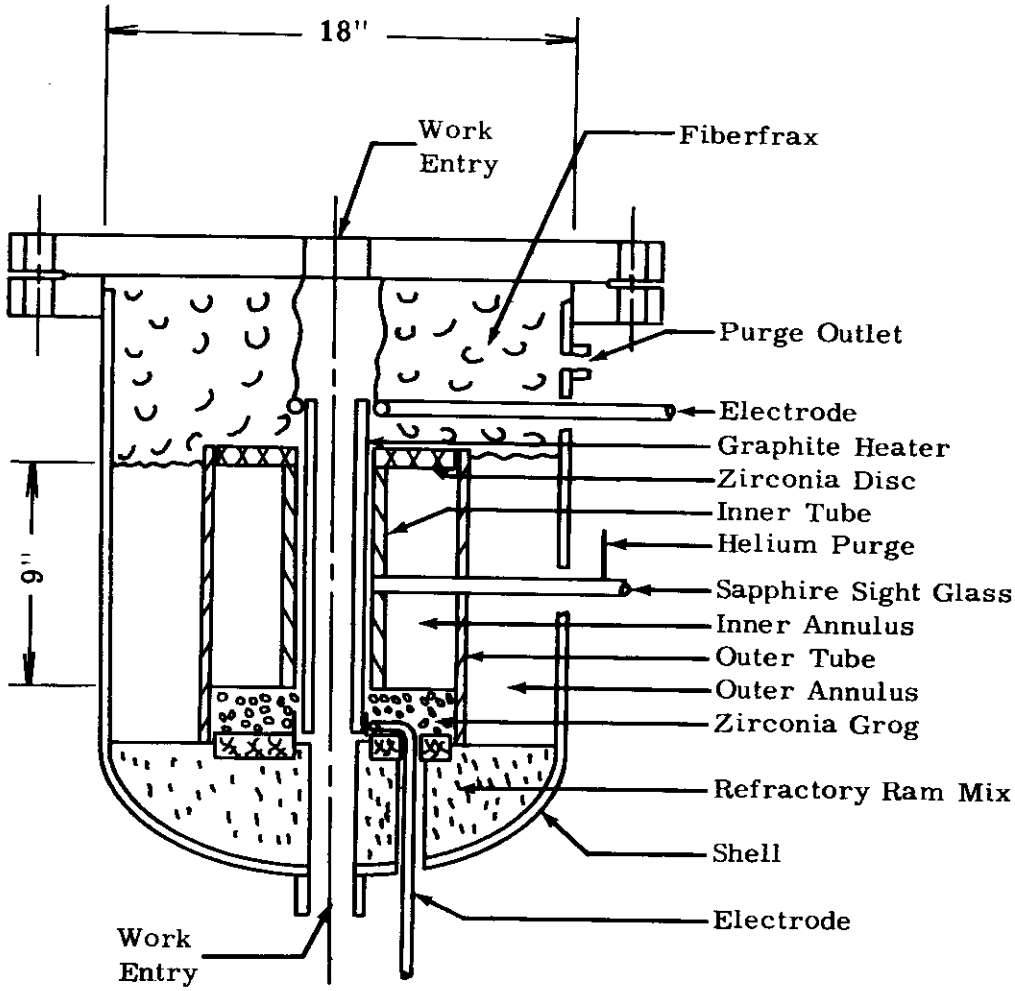

Figure 1. Schematic Cross Section of Numbers 1 and 2 5000° F Furnaces Employing Helical Graphite Heaters and Pressure and Vacuum Capability.

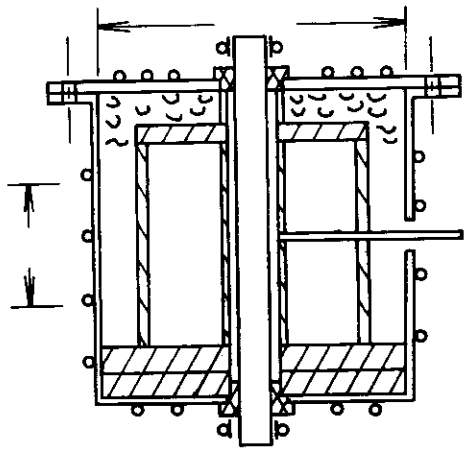

Figure 2. Schematic Cross Section of Numbers 3 and 4 5000° F Furnaces Employing Tubular Graphite Heaters for Atmospheric Pressure Operation.

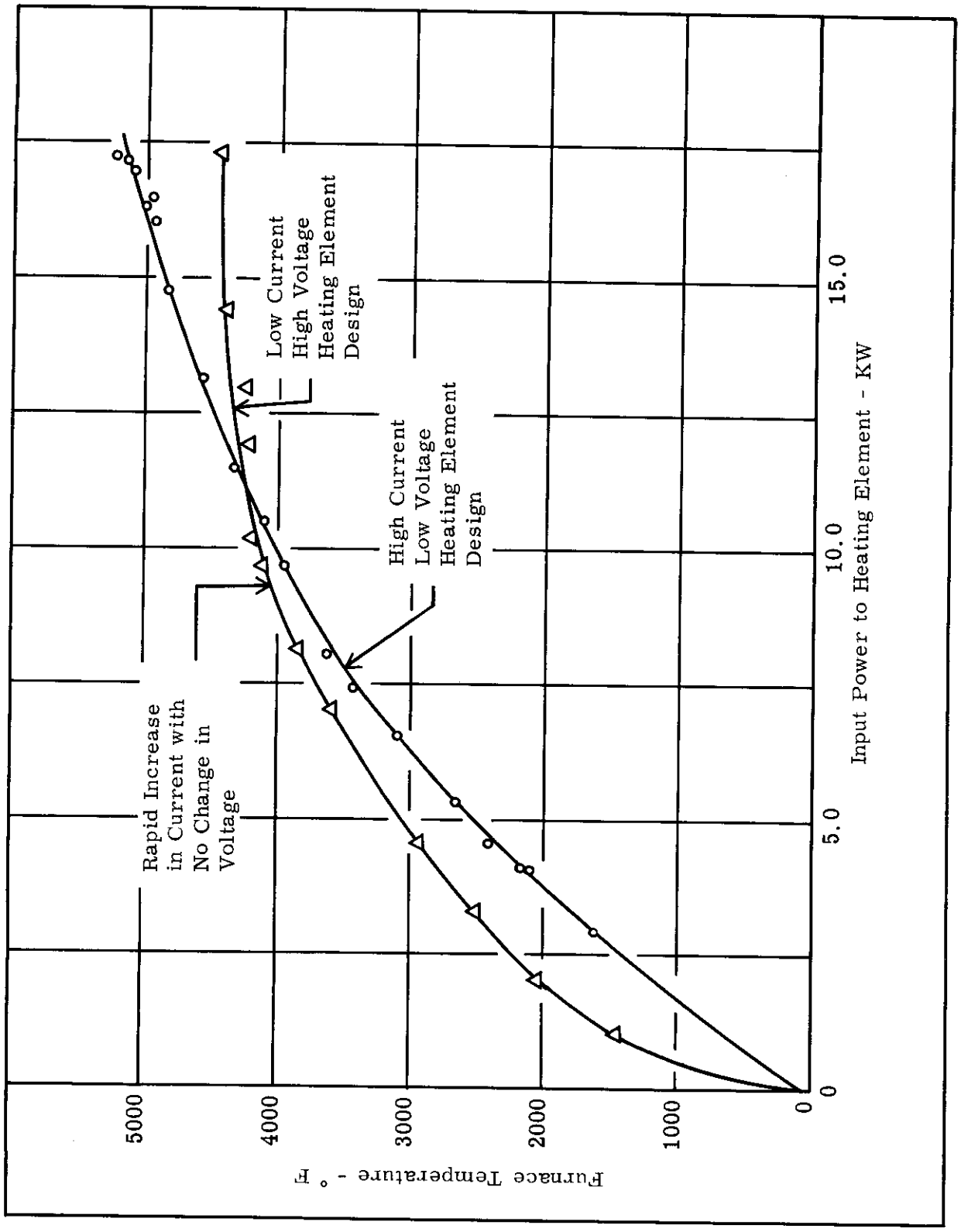

Figure 3. Relation of Furnace Temperature and Input Power.

in electrical properties, machineability, and apparent texture so that some changes in heater design were required between batches.

Zirconia end plugs and spacers around the heater and inner tube proved to be effective. Generally, the graphite and zirconia were compatible if the temperature range at their contact points was kept below 3500° F. Deterioration of the zirconia resulting from the carbon vapors in the gas phase was not excessive. If the two materials were permitted to contact physically within a zone at over 3500° F, then the deterioration of the zirconia was quite rapid.

All of the graphite heaters seemed to contain some silica, magnesia, calcia, sulphur, and other contaminants that apparently vaporized out of the heaters and could be found after a run condensed on the colder (2500° F) parts of the tubes.

Different purge gases were employed, including helium, argon, and nitrogen. No major difference in performance was noted so helium was selected as the primary purge. This gas was dried by a desiccant, but no serious effort was made to further clean it since the heater life was considered satisfactory. Usually, purge rates of about 5 to 20 scfh were employed.

In a subsequent contract, the chemistry of the gases in the hot zone will be determined by drawing samples out for analysis. Undoubtedly, carbon vapors will be detected, although none were visible to the eye except during faulty operation or on the initial exposure of new graphite parts and lamp black.

No difficulty was experienced with the water-cooled copper electrodes that were operated at current densities up to 300 amps per square inch. Undoubtedly, these electrodes could be made smaller and operated at even higher current densities.

Pictures of the different furnaces with the different apparatuses installed are shown in Figures 4, 5, 6, 7, and 8.

TEMPERATURE MEASUREMENT IN THE 5000° F FURNACES

The temperatures in the furnaces were determined by optical pyrometer readings through optical sight glasses with Pyrex and sapphire windows to 5000° F, tungsten-rhenium thermocouples to

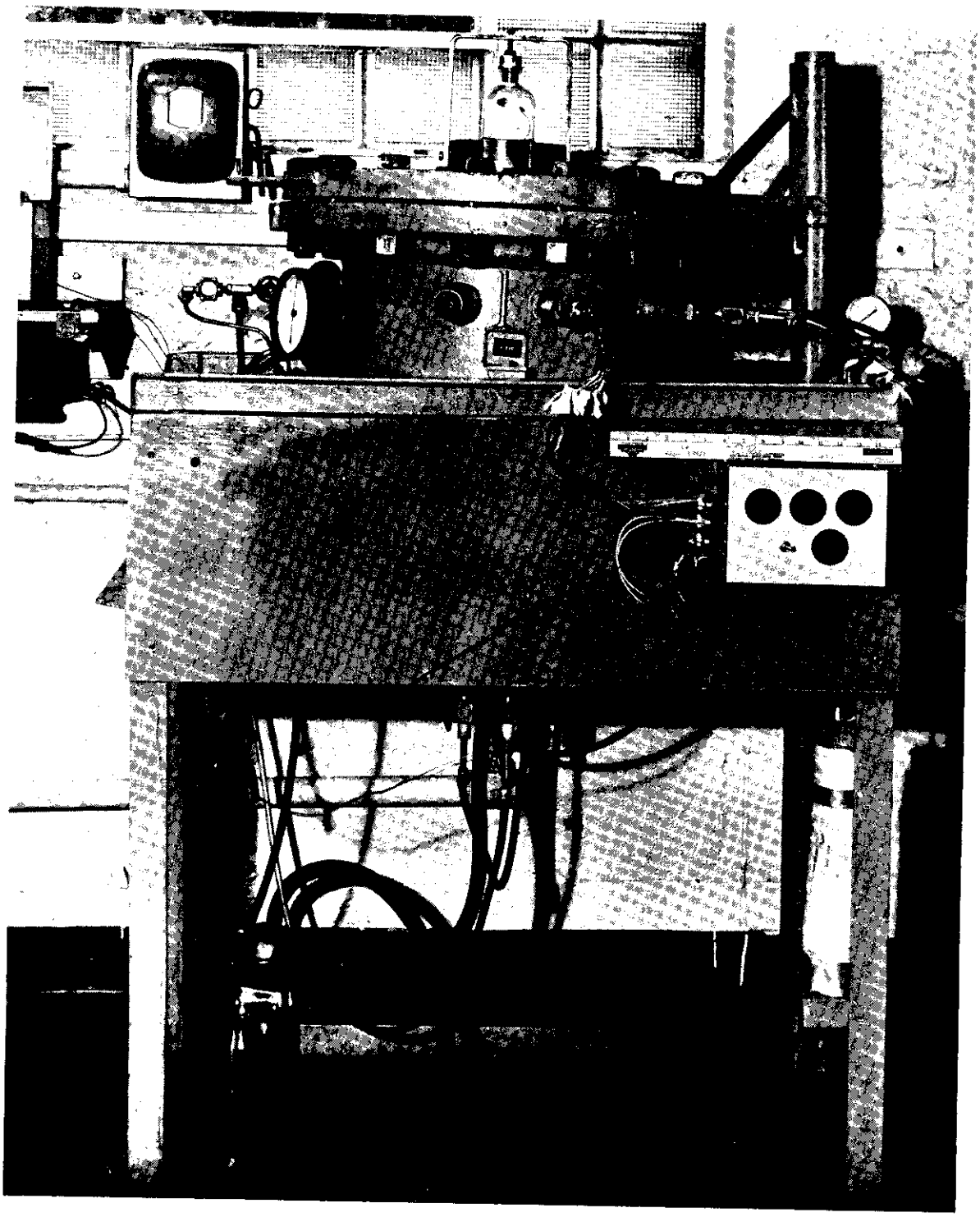

Figure 4. Furnace No. 1 with the Expansion Apparatus Installed

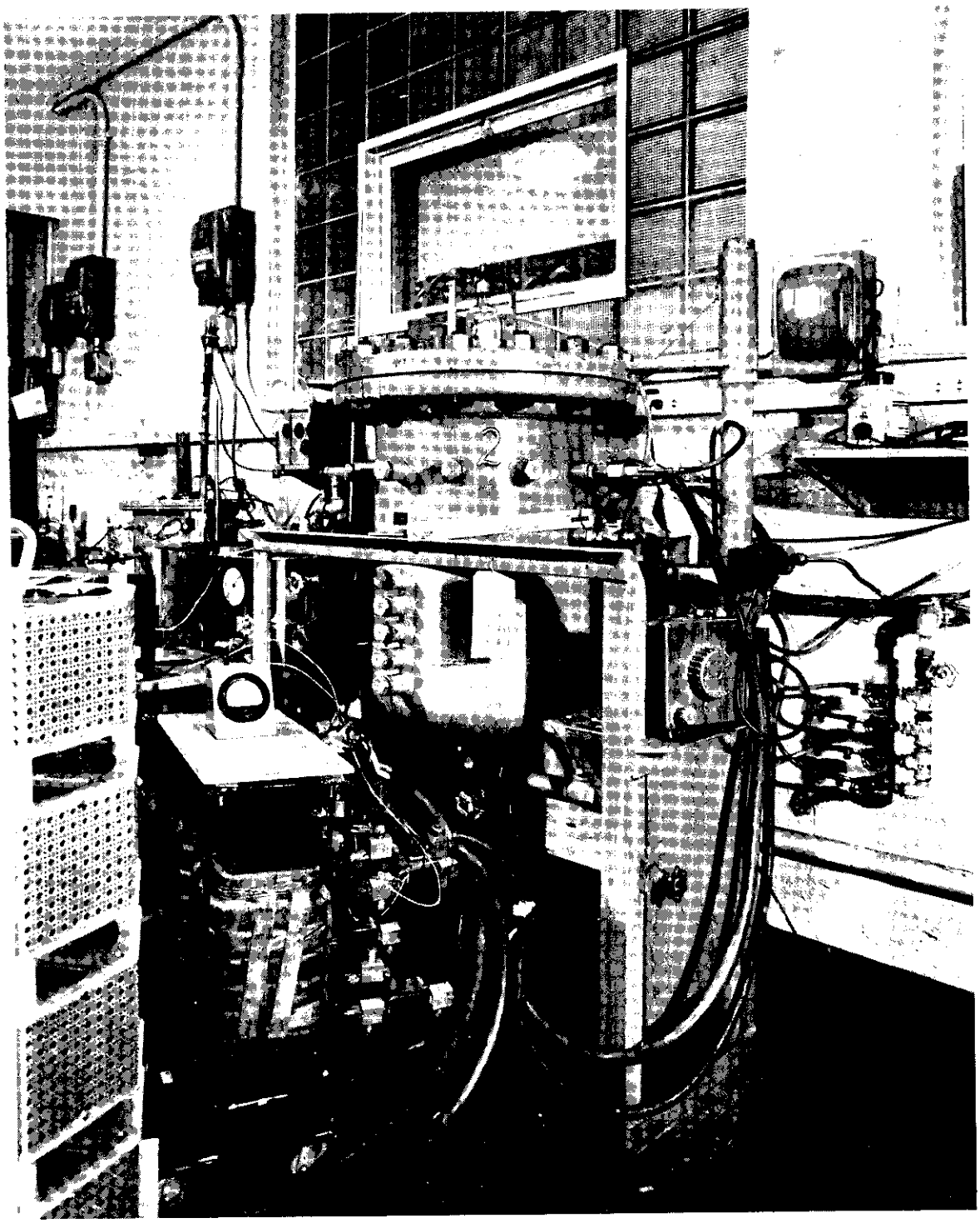

Figure 5. Furnace No 2 with the Expansion Apparatus Installed.

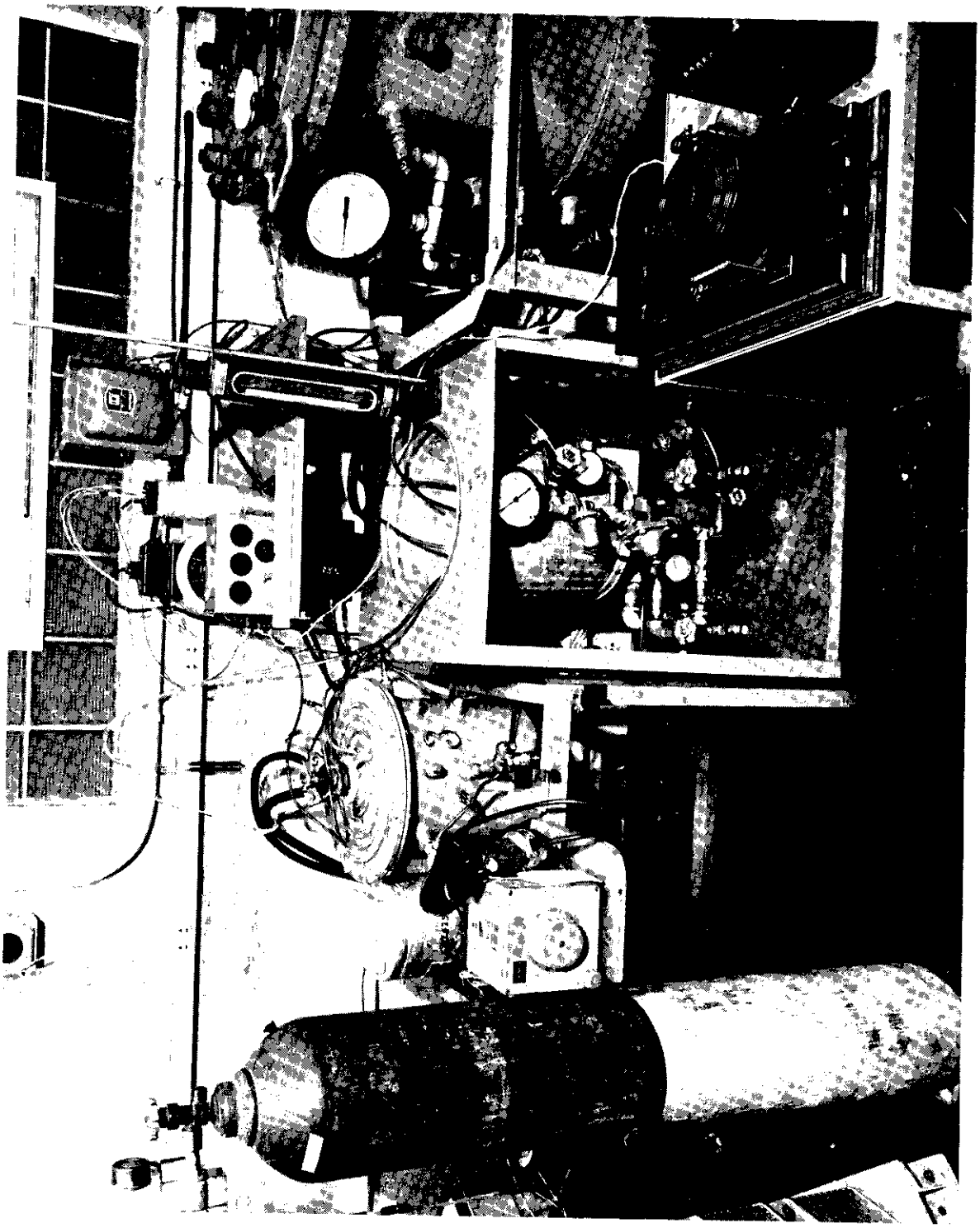

Figure 6. Furnace No. 3 with the Thermal Conductivity Apparatus Installed

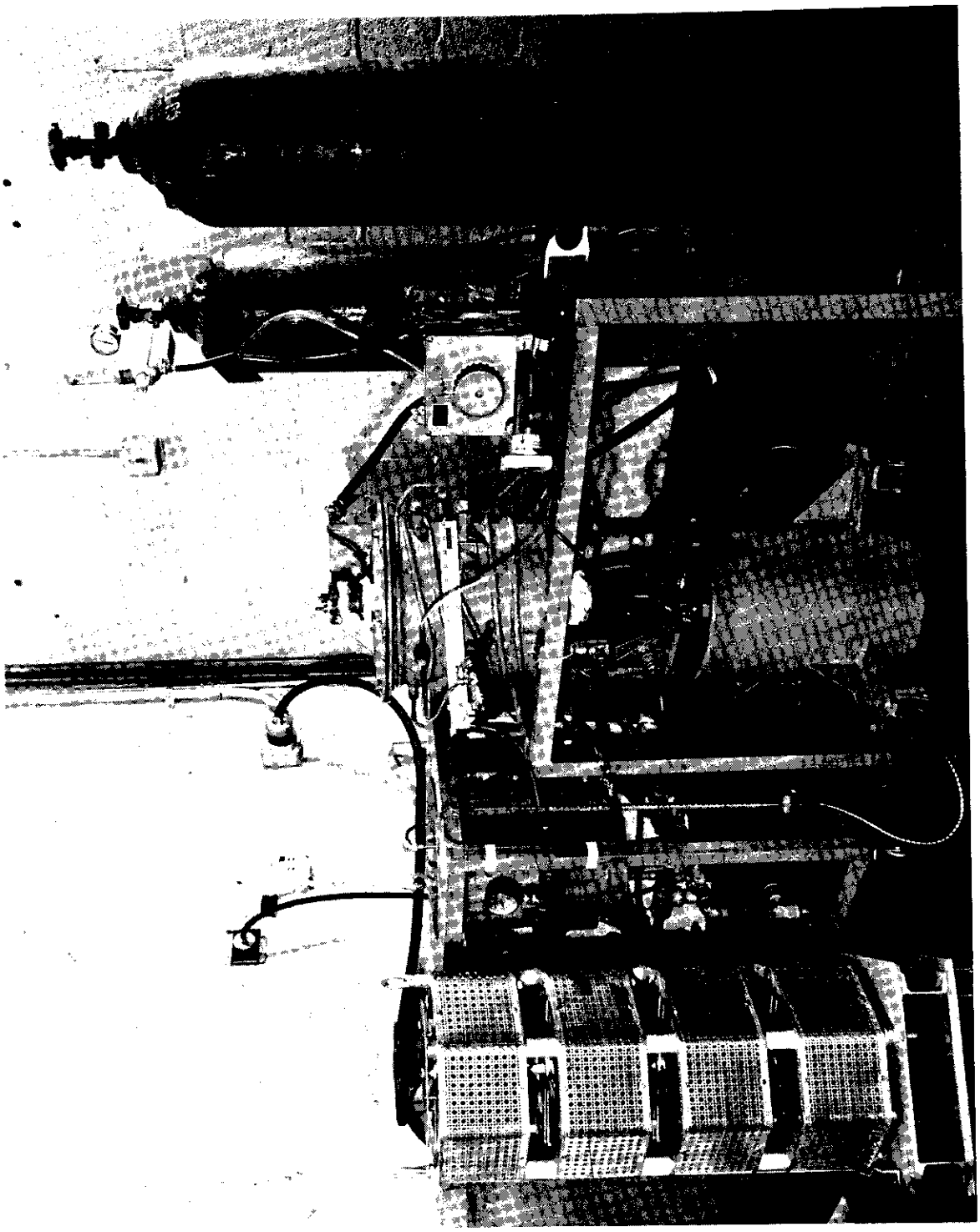

Figure 7. Furnace No. 4 with the Heat Capacity Apparatus Installed

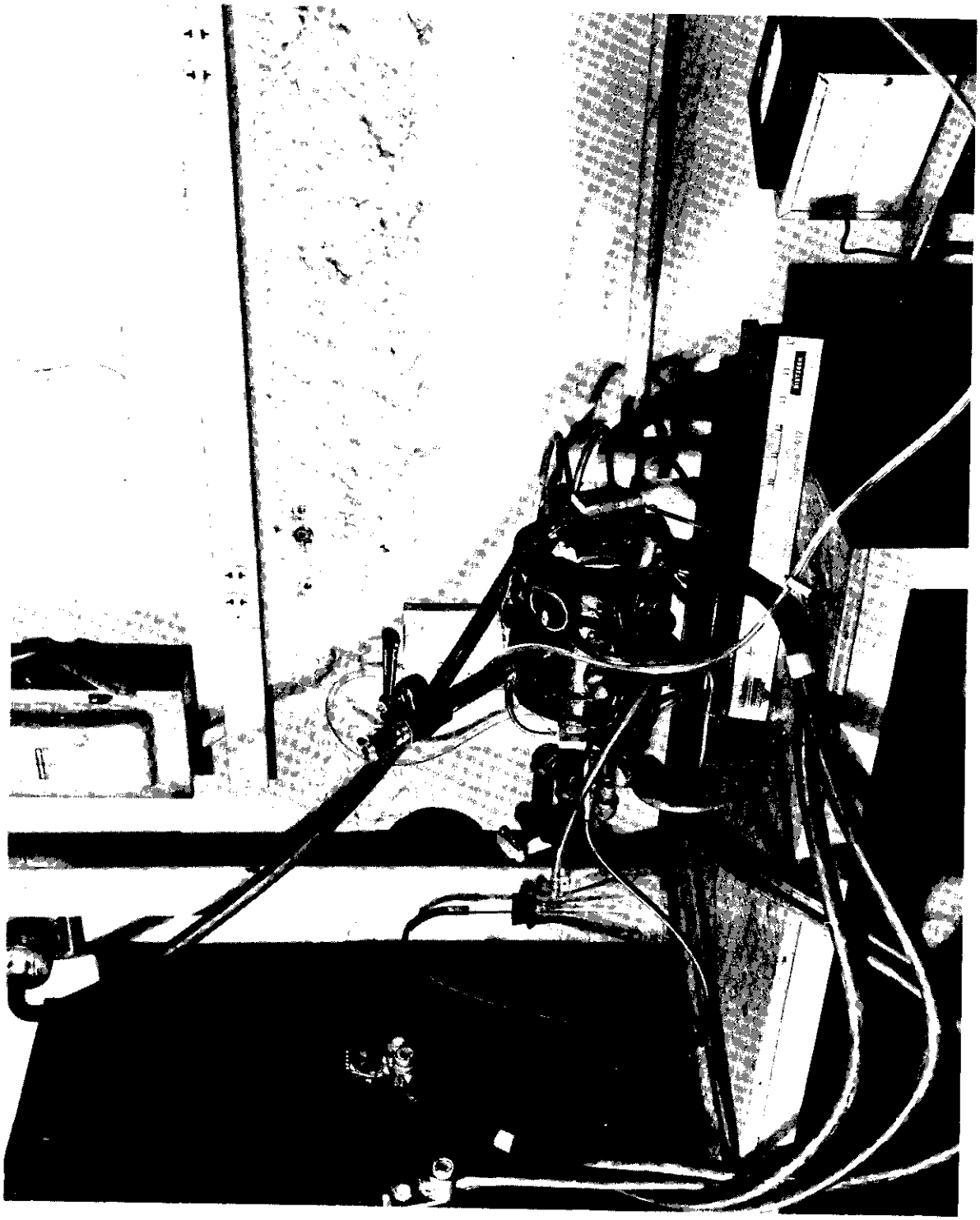

Figure 8. Furnace No. 5 with End Plugs in Place

4600° F, tungsten-molybdenum thermocouples to 4000° F, platinum-rhodium to 2800° F, and Chromel-Alumel to 2500° F. The greatest reliability was found using the optical pyrometer after techniques were developed to keep the optical tubes clear of fumes and condensing vapors or curtains.

In addition to the actual temperature calibration runs, cross checks were obtained during data runs between the optical pyrometer and the thermocouples in all three phases of the work in the temperature range above 1500° F and below the failure temperature of the particular couple being used.

In some preliminary investigations, the influence of the physical aspects of the sight tube on the resulting temperature reading was determined. As general conclusions, the temperature reading was independent of the distance of the focusing lens of the pyrometer from the source within the range of 5 to 20 inches with a normal deviation of about 10 to 15° F. However, the diameter of the sight tube had a major influence. Tubes larger than $\frac{1}{2}$-inch diameter had no effect. Tubes smaller than $\frac{1}{4}$ inch did reduce the temperature reading by as much as 100 to 200° F at about 3500° F. In between $\frac{1}{4}$ and $\frac{1}{2}$ inch, the diameter of the tube had the influence of reducing the temperature by an amount dependent also on the tube length. Any sight tube in this critical range or smaller should be calibrated in place in the furnace or errors as large as 100° F to 500° F can result.

During runs, measurements with optical pyrometers were made by viewing the specimen through a sight window. Windows of Pyrex and synthetic sapphire were used in the furnaces and introduced an error in the observed optical readings. To correct these readings, the windows were calibrated by comparing readings through the windows to readings with no window. The target used for calibration was the center of an inductively heated graphite crucible with a black body depth to diameter ratio of three to one. The correction curves for synthetic sapphire and Pyrex sight windows are shown in Figure 9. With a steady pyrometer mount and the cavity-type target, variation in pyrometer readings was about 10° F at constant source temperatures.

Several runs were made with tungsten/molybdenum and tungsten/rhenium thermocouples. Tungsten/iridium thermocouples were also evaluated, but the iridium became extremely brittle in these furnaces. The temperatures obtained were compared to corrected optical pyrometer

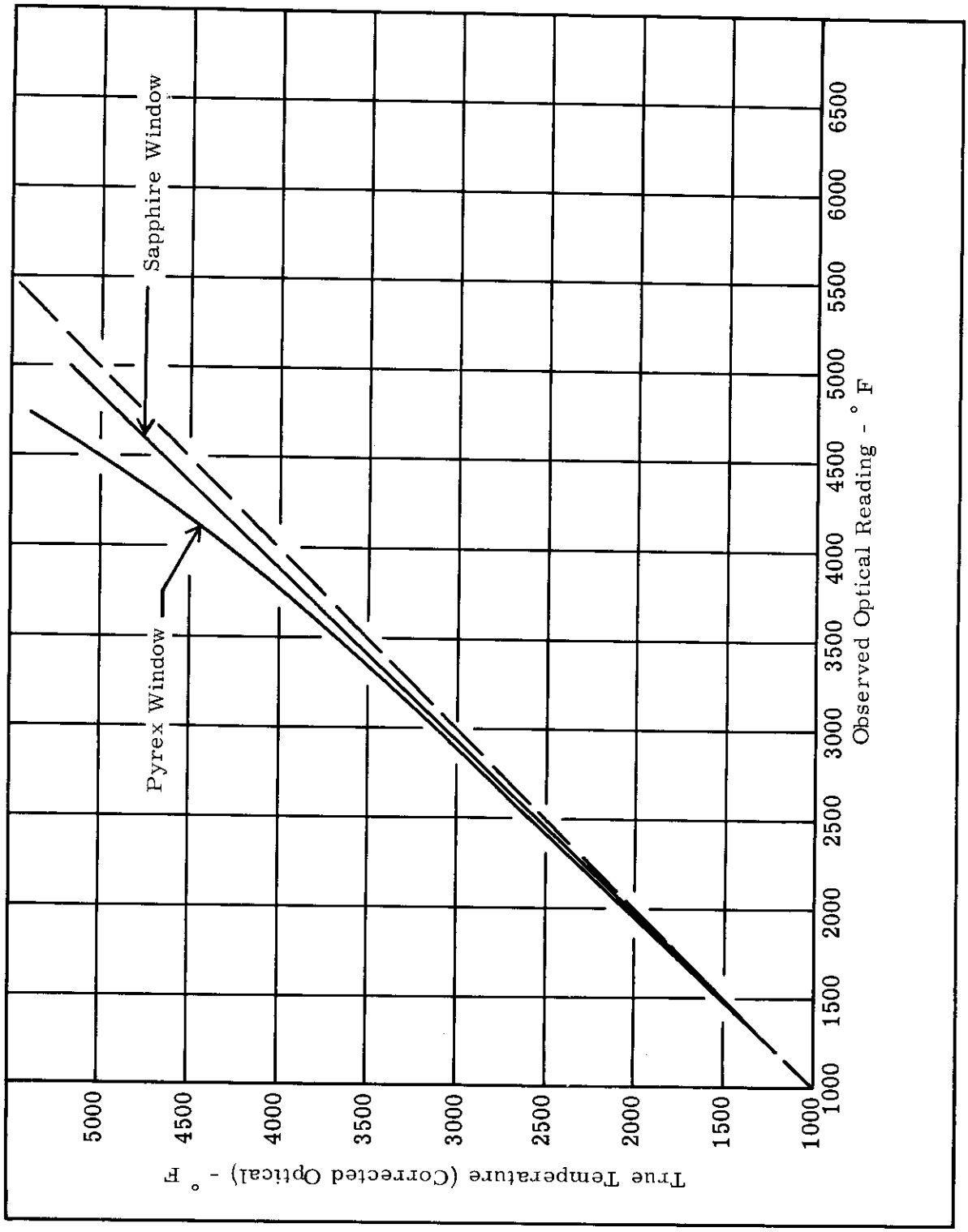

Figure 9. Temperature Calibration Curves for Optical Pyrometer.

readings, to temperature measurements made with established thermocouples, and to literature data. Curves of W/Mo thermocouple output versus temperature from both literature data and Southern Research Institute corrected optical readings are shown in Figure 10. Similar curves for W/Re thermocouples are shown in Figure 11. Southern Research Institute curves have the same character as the literature data but definitely indicate a lower EMF for a given temperature. The spread between data from different investigators is fairly large, and there is some spread between Southern Research Institute calibrations and the data shown in the literature although the character is the same. These variations can result from variations in thermocouple purity, failure to correct optical data for sight tube and window losses or variations in thermocouple technique. Figure 12 includes calibration curves for W/Mo and W/Re thermocouples, and optical readings through a sapphire window. Also shown in Figure 12 are points comparing established melting points of materials to the optical readings taken when these materials were melted in the furnaces.

For the work under this contract, the true temperatures above 1500° F were taken as the corrected optical readings. High temperature thermocouples calibrated by corrected optical readings were used extensively, especially in locations where optical readings were impossible. Although any one optical reading may be in error, the great number of points obtained in the calibration and during a run insured statistically accurate data.

During the runs, simultaneous observations were made of the specimen temperatures by calibrated optical pyrometer, standard thermocouples such as Chromel-Alumel and platinum-rhodium, and exotic thermocouples such as tungsten-rhenium and tungsten-molybdenum. The agreement was generally fair as shown by typical values in Table 1, but the reliability and internal consistency were invariably better for the optical data.

The furnace environment is important in the performance of practically all thermocouples. Wire aging was minimized by using new welded junctions on each run. With this procedure, no poisoning effect was really documented; however, it was observed that Chromel-Alumel was a little more reliable than platinum-rhodium, and both the tungsten-rhenium and tungsten-molybdenum couples demonstrated a shift in output EMF for a given temperature after a high temperature exposure. Also, both of these exotic couples melted at temperatures considerably below the melting point of the pure crystal of the metals.

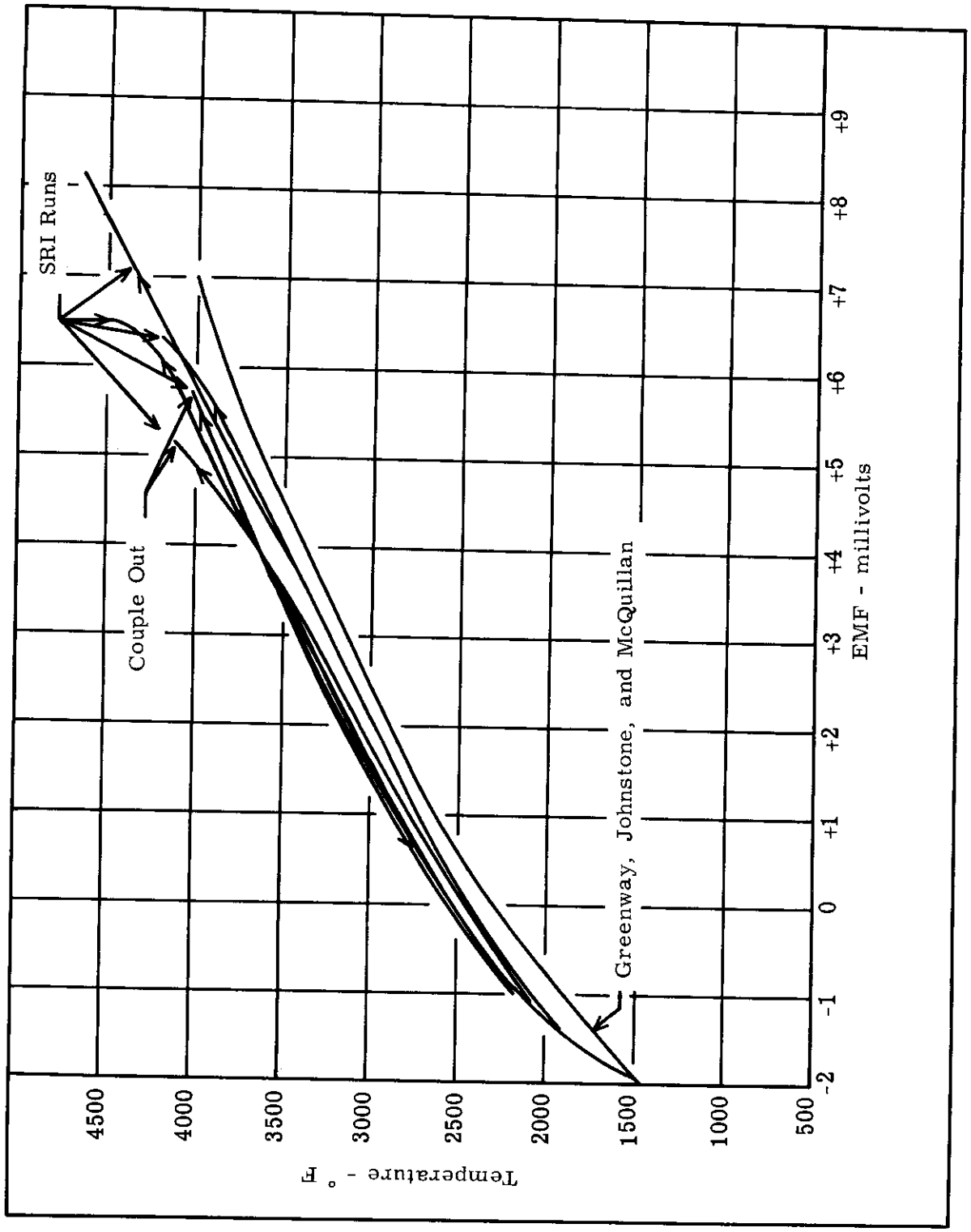

Figure 10. Calibration Curves - Tungsten vs. Molybdenum Thermocouples.

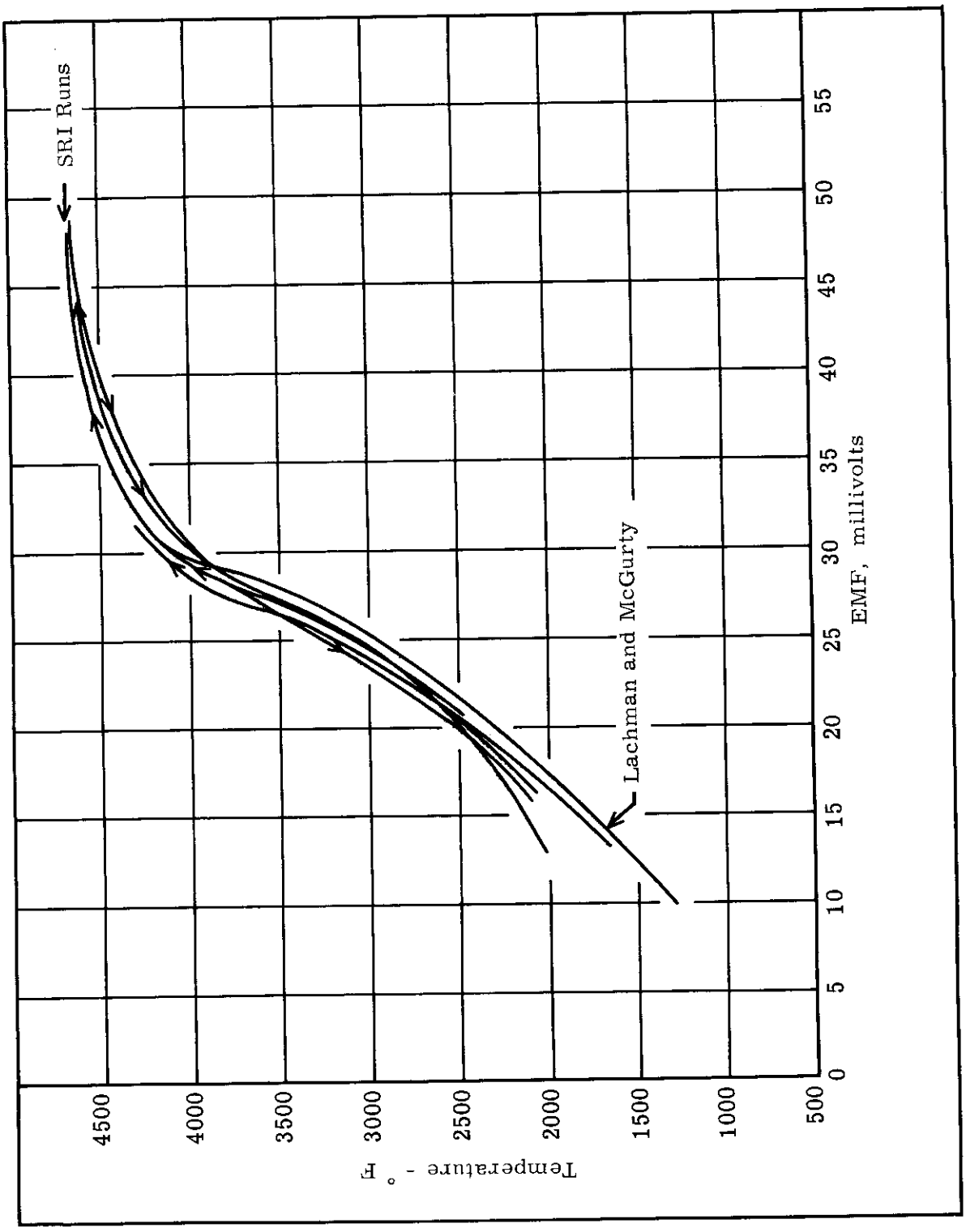

Figure 11. Calibration Curves - Tungsten vs. Rhenium Thermocouples.

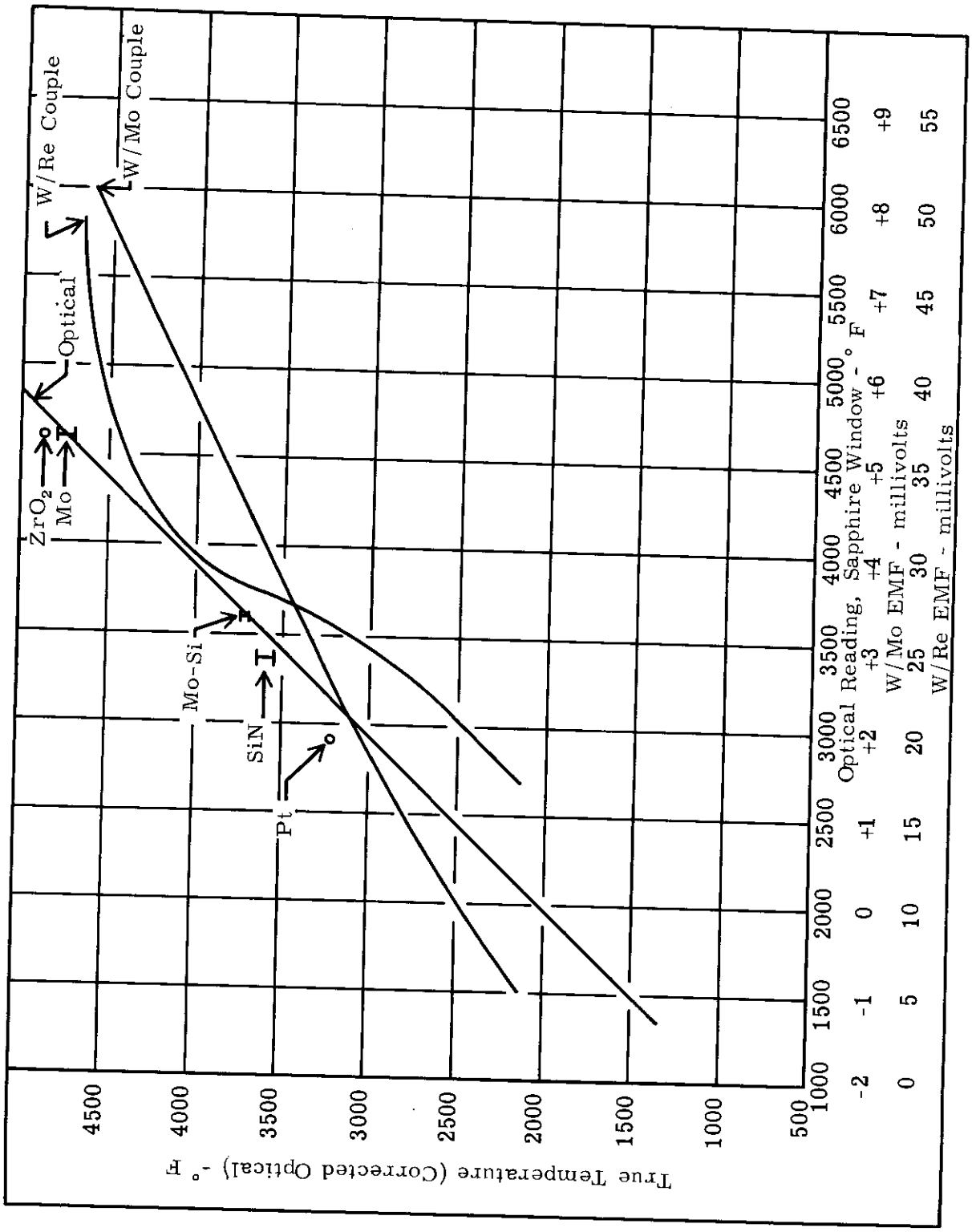

Figure 12. Calibration Curves for Optical and Couples.

Table 1

Cross Check of Temperatures in the Furnace During Runs
by Comparison of a Calibrated Optical Pyrometer and Thermocouples

True Temp. by Calibrated Optical Pyrometer ° F	Temp. by Standard Thermocouples ° F	Temp. by Exotic Thermocouples ° F
1890	1860	-
2075	2081	-
2060	2084	-
2040	2075	-
1570	-	1530
1780	-	1720
2230	-	2205
2840	-	2780
3150	-	3130
1570	-	1590
2840	-	2700
1570	1671	1530
1820	1945	1720
2045	2149	1900
2310	2386	2205
2840	-	2780
3000	-	3085
3150	-	3130

Different protection tubes were used. Alumina and magnesia performed well to 3000° F, but only thoria extended the range to over 4000° F. Some beryllia tubes were available but not used. Actually, unanchored bare wires invariably performed with the most reliability and minimum premature breakage.

THE SPECIMEN MATERIALS AND THEIR GENERAL PERFORMANCE

The refractory materials evaluated in this program were ordered under specifications requiring a maximum density, purity, and strength while employing a forming process compatible with either laboratory or production line techniques. Particle size was left to the discrimination of the supplier. Reliable performance as components at 5000° F was emphasized and the price left open. Generally, the best product for the current state of the art was anticipated. The suppliers were informed of the particular properties to be measured.

More than one supplier was found for every material; however, the price range and delivery dates were often orders of magnitude different. In every case, the supplier was selected either on the basis of a probable premium product, experience in a particular field, or a more firm guarantee of performance.

Within the very rigid confines of proprietary rights, all suppliers were very cooperative and assisted greatly in the over-all performance by expediting deliveries. In spite of this, the very nature of the work of producing the specimens resulted in some delays and, in some instances, in delivery of about a year. Also, some of the properties of some of the materials have not been received even yet. All pressed materials were pressed in the axial direction.

The specimen sizes were selected on the basis of maximum compatibility between the thermal property measurement apparatuses and the ability to produce a sound specimen Some suppliers could not produce a piece bigger than one-inch diameter nor longer than about three diameters. Other suppliers questioned the homogeneity that could be anticipated for special shapes and sizes. As a compromise, solid pieces about $\frac{3}{4}$-inch diameter by $\frac{3}{4}$ or 3 inches long were selected as the goal. Southern Research Institute then shaped the specimens with diamond grinding and ultrasonic drilling equipment.

In Table 2 the general information on all materials is presented as it is best known now. The density and chemical composition of the materials before and after the high temperature exposures will be determined by chemical and spectrographic analyses under a subsequent contract.

The table contains one column listing the theoretical melting temperature and another listing the temperature at which the specimens failed in these evaluations. Only three of the materials performed at over 5000° F. This limit was not the furnaces, but the specimen materials. In a few cases, such as for columbium carbide, the temperature range could have been extended to over 5000° F without melting the specimen; however, since the specimens failed at 4740° F in a fashion such as fracturing or exploding that precluded any further measurements, the runs were concluded. Most of the specimens failed by apparent disassociation, incipient melting, excessive softening, or a similar mechanism that indicated absolute material failure. Figure 13 shows the different materials before and after the exposures.

After the runs, the specimens were examined carefully to determine the type of failure and the possible contamination that may have resulted from carbon vapor in the furnace atmosphere. Generally, it did not appear that the presence of the trace carbon vapors actually caused any failures or induced premature temperature deterioration at other than the surface of the material. More specific data will be presented after the material analysis that is to be performed. One exception is anticipated. The tungsten melted at about 5000° F. Of course, the crystal melts at over 6000° F so it is probable that the carbon eutectic was formed. It is not known whether the carbon came from the furnace vapors or was in the material before exposure. The very gross melting as shown in Figure 14 suggests that the carbon may have been in the material. See Figure 15 for a picture of some small specimens of tungsten supplied by four different suppliers and exposed to 4940° F. Also, in one instance the tungsten specimen melted internally and broke through the solid shell, or skeleton, of the surface material. The analysis provided by the supplier does not indicate sufficient carbon to induce such gross melting without pickup from the furnace; however, the analysis was provided as typical of the melt and not for this particular series of specimens.

There is considerable evidence that many of these materials with crystal melting points of over 5000° F were actually fired during forming

Table 2

Properties of the Materials Evaluated in the Work

SRI No.	Material Name	Material Supplier	Chemical Symbols [1]	Chemical Composition by % Weight Except as Noted [2]	Density lb/ft³ [3]	Percent of Theoretical Density	Forming Method	Theoretical Melting or Destruction of Pure Material °F [4,5]	Maximum Exposure Temperature °F [6]	Remarks
1	Silicon Nitride	The Carborundum Company	SiN	0.05 Ca, 0.01 Cu, 0.01 Mg, 0.3 Al, 1.5 Fe, 0.01 Ti, and Trace Ba, Na, and Mn - Remainder Si and N	148		"A Casting Method"	≅ 3500 (Sublimes)	3420	Melting
2	Hafnium Nitride	The Carborundum Company	HfN	Wet Analysis: 95.4% Hf, 6.61% N_2, 0.9% O_2	877		Hot Pressed (Firing Temperature Near 6500° F)	5990	4750	Fracture
3	Titanium Nitride	Technical Research Group	TiN	Requested	255		Hot Pressed	5310	4700	Incipient Melting
4	Zirconium Nitride	General Electric Company	ZrN	Information Promised	427		Pressed and Sintered	5400	4810	Fracture
5	Tantalum Carbide	Kennametal, Inc.	TaC	6.14 C, ON, 0.1 W, <0.01 Si, Mg, Ca, Al, Ti, Cb, Sn, Zr, Fe, Na, Mn, Mg and Ni - Remainder Ta	866		Hot Pressed	7020	4800	Pitting and Spalling
6	Columbium Carbide	Kennametal, Inc.	CbC	11.3 C, 0.07 N, 0.1 Fe, 0.1 W, <0.01 Si, Mn, Mg, Cr, Sn, Ti, Zr, Ni - Remainder Cb	476		Hot Pressed	6330	4740	Cracks and Fissures
7	Zirconium Carbide	General Electric Company	ZrC	Information Promised	371		Pressed and Sintered	5750	4700	Exploded at 2800° F
8	Hafnium Carbide	The Carborundum Company	HfC	Requested	627		Hot Pressed (Firing Temperature Near 6500° F	7030	5220	Some Specimens Broke
9	Zirconium Boride	Norton Company	ZrB	78.7 Zr, 17.6 B, 0.36 C - Remainder Ti, Fe, Ni, Ca, Al, and Si	258	70 to 75	Hot Pressed	5500 (ZrB_2)	4750	Melting
10	Tantalum Boride	General Electric Company	TaB	Information Promised	756		Pressed and Sintered	5430 (TaB_2)	4810	Incipient Melting
11	ATJ Graphite	National Carbon Company	C	Requested	110.3		Molded and Fired	6600 (Sublimes)	5150	No Deterioration
12	Tungsten	Union Carbide Metals Company	W	In PPM: 30 Fe, 26 Si, 20 O, 10 S, 10 P and Ni, Cu, H and N - Remainder W	1178	98.4	Arc-Cast	6080	5010	Melting
13	Zirconium Silicate (Zirconium Orthosilicate) (Taylor Zircon CZ-5)	The Charles Taylor Sons Company	$ZrSiO_4$	ZrO_2 - 65-66%, SiO_2 - 33-34%, Al_2O_3 - 1% Max., Fe_2O_3 - 0.1% Max., TiO_2 - 0.3% Max., Others - 0.2% Max.	252	81.5	Slip-Cast and Sintered	(Dissociates) 3250	3710	Softening (Incipient Melting)
14	Synthetic Sapphire	Linde Company	Al_2O_3	100 Al_2O_3	233	100.0	Grown Single Crystal	3700	3006	No Deterioration
15	Armco Iron	Lapham-Hickey Steel Corporation		0.012 C, 0.017 Mn, 0.005 P, 0.025 S, Trace Si - Remainder Fe	470		Cold Drawn from Melt	2804	2250	No Deterioration
16	Grade 'A' Nickel	J. M. Tull Metal and Supply Company	Ni	0.25 Cu, 0.5 Fe, 0.35 Mn, 0.5 Si, 0.2 C, 0.02 S - Remainder Ni	546		Cold Rolled from Melt	2651	2100	No Deterioration

[1] The borides are claimed as borides - may contain considerable diboride.
[2] Information provided by suppliers - to be checked at Southern Research Institute in Part 2 of work.
[3] Measured at Southern Research Institute by volume displacement method.
[4] Information provided by suppliers.
[5] Supplier and handbook information for crystals and pure material.
[6] Maximum temperature exposure in Southern Research Institute work limited by material failure - some failures occurred at lower temperatures.

Note: No particle size information has been received although requested.

Material	Unexposed Specimen	Exposed Specimen	Exposure Temperature ° F	Theoretical Melting or Destruction of Pure Material ° F
ATJ Graphite			5150	6600 (Sublimes)
Tungsten			5010	6080
Tantalum Boride			4610	5430
Zirconium Boride			4750	5500
Columbium Carbide			4740	6330
Hafnium Carbide			5220	7030
Tantalum Carbide			4660	7020
Zirconium Carbide			4700	5750
Hafnium Nitride	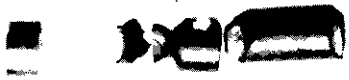		4750	5990
Silicon Nitride			3420	3500 (Sublimes)
Titanium Nitride			4700	5310
Zirconium Nitride			4810	5400
Zirconium Silicate			3710	3250 (Disassociates)

Figure 13. Picture of the Specimens Before and After the High Temperature Exposures.

Figure 14. Picture of the Melting of the Tungsten Specimen in the Expansion Apparatus

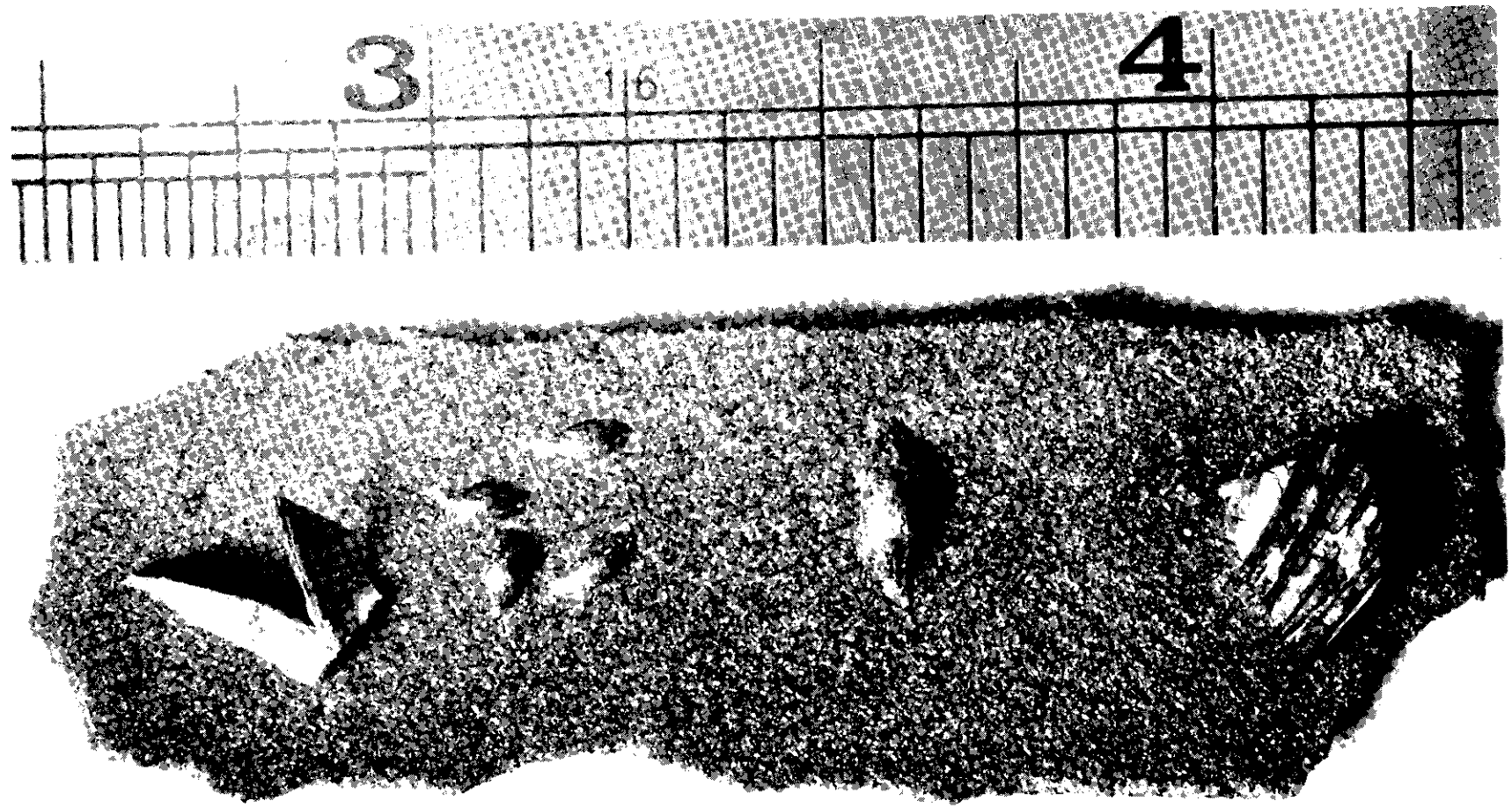

Figure 15. Picture of Tantalum, Tungsten Wire, Tungsten Sheet, and Part of Arc-Cast Tungsten Specimen After Exposure to 5000°F (Specimens in Listed Order from 3 to 4 on the Scale).

at considerably below the melting temperature of their crystals and even considerably below 5000° F. First, the data that was obtained on the thermophysical properties shifted considerably after the temperatures exceeded 4500° F to 5000° F. Reruns then indicated repeat data up to the level of the maximum temperature of the previous run and then again the data would shift. Second, heat soaking some of the specimens at a little over 4500° F for 15 minutes quite dramatically improved their subsequent performance in resistance to fracture and shifted their absolute thermophysical properties. See Figure 16 for a picture of the conductivity specimens showing the results of exposures on as-received and heat soaked specimens. Third, one supplier quoted on several materials with melting temperatures considerably over 5000° F and then declined to quote on another material with the comment that their facilities would not provide the required temperature of 5000° F for that material. Of course, different facilities may have been involved.

Specific details on the materials are presented in subsequent sections as they relate to the measurement of the particular properties; however, the nature of the materials, furnaces, and measurements should be kept in mind during the discussion of all observations.

HEAT CAPACITY

Apparatus and Procedure

The heat capacity was determined to 5000° F for all materials except those that melted, exploded, or otherwise deteriorated at lower temperatures. The apparatus employs the drop technique in which the specimen is heated in a tube-type graphite furnace and then dropped in an ice calorimeter in which an ice mantle has been frozen around the cup, and the heat from the specimen is sensed as the change in volume as some of the ice melts and changes into water. The annulus containing the flooded ice mantle communicates with the atmosphere through a mercury column so that the change in volume is read directly on a calibrated glass tube to provide a volumetric mercury accounting system.

A cross section of the apparatus is shown in Figure 17. Detailed pictures of the ice calorimeter, the ice mantle, and the drop rig are shown in Figures 18, 19, and 20.

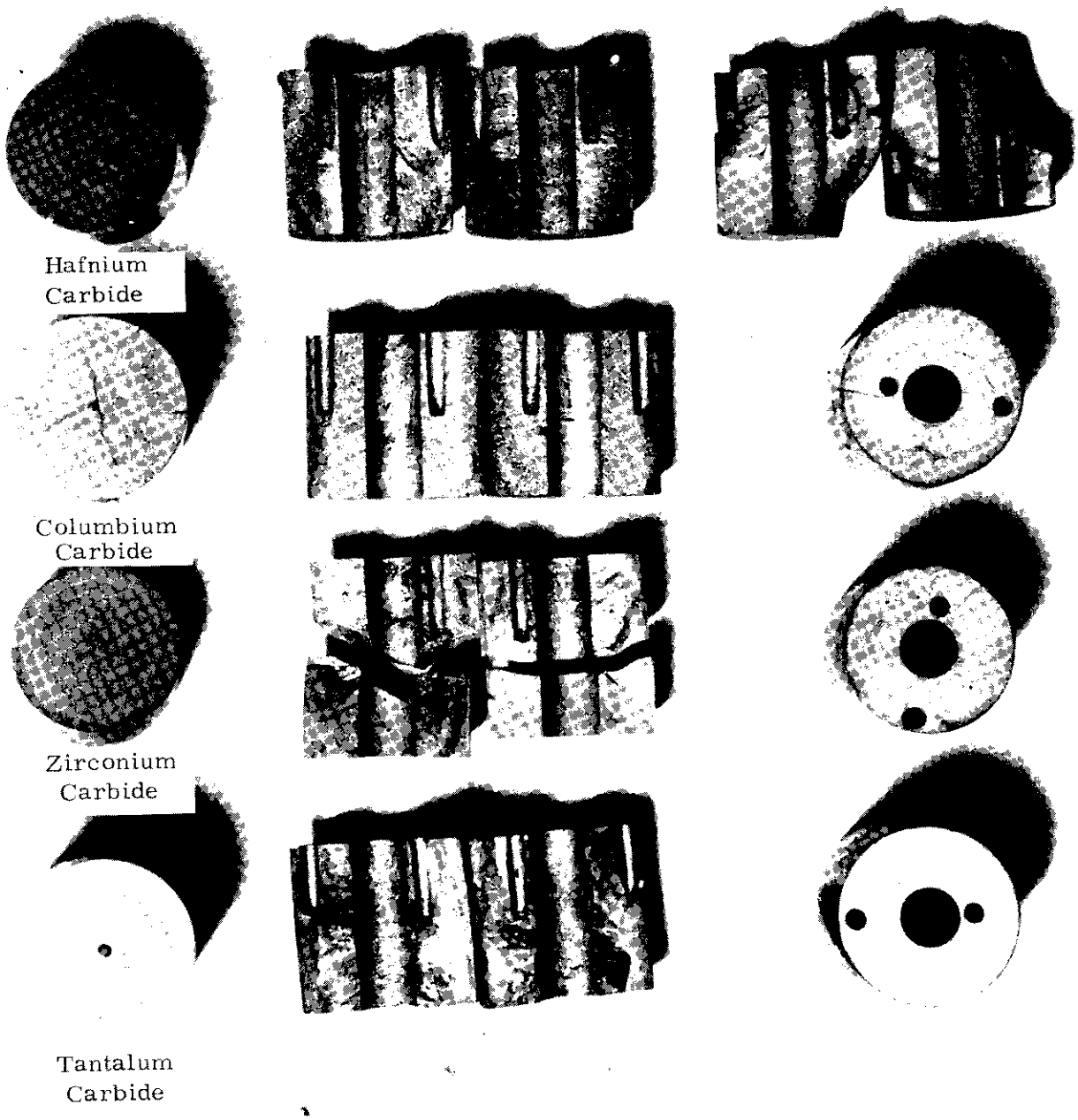

Figure 16. Pictures of Thermal Conductivity Specimens - Heat Soaked and Unsoaked - After the Conductivity Runs.

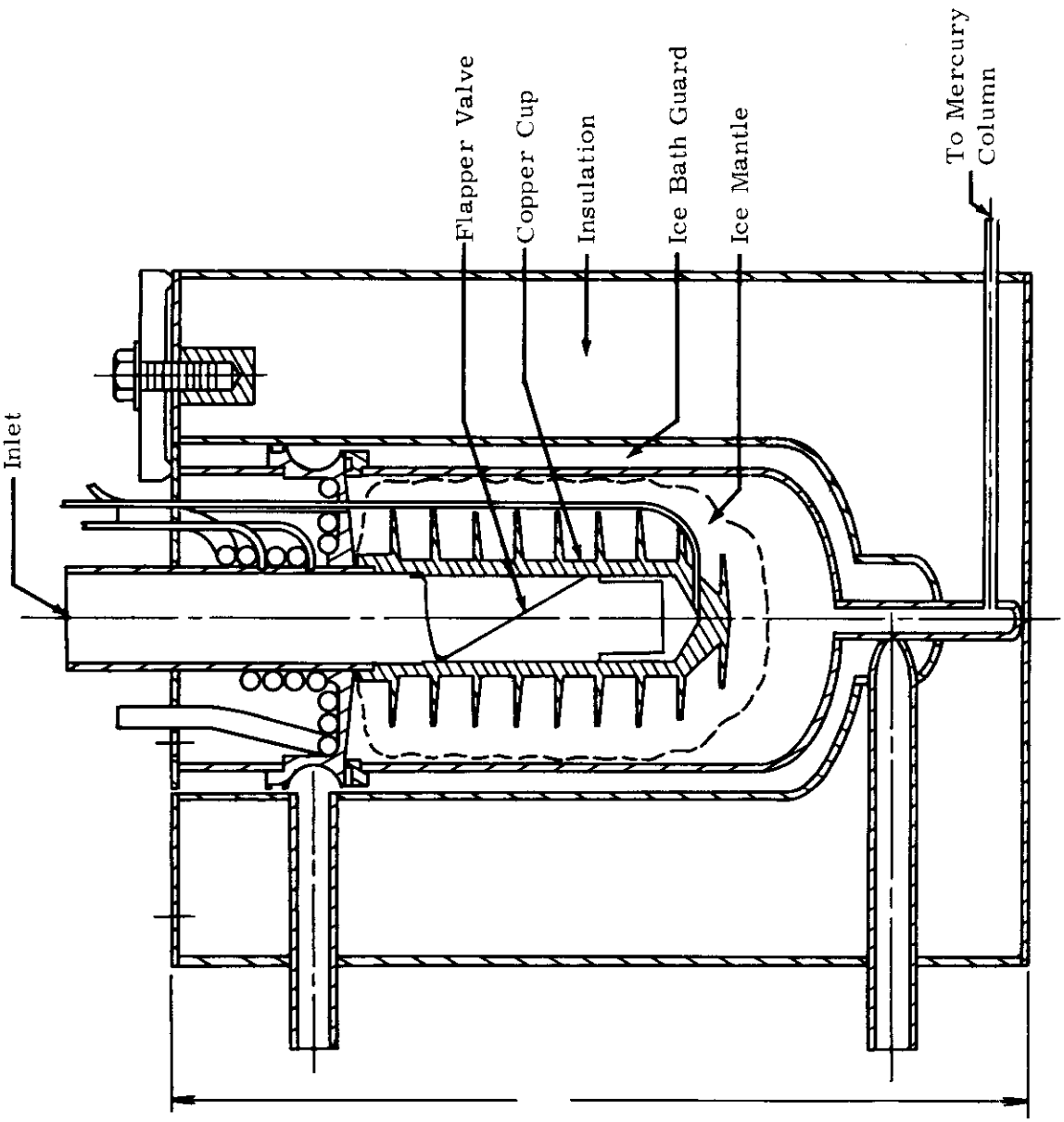

Figure 17. Cross Section View of Ice Calorimeter.

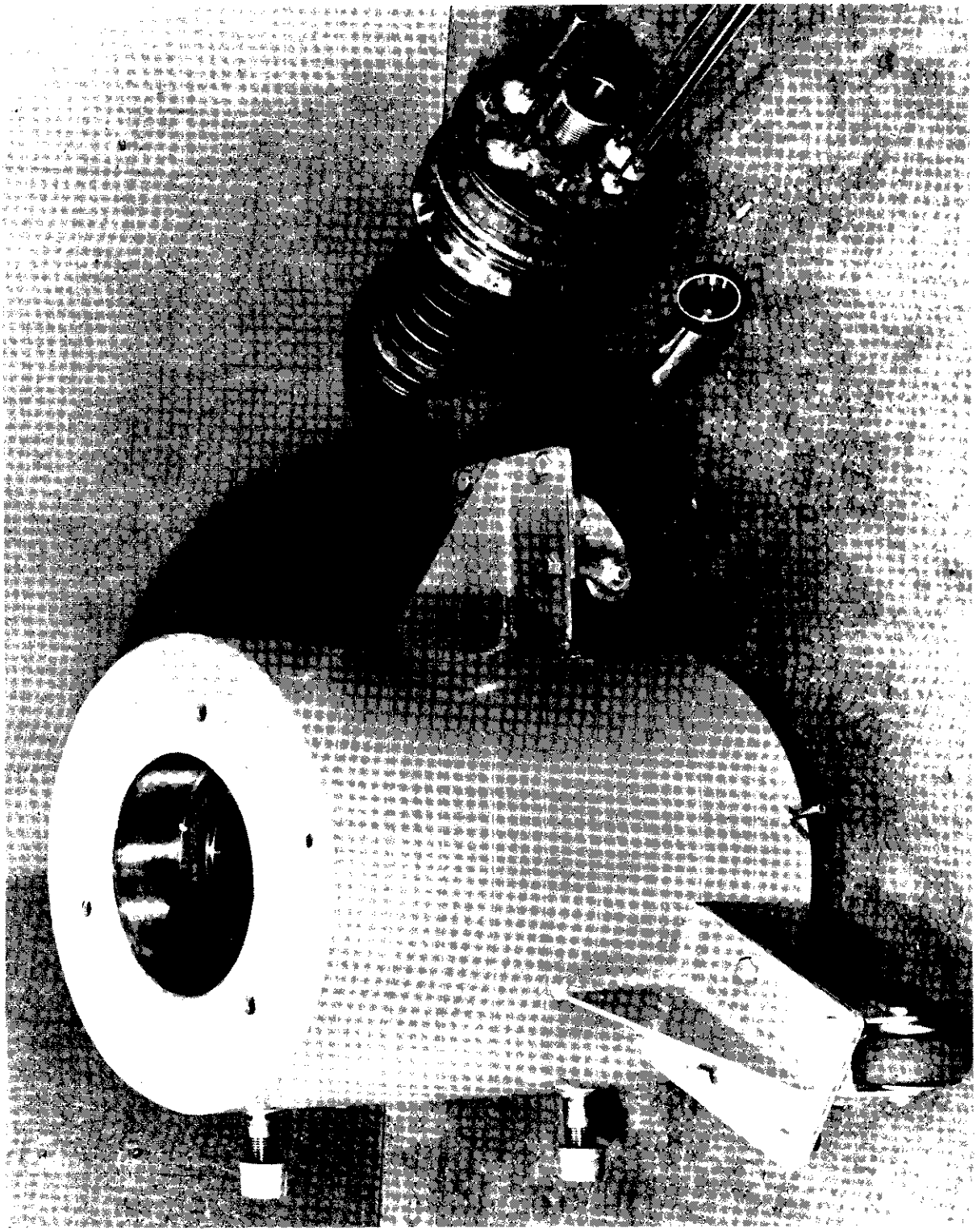

Figure 18. Picture of Ice Calorimeter Jacket and Drop Valve

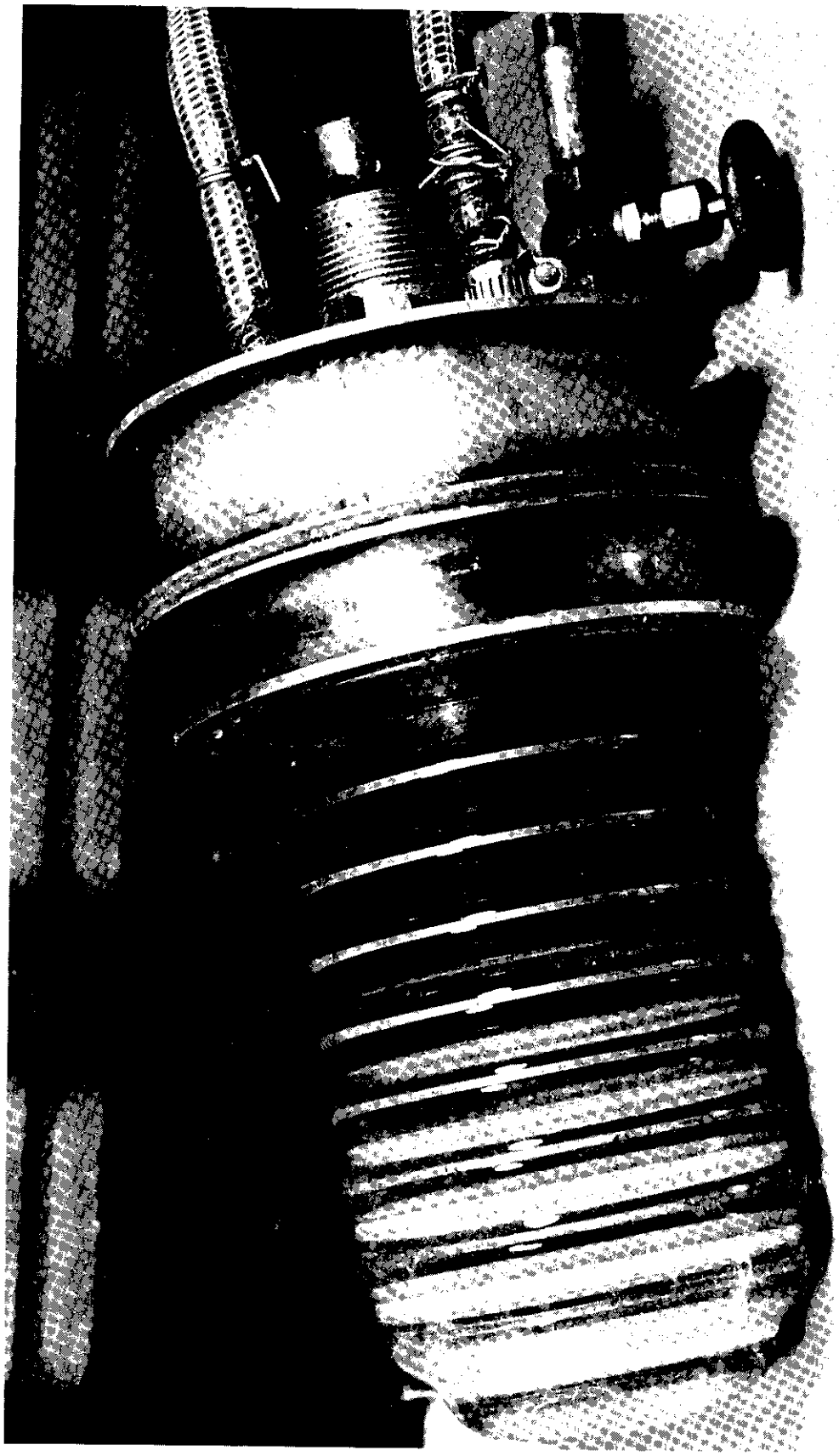

Figure 19. Picture of Ice Mantle

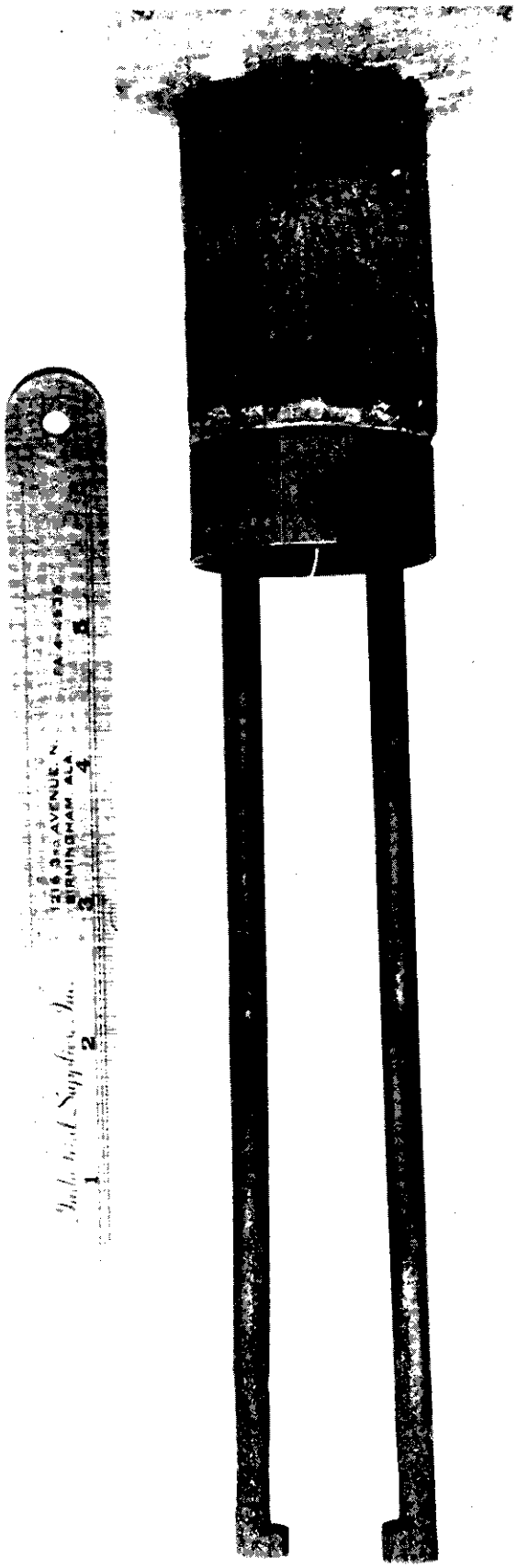

Figure 20. Specimen Holder and Drop Rig for Insertion into Top of Furnaces

The details of the furnace are presented in another section so are not repeated here. The section on calibration discusses many of the features of the ice calorimeter with emphasis on those aspects that contribute to minimum error. The calorimeter is very accurately guarded and has been thoroughly checked out against copper, sapphire, and graphite standards.

In operation, the specimen is enclosed in a basket and dropped into the ice calorimeter. The basket has been previously dropped and its heat content noted. Typical data showing the mercury displacement as a function of time before, during, and after the drop are plotted in Figures 21 and 22. The mercury displacement is a measure of the amount of ice on the mantle that has melted; the time is measured from any selected interval after freezing the mantle and permitting the sub-cooling to equilibrate at 32° F. For the first 30 minutes or so, the slope is a measure of the heat loss from the system. At the time of the specimen drop, the slope increases sharply. After the specimen has cooled to 32° F, the curve flattens out to the same slope that existed before the drop. The heat removed from the specimen is proportional to the ordinate displacement of the two slopes before and after the drop. The mercury displacement units have been calculated so that one cc is equivalent to 3.5 Btu. The enthalpy from a zero reference of 32° F is then calculated from this heat removal and the weight of the specimen.

To determine the enthalpy of the specimen alone, it is necessary to know the effect of the drop basket, radiation losses, drop losses, and unknowns upon the system. This is determined by making runs with the drop basket alone. The mercury displacement caused by dropping the basket includes the above-mentioned losses and provides a convenient way to correct for system unknowns.

To determine the mercury displacement caused by a specimen, the displacement caused by the drop basket must be subtracted from the total displacement caused by a specimen enclosed in a drop basket.

The mercury displacement units have been calculated so that one cc is equivalent to 3.5 Btu. The enthalpy from a zero reference of 32° F is then calculated from this heat removal and the specimen weight as follows:

$$\text{Enthalpy} = \frac{(\text{Mercury Displacement, cc})(3.5\ \frac{\text{Btu}}{\text{cc}})}{(\text{Specimen Weight, lbs})}$$

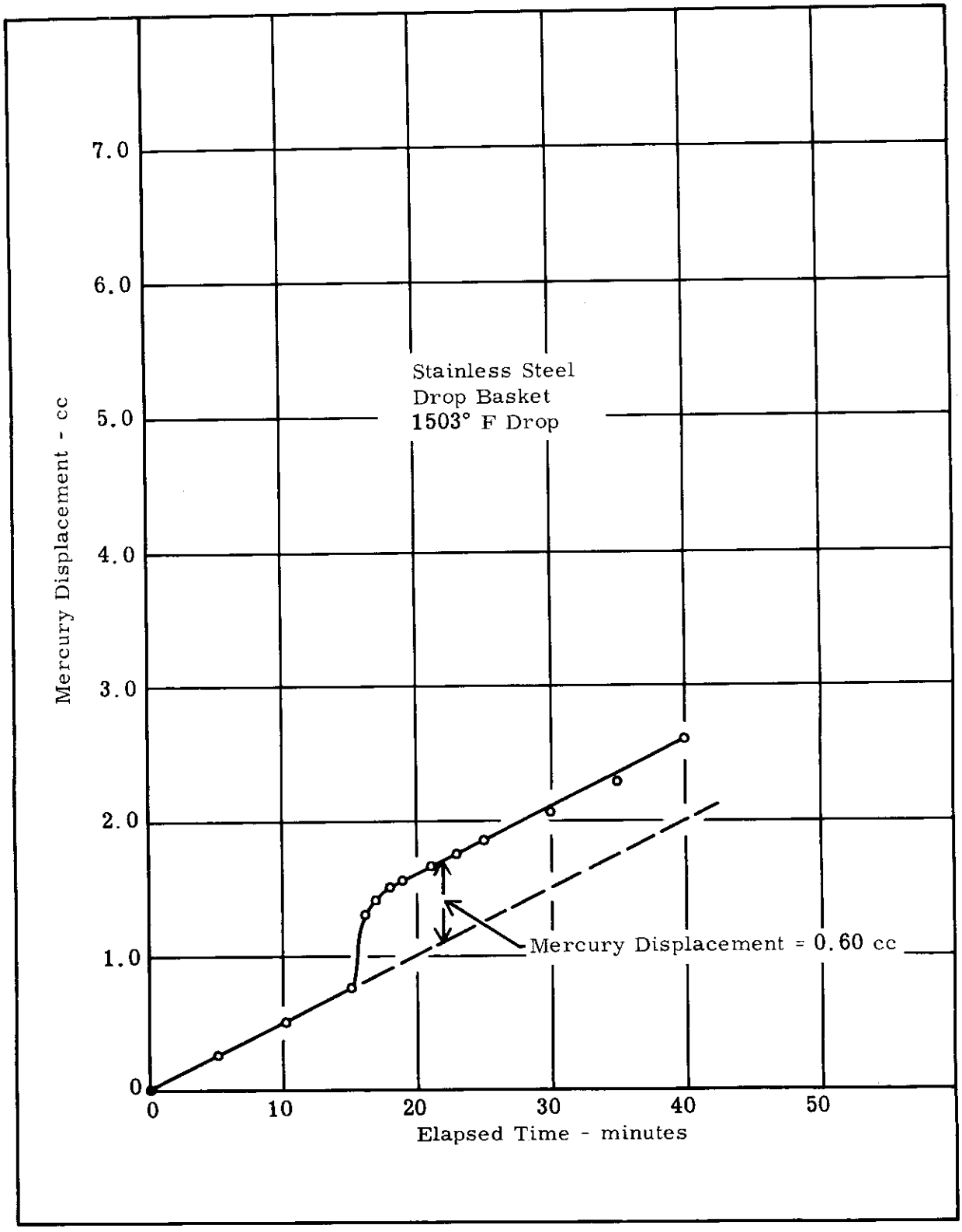

Figure 21. Mercury Displacement Due to 304 Stainless Steel Basket.

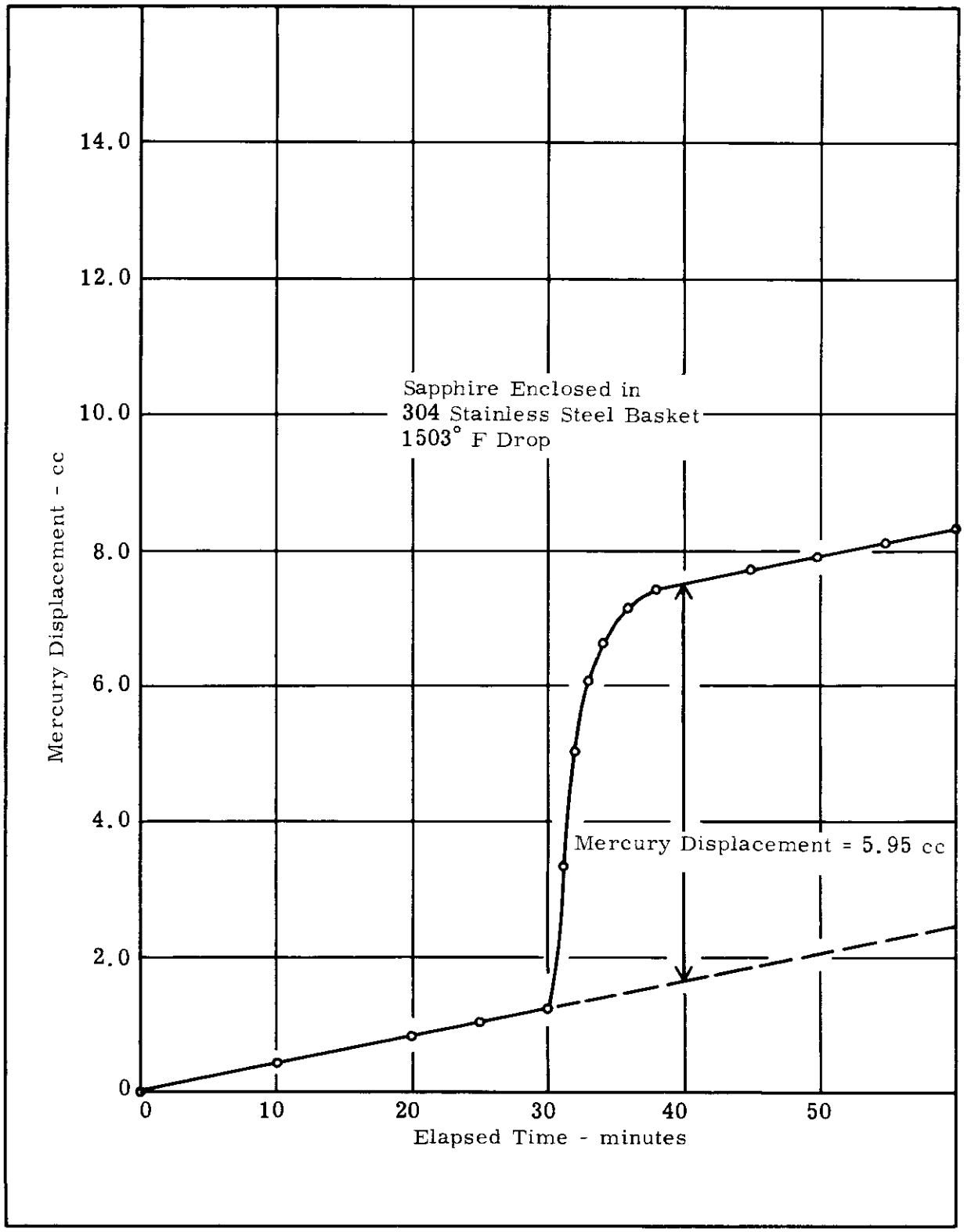

Figure 22. Mercury Displacement Due to Sapphire Enclosed in 304 Stainless Steel Basket.

As an example, the mercury displacement due to synthetic sapphire dropped at 1503° F is as follows:

From Figure 22, total displacement = 5.95 cc

From Figure 21, basket displacement = 0.60 cc

By subtraction, displacement due to specimen = 5.35 cc

Specimen Weight = 21.765 grams = 0.048 lbs

$$\text{Enthalpy} = \frac{5.35 \times 3.5}{0.048}$$

Enthalpy = 390 Btu/lb ° from drop temperature to 32° F

Drops were made at 500° F temperature increments and enthalpy versus temperature plots obtained. Three different techniques were employed to reduce this enthalpy data to heat capacity versus temperature information.

First, the slopes of the enthalpy plots were read from the curves at 1000° F total increments around a mean temperature. This slope is then the average heat capacity of the material at this temperature. The technique has the major advantage of being insensitive to odd inflections in the curve and of providing reliable data that is not distorted by the practical inability to write a precise equation that matches the enthalpy plot throughout its entire range.

As a second method of treating the enthalpy data to obtain heat capacity versus temperature information, equations were written for the best visual curve fit of the enthalpy plot (Enthalpy = $a + bT + cT^2 + dT^3$). After solving these equations, the heat capacity is the derivative ($HC = b + 2cT + 3dT^2$). Unfortunately, most of the materials over the wide temperature ranges employed had several inflections so that the equation actually fit only the four points selected for simultaneous solution rather than the entire range. Since heat capacity is the derivative of the enthalpy plot, any deviation of the equation from the observed data introduces a magnified error in heat capacity. Figure A-3 in the Appendix shows plots of the heat capacity as determined by these first two techniques for the hafnium nitride specimen.

Third, equations were developed on a computer from a least squares fit of all observed data. The equations for all materials are

included in Table A-18. Although data from these equations is subject to the same anomalies described for the second analysis, they do present the function in a relation required for many applications.

After careful consideration, the technique of data analysis employing the slope measurements was selected and used in the preparation of all data on heat capacity.

Date and Results

The enthalpy and heat capacity data for all specimen materials, the stainless and graphite baskets, and the copper and sapphire calibration specimens are shown in Figures A-1 through A-17 in Appendix 1 and Tables A-1 through A-17 in Appendix 2. The data points on the enthalpy plots are observed readings with the maximum temperature point being the top exposure temperature. At these maximum temperatures, many of the materials deteriorated; however, no attempt has been made at this time to relate precisely the type of deterioration with the change in heat capacity.

Also, many of the inflections in the high temperature range can be related to inflections in the thermal expansion and thermal conductivity data. Again, these inflections can be more thoroughly analyzed and discussed after the chemistry of the material is better established.

Both of the elements, graphite and tungsten, demonstrated an increase in heat capacity to about 3000° F and then a slight decrease with the graphite again increasing above 4000° F. No difficulty was experienced in extending the exposure on graphite to over 5100° F, but the tungsten completely melted at 5300° F, and even the 4950° F run showed signs of melting. Chemical analysis will probably indicate that either the tungsten contained carbon as it was received or else picked up carbon from the furnace since tungsten and carbon do form a eutectic melting at about 5000° F. Once this melting started, the specimen would probably continue to failure.

Although the nitrides appeared to disassociate and undergo rather serious changes in physical appearance (and odd thermal expansions) at temperatures above 3500° F, the hafnium nitride was taken to over 4900° F and the titanium nitride and zirconium nitride to over 4500° F. Only titanium nitride had an odd inflection at about 2500° F. The other nitrides had rather smooth curves over the entire temperature range with a gradual increase in heat capacity at up to 2000° F.

The heat capacity of the borides increased with temperature up to about 2000° F and then remained constant to over 4000° F. Neither boride behaved in an erratic fashion.

After an orderly increase at up to about 2000° F, the heat capacity of the zirconium silicate again increased slightly. This higher temperature inflection was probably associated with material change since almost complete destruction occurred at less than 3500° F.

All of the carbides had an increasing heat capacity at up to about 2000° F. The slope of the hafnium carbide curve then remained flat to 5000° F; whereas the columbium carbide data had a slight inflection, and the zirconium carbide demonstrated an increasing value beyond 3700° F. Although the zirconium carbide and columbium carbide data were only extended to 4700° F, they probably could have been exposed to 5000° F. However, these materials had a tendency to spall and fracture catastrophically so that the probability of seriously damaging the furnace did not make the risk seem worth while.

The data on the sapphire and copper indicate the very little scatter that was obtained with homogeneous specimens of stable composition. Actually, the scatter was not particularly bad with most of the specimens, and the observed inflections were undoubtedly real. These standard specimens are discussed further in the section on calibration.

The heat capacity data on the baskets are included primarily to record the information. The increased scatter with the very small specimens should be expected; however, it is interesting to note that the heat capacity still checks rather closely with that anticipated for the two materials even though the baskets suffer practically all of the drop losses that do occur.

CALIBRATION AND ERROR ANALYSIS OF THE HEAT CAPACITY APPARATUS

The drop-type ice calorimeter has no inherent limitations for service up to 5000° F and demonstrates good performance throughout the entire temperature range. Since this method employs direct measurements of the variables rather than a comparison technique, the accuracy is as good as the total of the separate measurements. Specifically, the precision of the data is dependent on (1) the accuracy of the temperature measurement of the specimen in the furnace immediately before the drop, (2) the absence of temperature gradients in the specimen before the drop, (3) minimizing the already small heat loss from the specimen during the fall from the furnace to the cup,

(4) eliminating heat losses by radiation of the specimen out of the cup after the drop, (5) guarding the cup and accurately accounting for any losses during the specimen cooling from drop temperature to 32° F, and (6) measuring the change in volume of the ice and water in the cavity containing the ice mantle as the ice absorbs the heat and changes in volume while proceeding from ice to water.

The specimen size must be selected to provide large heat contents for accurate readings, and the material chemistry must be stable in the furnace environments. These two requirements are aggravated by the high temperature aspects since large specimens are inclined to thermal shock and the graphite heater does emit carbon vapors. By enclosing the specimen in heat-aged graphite baskets, broken specimens could be handled and the contamination from heater fumes was minimized. Lining the cups with tungsten foil and a zirconia cement wash has also proven effective. The best protection is to introduce fresh helium right at the specimen.

A compilation of these possible errors indicates that the apparatus is accurate to well within 5% over the entire temperature range. Comparison of Southern Research Institute data on copper, Linde synthetic sapphire, ATJ graphite, and many other isolated check points on the specimen materials all confirm the 5% accuracy.

A detailed discussion of the different variables is necessary. The specimen temperatures were measured by thermocouples at up to 2000° F and then by calibrated optical pyrometer to 5000° F. A selenium-cell radiation pyrometer was also used regularly as an operation aid. A detailed discussion of the temperature calibration is included in another section; however, it should be noted that at various times the specimens were monitored by platinum-rhodium, Chromel-Alumel, tungsten-molybdenum, and tungsten-rhenium thermocouples concurrent with optical measurements on a different part of the specimen. No gradients over about 10° F were normally detected. The long 5-inch hot zone undoubtedly minimized any end cooling of the specimen. Also, the end plugs of the furnace were usually zirconia, molybdenum, tungsten, or graphite, all of which were permitted to come to near specimen temperature so that a cold end surface was simply not present. The soak time for the specimen was always at least five times the theoretical that would be required from diffusivity calculations.

Very little heat can be lost from the specimen during the drop. About $\frac{1}{3}$ second is required for the fall. If the specimen were at 5000° F and the emission were all lost, then about 0.2 Btu would be involved.

The enthalpy change for the ATJ specimen at 5150° F, for example, was about 70 measured Btu so that only 0.3% could be lost. Since the specimens are actually dropped in an enclosing basket, and since the basket has been previously dropped and the heat content noted, the thermal diffusivity is such that all of the 0.2 Btu that is lost departs from the calibrated basket—not the specimen. Assuming even a 10% error in calibrating the lightweight baskets, the net effect on the heat content of the specimen could be no more than 0.03%. The thermal diffusivity of the basket is such that the specimen temperature itself does not have time to decrease.

To minimize heat pickup by the cup from the furnace immediately before the drop and to eliminate heat loss radiating from the specimen out of the cup, a spring-loaded flapper valve was installed within the cup. This molybdenum flapper reflects the heat from the furnace up out of the cup during the few seconds the bottom plug of the furnace is pulled and the drop made and reflects the specimen radiation down into the cup during the specimen cooling. Any heat that is absorbed by the flapper during the 15 minutes required for the specimen to cool is conducted to the cup walls and hence contributes to melting the ice mantle and is not lost. Proper design and operation of this flapper valve, coupled with the use of lightweight calibrated baskets, are probably the two key features of a successful drop-type calorimeter of this type. Without the flapper, over 10% error is introduced at high temperatures.

The cup zone is completely guarded by the flapper and recirculated ice water that enters the guard zone at 32° F and leaves at not over 33° F. With this high circulation rate and resulting good guarding, the normal heat loss from the empty cup over a 10-minute period is no more than 7% of the heat absorbed from a specimen dropped at 1500° F. However, this heat loss is not error. The slopes of the heat loss versus time curves before and after the drop (and subsequent specimen cooling) are essentially equal so that the slope before the drop can be extended to the time after specimen cooling, and the heat absorbed from the specimen is the difference on the ordinate between these two parallel slope lines. Data inspection reveals that the slopes practically always remain constant; however, assuming even a 10% error in slope extension, the error introduced in determining the heat content would be no more than 0.7% for the specimen and 6% for the basket. Since the basket is so lightweight and has a small heat content, it has only about a 10% influence and so contributes only 0.6% to any accumulative error. On this basis, the total error resulting from improper guarding could total

no more than 1.3% at 1500° F and is proportionately less at higher temperatures. The fact that accurate and reproducible data are obtained even at 300° F indicates that the slope extension results in data that is considerably better than the over-all 1.3% error that has been allowed.

The mercury accounting system involves simply the accuracy of reading a mercury column in a calibrated glass tube. At 1500° F drops, this readout is within better than 1%. At higher temperatures, the readout is proportionately better. When more accuracy is needed, the system can be modified by using a resistance-wire technique or mercury weighing system; however, for these runs, the change in mercury column height was sufficient to use the volumetric measure. To insure a minimum influence of any air bubbles that could be entrapped in the ice-mantle cavity or in the mercury system, a constant pressure head was maintained on the ice-mantle part of the system during all readings.

A comparison of data obtained from the Southern Research Institute ice calorimeter and that published by other investigators on synthetic sapphire is shown in Table 3. Generally, some investigators have found values a little higher and others have found values a little lower. An inspection of Figure A-15 showing the enthalpy versus temperature plot for sapphire reveals that the maximum deviation of a measured data point from the smooth curve fit was only 2%. All other data points matched even better. Data on copper is presented in Figure A-14 indicating very close agreement between the Southern Research Institute and literature data. Also, the ATJ data in Figure A-1 is in good agreement with the literature and is considered as a calibration standard to 5000° F. Other specimens such as tungsten also check well with published information.

The data treatment introduces no additional error since readout on the enthalpy versus temperature curves is to three significant figures. The slope is the heat content in Btu/lb/° F so no additional treatment is necessary. The procedure of writing an equation for the enthalpy versus temperature plot and taking the derivative to obtain heat content data does introduce error in those ranges on the curve at which the derived equation deviates from the observed data points. Since the equation is a perfect match only at 3 or 4 points, depending on the treatment, some deviation at midpoints is inevitable. Of course, the derived equation should never be extrapolated beyond the range of the points used to obtain the constants so that the equation really adds nothing to the information.

Table 3

Comparison of the Heat Capacity of Sapphire Obtained by the Ice Calorimeter to Several Other Sources

SRI Ice Calorimeter		SRI Adiabatic Calorimeter		Armour Research Foundation		Linde Company		International Critical Tables		NBS	
Temp. ° F	Heat Capacity Btu/lb/° F	Temp. ° F	Heat Capacity Btu/lb/° F	Approx. Temp. ° F	Heat Capacity Btu/lb/° F	Approx. Temp. ° F	Heat Capacity Btu/lb/° F	Temp. ° F	Heat Capacity Btu/lb/° F	Temp. ° F	Heat Capacity Btu/lb/° F
497	0.240	490	0.223	500	0.263	500	0.2125			500	0.254
1008	0.275	996	0.240	1000	0.280	1000	0.2265	922	0.239	1000	0.283
1503	0.320			1500	0.297	1500	0.234			1500	0.296
2005	0.330			2000	0.314			1832	0.260	1750	0.300
2148	0.330										
2456	0.320			2500	0.331			2732	0.275		
3006	0.315										

The probable error was statistically determined for the enthalpy versus temperature curves to establish the maximum deviation that should be expected for 50% of the observed data points from the smooth curve. This deviation was more enthalpy dependent than temperature dependent and was found to be about 3% at the 100 Btu/lb range and $1\frac{1}{2}$% at the 1500 Btu/lb range. The over-all probable errors for ATJ, TaB, ZrB, HfC, and SiN were about 3% for all. Except for temperatures at which the specimens were deteriorating, these data are representative.

THERMAL EXPANSION

Apparatus and Procedure

Thermal expansion measurements were made on all specimens, axially, in graphite tube dilatometers to over 5000° F or the destruction point of the material. The dilatometers consisted of (1) graphite tubes into which the specimens were placed, (2) graphite rods which transmitted specimen motions to the dial gages, (3) short stainless steel tube and rod extensions, and (4) the dial gages. The dilatometers were self-contained units that were placed in the high temperature furnaces with the dilatometers hung from the top flanges of the furnaces and not in contact with the furnace inner parts. A typical dilatometer assembly and the dilatometer parts are shown in Figure 23.

Dilatometer tubes and rods were machined from National Carbon Company's Grade CS graphite stock. The effective lengths of the dilatometer tubes were equal to the combined lengths of the specimens and the dilatometer rods. The stainless steel tube and rod extensions were of equal effective lengths, eliminating errors due to the differences in coefficients of expansion. The dial gages used in the dilatometry apparatus were graduated in 0.0001-inch divisions with a total range of 0.200 inch. The mechanical accuracy of the B. C. Ames Company Model 212 shockless dial gages is stated by the manufacturer to be $\pm$ 0.0001 inch for any given reading at any point in the range.

The dial gage movement during any expansion run must be corrected by the movement of that corresponding length of graphite dilatometer tube. The true total elongation of the specimen is then equal to the sum of the dial gage movement and the calibrated movement of the graphite dilatometer over the specimen length. Other than in the specimen zone, the expansion of all dilatometer parts is cancelled by an equal expansion

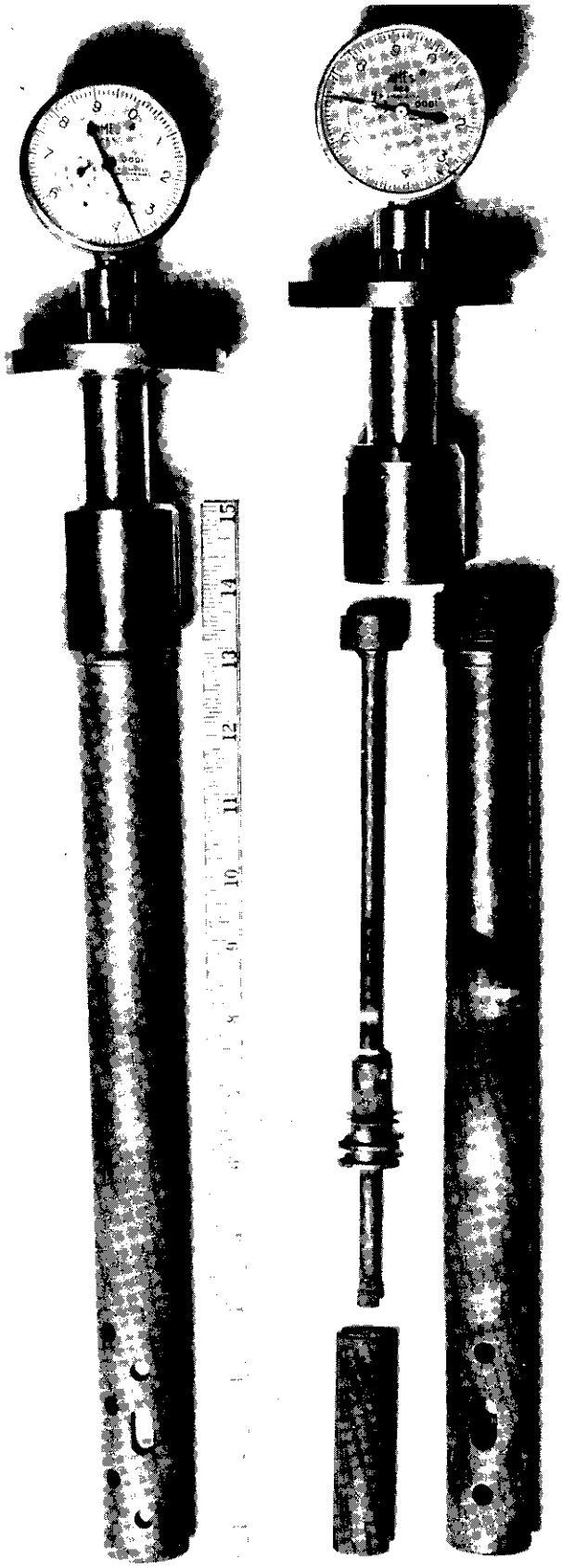

Figure 23 . Picture of Typical Arrangement of the Graphite Dilatometers

of a corresponding part of the same material at the same temperature. The expansion of the tube reduced the indicated expansion of the specimen, making a dilatometer tube movement correction necessary.

Careful measurement of the graphite dilatometer parts before and after temperature exposures indicated a permanent change in length on the initial high temperature exposure. No significant dimensional changes occurred on subsequent exposures, so a preliminary heat soaking run was standard procedure for new graphite dilatometer parts.

In preparing a specimen for the thermal expansion run, the ends were ground to a radius equal to the specimen length. This provided that one end of the specimen could shift without causing any change in dial gage indication. On some of the early runs, thermocouples were placed in three locations on the specimen to determine temperature gradients. On several other runs, thermocouples were placed at the center of the specimens for temperature measurements.

Furnaces No. 1 and No. 3 shown previously in Figures 4 and 6 were used for the thermal expansion measurements. Most of the specimens were evaluated in Furnace No. 1 which employs a graphite helix heating element enclosed by a graphite tube and lamp black insulation. Furnace No. 3 has a slotted graphite tube heating element enclosed by a graphite tube and lamp black insulation.

The following paragraphs contain a discussion of the general procedure for thermal expansion runs.

The specimen, and usually the dilatometer tube and rod, were measured for initial length before assembly of the dilatometer unit. The dial gage housing was anchored to the stainless steel extension tube and the dial gage was zeroed. The unit was then inserted into the furnace and hung from the top. The bell glass was attached, the furnace sealed and evacuated several times, and purged with helium gas. At this point, the power was turned on and the furnace heat-up started. The furnace was evacuated several more times while below 800° F to remove boil off and assure an inert atmosphere.

Data points were taken at approximately 250-500° F intervals throughout most of the temperature range. At a given power setting at least three times the theoretical soak time was allowed for complete elimination of specimen temperature gradients. As an operational aid

to indicate heating rates and furnace equilibrium, a selenium-cell radiation pyrometer was used to view the specimen during runs.

Throughout all runs, careful attention was directed to the indication of inflections in the expansion of specimens. When slope changes were evident, readings were taken much more regularly to insure true analysis of specimen behavior.

Data points were taken at less frequent intervals during the cooling off period on most runs. The room temperature zero return was recorded on all runs and compared to the original zero setting.

At the completion of all runs, the specimen length was measured and recorded. On most runs, the tube and rod were measured to determine the permanent change in length. The conditions of the specimens following the runs were very carefully observed and recorded.

The thermal expansion data recorded during all specimen runs provided dial gage readings at given absolute temperatures. The treatment of the raw data required that the dial readings (observed total elongation) be converted to observed unit elongation, that the unit correction for the expansion of the graphite dilatometer tube be applied, and that the correction be algebraically added to the observed unit elongation to obtain the corrected specimen unit elongation.

Data and Results

Tables A-19 through A-31 in Appendix 2 contain the complete thermal expansion data for the thirteen specimens evaluated under this contract. Data points for each specimen are plotted on the curves shown in Figures A-18 through A-30 in Appendix 1. For each material, the over-all slopes of the curves over a given temperature range are noted. In addition, curve slopes at given temperatures, ± 500° F are included.

From an inspection of the expansion curves, it can be seen that most of the materials had a reasonably constant expansion from room temperature to about 3500° F. Only three materials, ATJ graphite, tungsten, and hafnium carbide, maintained reasonably constant expansion throughout the temperature range. Tantalum boride, zirconium boride, and tantalum carbide maintained reasonably constant expansion to the 4200-4500° F range. Above about 3500° F, columbium carbide and zirconium nitride showed a marked increase in the rate of expansion.

The two silicon-containing materials, silicon nitride and zirconium silicate, expanded at a reasonably constant rate from room temperature to the vicinity of their deterioration temperatures of 3420° F and 3710° F, respectively. Two materials broke prematurely. Hafnium nitride fractured at about 2550° F, causing the apparent expansion to decrease quite rapidly. Zirconium carbide essentially exploded on two occasions once at about 2000° F, later between about 2500° F and 3000° F. The final material, titanium nitride, expanded constantly to 2975° F, suddenly began contracting, and continued to contract throughout the exposure. Measurement of the specimen of this material after the run indicated that a permanent length reduction of about 3% had occurred.

A discussion of the expansion behavior of each material, individually points out some interesting observations. From Figure A-18, it can be seen that four runs are plotted for ATJ graphite. The first two runs to 3780° F and 4950° F were almost identical; however, the two final exposures indicated that the specimen expansion rate was changed by the prior 4950° F exposure. Generally, zero return of the dial gage checked closely with specimen length.

From Figure A-19, it can be seen that the expansion of the arc-cast tungsten specimen remained stable up to about 4800 F From 4800° F to 5010° F, the specimen length decreased and the specimen melted over its entire length (see prior Figure 14) Figure A-20 showing the expansion curve for tantalum boride, illustrates the fact that incipient melting occurred at about 4200-4300° F. Figure A-21, for zirconium boride, shows that the curve slope stayed constant for about an extra 500° F of the temperature range on each succeeding exposure up to the deterioration temperature of the material. From Figure A-22, on columbium carbide, it can be seen that at about 3500 F, the expansion increased to more than twice the original level, indicating a stress relief in the material. Post inspection disclosed several axial and circumferential cracks in the specimen.

Figure A-23, on hafnium carbide, requires a detailed discussion. The first exposure represents the true expansion data to 4810° F for the material. This curve shows that the material had a reasonably constant expansion with an indication of a gradual slope reduction above 4000° F The specimen also underwent a small length reduction due to the exposure. A comparison of the zero return of the dial gage to the measured specimen length change checks very well. The curve on Figure A-23 representing the second specimen exposure provides an

excellent illustration of the necessity of heat soaking new graphite dilatometer parts before making data runs. A new dilatometer tube and rod were used for this particular run and, because of permanent length changes during this initial dilatometer exposure, caused a very definite shift in the apparent expansion of the specimen. Between 1000° F and 2000° F, an unusual inflection is quite evident and the slope of the curve remains greater thereafter. It is possible that some of the slope change could be an actual specimen change after exposure to 4810° F; however, this could not reasonably account for a 50% to 90% slope increase and most probably could not cause the slope inflection between 1000° F and 2000° F.

It is interesting to note that the second exposure for hafnium carbide reached a maximum temperature of 5220° F with no specimen damage.

From Figure A-24, on tantalum carbide, it can be seen that the first and second exposures established expansion curves that were essentially identical. The final exposure resulted in a slightly steeper curve slope that became very steep near the specimen deterioration temperature. Figure A-25, on zirconium carbide, indicates the point of rapid growth and explosion of the first specimen. The breakage of the second specimen was almost identical on post inspection to the breakage of the first specimen even though the expansion curves do not indicate this. Probably, the second specimen broke, or exploded, at about 2800° F. Figure A-26, on hafnium nitride, shows that the specimen expanded rather rapidly from 2000° F to 2500° F where the material broke.

From Figure A-27, on silicon nitride, it can be seen that a smooth expansion curve was established up to the deterioration temperature of the specimen. In the 1000° F to 2000° F range, the specimen was heated, cooled, then reheated to check on the repeatability of the temperature-dial gage reading relationship. The specimen did not return along the established curve, but upon reheating returned to the same point and verified the over-all curve slope as well as indicating a permanent shift in the specimen length.

Figure A-28, on titanium nitride, illustrates the severe change that the material underwent during the exposure. The expansion was reasonably constant to 2960° F; however, at that point, the material began a contraction, which continued throughout the exposure. Figure A-29, on zirconium nitride, shows a rather erratic expansion through most of the temperature range. The specimen was found broken

on post inspection. Breakage probably occurred around 4500° F to 4700° F. From Figure A-30, on zirconium silicate, it can be seen that a reasonably constant expansion occurred until the material disassociated at about 3300° F.

Two failures of the specimens during runs are shown in Figures 24 and 25 for silicon nitride and zirconium carbide. The first failure is a typical disassociation and the second is a catastrophic fracture.

CALIBRATION AND ERROR ANALYSIS OF THE THERMAL EXPANSION APPARATUS

Precision dilatometry requires that (1) the specimen temperature be known accurately; (2) no serious thermal gradients exist between the tube specimen, and rod at the same position within the length; (3) the tube and rod do not change length during a run in an unknown manner and have both a relatively small and known motion; (4) there be no deleterious reaction between the tube, rod, and specimen materials; and (5) an accurate linear motion device be used to measure the relative motion of the tube, rod, and specimen. As a further check on these parameters, the dilatometer should provide data that agrees with published information on standard materials, and any failure of zero return should match a growth or shrinkage in the specimen. Of course, the specimen must not shift during a run, although provisions can be made in preparing the ends of the specimen to prevent a serious error by grinding the ends on a radius equal to the length of the specimen.

A special requirement emphasized by the high temperature aspects is that the specimen size and chemistry must receive careful attention. Many refractory materials are very subject to thermal shock in large sizes; therefore, the size must be a compromise between a minimum length to obtain large total readings and a maximum length that will not induce premature specimen failure. Also, the chemistry of the specimen must not be altered by the furnace environment. Fresh helium introduced down through the dilatometer tubes greatly minimizes this furnace vapor contamination. Finally, the heat aging of the specimen and its thermal history must be carefully noted and recorded. For example, the expansion coefficient of the ATJ graphite shifted considerably after exposure at 5000° F.

All of these requirements of good dilatometry have been considered in this system; and considering that the exposures must be to 5000° F,

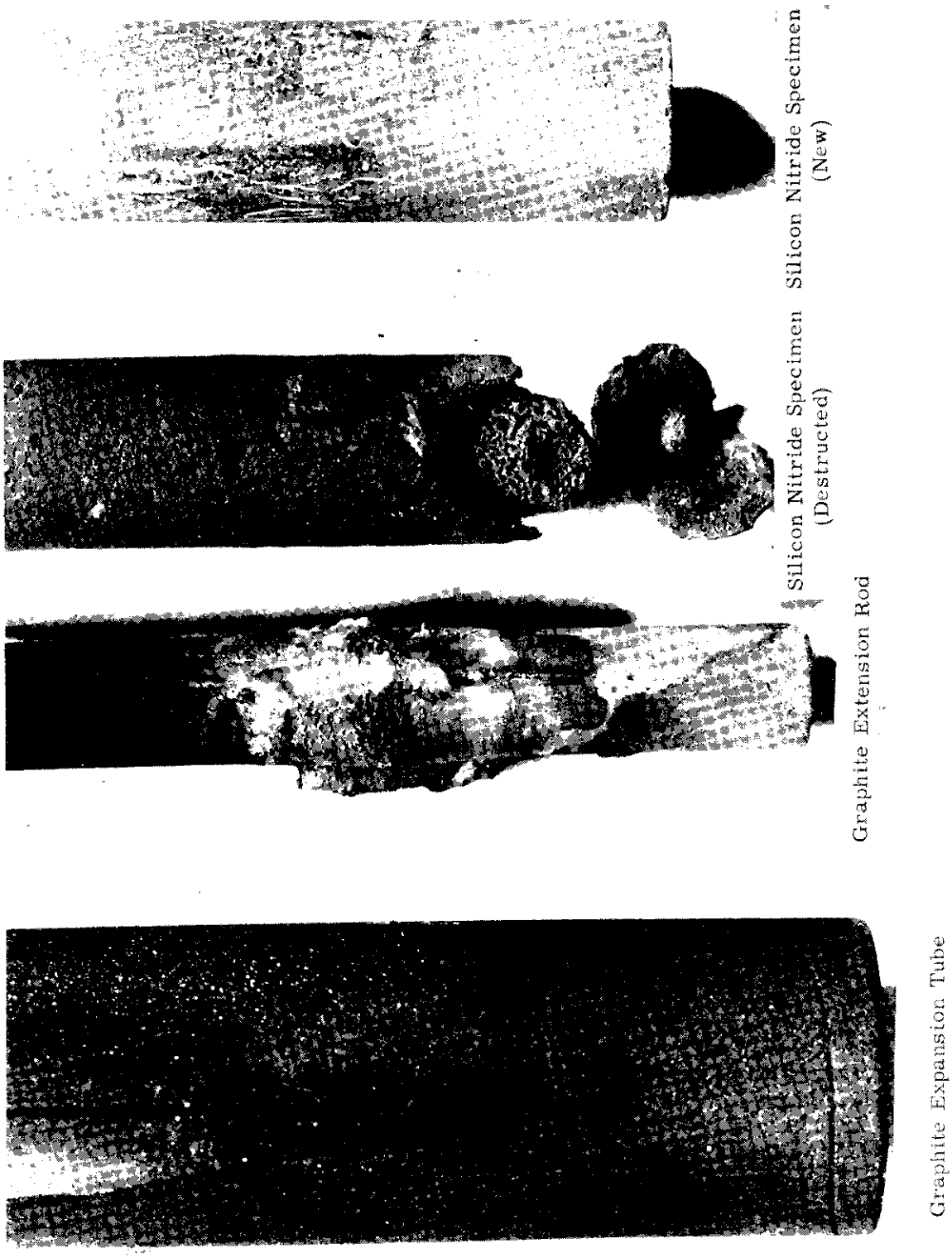

Figure 24. Picture of Failure of Silicon Nitride Specimen During a Run.

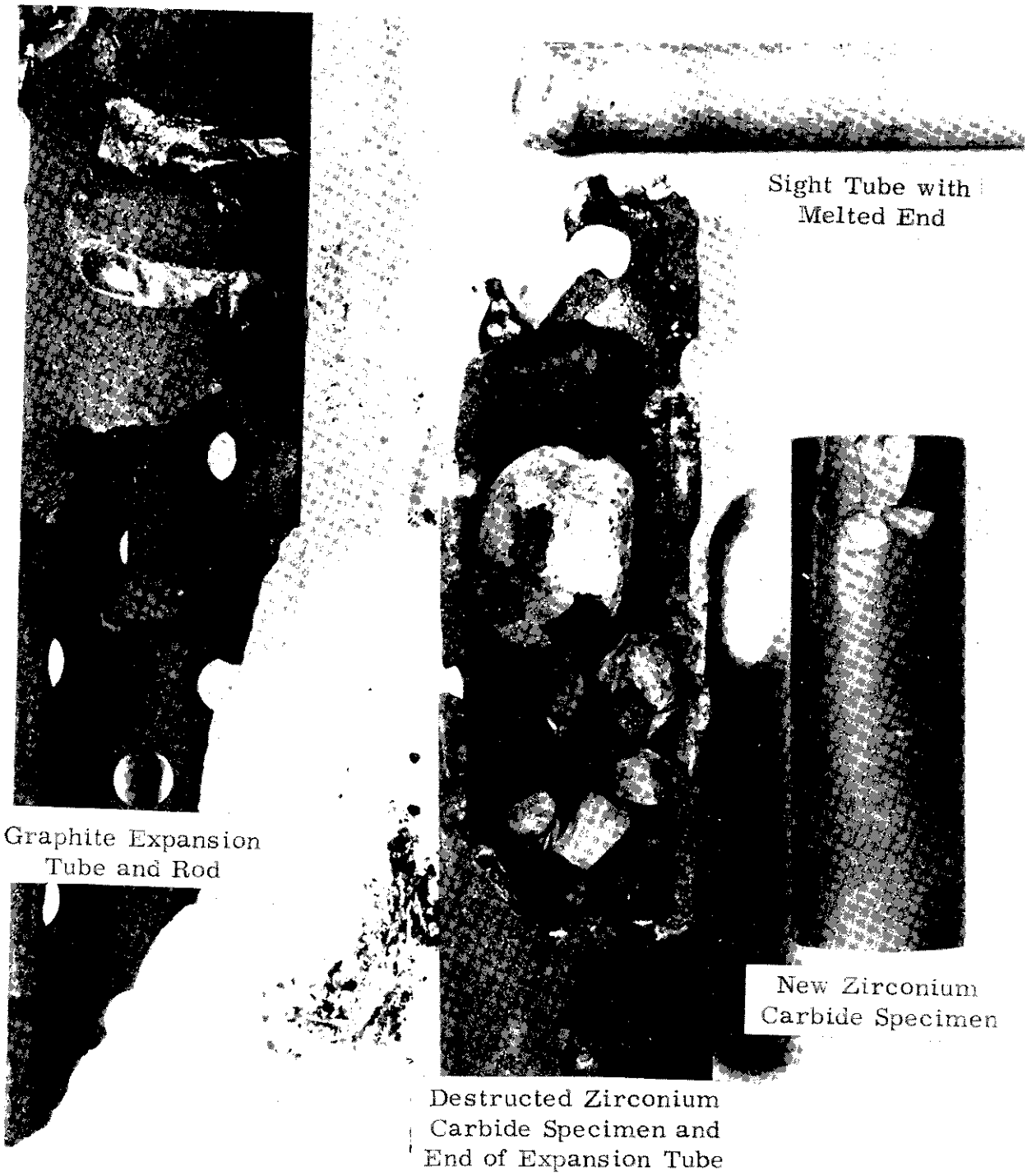

Figure 25. Picture of Failure of Zirconium Carbide Specimen During a Run.

all requirements seem well satisfied. From a study of the calibration runs and the specimen data obtained, results are repeatable to about 0.00025 inch per inch at any given finite temperature range; and rod, tube, and specimen growth accountability is within 0.0005 inch per inch over the entire exposure. The agreement with standards is also good so that the accuracy is estimated within 5%.

Some of the specific parameters of the calibration require more detailed discussion. Absolute temperature measurements were made by thermocouple up to 2000° F and then by a calibrated optical pyrometer up to 5000° F. As an operational aid to indicate heating rates and provide a continuous plot of temperature versus time, a selenium-cell radiation pyrometer was also employed to view the specimen during the entire run. The method of calibrating the optical pyrometer and a comparison of Chromel-Alumel and platinum-rhodium thermocouples are discussed in another section and will not be repeated here; however, it should be emphasized that on many of the runs, two different types of thermocouples were attached to the specimen to observe the temperature at up to the range of the optical pyrometer. The agreement between the thermocouples and the optical pyrometer during the overlap range was noted to be well within 50° F. Above 3000° F, the individual calibrated optical readings are estimated to be within 20° F. The data plots on the specimens show little scatter and confirm this close agreement. For some of the runs, the thermocouples were omitted, since the extremely high temperatures would vaporize the thermocouple insulators and this fume would destroy some specimens.

Considerable effort was directed to determine the temperature gradients that might exist across the dilatometer tubes. These were concluded to be negligible or less than a 1% influence on the expansion. The various temperatures within the tube, rod, and specimen are shown in Table 4 up to 4040° F. In columns 3, 4, and 5, note that the maximum gradient at up to 2100° F was 34° F and at up to 3300° F only 100° F. Actually, it is probable that this gradient at 3300° F was primarily the result of a faulty thermocouple, since the higher radiation heat transfer rates at the higher temperatures undoubtedly reduce the gradients. Even a 100° F gradient at this higher temperature range would induce a motion error of less than 0.0002 inch per inch.

The close agreement between the temperatures of the rod, tube, and specimen at a particular cross section are also shown in Table 4 in columns 1, 2, 3, 4, 5, and 6. The agreement at the midpoint of the

Table 4

Study of Temperature Gradients in Specimen Rod and Tube of Graphite Dilatometers in Thermal Expansion Equipment

Temp. of Tube at Bottom of Specimen ° F	Temp. of Tube at Middle of Specimen ° F	Temp. of Tube at Top of Specimen ° F	Temp. at Bottom of Specimen ° F	Temp. at Middle of Specimen ° F	Temp. at Top of Specimen ° F	Temp. at Top of Rod ° F	Temp. at Top of Tube ° F
218	218	211	209	207	203	124	130
616	628	637	667	659	662	329	351
1180	1190	1143	1150	1122	1118	357	391
1370	1386	1335	1341	1315	1346	399	433
1570	1600	1550	1549	1525	1559	430	469
1790	1800	1770	1760	1745	1778	243	267
1990	2045	1985	1956	1947	1988	484	527
2270	2290	2250	-	2170	-	540	590
-	3000 ± 20	-	-	3000	-	656	714
-	3240 ± 20	-	-	3240	-	731	<1000
-	3580 ± 20	-	-	3580	-	281	<1000
-	4040 ± 20	-	-	4040	-	892	<1000
-	-	-	-	2310	2386	-	-
-	2840 ± 20	-	-	2840	2780	-	-
-	3000 ± 20	-	-	3000	3085	-	-
-	3300 ± 20	-	-	3300	3200	-	-
-	-	-	-	1980	1966	-	-
-	2840 ± 20	-	-	2840	2770	-	-
-	3130 ± 20	-	-	3130	3070	-	-
-	-	-	218	218	215	-	-
-	-	-	991	940	942	-	-
-	-	-	1611	1571	1565	-	-
-	-	-	2100	2081	-	-	-
-	-	-	1826	1815	-	-	-
-	-	-	1465	1450	-	-	-
-	-	-	1010	995	-	-	-
-	-	-	570	565	-	-	-

specimen at over 3000° F was so close that no difference could be detected on the optical pyrometer with the hot wire spanning both the specimen and the tube.

From columns 7 and 8 in Table 4, the temperatures at the top of the rod and tube are seen to be in close agreement so that no spurious motions were introduced by the axial gradients. Probably the best indication of the absence of thermal gradients was obtained with the run using a graphite specimen of identical composition of the tube and rod and observing only 0.0004 inch per inch motion of the dial gage between 500° F and 3000° F; see Table 5.

The next consideration is the thermal motions that are induced in the tube and rod during an exposure. New tubes and rods did show a permanent dimensional change in the order of 0.001 inch per inch. After this initial exposure, the lengths checked within 0.0001 inch per inch as measured by a micrometer before and after the runs. Most exceptions were considered as human error and reruns made. To determine the repetitive thermal expansion of the exposed, or aged, tube and rod, the system was calibrated against 'A' nickel, quartz, and slope data on graphite published by the National Carbon Company. These data are shown in Figures 26 and 27 and Tables 6 and 7. From Figure 26, note that on three successive runs to 2000° F on 'A' nickel, and with no reset of the dial gage, the slopes of the motion versus temperature curves were repetitive and the absolute shift was no more than 0.0008 inch per inch out of the three excursions of 0.015 inch per inch each. Also, observe that the data using the Southern Research Institute quartz dilatometers and the literature data are in about as close agreement with the graphite dilatometer data as can be expected. The absolute calibration data to 2100° F is then extended to 5000° F, as shown in Figure 27, by using slope measurements made by National Carbon Company to extend graphite data to these higher temperatures. The subsequent run on the ATJ graphite specimen is also considered as a calibration at the higher temperatures, since that motion versus temperature curve showed no inflections and provided close agreement with literature data on this fine grain graphite. Also, the zero return indicated complete accountability of all motions. In these four ATJ runs, it is particularly striking that after the 5000° F exposure shifted the motion curve, a rerun on the same specimen using a different dilatometer resulted in agreement with the shifted data to within 0.0005 inch. The correction of the specimen motion by the tube motion as indicated in Figure 27 gains further confidence, since the tube motion usually accounted for no more than 20% of the total.

Table 5

Expansion Run on Electrode Graphite Calibration Specimen
in Graphite Dilatometer of Same Composition

Avg. Tube Temp. ° F	Avg. Specimen Temp. ° F	Avg. Specimen Gradient ° F	Temp. Difference Between Upper Rod and Upper Tube ° F	Dial Gage Reading 0.0001"
502	489	11	18	0.9959
1171	1130	16	34	0.9957
949	926	18	27	0.9954
1182	1129	29	29	0.9953
1364	1334	28	34	0.9952
1573	1544	29	39	0.9951
1787	1761	24	24	0.9951
1185	1157	28	30	0 9946
1579	1539	27	37	0.9945
2007	1964	25	43	0 9946
2270	2170	-	49	0.9948
2660	2570	-	53	0.9948
3010	2930	-	-	-
3000	2920	-	58	0.9948
70	70	-	-	0.9950

Note: 1. Total run time of 88 hours to determine time influence.
2. Specimen $\frac{3}{4}$" diameter by 3" long.

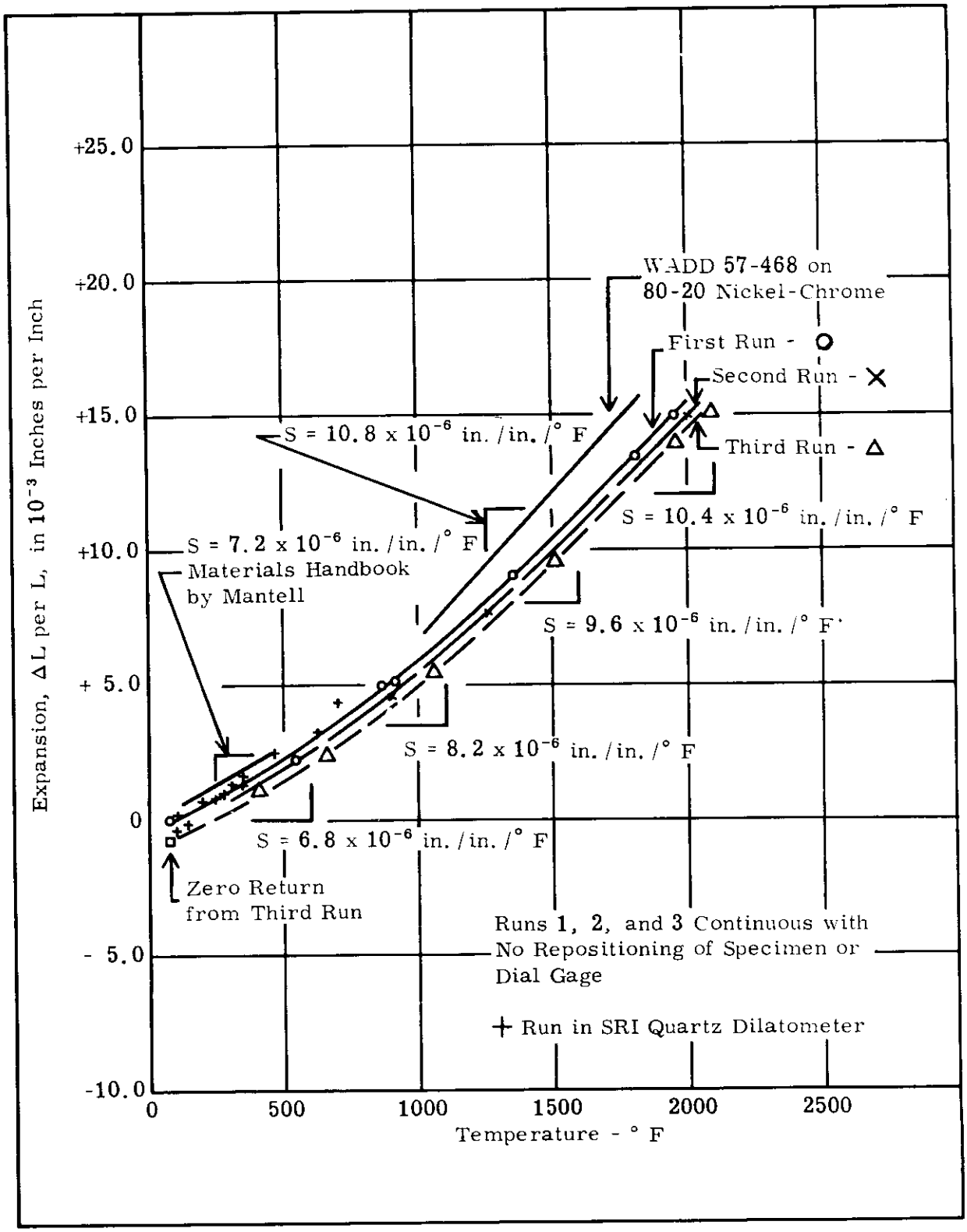

Figure 26. Thermal Expansion of 'A' Nickel Calibrator in Graphite Dilatometer.

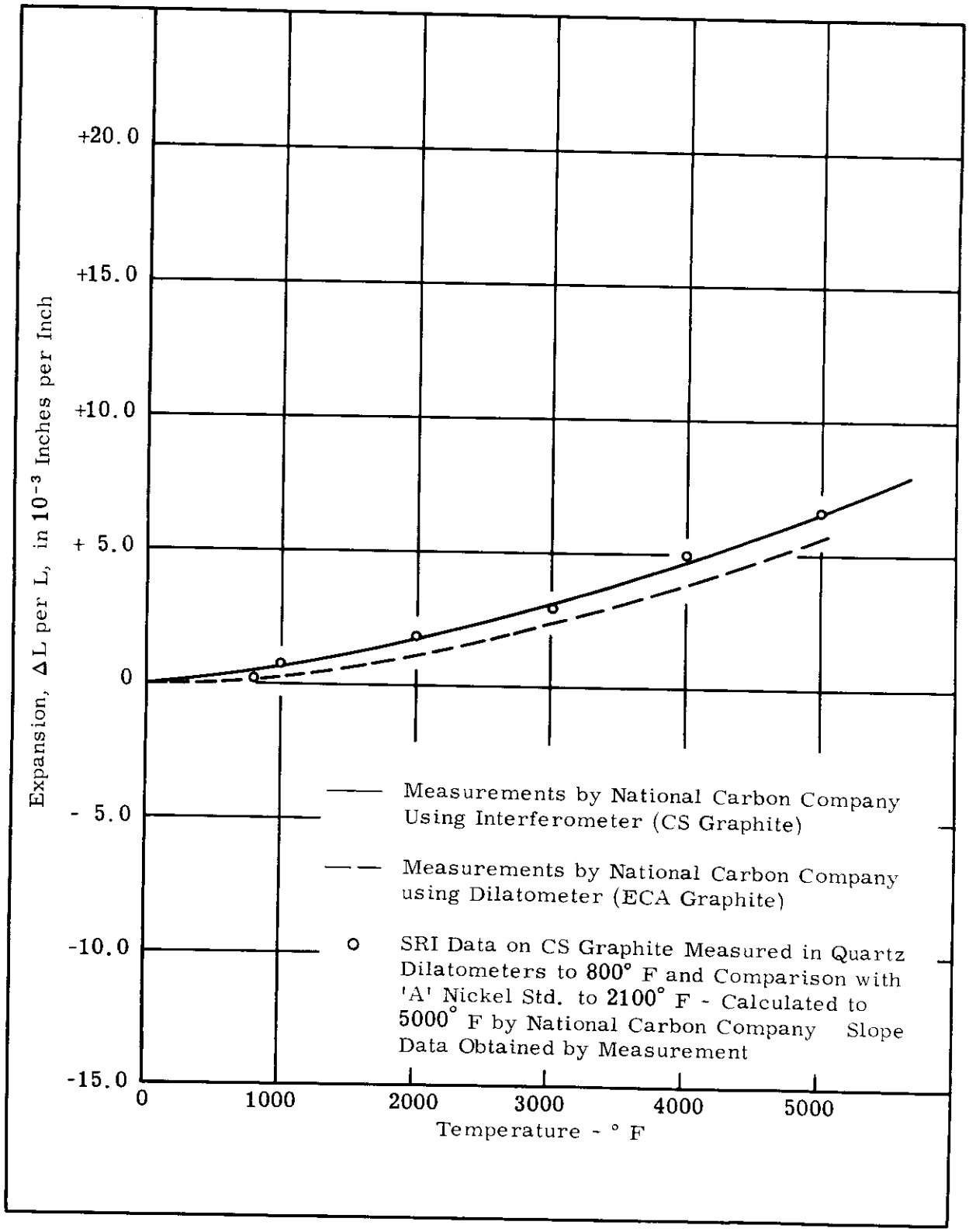

Figure 27. Thermal Expansion of CS Graphite Dilatometer Tubes.

Table 6

Expansion Run on 'A' Nickel Calibration Specimen
in Quartz Dilatometer

Temperature Bottom of Specimen ° F	Temperature Middle of Specimen ° F	Unit Elongation in 10^{-3} inches/inch
112	94	0
295	252	0.9
367	360	1.4
411	403	1.8
104	104	-0.6
164	163	-0.3
332	327	0.9
414	409	1.6
561	558	2.5
650	642	3.2
741	-	4.7

Note: 1. Run made in same order as listing of data points.
2. Specimen $\frac{3}{4}$" diameter by 3" long.
3. Data not corrected for motion of quartz tubes.

Table 7

Thermal Expansion of 'A' Nickel Calibrator in Graphite Dilatometer

Temperature ° F	Observed Total Elongation inches	Observed Unit Elongation inches/inch	Unit Elongation Correction for Dilatometer Motion inches/inch	Corrected Specimen Unit Elongation inches/inch
70	0	0	0	0
207	0.0013	0.0004	0.0001	0.0005
540	0.0060	0.0020	0.0003	0.0023
858	0.0135	0.0045	0.0005	0.0050
911	0.0138	0.0046	0.0006	0.0052
1354	0.0241	0.0080	0.0011	0.0091
1798 (2000 optical)	0.0360	0.0120	0.0015	0.0135
1951	0.0399	0.0133	0.0017	0.0150
909	0.0121	0.0040	0.0006	0.0046
1283 (1988 optical)	0.0206	0.0069	0.0009	0.0078
2020	0.0397	0.0132	0.0018	0.0150
415	0.0031	0.0010	0.0002	0.0012
674	0.0061	0.0020	0.0004	0.0024
1069	0.0142	0.0047	0.0008	0.0055
1509	0.0251	0.0084	0.0012	0.0096
1970 (2193 optical)	0.0368	0.0123	0.0017	0.0140
2100	0.0397	0.0132	0.0019	0.0151
70	-0.0021	-0.0007	0	-0.0007

In only a few runs were serious reactions noted between the tube and rod and the specimen ends. In these cases, the tube and rod measured very close to the pre-exposure lengths so that practically all of the reaction was within the specimen. In these instances, the specimens wholly melted, softened, broke, or otherwise deteriorated so that no particular effort was made to minimize the end reaction. When necessary to prevent reaction, as on an oxide prone to carbide at the elevated temperatures, tungsten foil has been placed between the specimen and tube and rod to minimize the carbon diffusion. The foil acts as a diffusion barrier and is very effective in preserving the end surfaces of both the specimen and the tube and rod.

An Ames dial gage calibrated to 0.0001 inch was used for all measurements. A differential transformer was considered but the large motion of the specimens, particularly at the deterioration temperature and the observed reliability of the dial gage precluded changing the system.

The final treatment of the data provides readout to three significant figures so additional error is not introduced. The slope measurements on the motion versus temperature curves are at least to within 0.00025 inch per inch and 25° F. Since this slope measure is the unit expansion per degree F, no additional treatment is necessary.

The probable error was statistically determined for the motion versus temperature curves to establish the maximum deviation that should be expected for 50% of the observed data points from the smooth curve. This deviation was more motion dependent than temperature dependent and was found to be about 4% at the 3×10^{-3} inch per inch range and less than 1% at the 15×10^{-3} inch per inch range. The over-all probable errors for ATJ, TaB, ZrB, HfC, and SiN were $2\frac{1}{2}$%, 1% 1%, 2%, and 2% respectively. Except for temperatures at which the specimens were deteriorating, these data are representative.

THERMAL CONDUCTIVITY

Apparatus and Procedure

Thermal conductivity measurements were made to 5000° F with a radial heat flow apparatus that utilized a miniaturized specimen $\frac{3}{4}$ inch in diameter and $\frac{3}{4}$ inch long. A cross section schematic and a picture of

the conductivity apparatus are shown in Figures 28 and 29, respectively. In addition to the specimen itself, the apparatus consists primarily of (1) a water calorimeter that passes through the center of the specimen, (2) guards made from the specimen material at both ends of the specimen to prevent axial heat losses, (3) optical or thermocouple temperature measuring devices in the specimen, and (4) an external heat source. The water calorimeter provides a heat sink at the center of the specimen to create a substantial heat flow through the material. Thermocouples mounted $\frac{1}{4}$ inch apart in the calorimeter water stream measure the increase in the temperature of the water as it passes through the gage portion of the specimen. By also metering the water flow through the calorimeter, all variables necessary for calculating heat flow are determined. The total radial heat flow through the $\frac{1}{4}$-inch specimen gage section into the calorimeter is calculated from the standard relation of $Q = MC\Delta T$. In this particular case, M is the weight of water flowing per hour, C is unity for water, and ΔT is the temperature rise of the water as it passes through the gage section.

The specimen configuration is $\frac{3}{4}$ inch long, $\frac{3}{4}$ inch outside diameter, $\frac{1}{4}$ inch inside diameter, with $\frac{3}{8}$ inch deep, $\frac{5}{64}$ inch diameter holes on radii of $\frac{3}{16}$ inch and $\frac{5}{16}$ inch to permit temperature measurement within the specimen. Guards of specimen material $\frac{3}{8}$ inch long are placed above and below the $\frac{3}{4}$-inch specimen to maintain a constant radial temperature gradient over a sufficient axial distance and so minimize axial heat flow. The ends of the specimen guards are insulated with lamp black-filled graphite tubes, which also hold the specimen in alignment. The combined effect of specimen guards and excellent lamp black insulation permit a minimum axial temperature gradient not detectable by optical pyrometer readings sensitive to 10° F.

To provide controlled radial heat flow from the $\frac{1}{4}$ inch inside diameter of the specimen to the $\frac{7}{32}$ inch outside diameter of the water calorimeter tube, the annulus was packed with copper, graphite, or lamp black. The filled annulus permits heat flow through the material and also provides a positive method of centering the water calorimeter within the specimen. Generally, copper granules are preferred as the packing on low temperature runs to increase the heat flow, and graphite lathe dust is best on high temperature runs. Some exceptions were encountered, especially on materials with a high conductivity. To prevent swamping of the calorimeter by excessive heat flow in these cases, low conductivity packing materials were used. Copper was replaced by graphite, and in one instance graphite was replaced by lamp black. The

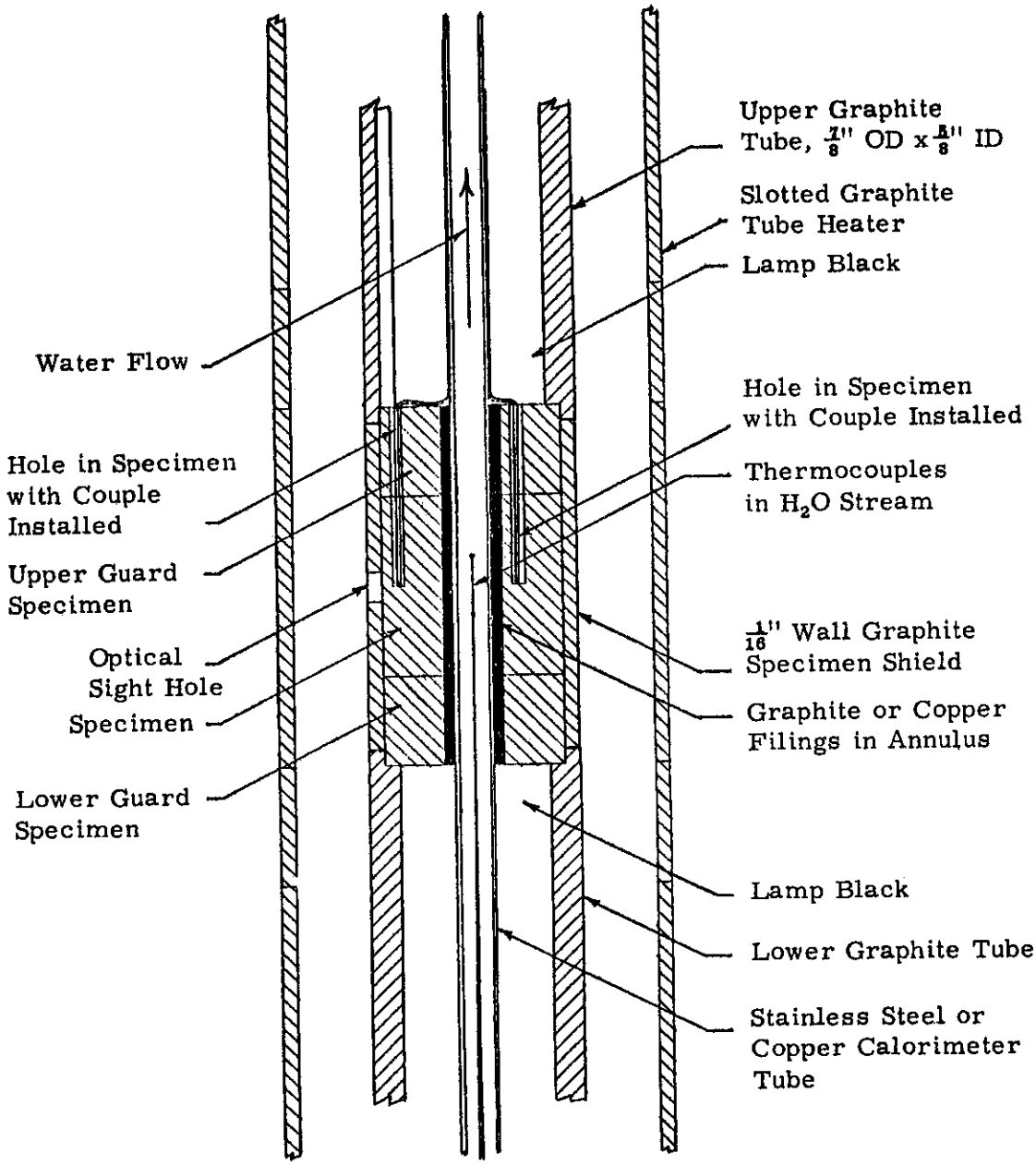

Figure 28. Cross Section of Radial Conductivity Unit.

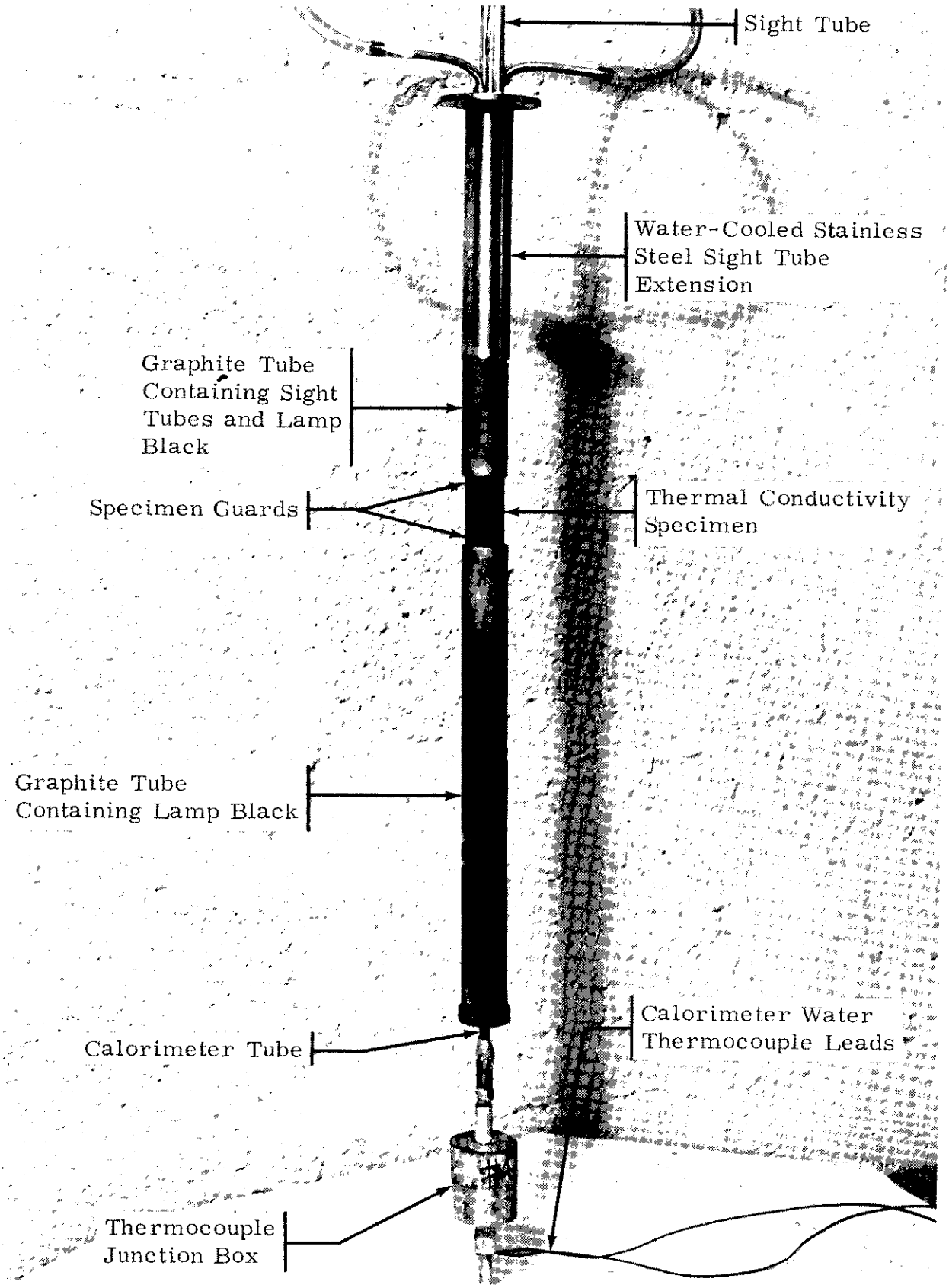

Figure 29. Picture of the Radial Thermal Conductivity Apparatus

use of lamp black in the annulus between the specimen and tube also assisted in reducing the over-all system power requirement for the elevated temperatures.

On low temperature runs (to 2000° F), the specimen temperatures were measured with Chromel-Alumel or platinum-platinum + 10% rhodium thermocouples. At high temperatures, optical sight tubes were aligned to view the bottoms of the specimen temperature holes from the top of the furnace. The temperature drop across the $\frac{1}{8}$-inch specimen distance was then read with an optical pyrometer sighted through a right-angle mirror device.

In the prior Figure 29 showing a typical conductivity calorimeter apparatus ready for insertion in a furnace for a run, the specimen and specimen guards can be seen at the center of the unit. The specimen guards are shouldered within the graphite extension tubes that contain lamp black insulation. A water-cooled, stainless-steel section can be seen at the top of the unit. This section provides permanent optical sight tubes to within about $2\frac{1}{2}$ inches of the guard specimen, in addition to a permanent mount for the right-angle mirror device. Within the short graphite tube between the water-cooled section and the top specimen guard, graphite sight tubes are fitted. The remainder of the annulus is filled with lamp black insulation.

For low temperature runs, thermocouples were placed in the specimen temperature holes, the leads were passed through the lamp black above the top of the guard specimen, and out of the water-cooled sight tubes. In the short section containing lamp black, the thermocouple leads were tied to the water calorimeter tube for low temperature protection. Attempts were made at the low temperatures to install the graphite sight tubes used on high temperature runs and pass the thermocouple leads out through both the graphite and water-cooled tubes. Heat losses caused by this procedure were excessive at low temperatures, however, so the tubes were removed and the entire annulus was filled with lamp black. The necessity of omitting the graphite sight tubes at low temperatures made separate low and high temperature runs necessary. If the presence of the tubes and the resulting openings had been permissible, thermocouples for low temperature data could have been easily pulled out before melting, making only one run necessary to cover the entire temperature range; however, the duplicate runs at the overlap temperature range provided a good check on that data.

During thermal conductivity runs, the following data were recorded: (1) power input, (2) specimen face temperature, (3) specimen temperatures in the gage section at the $\frac{3}{16}$-inch and $\frac{5}{16}$-inch radii, (4) temperature of the water in the calorimeter at two points $\frac{1}{4}$ inch apart axially within the specimen center, and (5) flow rate of the water through the calorimeter. Several readings (four to six) were made at each general temperature range to establish data scatter, to eliminate the error due to stray points, and to determine the influence of water flow rates through the calorimeter and provide a method of observing internal consistency in the data. Generally, a series of readings was made about every 500° F through the temperature range.

All thermocouple readings were measured on a Leeds and Northrup K-2 null balance potentiometer used in conjunction with a galvanometer of 0.43 microvolts per mm deflection sensitivity. All optically measured temperatures were read with a Leeds and Northrup Type 8622 optical pyrometer. The flow rate of the calorimeter water was measured with a Fischer and Porter Stabl-Vis Flowrator.

The thermal conductivity values for the materials were computed from the basic heat flow equation $K = QL/A\Delta T$ where Q is the heat flow in Btu/hr, A is the area through which the heat is flowing, ΔT is the temperature drop, and L is the length between inner and outer temperature measuring holes. For a cylindrical specimen, the area is not constant and is usually taken as the log mean area. For the particular specimen configuration, the temperature measuring holes were $\frac{5}{64}$ inch in diameter and located on $\frac{5}{16}$- and $\frac{3}{16}$-inch radii. Therefore, the area (0.00272 square feet) would be defined by these two radii and the axial gage length ($\frac{1}{4}$ inch) determined by the placement of the thermocouples in the calorimeter. Since the specimen is axially guarded, the end areas are not involved. Also, since the temperatures are determined over a finite area including parts of each hole, the distortion of the temperature gradient would be greater than the deviation from linearity caused by the changing area between the temperature holes. For this reason, the area was taken as the arithmetic mean rather than log mean, thus employing the minimum sophistication. The error involved in this simplification is 2.2% and is less than the observed data scatter. Sample calculations for the area computation are given in Appendix 3.

Mean temperatures for the conductivity values were taken as the arithmetic average of the two thermocouple readings at the lower temperatures. When optical pyrometers are used to measure specimen

temperatures, the observed temperatures are low because of losses through the viewing tubes. This deviation of observed temperature varies from about 25° F at 2000° F to around 200° F at 4000° F. Since the viewing tubes are identical, the temperature differences are not influenced by these losses. However, the mean temperature would be in error if an arithmetic average were used. Consequently, to get a more accurate mean temperature measurement, the outer face temperature was measured optically, and the temperature at the center of the gage section was computed from the observed temperature drop across the holes and the specimen configuration. For this particular specimen size, the distance between the outer face of the specimen and the center of the gage section between the two temperature holes is equal to the distance between the two temperature holes. However, the average cylindrical area (A) between the temperature holes is only 80% of that between the outer face and the midpoint between the temperature holes. Therefore, the temperature drop between the outer face and the mean position between the temperature holes is 80% of the observed temperature difference between the holes. It follows that the mean temperature of the gage section is equal to the outer face temperature minus 80% of the observed ΔT. The furnace configuration insures essentially a black body condition for the outer face of the specimen, providing a good reference temperature at that point on the specimen. A sample calculation is included in Appendix 3.

No correction to the value of the ΔT is necessary because both temperature holes are physically similar and the temperatures are sufficiently close so that the deviation from absolute true value is equal for each and is cancelled out in the subtraction process to obtain the ΔT. A study of the tables including the recorded data indicates that for practically all readings employing optical temperatures, the temperature drop (ΔT) across the specimen was fairly high so that small errors in reading the temperatures would have similarly small effects on the calculated conductivity value.

Data and Results

The thermal conductivity values for the materials evaluated in this work are shown in Tables A-32 through A-44 in Appendix 2. The curves resulting from the plotted values are shown in Figures A-31 through A-43 in Appendix 1.

An extensive number of runs were made on CS graphite and ATJ graphite for calibration purposes. Also, to determine the sensitivity of the apparatus for a wide range of conductivities, runs were made on copper (very high K), Armco iron, 316 stainless steel, and silica (very low K). The sensitivity of the apparatus was good for the full range, and agreement with the literature was generally within 10% to 15%. A complete discussion of the calibration of the radial conductivity apparatus is discussed in the next section of this report.

On specimen materials for which literature data were available, comparisons of Southern Research Institute values were made. Good agreement was found in some cases such as for ATJ graphite and the 2500° F temperature range for ZrN, TiN, and $ZrSiO_4$. The absolute values and curve characteristics compare very closely to several literature references for ATJ and GBH graphite. For tungsten, literature references differ from Southern Research Institute data by about a 2 to 1 ratio. For example, at 3000° F, literature data for single crystal tungsten is about 740 Btu/hr ft^2 ° F/in. compared to a Southern Research Institute value of about 430 Btu/hr ft^2 ° F/in. The large difference between the two sets of data is quite possibly due to the fact that the literature data is for single crystal tungsten while the Southern Research Institute data is for arc-cast polycrystalline tungsten. The large influence of heat treatment is discussed later in this section.

After studying Southern Research Institute data and several literature references, it appears that considerable differences in thermophysical properties of refractory materials can exist as a result of different batches of the same material, different forming methods for the same material, and different temperature exposure histories on the same material.

A discussion of the thirteen thermal conductivity curves and the circumstances related to the individual runs should provide a clearer understanding of the data. On each curve, the plot is extended beyond the mean temperature of the data point to the maximum hot face temperature for that material on a conductivity run.

Figure A-31 shows data points and the resulting curves for ATJ graphite. On several runs below 4000° F, the data repeated itself quite well. However, runs on the material after exposure to 4000° F resulted in a significant increase in its thermal conductivity. Later runs after specimen exposure to 4800° F showed no additional increase in

conductivity. Apparently, the high temperature exposures contribute to increasing the bond between the grains and reducing the resistance to heat flow. This influence diminishes on subsequent exposures.

Figure A-32 shows the data for arc-cast tungsten. Several runs were made to establish curve inflections as accurately as possible. The data established an upward inflection of the curve in the vicinity of the softening point of tungsten. Above 2500° F, the conductivity decreased until at about 3600° F it had returned to a value about equal to the value at 1500° F. From the 3600° F range until the end of the exposure, the conductivity increased reasonably constantly. Observe that the conductivity at 4800° F is about as would be expected if the literature data were extrapolated. Perhaps the high temperature exposure induced a stress relief and grain growth or lattice alignment. Reruns on the heat-exposed specimen could not be made because it was inadvertently melted.

Figures A-33, A-34, A-35, and A-36 show the thermal conductivity versus temperature curves for the nitrides evaluated in this program. The hafnium nitride specimens were inclined to break during a run, although they did not appear to disassociate or form a carbide. Because of the breakage, the temperature exposure did not exceed 3700° F. The thermal conductivity values were quite possibly affected by the specimen breakage; however, the curve established by the data shows a decrease in K from 500° F to 1000° F, then an increase throughout the remainder of the temperature exposure.

Silicon nitride and titanium nitride runs established smooth curves up to the deterioration temperatures of both materials. Silicon nitride maintained a smooth curve with no notable inflections. Titanium nitride had a constant K increase up to about 3200° F before the slope gradually reversed and the conductivity decreased steadily to 4700° F face temperature.

Zirconium nitride established a conductivity curve with a general K increase up to about 2900° F, then a rather rapid decrease thereafter. The material once again broke. It is possible that the apparent decrease in thermal conductivity was a result of specimen breakage.

Figures A-37 and A-38 for tantalum boride and zirconium boride show that the thermal conductivity of each material decreased as the temperature was raised from 500° F to 1800° F, remained about constant up to the 3200° F to 3700° F range, then increased slightly

through the remainder of the temperature range. Both materials deteriorated at a little above 4000° F face temperature.

Figure A-39 shows the curve for the thermal conductivity of zirconium silicate. Throughout the temperature range, the conductivity decreased gradually with only slight curve inflections. Around 3300° F, vapors were emitted in the optical sight holes indicating specimen disassociation.

Figures A-40, A-41, A-42, and A-43 show the curves for the carbides of columbium, hafnium, tantalum, and zirconium. All four of these materials broke prematurely during the runs so a process of annealing the specimens by heat soaking them at about 4500° F for 15 minutes was introduced. Three of the materials had greatly improved thermal shock resistance as indicated in the picture in Figure 16. The other material, hafnium carbide, broke prematurely even after being heat soaked. The most notable fact discovered was that the thermal conductivities of the materials were changed by the heat soaking procedure

The curve of thermal conductivity versus temperature for columbium carbide shows a decrease in K between 500° F and 1000° F, then a reasonably smooth increase through the remainder of the temperature range. The large scatter for specimens that had not been heat soaked (hereinafter referred to as unsoaked specimens) is probably the result of fractures and fissures formed internally. No clear difference in conductivities is noted for the heat soaked and unsoaked specimen.

The hafnium carbide data is rather difficult to analyze. The low temperature data on an unsoaked specimen established a conductivity in the vicinity of 100 Btu/hr ft^2 ° F/in. The heat soaked specimen, however, established the top curve in Figure A-41, which showed a decrease in conductivity from about 390 at 500° F to about 290 at 1000° F. Between 1000° F and 2000° F, the conductivity values for the heat soaked specimen fell well below 200 Btu/hr ft^2 ° F/in.; but from 2000° F to 3800° F, the conductivity was again between 200 and 300, establishing the curve in that range. It is difficult to believe that the heat soaking really shifted the data so much; however, observe that duplicate runs were made on the unsoaked specimen rather firmly establishing that data.

The tantalum carbide data for the unsoaked specimen established a reasonably smooth curve throughout the temperature range. The heat soaked specimen had a conductivity about 40% below the original

values in the 2000° F vicinity. The slope of the curve for the heat soaked specimen was steeper, however, and approached the original curve at above 4500° F. This would be expected since the high temperature exposure during the run on the unsoaked specimen would tend to produce the same conditions within the specimen as the separate heat soaking.

The data for zirconium carbide indicated a high initial conductivity, a rapid decrease with temperature increase up to about 2000° F, then an increase with temperature up to about 3500° F and then an essentially constant K for the remainder of the temperature range. At the top temperatures, the thermal conductivities of the heat soaked and unsoaked specimens tended to converge as expected. Again, the high temperature exposure provides similar results to the heat soaking.

All of the carbide materials had both radial and circumferential fissures perhaps about $\frac{1}{16}$ inch to $\frac{1}{8}$ inch long. Undoubtedly, these interfaces distorted the temperature gradients and had a real influence on the thermal conductivity. This physical feature also probably caused the greater data scatter found for the carbides.

In Part 2 of this work, the chemical analysis of these specimens is to be made. At that time, perhaps an analysis can be made of the conductivity data relating inflections and values with property changes of the materials.

CALIBRATION AND ERROR ANALYSIS OF THE RADIAL THERMAL CONDUCTIVITY APPARATUS

The radial thermal conductivity apparatus employs the direct measure of heat flow, area, and temperature drop per unit length parallel to the heat flow so that the accuracy is as good as the total of the separate measurements. The following variables require precise determination: (1) the radial heat flow into the axial calorimeter and (2) the radial temperature drop over a known finite increment of the radius. Spurious detrimental influences must be eliminated such as (1) axial heat flow in the specimen, (2) distorted circumferential isothermals in the specimen, and (3) faulty calorimeter measurements.

The specimen size must permit the existence of large variables such as heat flow and temperature drop so that the sensing accuracy is sufficient to minimize excessive measurement errors associated with the

basic instrument sensitivity. Sometimes these requirements are in conflict. For example, larger diameter specimens would permit larger radial lengths between the temperature measurement points but would seriously reduce the rate of heat flow into the calorimeter. Specimen size is also important in the ability to maintain a sound specimen. Large refractory pieces are prone to heterogeneity and thermal cracking, particularly under radial temperature gradients. The chemical and metallurgical make-ups of the specimen are also often critical in that they must be stable in the furnace environment and must not change during a run. For example, the conductivities of ATJ graphite and zirconium carbide were found to vary with heat soaking of the specimen. Considering that many refractory materials are simply small particles bonded at their junction points (rather than containing a continuous lattice like a metal), the major influence of the thermal history of a material on its thermal conductivity is easily understood. Also, the data scatter was observed to relate closely with the deterioration of the specimen.

The accuracy of the Southern Research Institute radial conductivity apparatus is estimated to be 10% with a data scatter of 15% for materials that are reasonably homogeneous and constant in physical and chemical properties. This accuracy was confirmed with runs on several "standards" such as silica, Armco iron, 316 stainless steel, CS graphite, and copper. The ATJ graphite specimen is also considered as a "standard" since considerable literature data are available on this, and similar, fine-grain graphites. The reliability is further enhanced by the consideration that for each material separate runs were made with one using thermocouples and the other using an optical pyrometer to measure the radial temperature difference. The continuous lineup of the two curves demonstrated a regular internal consistency.

A major concern in this high temperature measurement that requires an intimate knowledge of both the technique and the materials is that gross errors in the conductivity value can be obtained with no ostentatious warning. For example, silica boil off (from specimens containing silica as a binder or an impurity) can provide a condensing curtain in the optical sight ports and cause the apparent temperature in the hole to be that of the curtain rather than that at the bottom of the hole. Also, the calorimeter can become swamped at excessively large heat inputs so that gas or steam bubbles form around the thermocouple junctions insulating them from the water stream and giving uniform appearing, but actually erroneous, temperature indications. Difficulties of these types can usually be detected by a careful study of the internal consistency

of the data both at a single and over a large temperature range. Obtaining many data points (six, usually) at a single specimen temperature while varying only the water flow rate through the calorimeter was a great assist in noting the internal consistency of the data as well as in supplying multiple points to allow a statistical treatment of the data.

Some of the specific measurements require a detailed discussion. The absolute temperature of the outer face of the specimen was obtained using thermocouples and an optical pyrometer. The calibration of the sight ports is discussed in another section of this report. The radial temperature drop thrcugh the specimen was measured by thermocouples at up to 2000° F and by optical pyrometer at over 2000° F. The error in the optical reading is primarily one of human judgment and will show a scatter of about ± 10° F. Above 3000° F, the temperature drop through the gage length was usually about 150° F or better so that any one reading could contain an error of 14%. Since six readings were obtained at each temperature point, the actual error of the arithmetic average was undoubtedly much less than the scatter—perhaps half of the statistical probable error or about 4%.

The radial distance between the points of temperature measurement was inherently small because of the small specimen. The spacing was $\frac{1}{8}$ inch. The holes in the center specimen were $\frac{5}{64}$-inch diameter at the top and about $\frac{1}{32}$ inch at the bottom. Since these holes were ultrasonically ground with a precision machine, and since the holes and sight tube were aligned before the run, the major error in determining the gage length was undoubtedly in aligning the hot wire of the pyrometer with the hole. See Figure 30 for a picture of the hole with the hot wire shifted slightly off center. It seems reasonable that the hot wire was regularly aligned within one quarter of the diameter of the bottom of the hole or one eighth of the diameter of the top of the hole. Generally, the eye can read to within one tenth of a one-sixteenth inch spacing between finely spaced lines. This same accuracy should apply to placing the hot wire on the diameter of the hole. On this basis, any one reading should be within 15% of the actual gage length. Again assuming that the multiple readings would result in an error of about half of the probable error, a 4% error in data could be experienced.

The water calorimeters were calibrated by passing electric current through the outer metal tube and comparing the input KW energy over the gage section containing the thermocouples with the output energy rate as picked up by the water; see Figures 31, 32, and 33. In all cases,

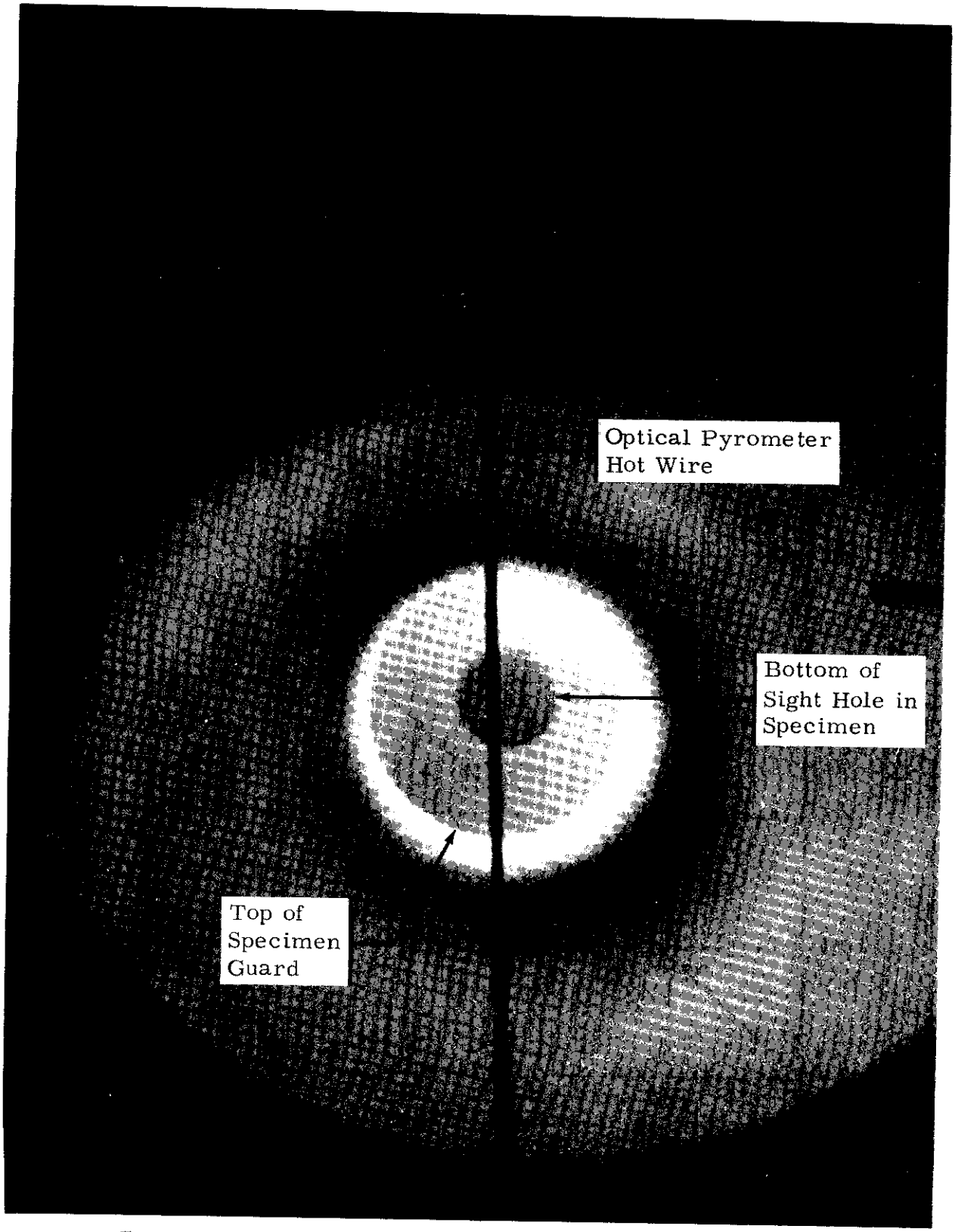

Figure 30. Picture of the Hot Wire of the Optical Pyrometer and the Sight Hole in the Specimen.

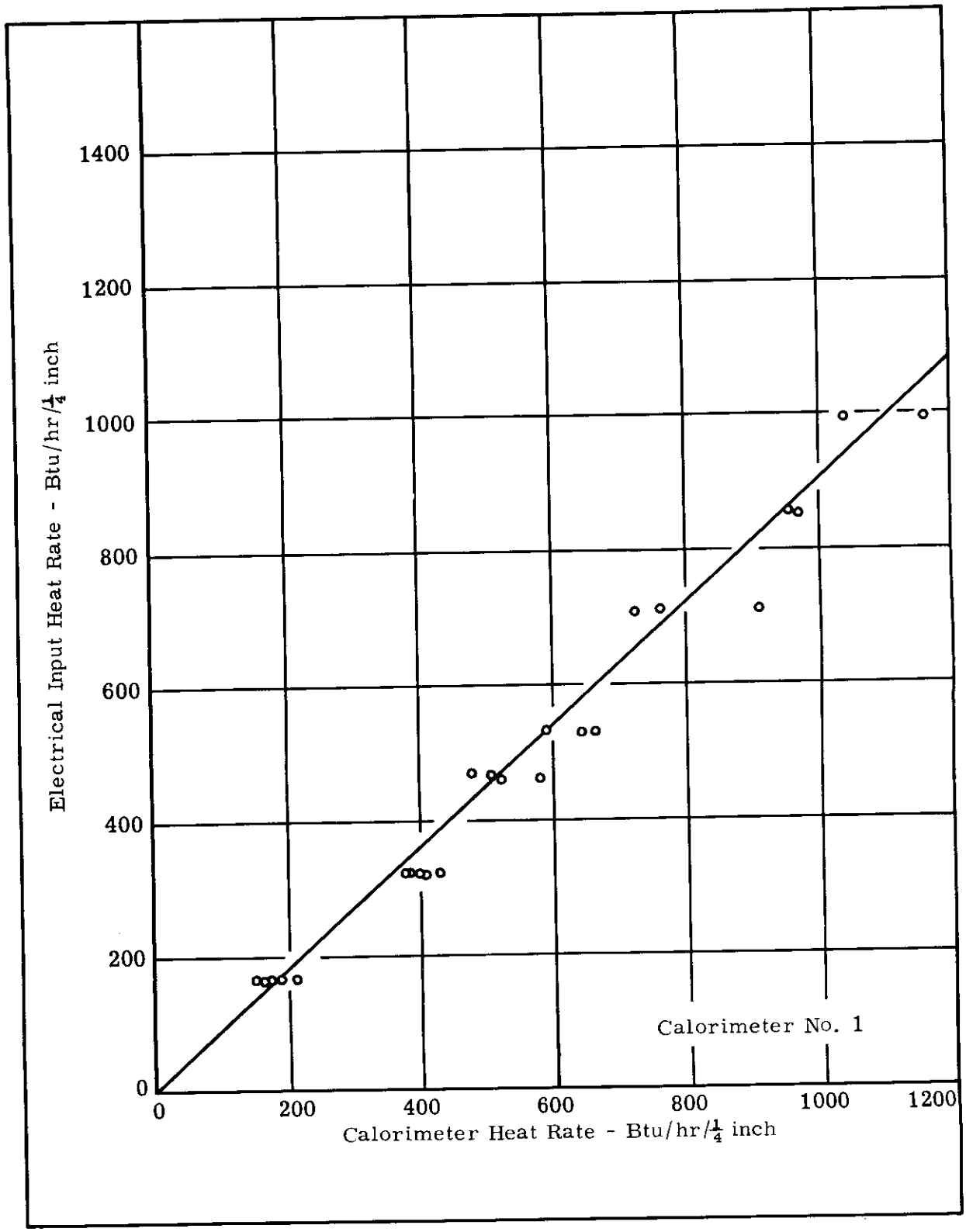

Figure 31. Thermal Conductivity Calorimeter Linearity with Heat Rate.

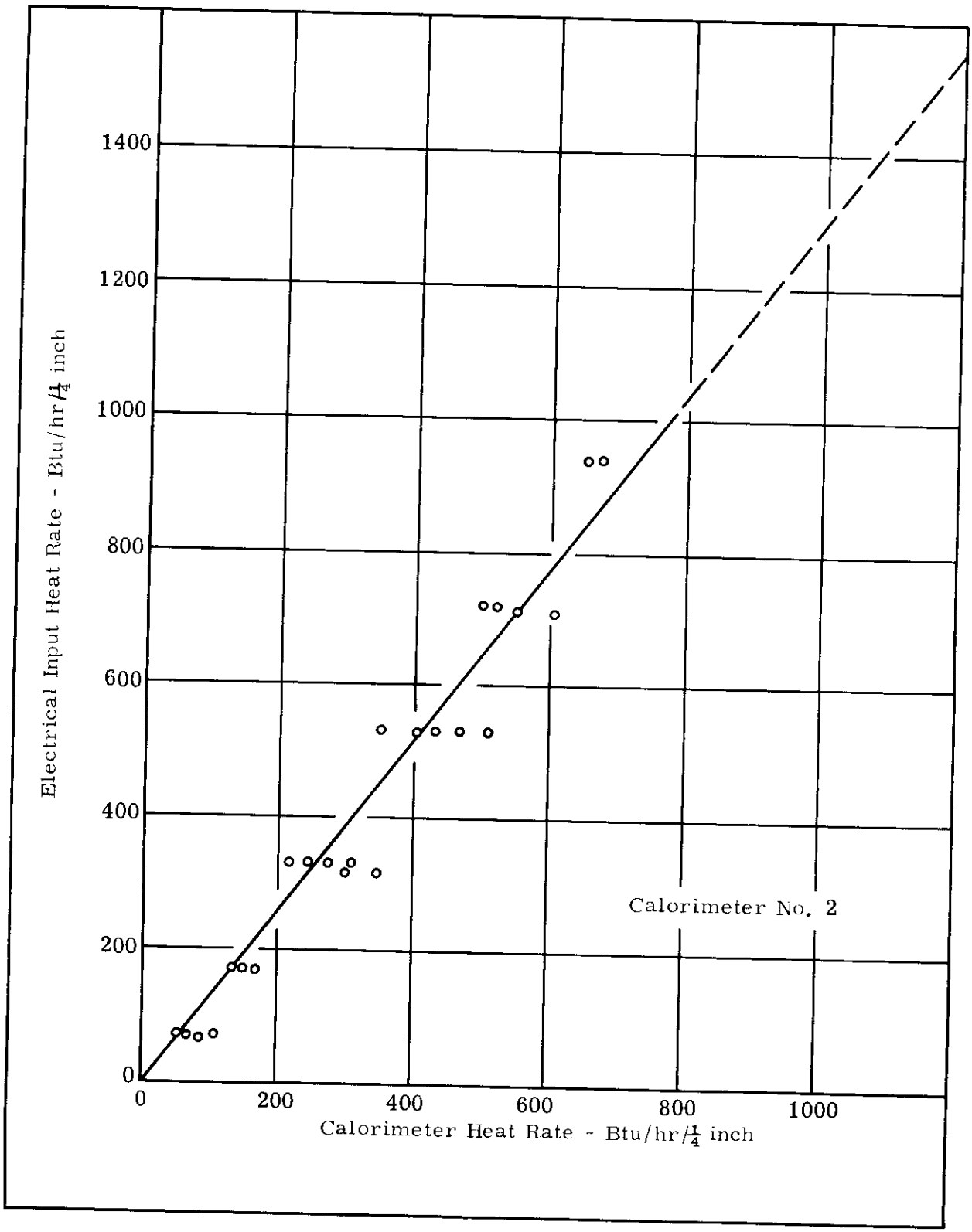

Figure 32. Thermal Conductivity Calorimeter Linearity with Heat Rate.

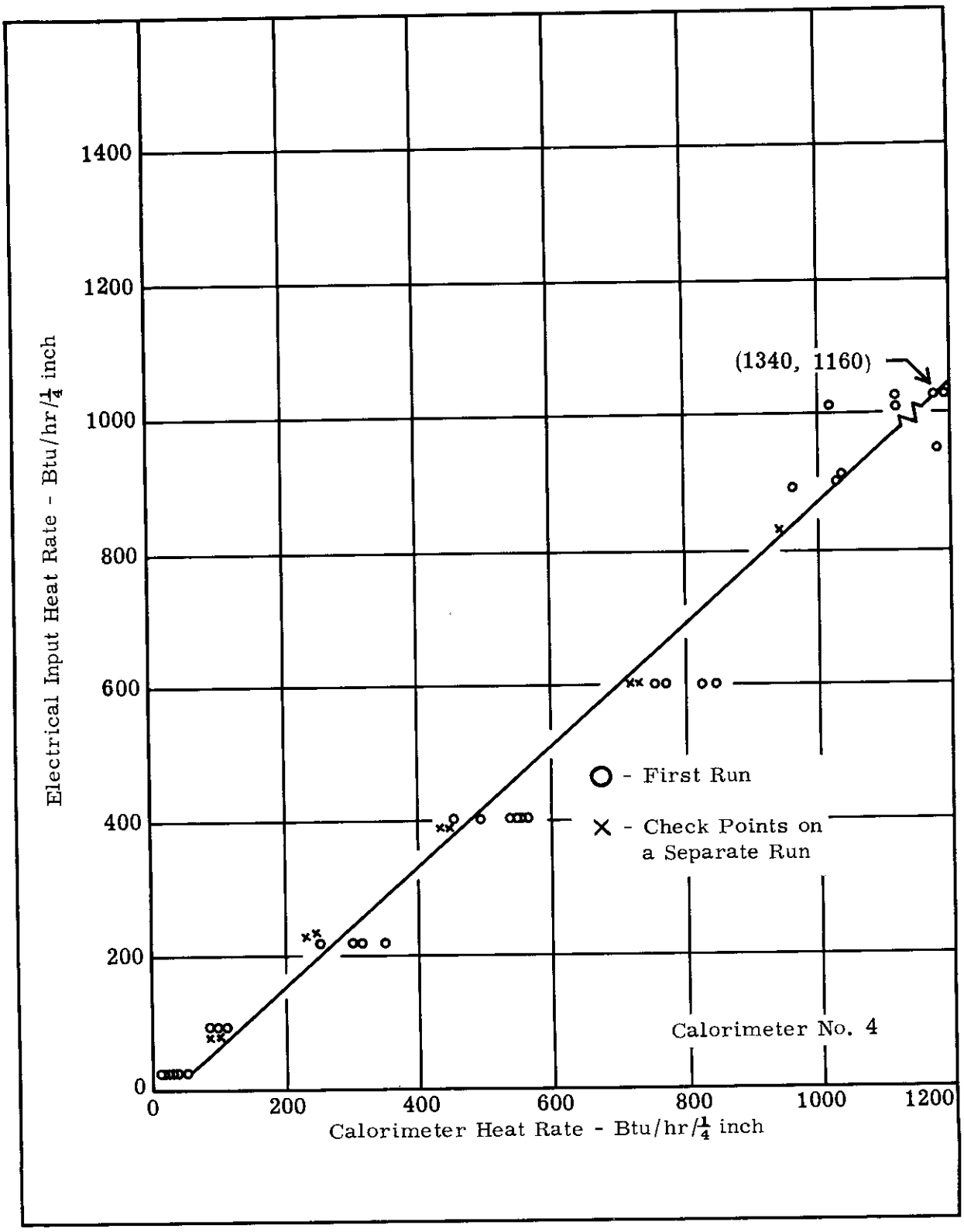

Figure 33. Thermal Conductivity Calorimeter Linearity with Heat Rate.

the calorimeters had a linear relation between input and output. Generally, the absolute value of the output ranged from 20% higher to 20% lower than the input. This deviation was not considered important since the main requirement was to demonstrate linearity and since the actual electrical input varied down the metal tube as the wall thickness and electrical resistance varied. About a 20% variation in voltage drop down the tube was noted at constant current by direct measurement with a voltmeter. At a constant input electrical KW, the output KW indicated by the calorimeter temperature and water flow rate measurements varied by an average of about 10%. Again assuming that the actual error would be about half of the probable error when the arithmetic mean of several readings is used, about 3% error could be expected. The water flow rate and water temperature rise measurements were both within 1% at 1500° F specimen temperature and higher so the absolute measurements were precise. Generally, the water flow was 15 to 20 gph and the temperature rise in the water was about 2° F at the 500° F specimen temperature and 10° F or better at over 2000° F specimen temperature.

Some calorimeters were a little more sensitive than others to the water flow rate. From Figure 34, note that the heat pickup rate for calorimeter number four was independent of the water flow rate; whereas, the heat pickup rate for calorimeter number two fell off at increased water flow rates. It is suspected that as a calorimeter aged and an insulating film formed on the thermocouple junctions, the water flow rate sensitivity increased.

There are other factors that could influence the accuracy of the apparatus but which defy a very rigid discussion. It is doubtful if axial heat flow was a serious problem. Performance was constant whether a stainless or copper calorimeter tube was used and the conductivity ratio of the two metals is one to ten. The use of graphite or copper powder to fill the annulus between the specimen and calorimeter had no error influence except when copper permitted swamping of the calorimeter. The removal of the upper guard specimen did not seriously influence the data. The very low conductivity of the lamp black at either end of the guard specimens could not permit much axial heat flow.

Another difficult variable to evaluate is the distortion of the circumferential isothermals by the holes drilled in the specimen. Observation of the top of the specimen through the optical sight ports indicated no disruption; however, this instrument could not detect a gradient less than 10° F. Post inspection of the specimens indicated

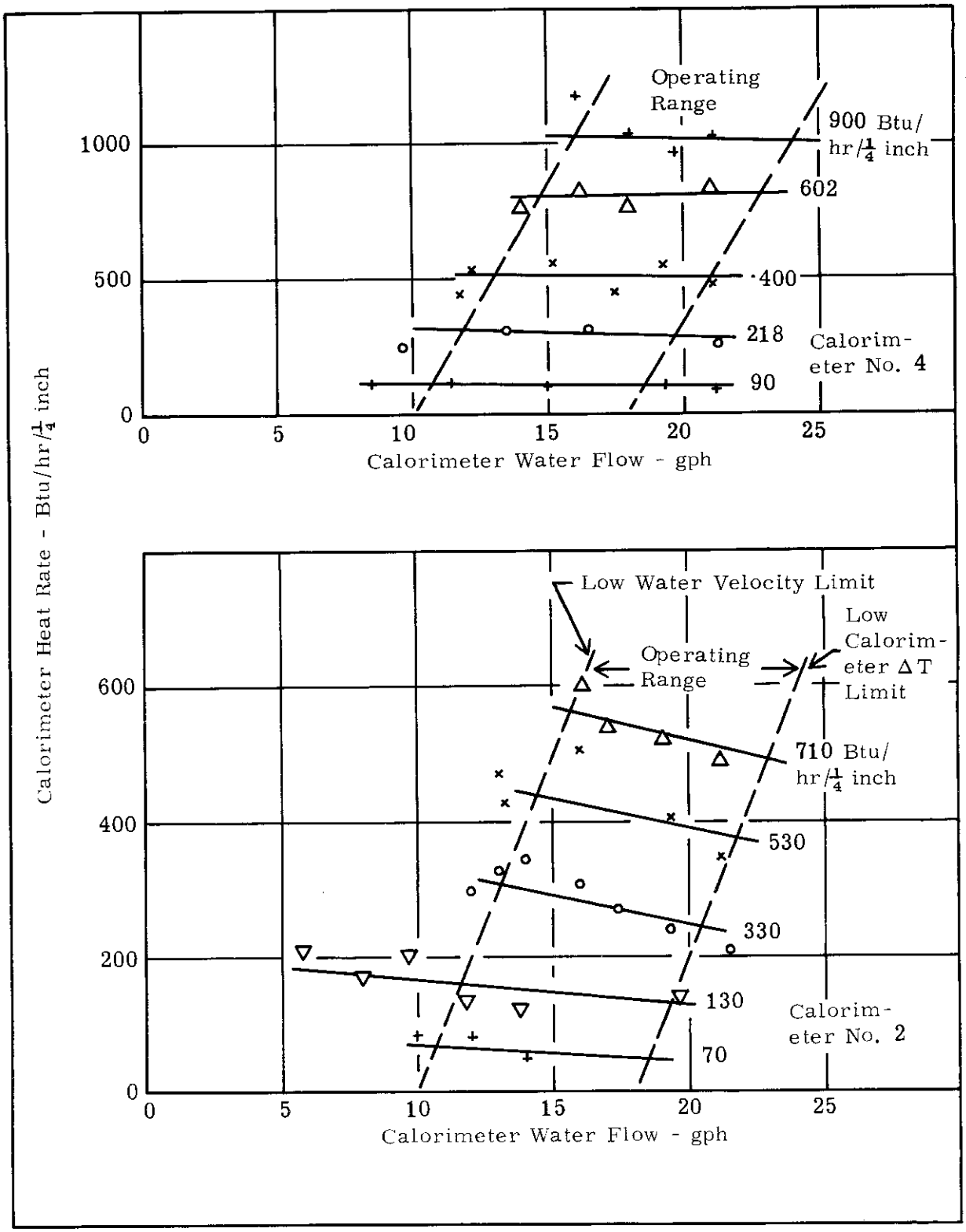

Figure 34. Thermal Conductivity: Influence of Water Rate on Calorimeter Performance.

color rings and circumferential melting and disassociation that inferred no detectable isothermal contortion. It is doubtful if this were a serious parameter. It is important to recall that even though the specimen diameter was small, the length to diameter ratio was 2 to 1, or more than is often used in apparatus of this type using larger specimens. The picture in Figure 35 shows isothermal color lines that were formed in two specimens during normal runs to 4500° F. Although the specimens broke upon cooling, observe that there are no disruptions of the isothermal lines even at the sight holes.

This apparatus was calibrated against several "standards" with thermal conductivities ranging from 50 Btu/hr/ft²/° F/in. for silica, 200 for Armco iron and 316 stainless steel, 700 to 200 for graphite, and 2400 for copper; see Figure 36. All of the other data agreed well with the Southern Research Institute results. The deviation averaged about 10% and demonstrated no trend.

The final data treatment involves the plotting of the data and then visual curve fitting to obtain conductivity versus temperature. No error is introduced by this treatment. Generally, only data was rejected that was either internally inconsistent or else that was a high and a low out of multiple readings and significantly influenced only the scatter, not the arithmetic mean. All data points are plotted on the conductivity curves unless specifically noted as when the scatter of separate runs would overlap and confound a comparison.

The probable error was statistically determined for the conductivity versus temperature curves to establish the maximum deviation that should be expected for 50% of the observed data points from the smooth curve. This deviation was more dependent on the thermal conductivity range than on the temperature and was found to be about 4% at the 50 Btu/hr/ft²/° F/in. range and 2% at the 700 range. The over-all probable errors for ATJ, TaB, ZrB, and SiN were about 4½%, 6½%, 3%, and 2½%, respectively. In those cases in which the specimen was found to be, or suspected of, remaining thermally sound, these data are representative. When the specimen suffered from fissures, breaks, cracks, composition change, or the influence of the heat soaking, then these limits of probable error do not apply and the data for the material must be evaluated in the light of the particular material change or history. For example, the fissures in most of the carbide specimens undoubtedly contributed to the increased data scatter for these materials.

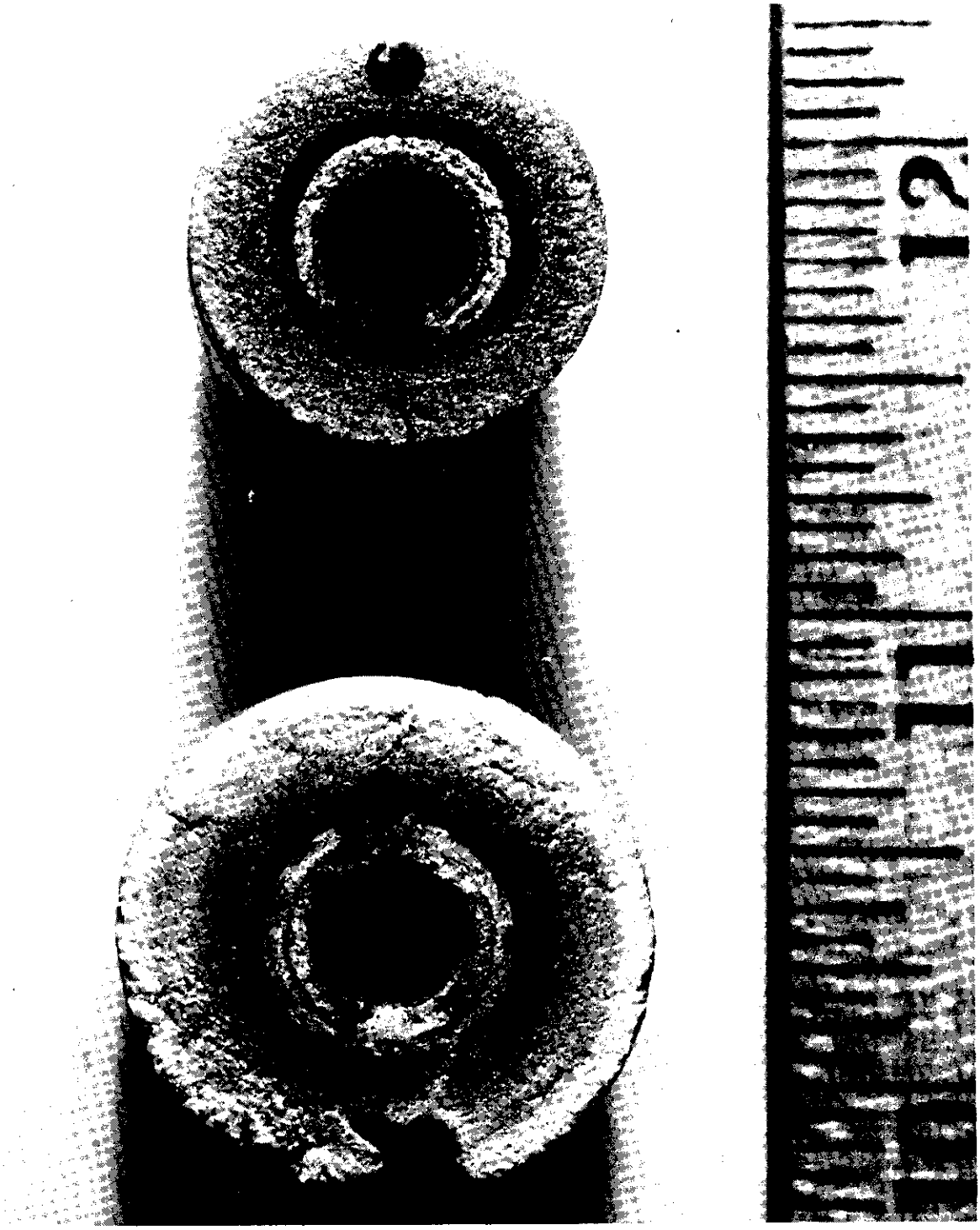

Figure 35. Picture Showing Isothermal Coloration Lines on the Surface and Extending Through Conductivity Specimens

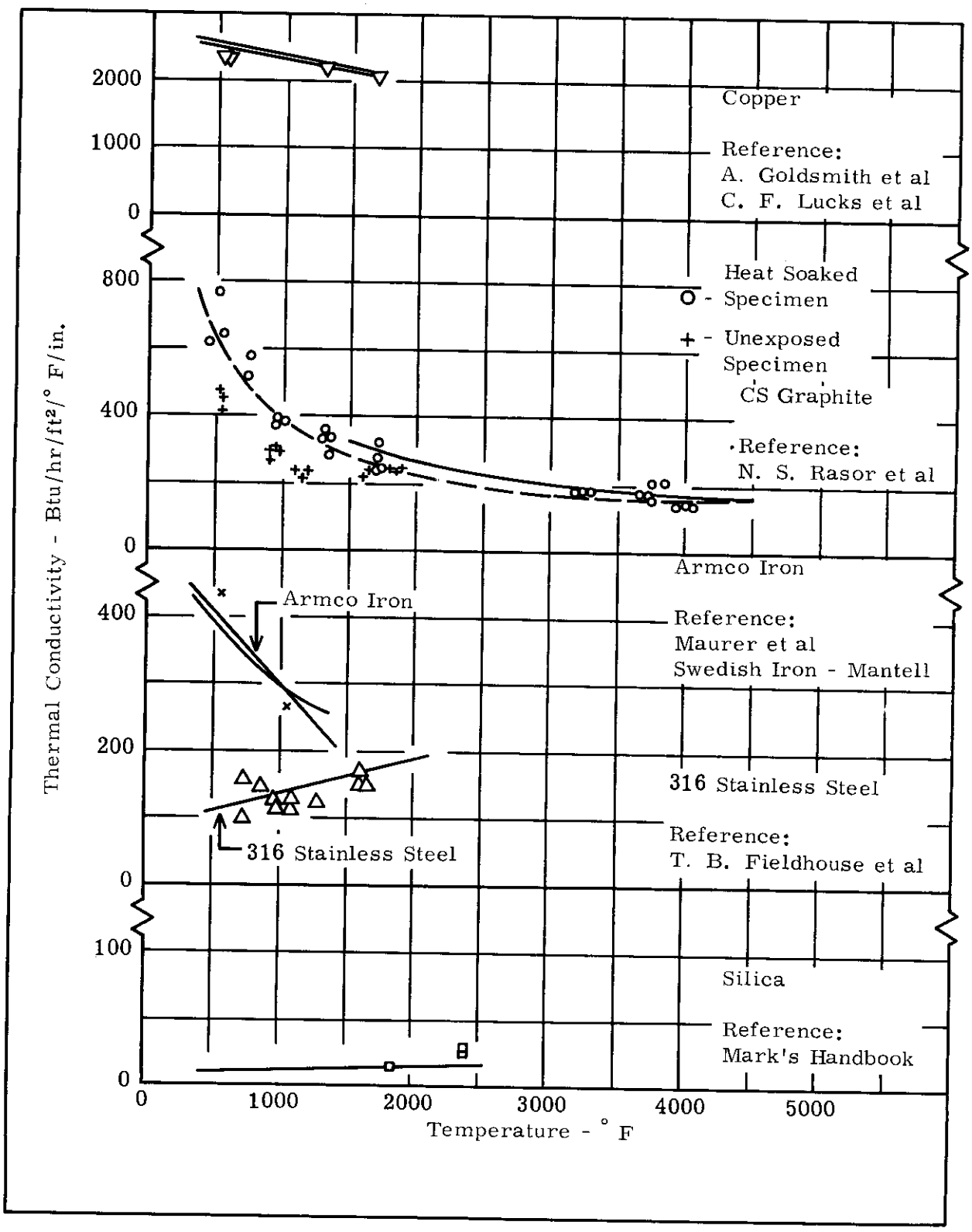

Figure 36. Thermal Conductivity on Five Reference Materials Used as "Standards."

MISCELLANEOUS OBSERVATIONS

Some interesting observations developed concerning the molybdenum and tungsten wire used inside the furnace. The molybdenum wire lost its ductility after being heated above 2500-2600° F. At about 3700-3750° F the molybdenum wire began melting and flowing together, forming a good weld between pieces. Even though the area just out of the welded zone was quite brittle, the weld itself seemed to have good strength. The tungsten wire behaved in much the same manner as the molybdenum, except that the melting of tungsten did not begin until above 4000° F. Welds were made between two pieces of molybdenum, two pieces of tungsten, and between tungsten and molybdenum. In the Mo-Mo, W-W, and W-Mo welds, the adjacent wires were all quite brittle. It is likely that the presence of silicon was responsible for the lowering of the melting points of tungsten and molybdenum. The presence of 5.5% silicon forms a eutectic of molybdenum, which melts at about 3750° F. Four percent silicon causes tungsten to melt at about 4070° F. Since the melting points of molybdenum and tungsten are about 4760° F and 6170° F, respectively, it appears that the eutectic was forming. The silicon probably vaporized from the silica in the end plug insulator bricks as they were originally made. A picture of the welds formed in the heat capacity furnace is shown in Figure 37.

A graphite batting for insulating purposes was used during one run in the expansion furnace. The batting was not suitable for this high temperature insulation application and was removed. The fiber did not seem to maintain any strength—and very little soundness or integrity—after heating, permitting the batting to fall apart.

A piece of tantalum sheet was placed in the heat capacity furnace along with tungsten/molybdenum and tungsten/rhenium thermocouples. The tantalum performed as a "getter," keeping impurities in the atmosphere from contaminating the thermocouples. The useful range of the thermocouples was increased by several hundred degrees.

During the many runs on the graphite helices and the thin tubes, much data were collected on the electrical resistance of the graphite. Contrary to many reports in the literature, the resistance did not seem to decrease appreciably with temperature from 2000° F up to 5000° F.

The apparent current bypass around the helices was eliminated. It appears that the 4000° F breakdown did occur at 20 volts per inch AC and did not occur at 5 volts per inch AC or DC.

Figure 37. Picture of Melted Tungsten and Molybdenum Pieces at Temperatures Well Below the Crystal Melting Range.

CONCLUSIONS

The heat capacity was found to vary considerably with temperature over the full temperature range; however, very few serious inflections were observed.

The thermal expansion was observed to be very dependent on the prior thermal history of the specimen. Considerable nonlinearity was noted at temperatures within 1000° F of the deterioration temperatures.

The thermal conductivity values were similar for families of materials but varied considerably over the temperature range. The prior thermal history of the material significantly altered this property.

The specimen materials did not perform to temperatures anticipated from handbook values. Much more understanding is required on the influence of extreme temperatures on the behavior of refractory materials.

APPENDIX 1

Data Curves for the Heat Capacity, Thermal Expansion, and Thermal Conductivity Specimens and Calibrators

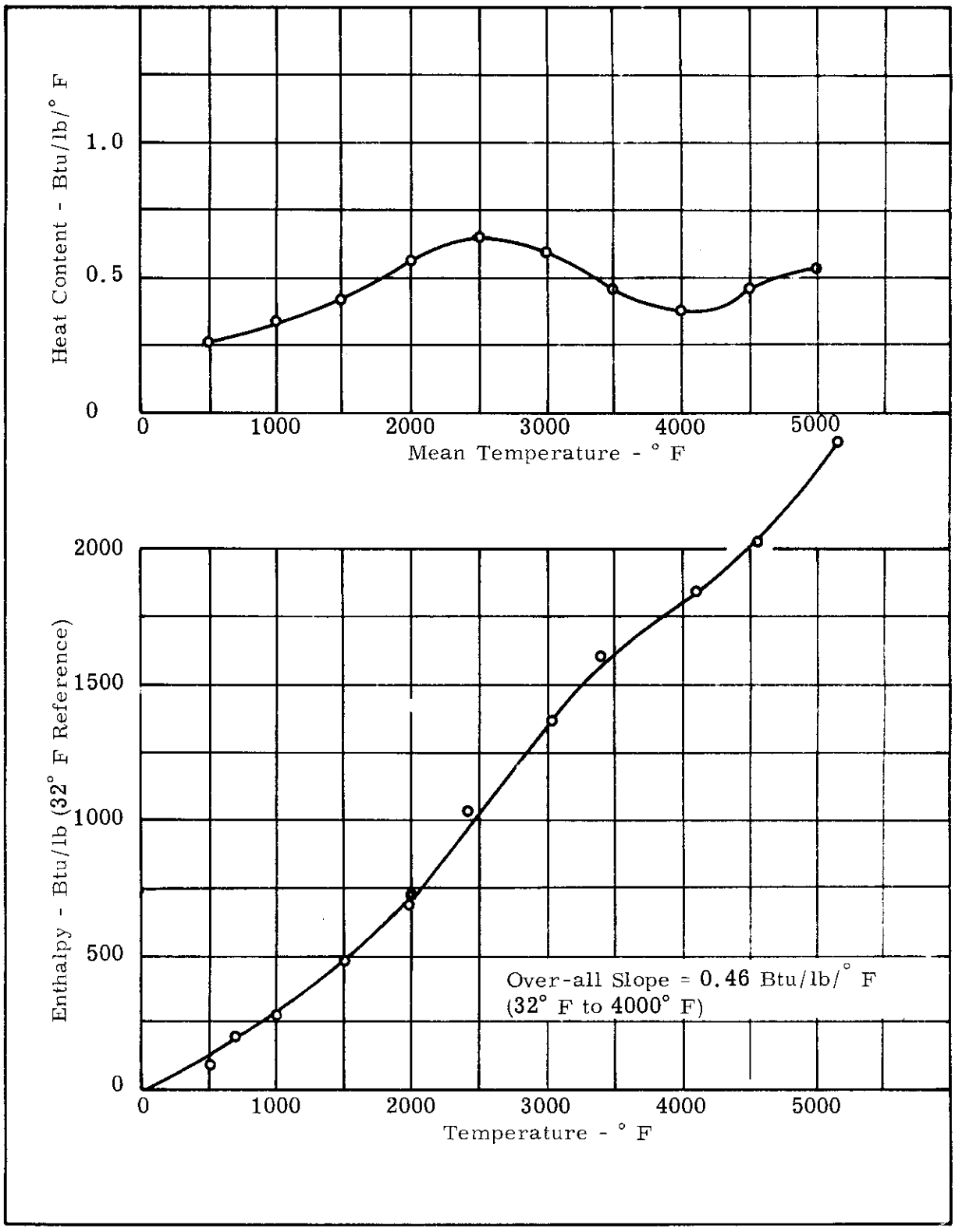

Figure A-1. Enthalpy and Heat Content for ATJ Graphite.

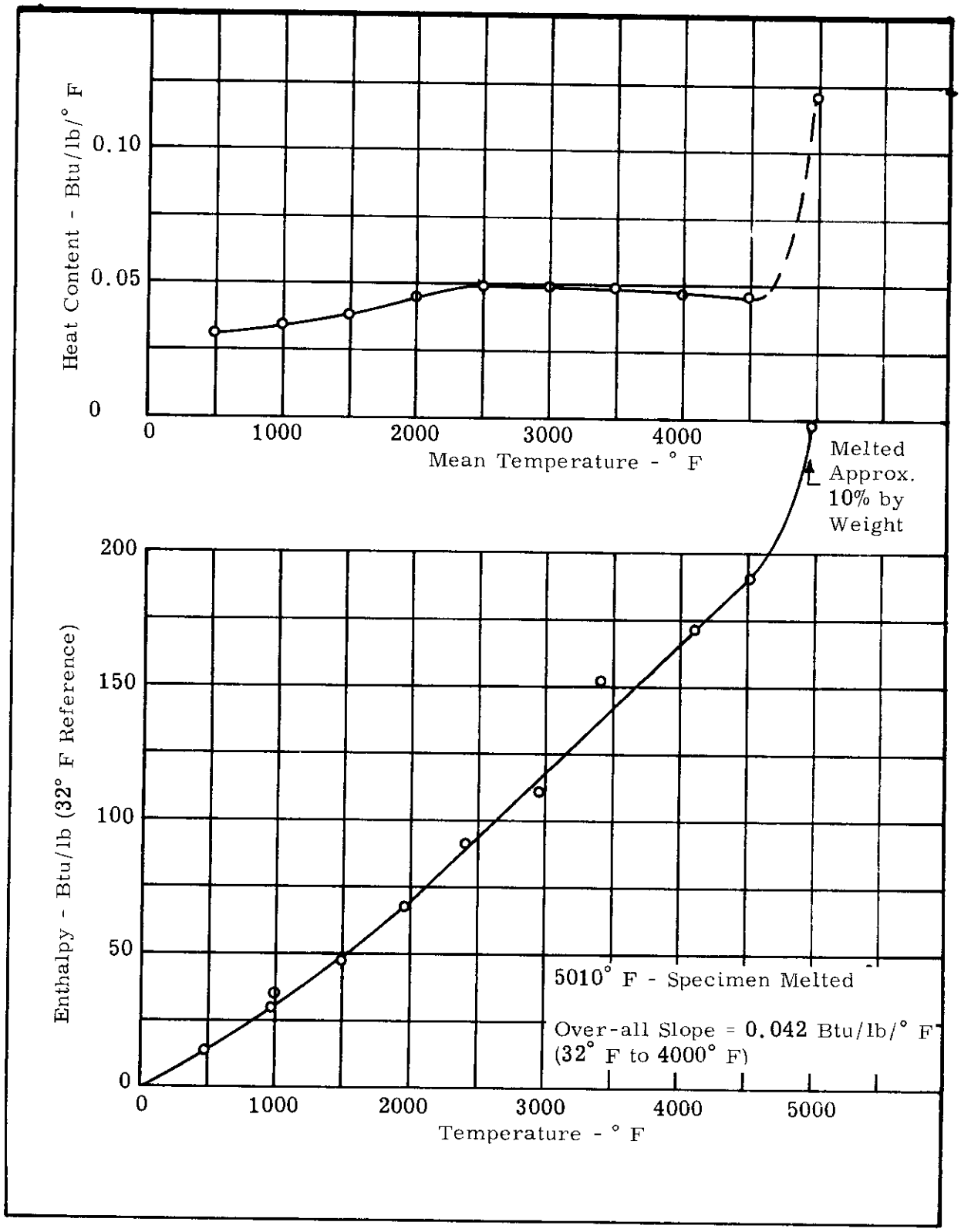

Figure A-2. Enthalpy and Heat Content for Tungsten.

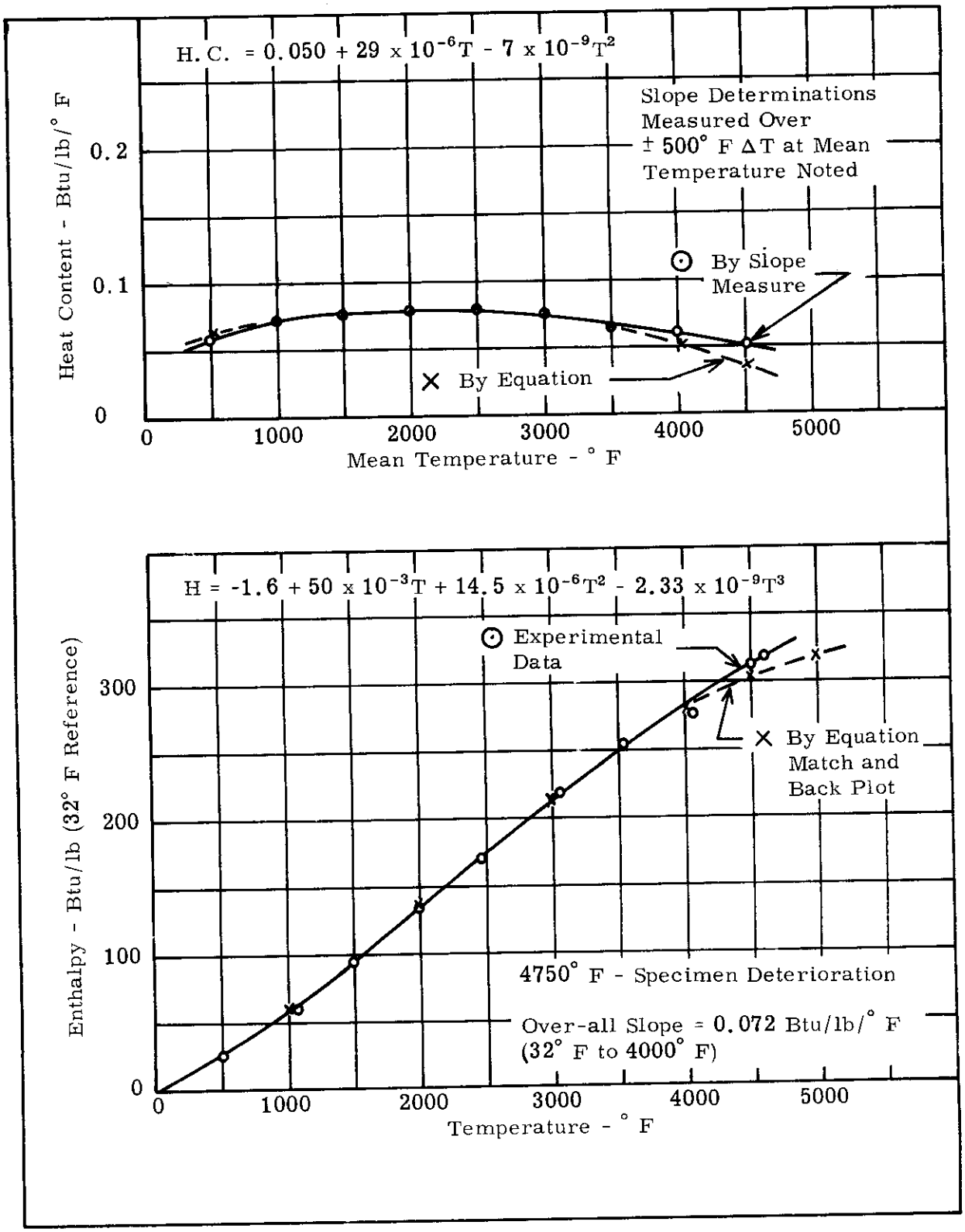

Figure A-3. Enthalpy and Heat Content for Hafnium Nitride.

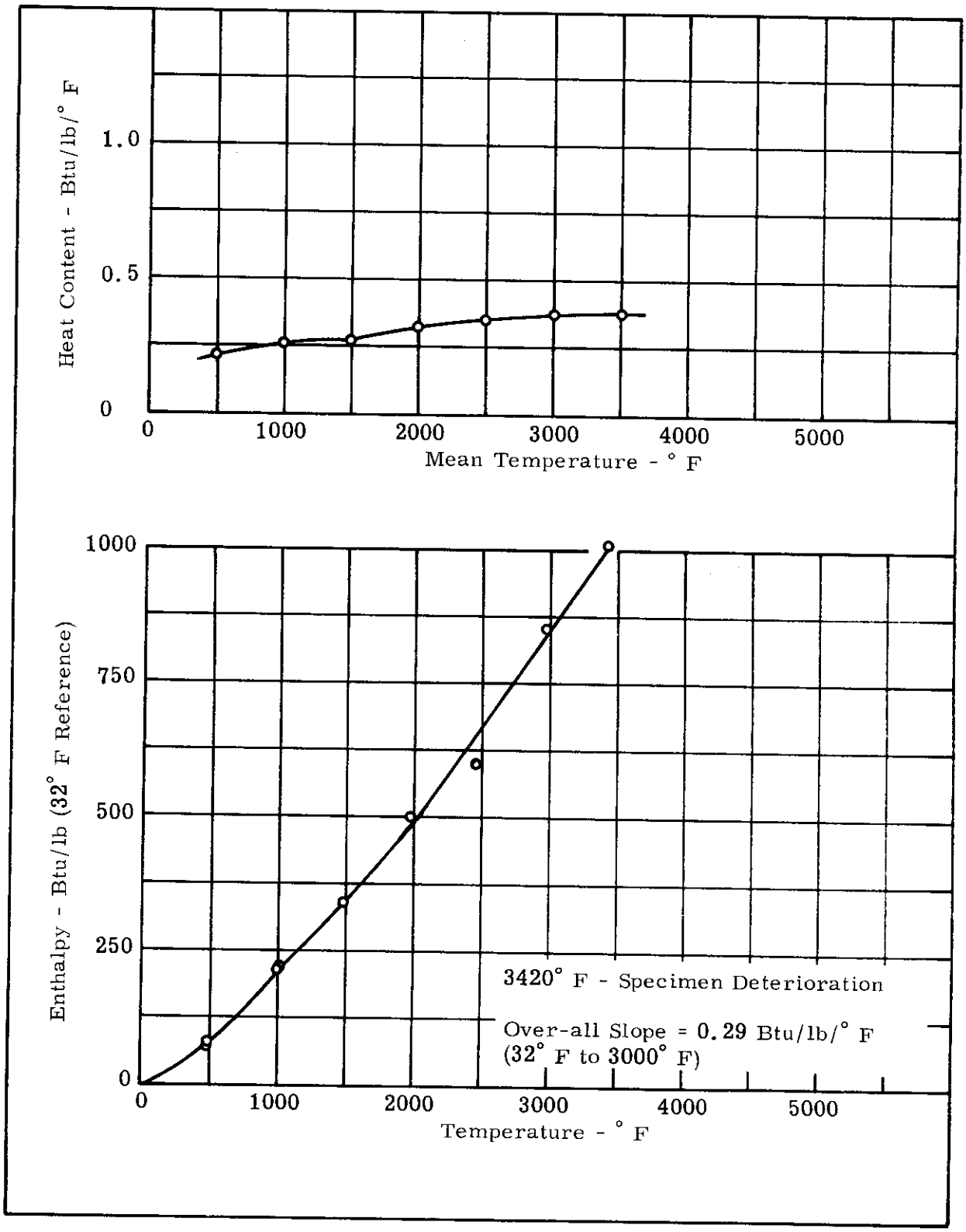

Figure A-4. Enthalpy and Heat Content for Silicon Nitride.

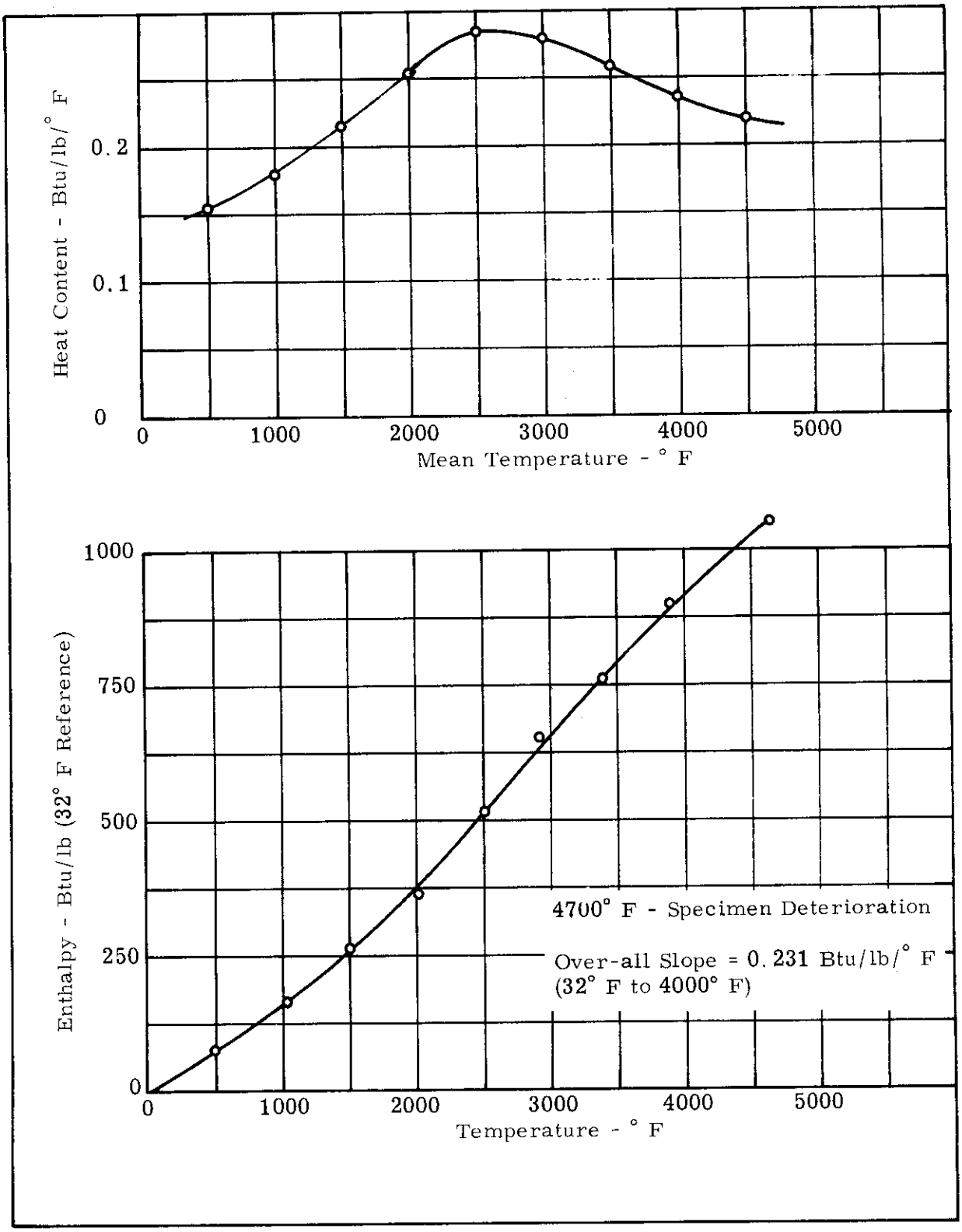

Figure A-5. Enthalpy and Heat Content for Titanium Nitride.

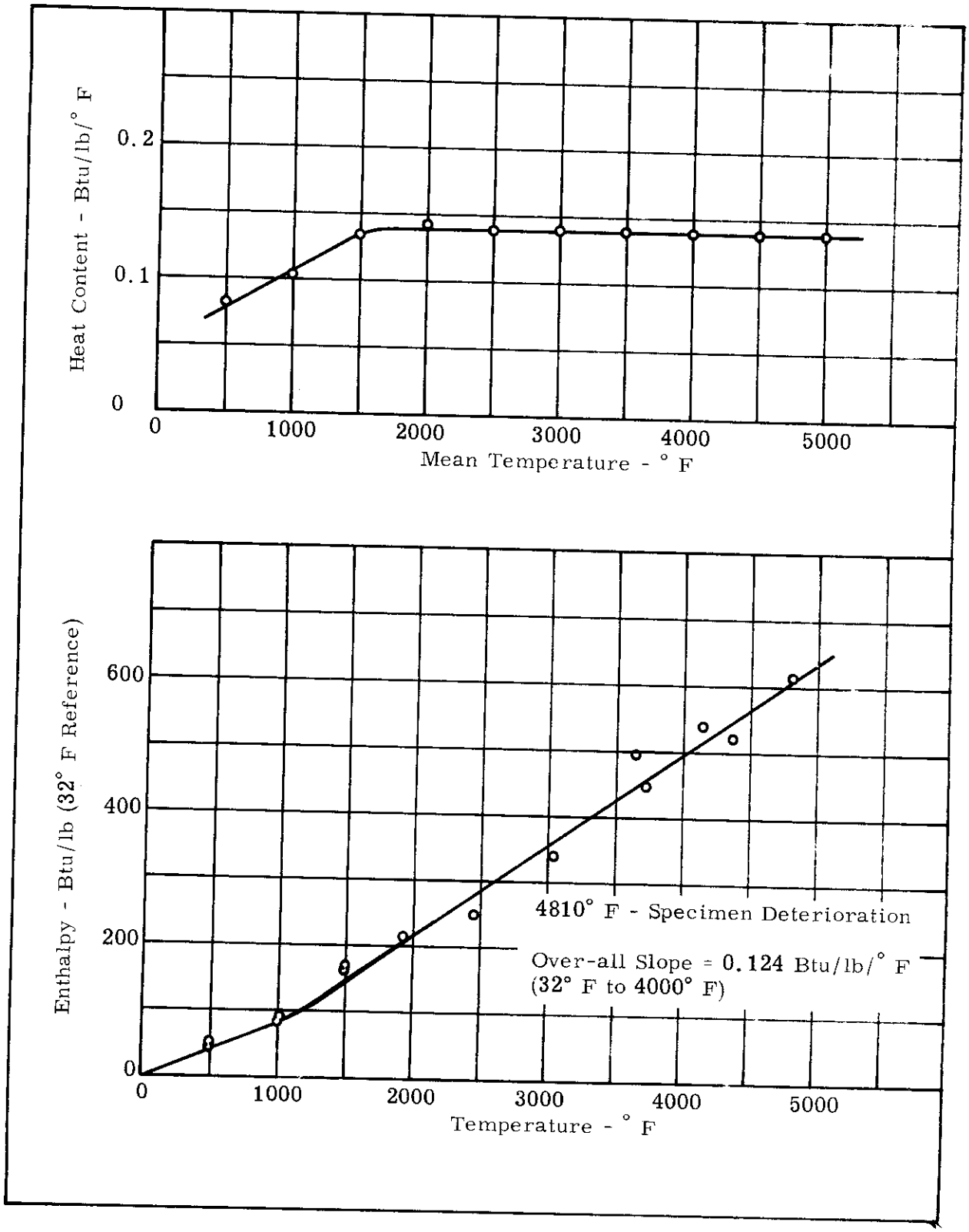

Figure A-6. Enthalpy and Heat Content for Zirconium Nitride.

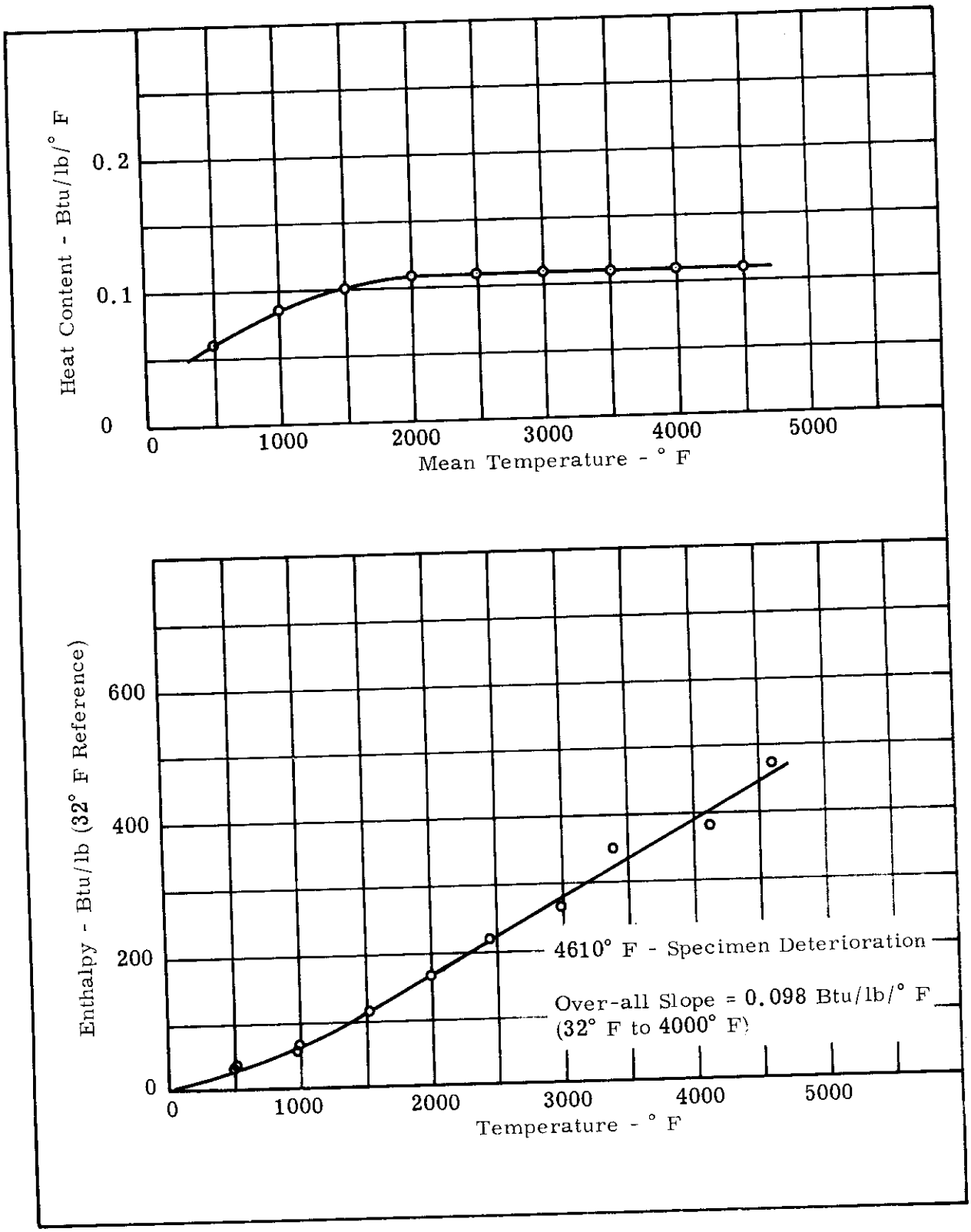

Figure A-7. Enthalpy and Heat Content for Tantalum Boride.

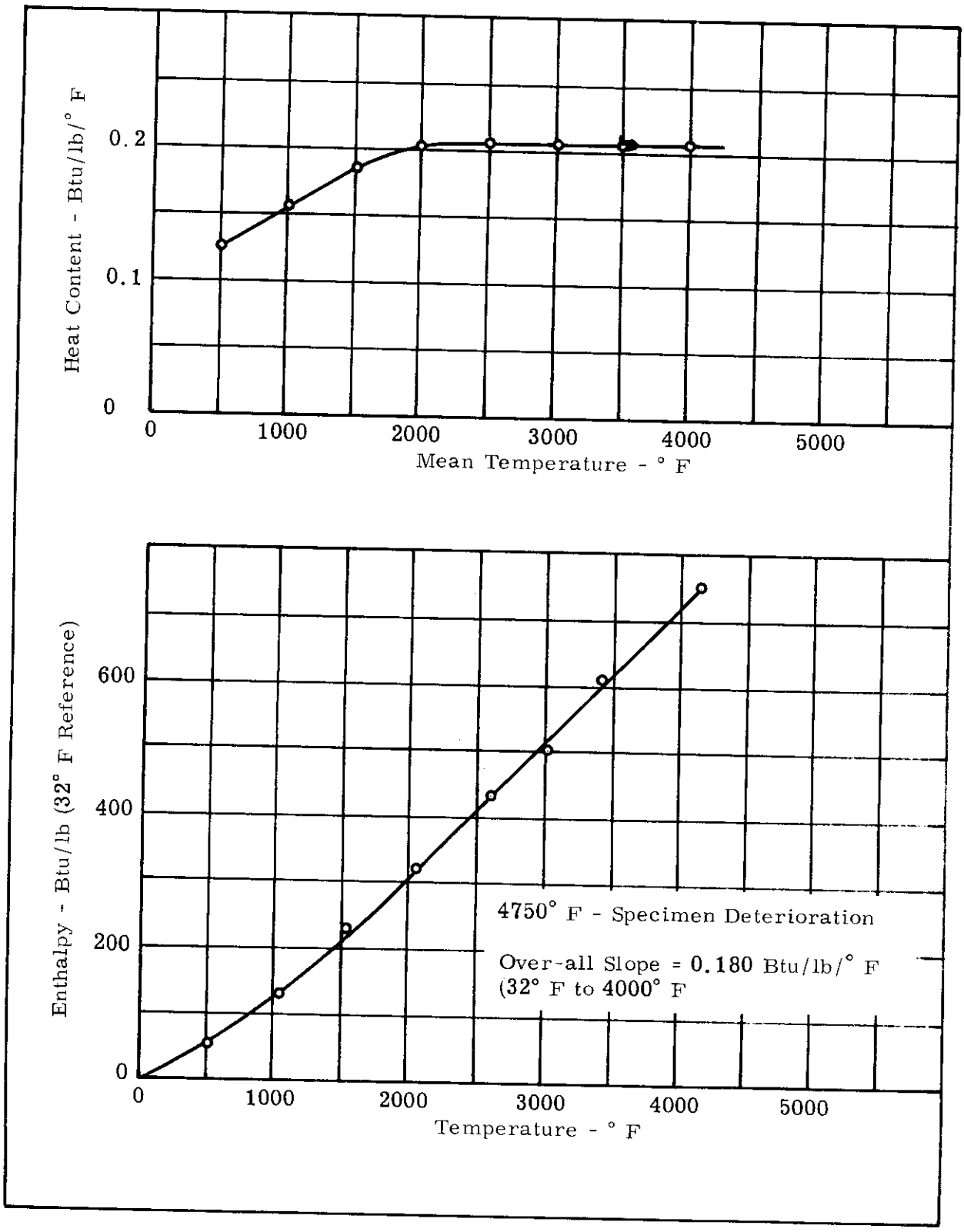

Figure A-8. Enthalpy and Heat Content for Zirconium Boride.

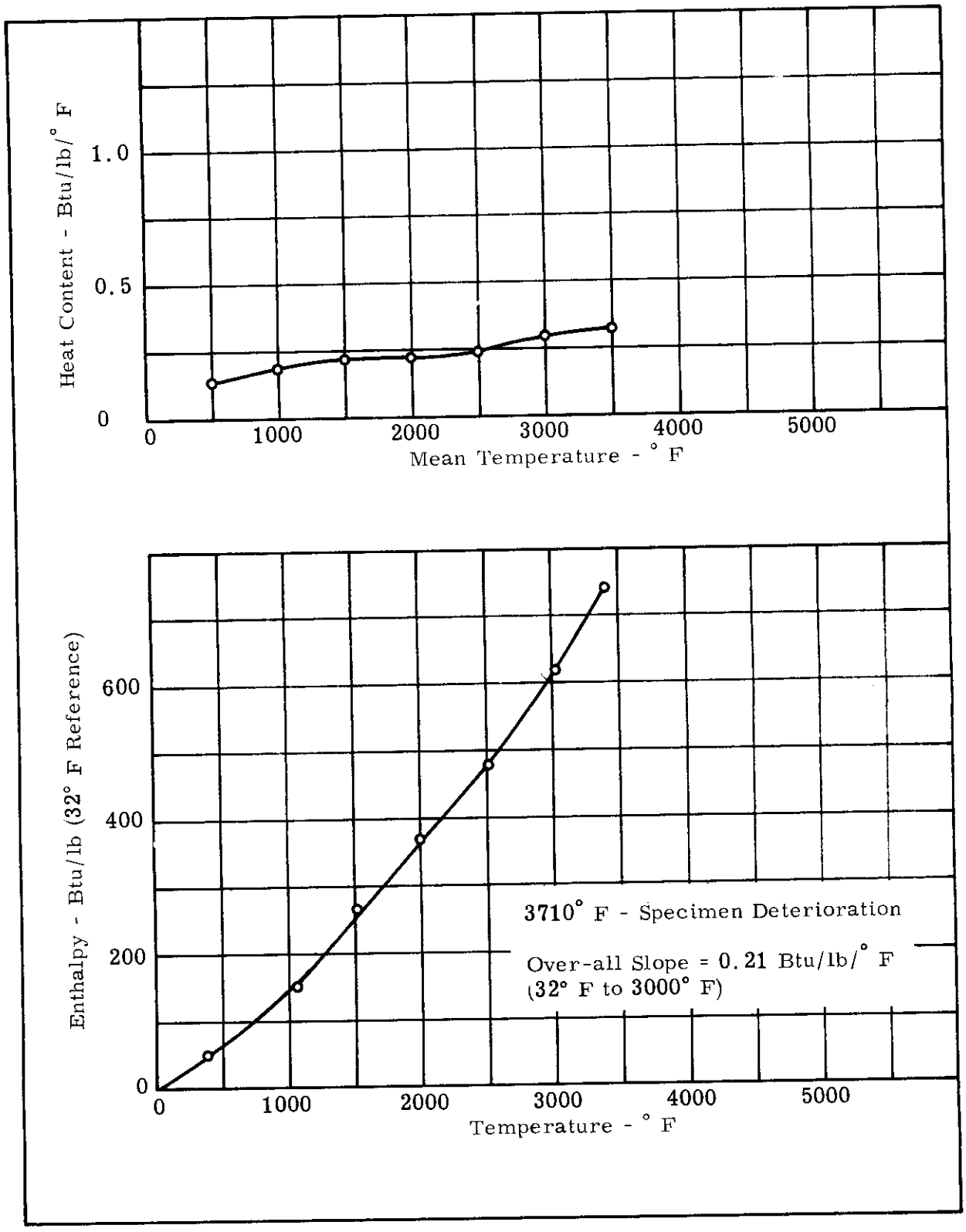

Figure A-9. Enthalpy and Heat Content for Zirconium Silicate.

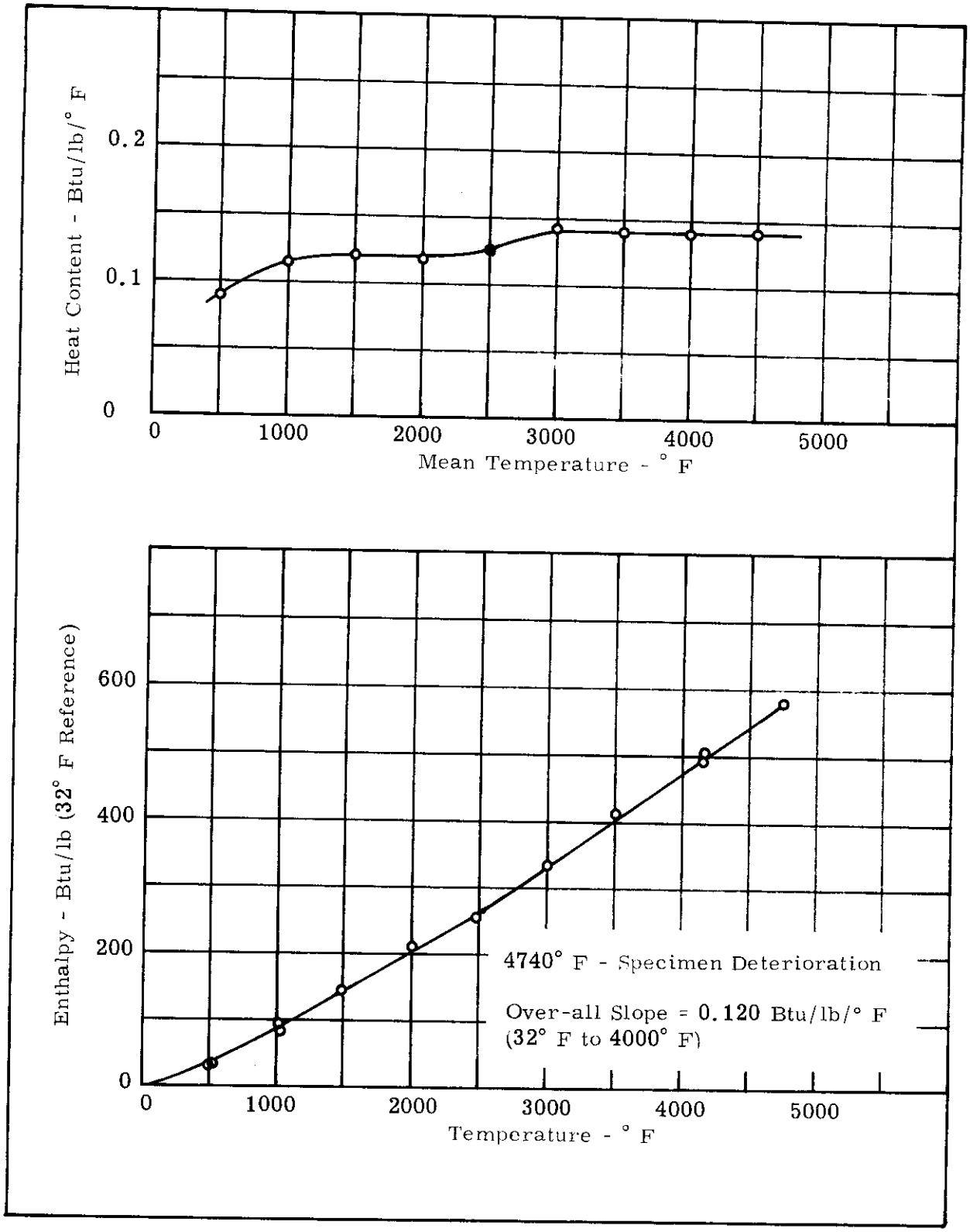

Figure A-10. Enthalpy and Heat Content for Columbium Carbide.

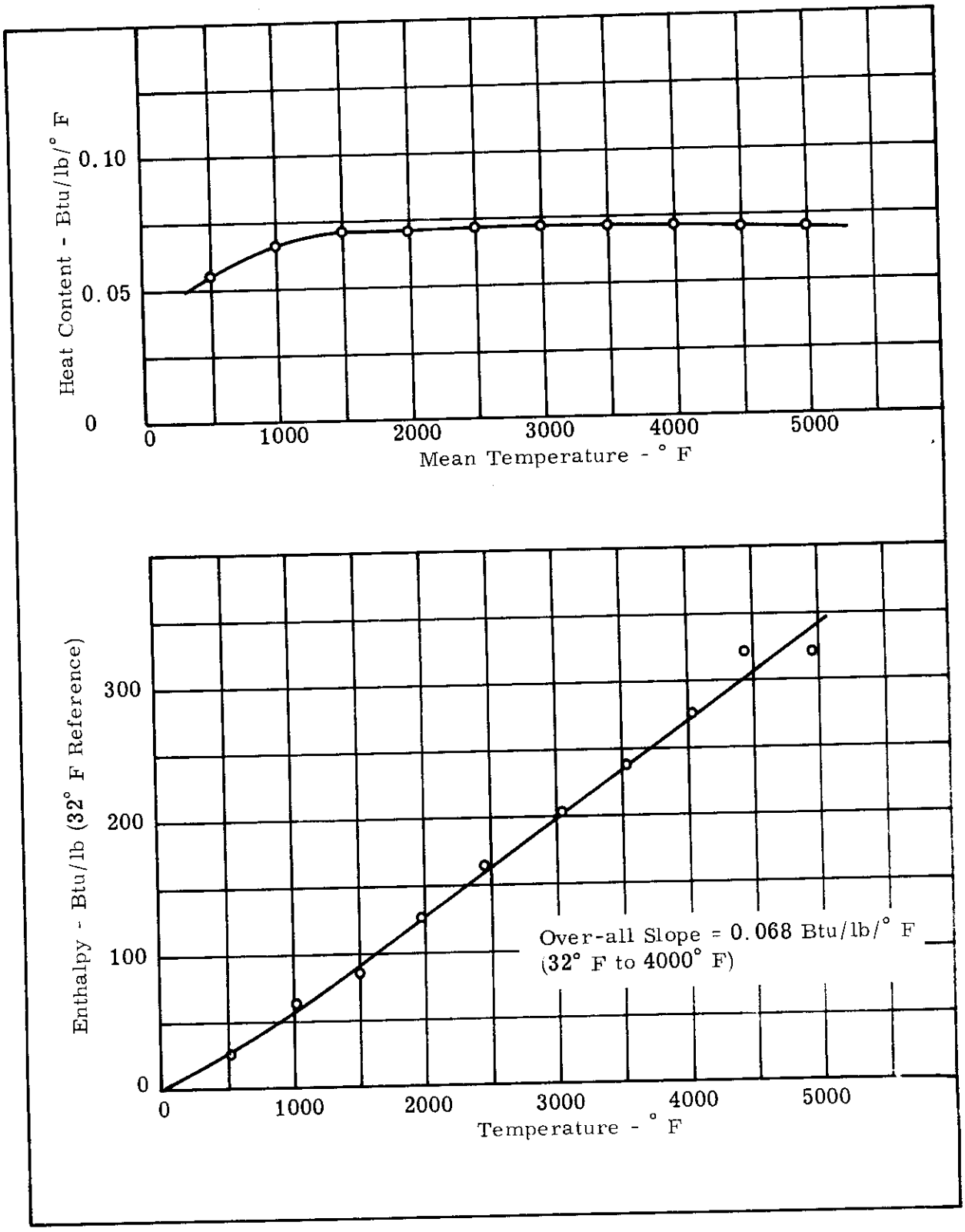

Figure A-11. Enthalpy and Heat Content for Hafnium Carbide.

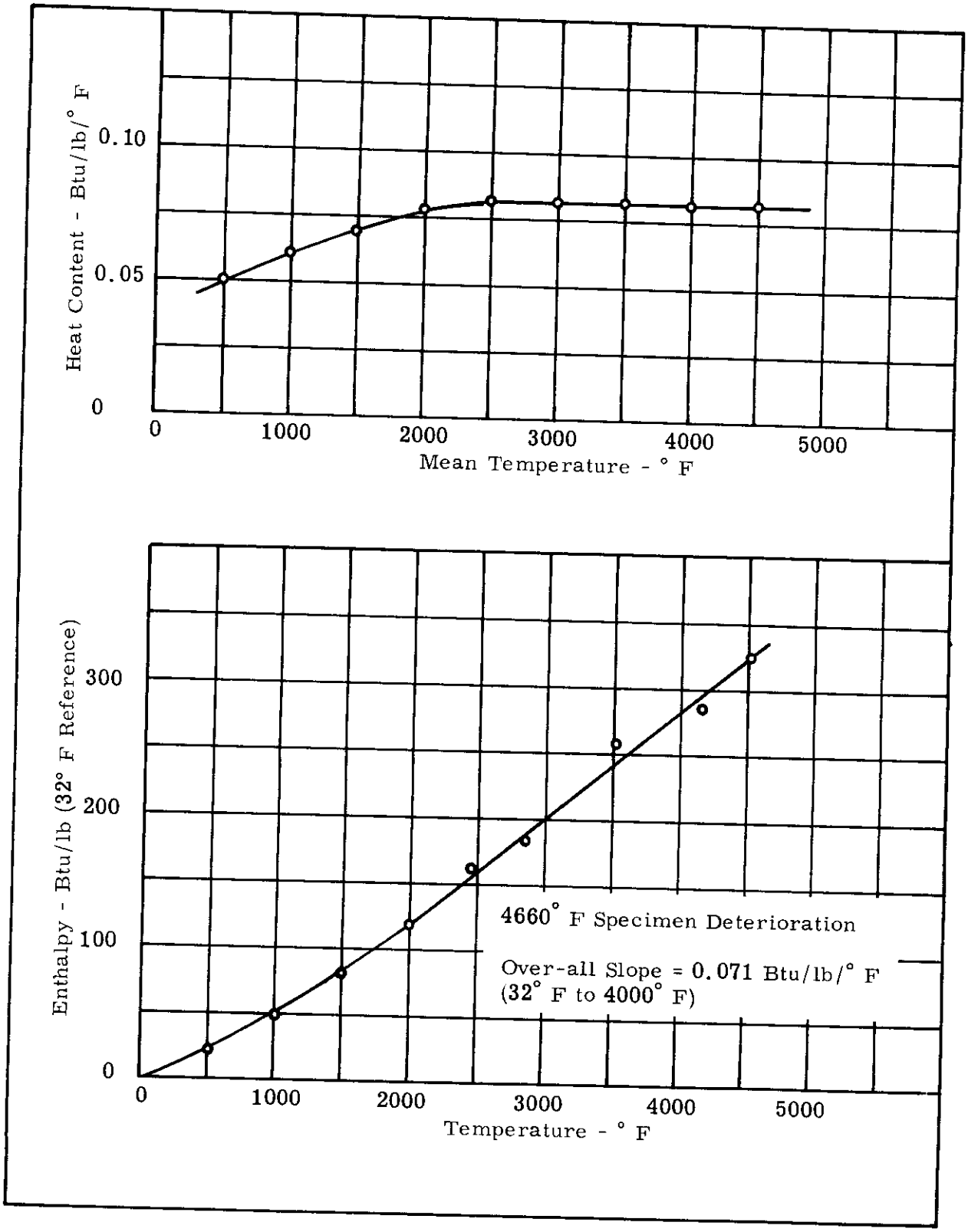

Figure A-12. Enthalpy and Heat Content for Tantalum Carbide.

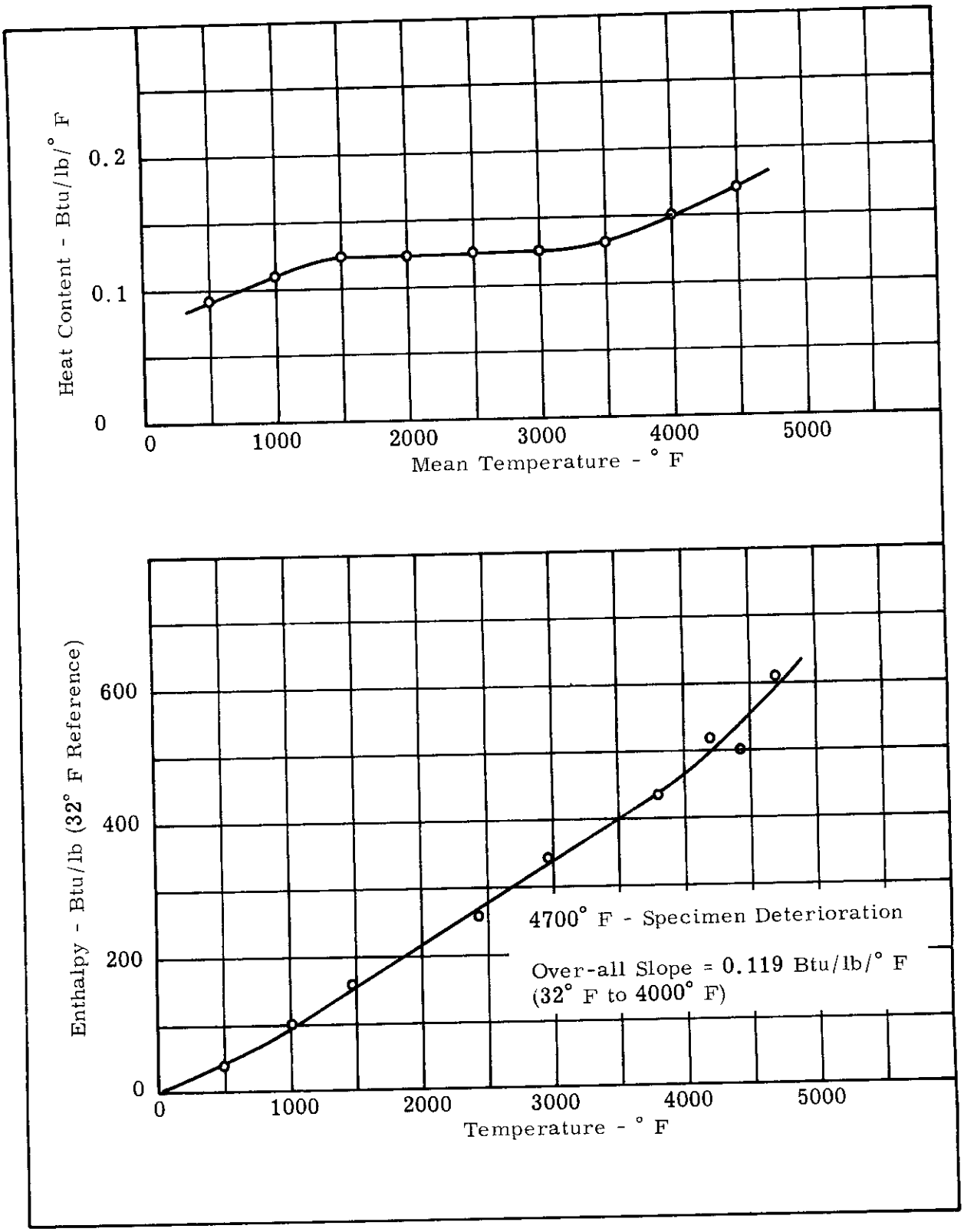

Figure A-13. Enthalpy and Heat Content for Zirconium Carbide.

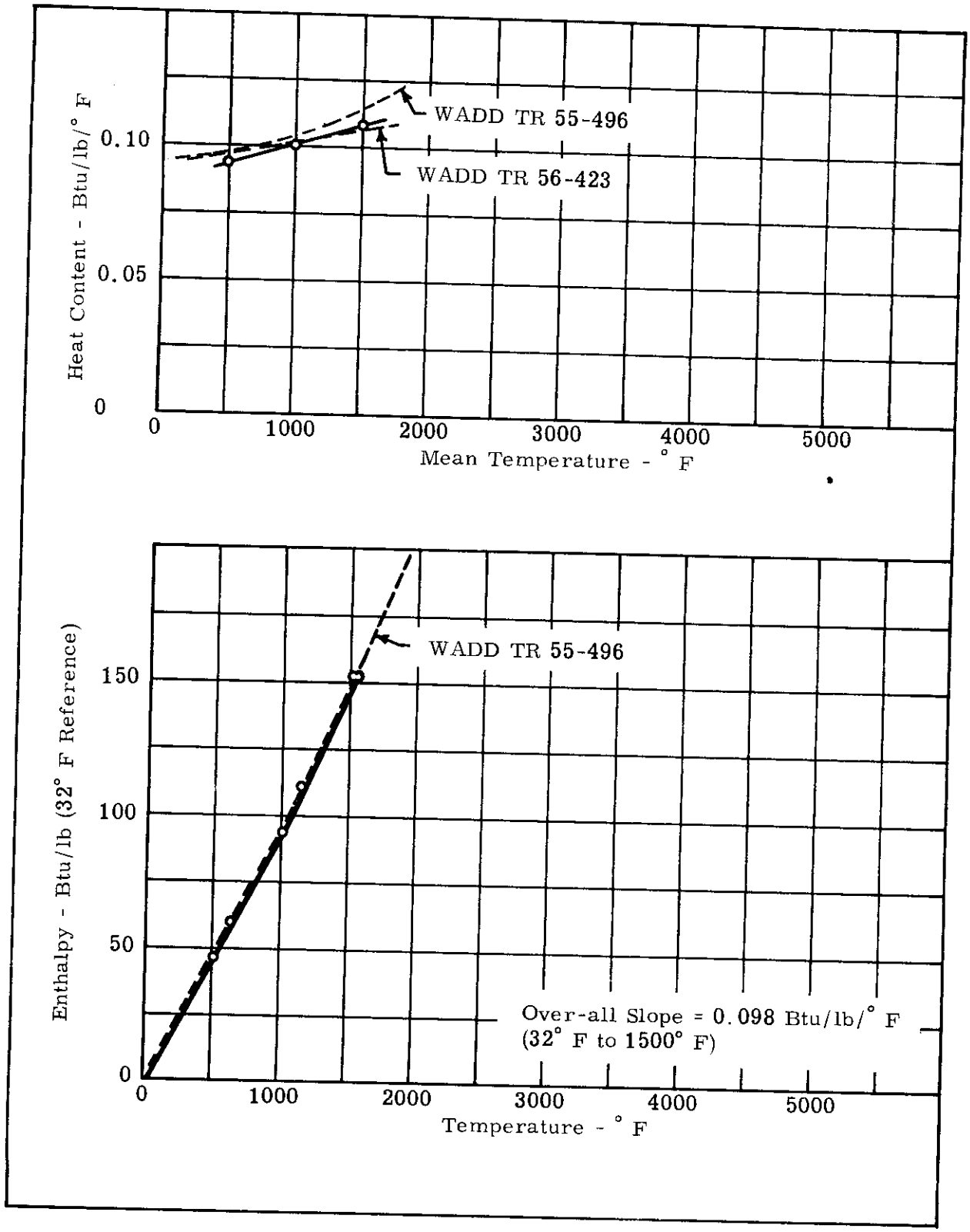

Figure A-14. Enthalpy and Heat Content for Electrolytic Copper.

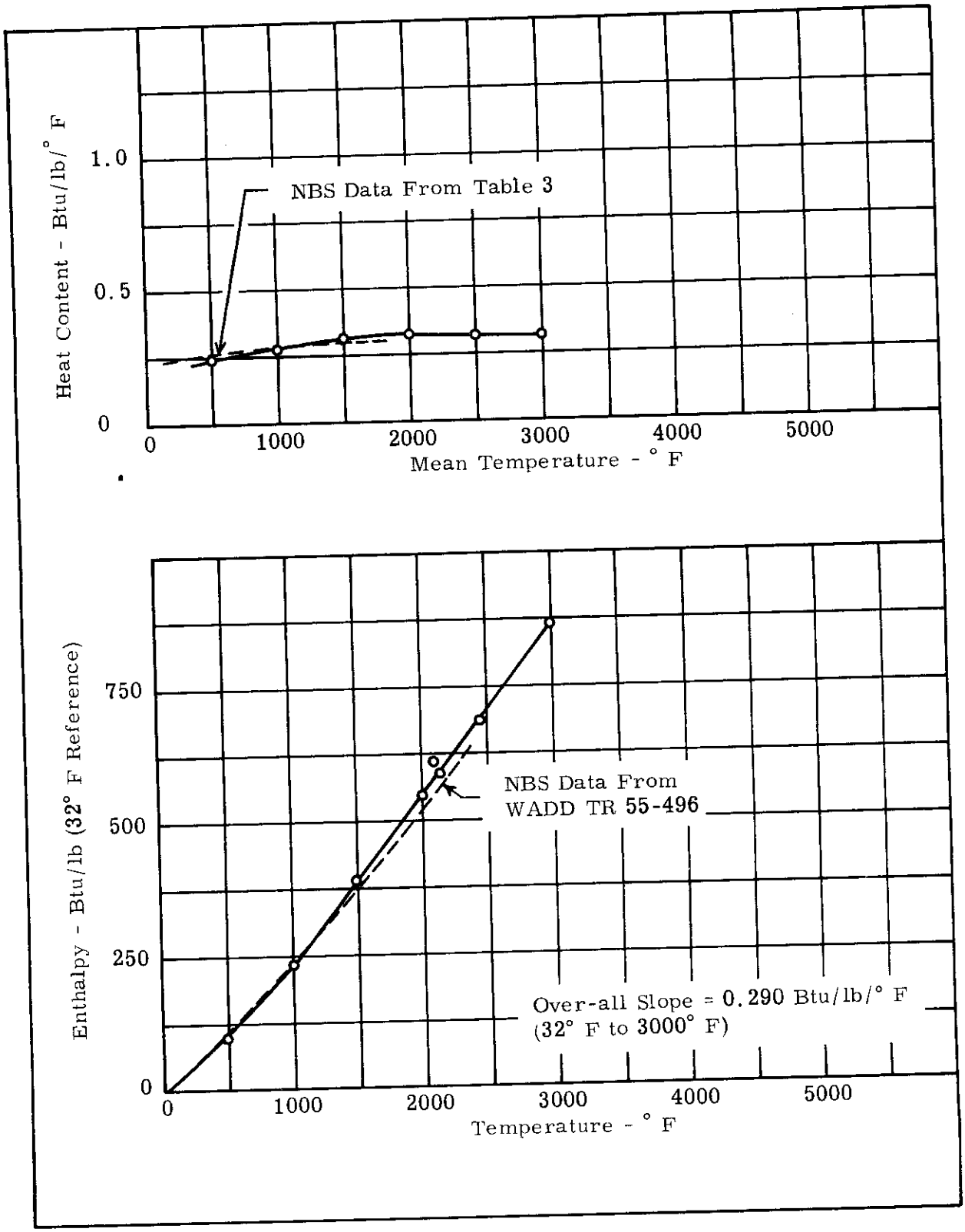

Figure A-15. Enthalpy and Heat Content for Sapphire.

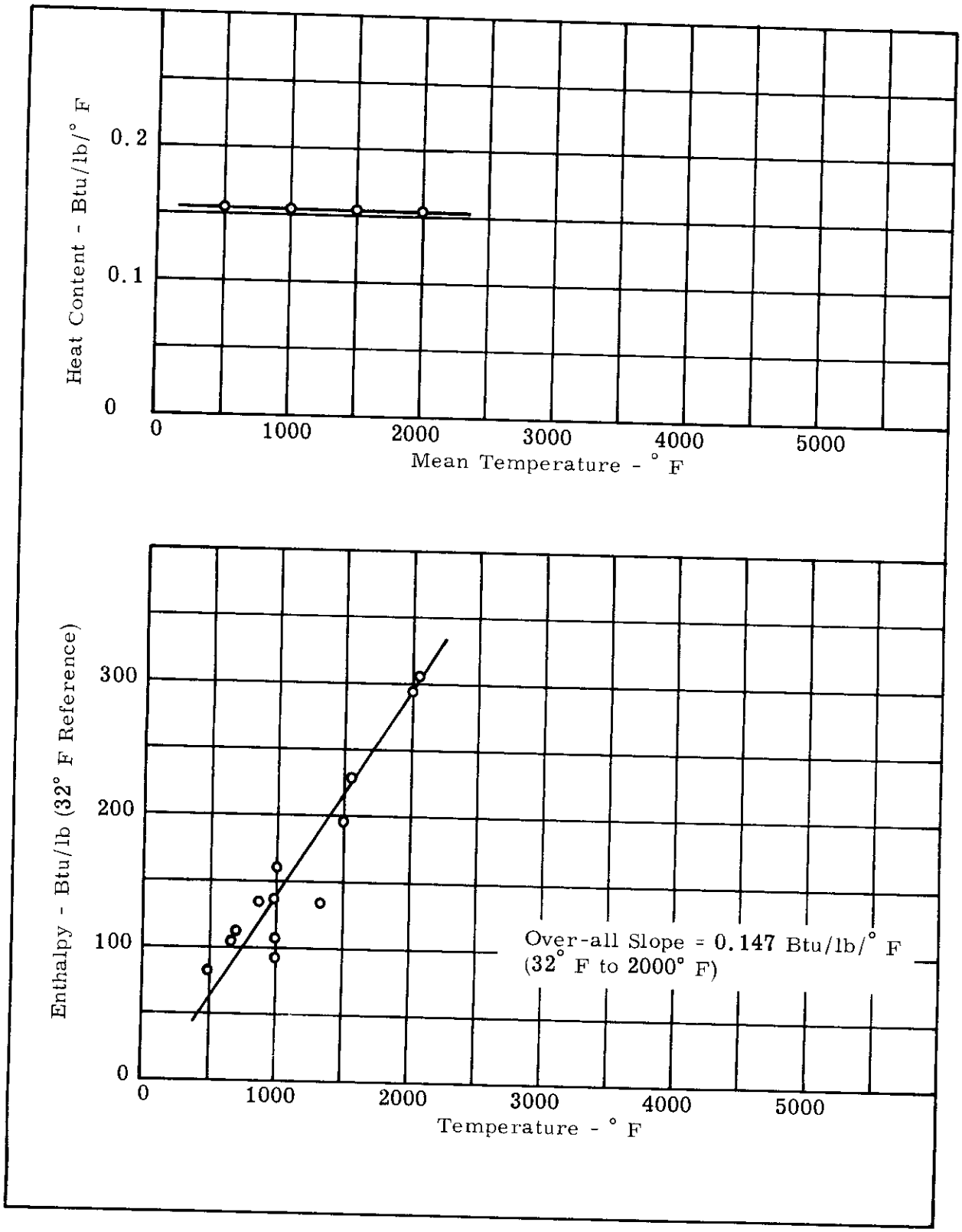

Figure A-16. Apparent Enthalpy and Heat Content for 304 Stainless Steel Basket.

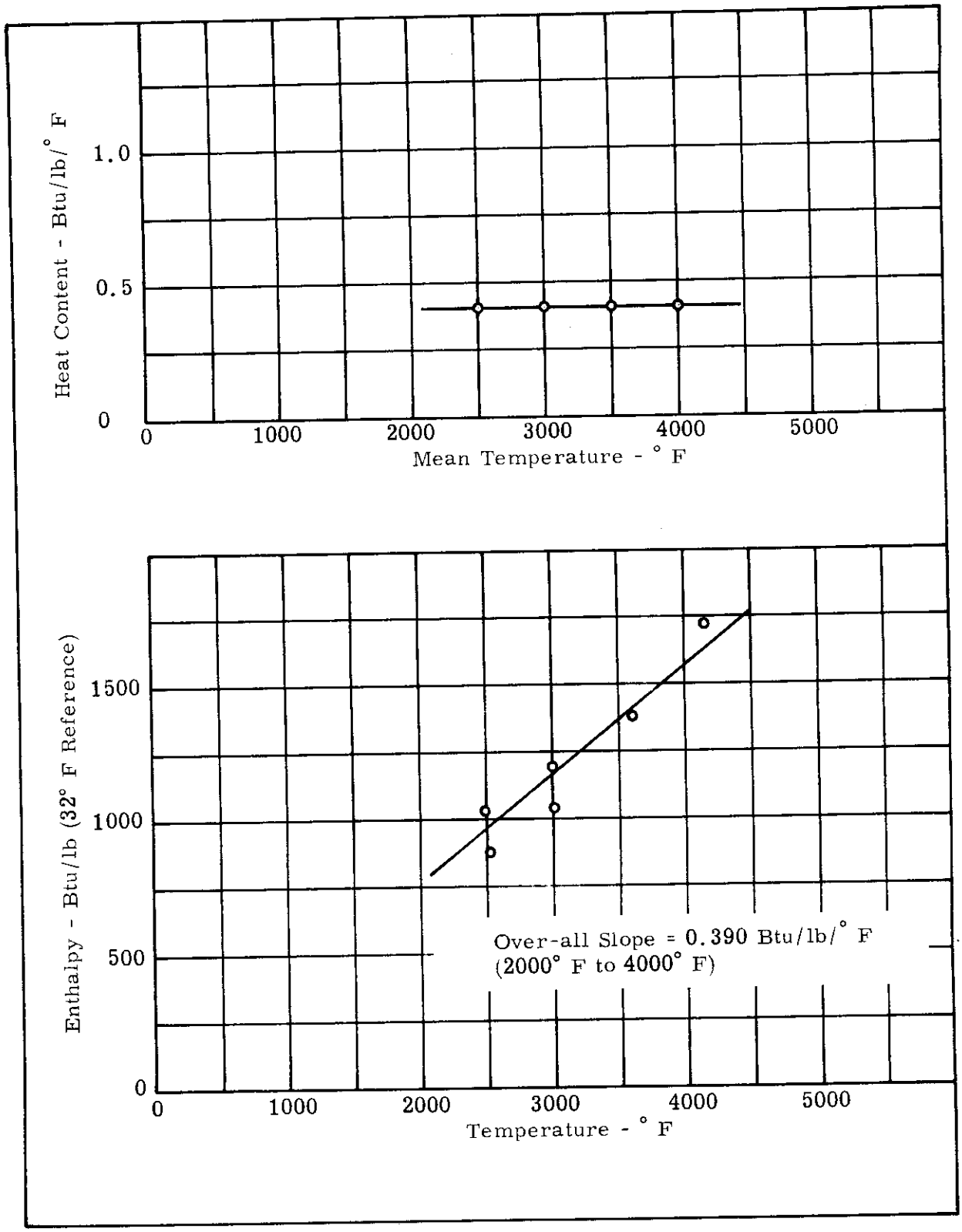

Figure A-17. Apparent Enthalpy and Heat Content for CS Graphite Basket.

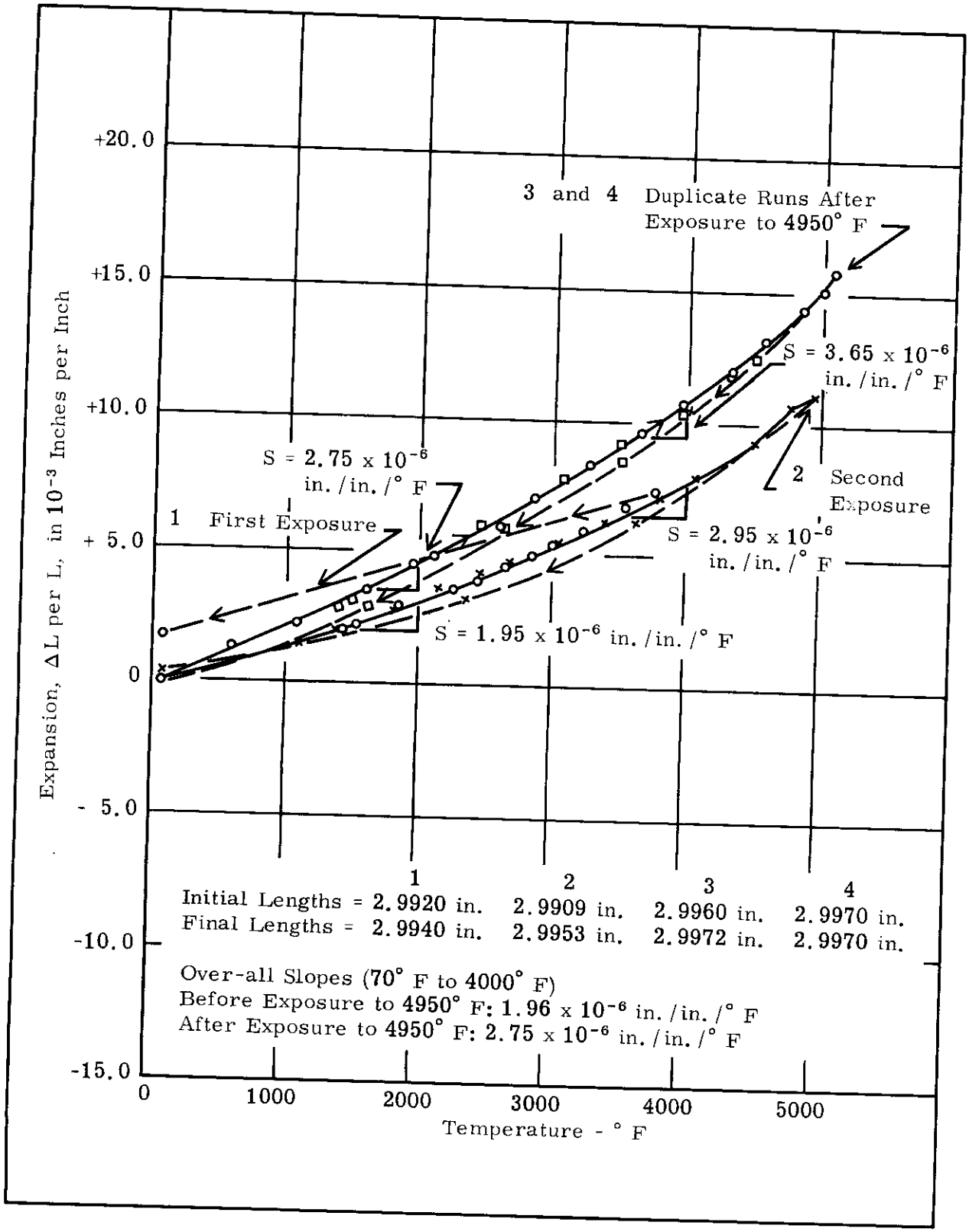

Figure A-18. Thermal Expansion of ATJ Graphite.

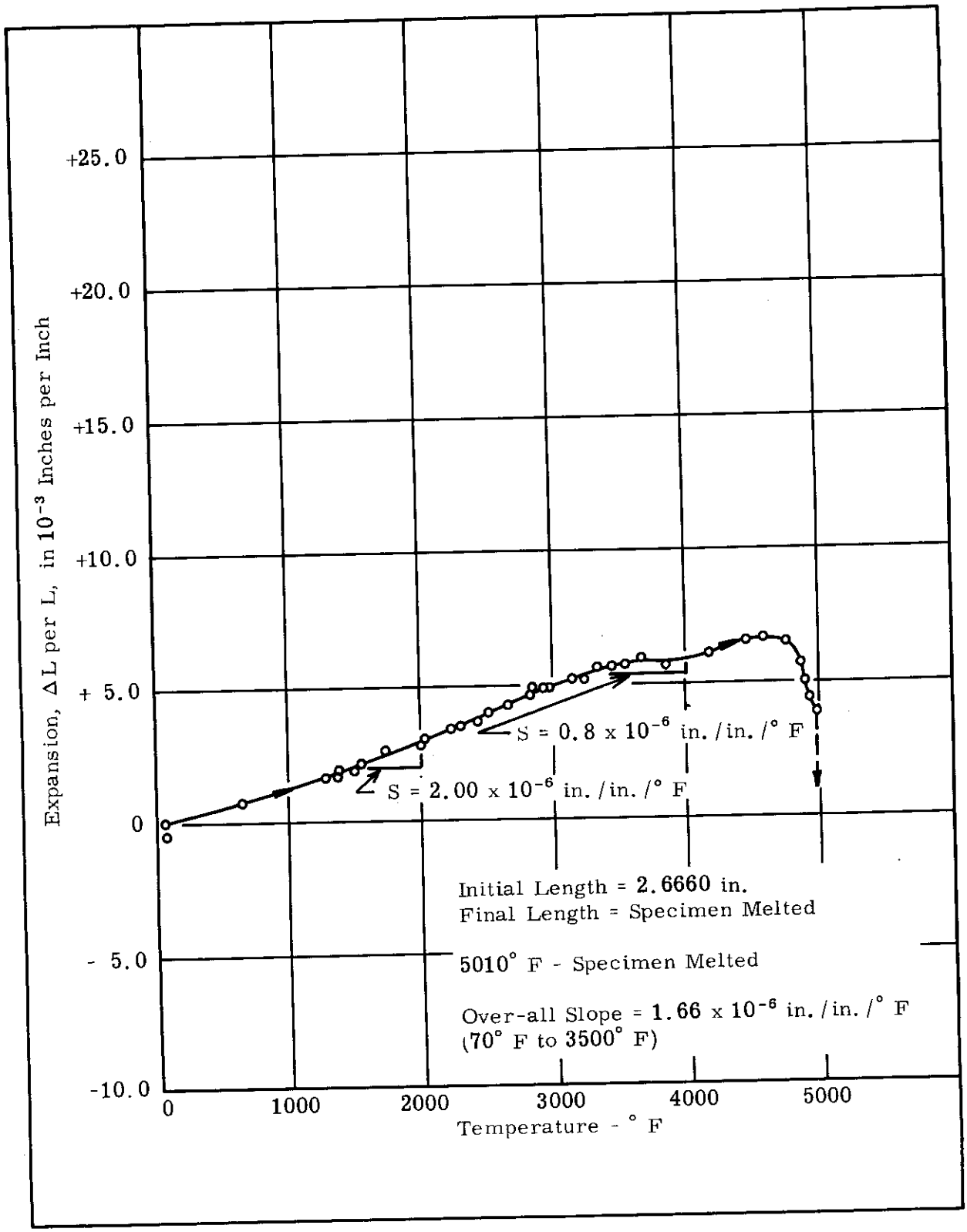

Figure A-19. Thermal Expansion of Tungsten.

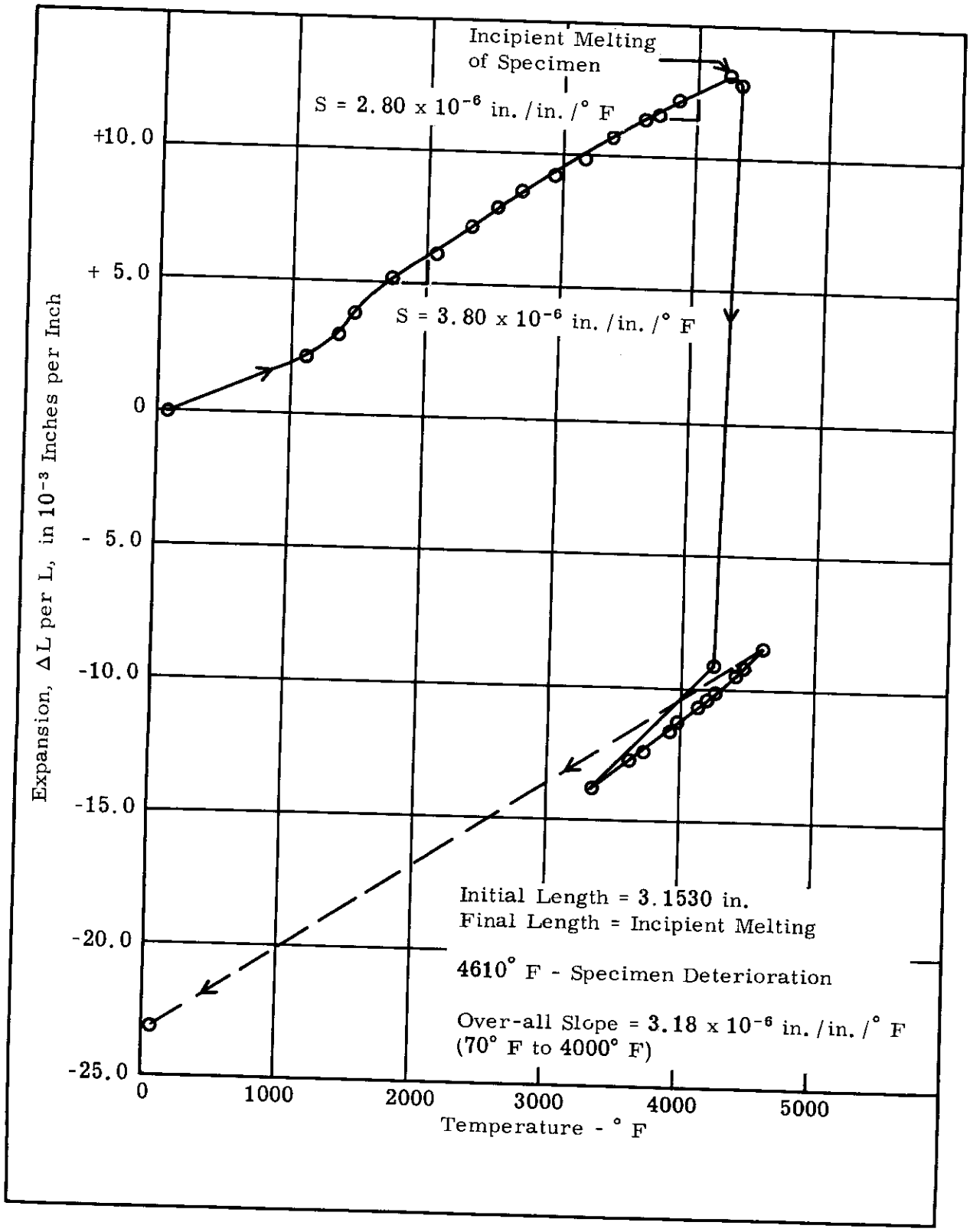

Figure A-20. Thermal Expansion of Tantalum Boride.

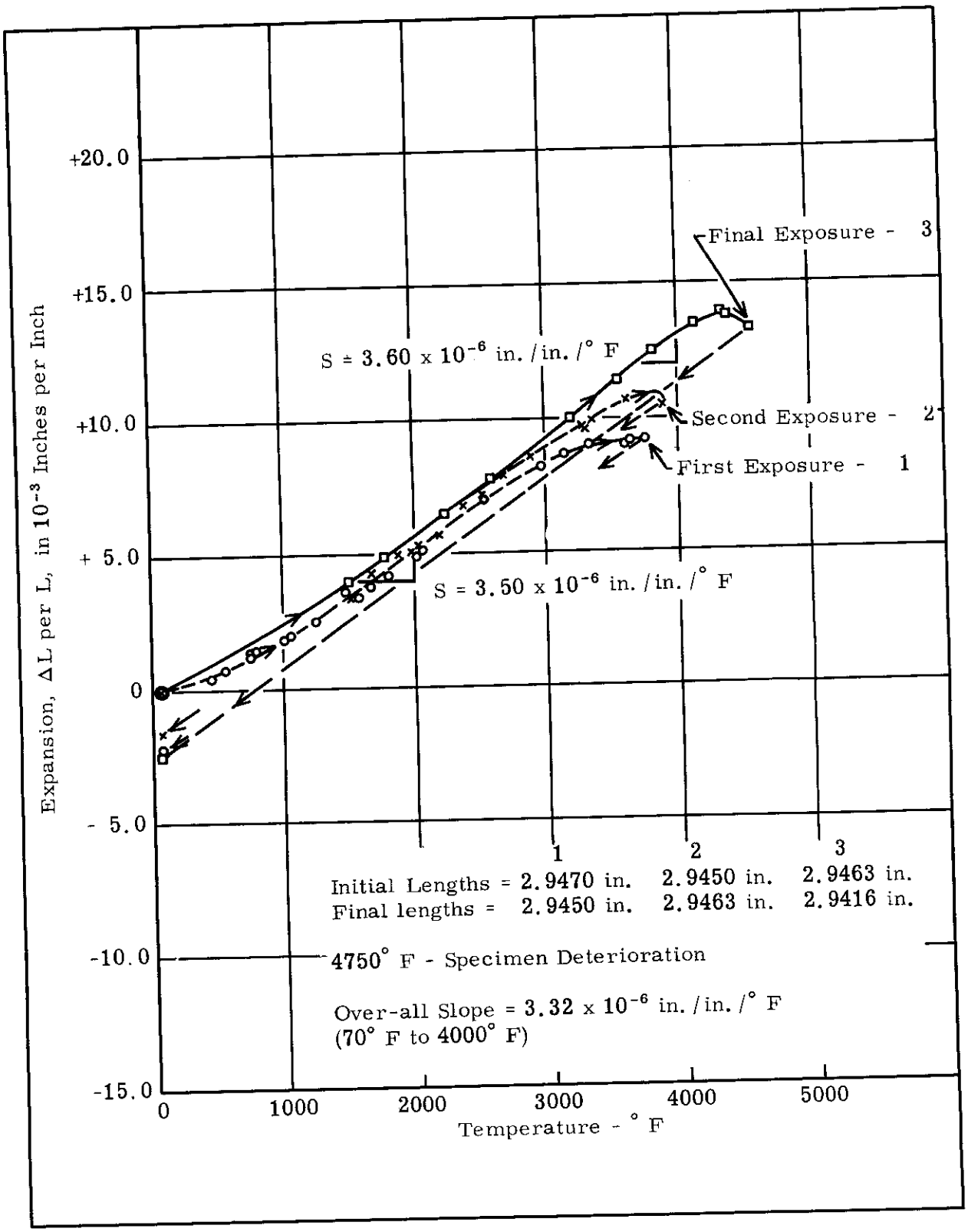

Figure A-21. Thermal Expansion of Zirconium Boride.

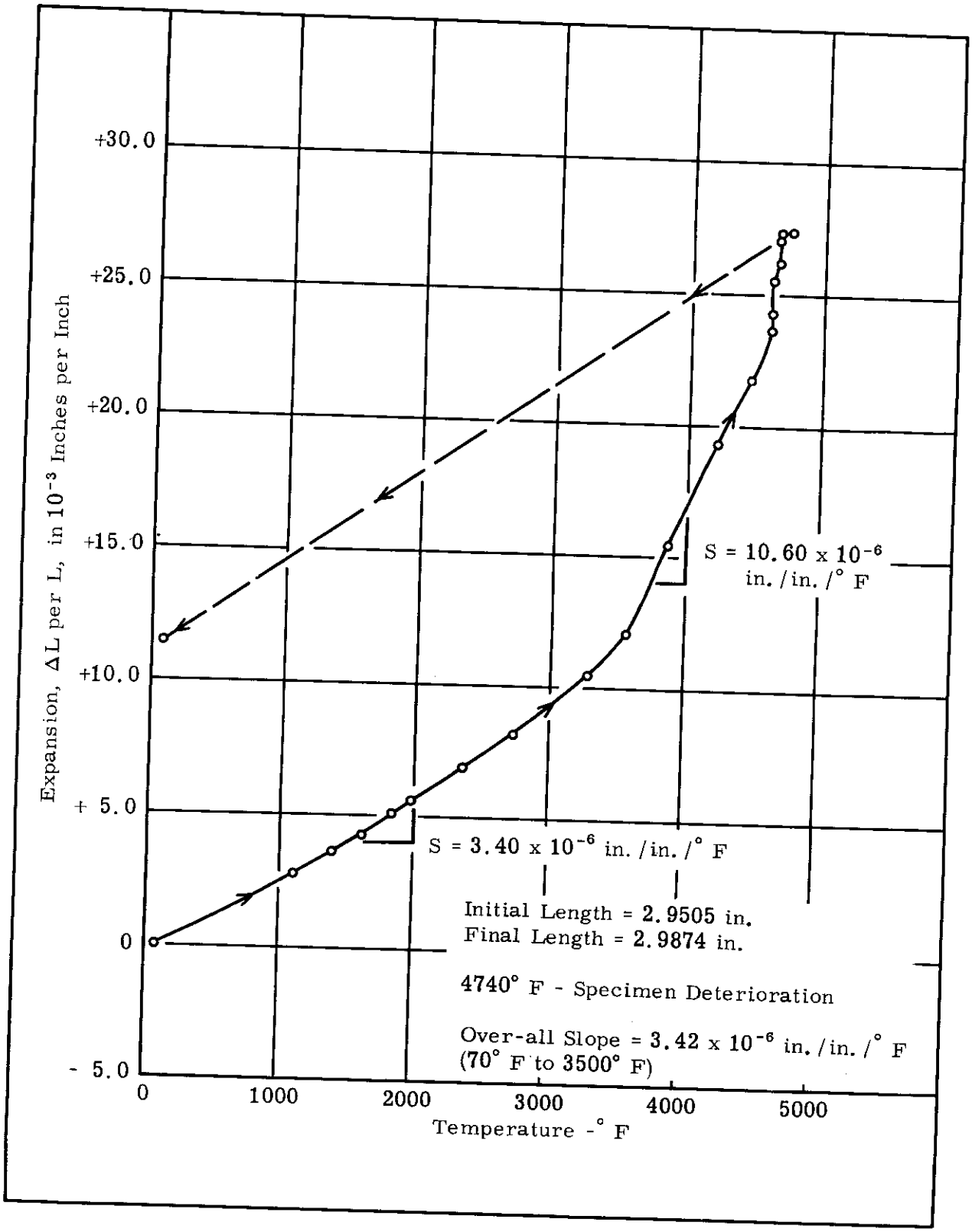

Figure A-22. Thermal Expansion of Columbium Carbide.

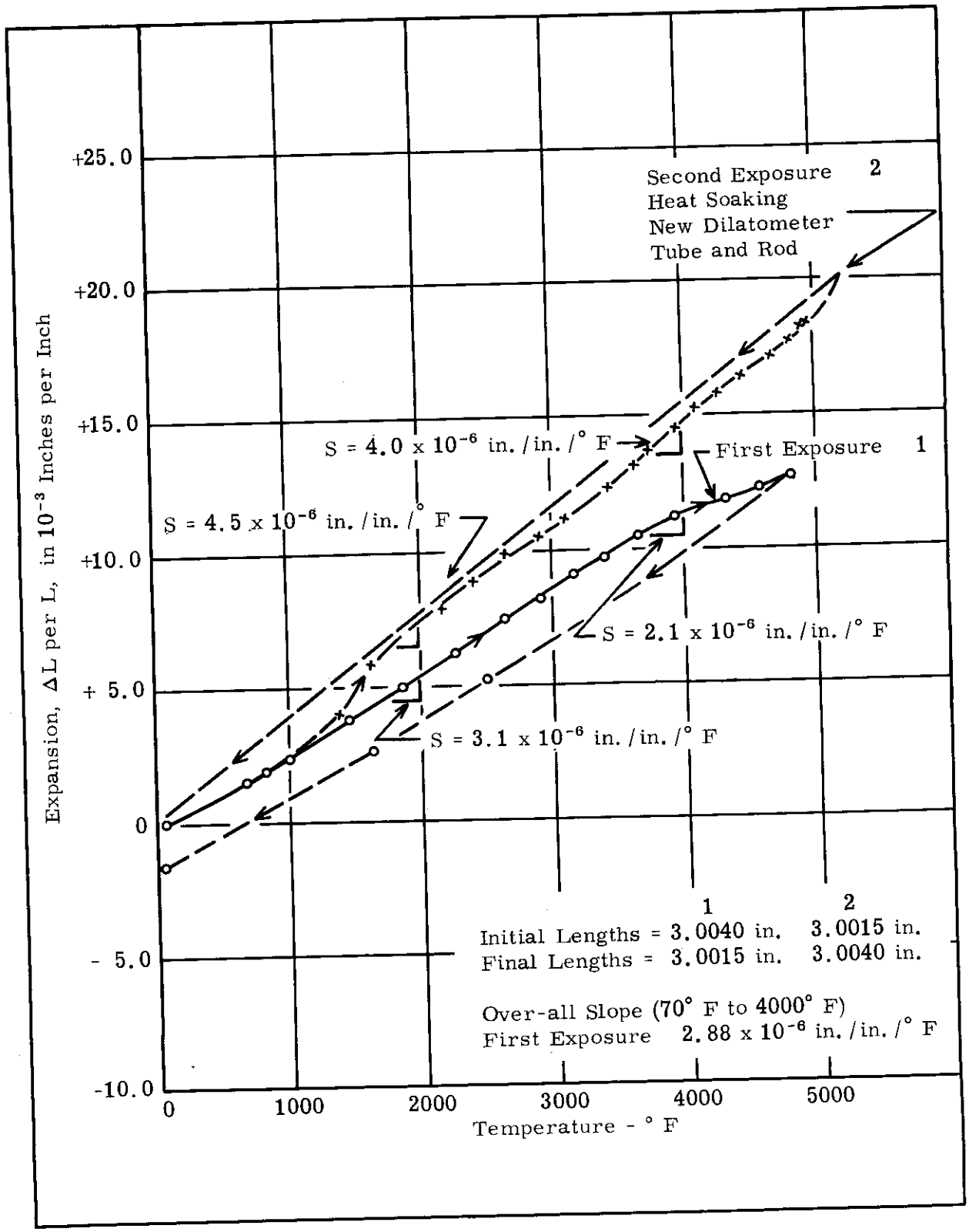

Figure A-23. Thermal Expansion of Hafnium Carbide.

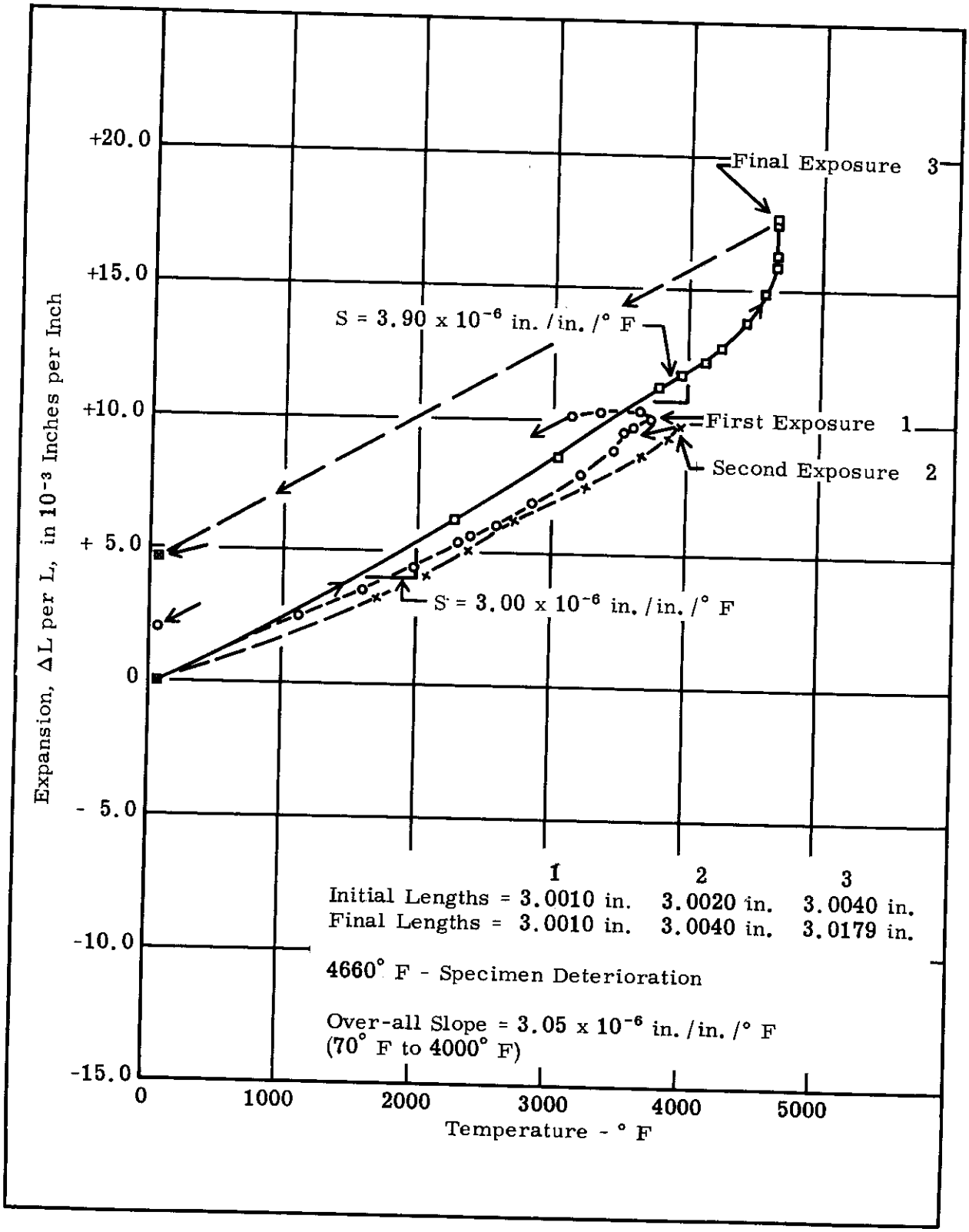

Figure A-24. Thermal Expansion of Tantalum Carbide.

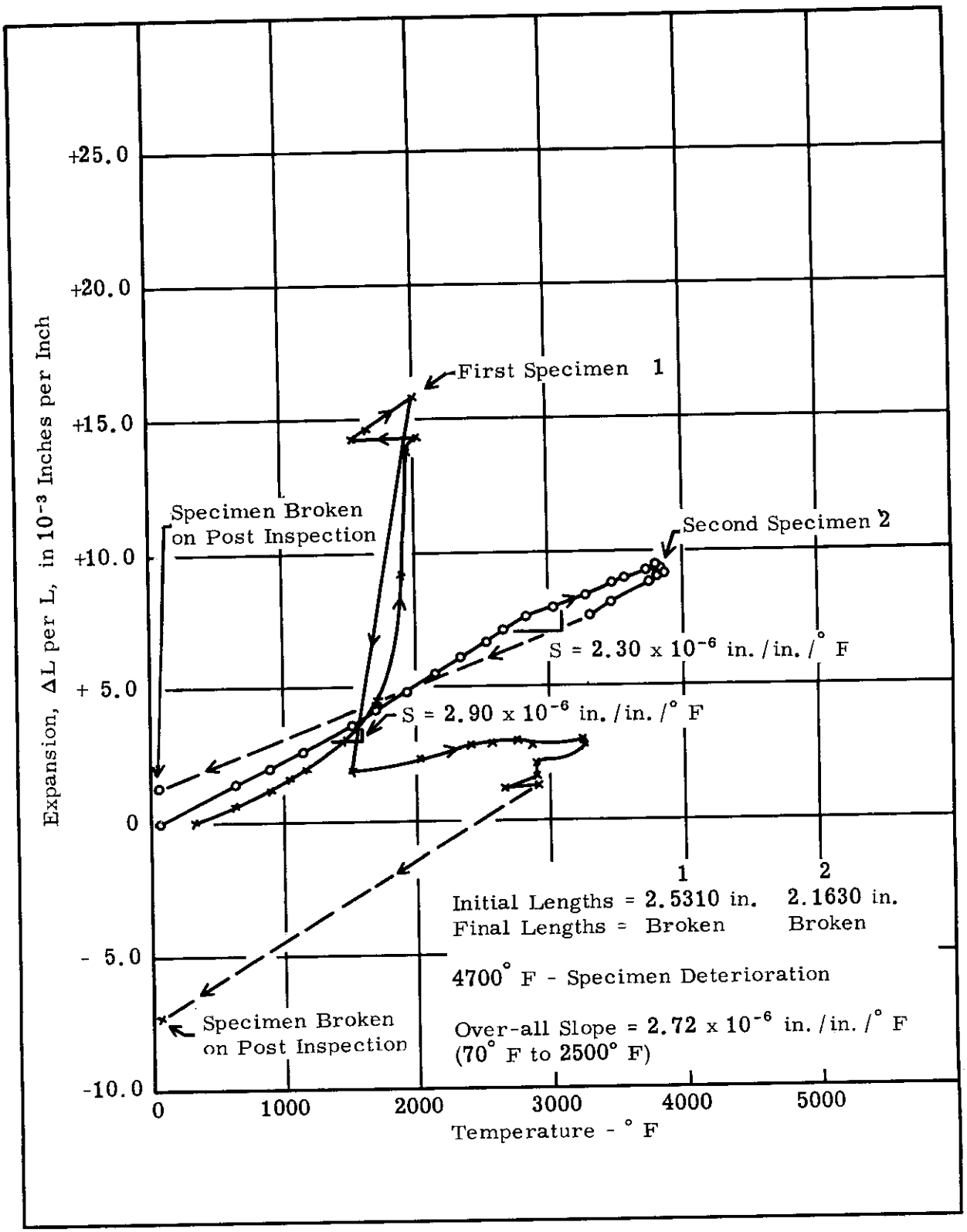

Figure A-25. Thermal Expansion of Zirconium Carbide.

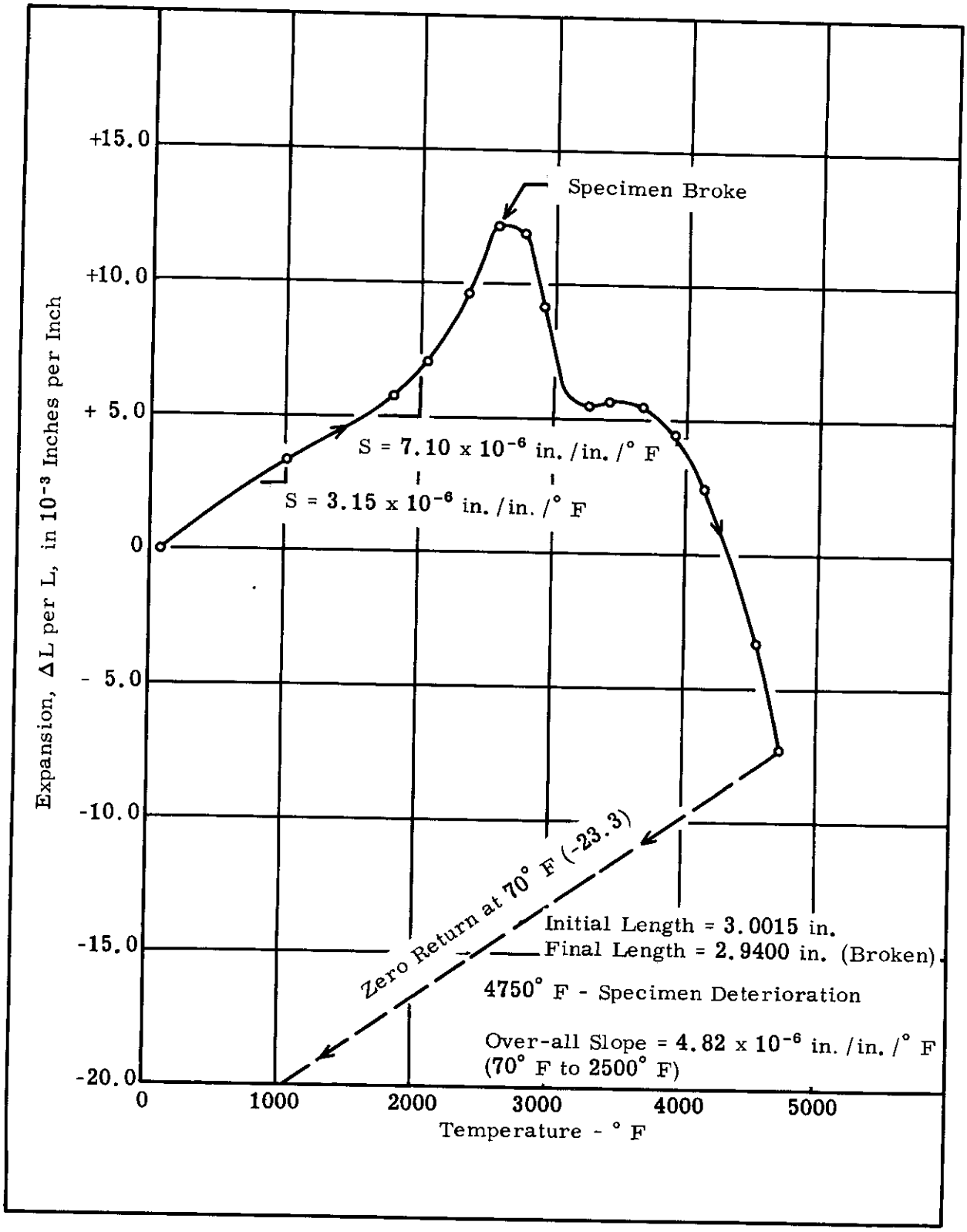

Figure A-26. Thermal Expansion of Hafnium Nitride.

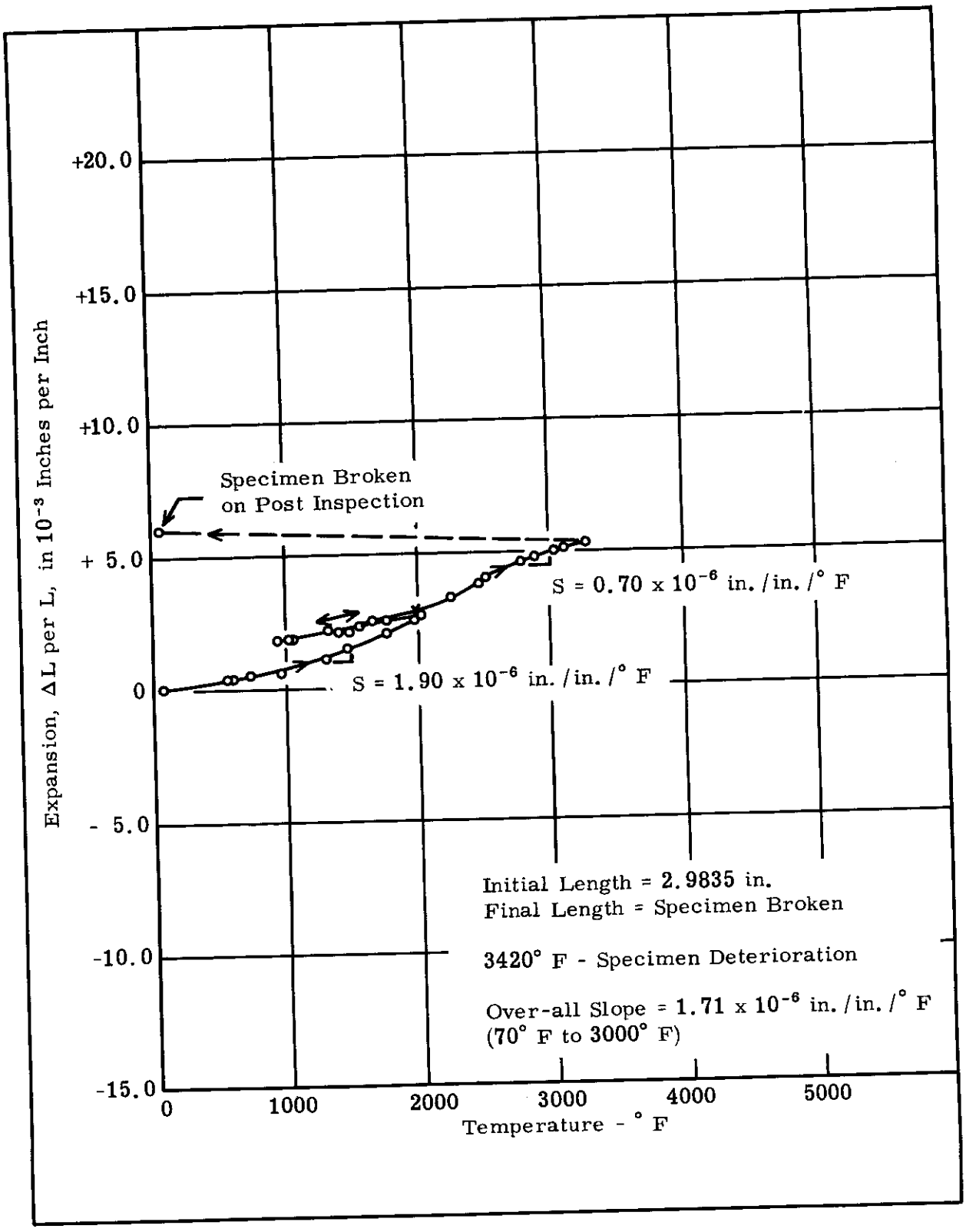

Figure A-27. Thermal Expansion of Silicon Nitride.

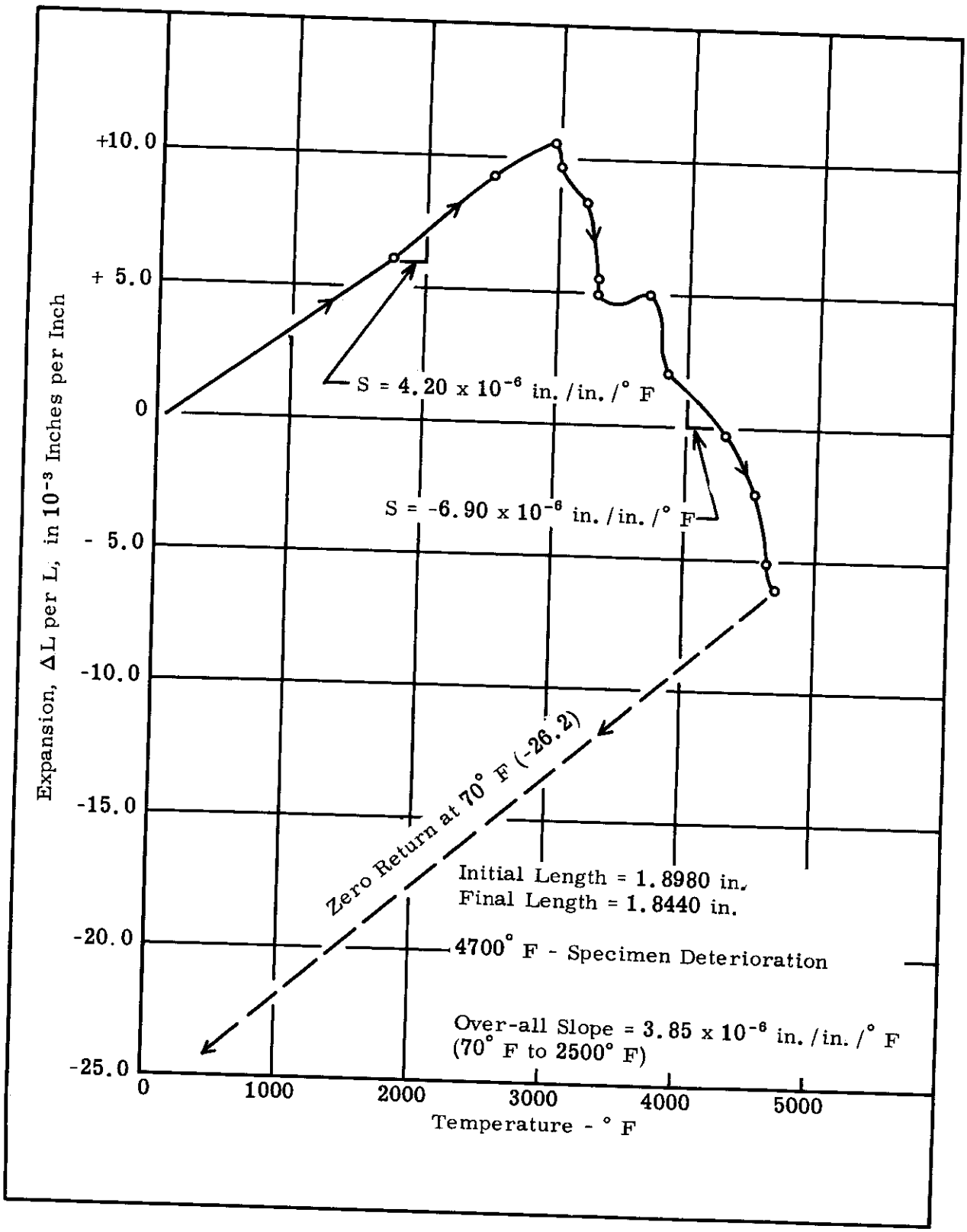

Figure A-28. Thermal Expansion of Titanium Nitride.

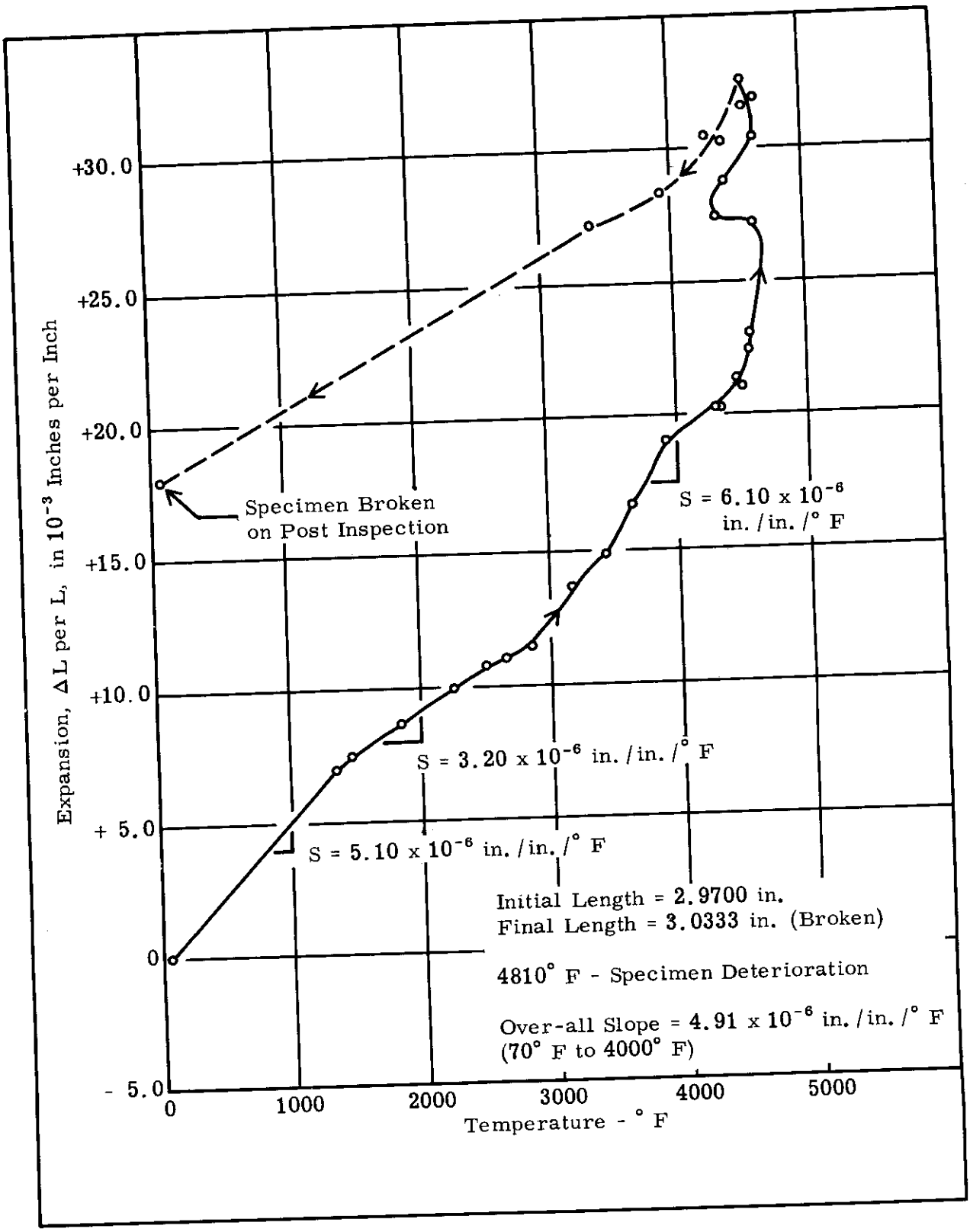

Figure A-29. Thermal Expansion of Zirconium Nitride.

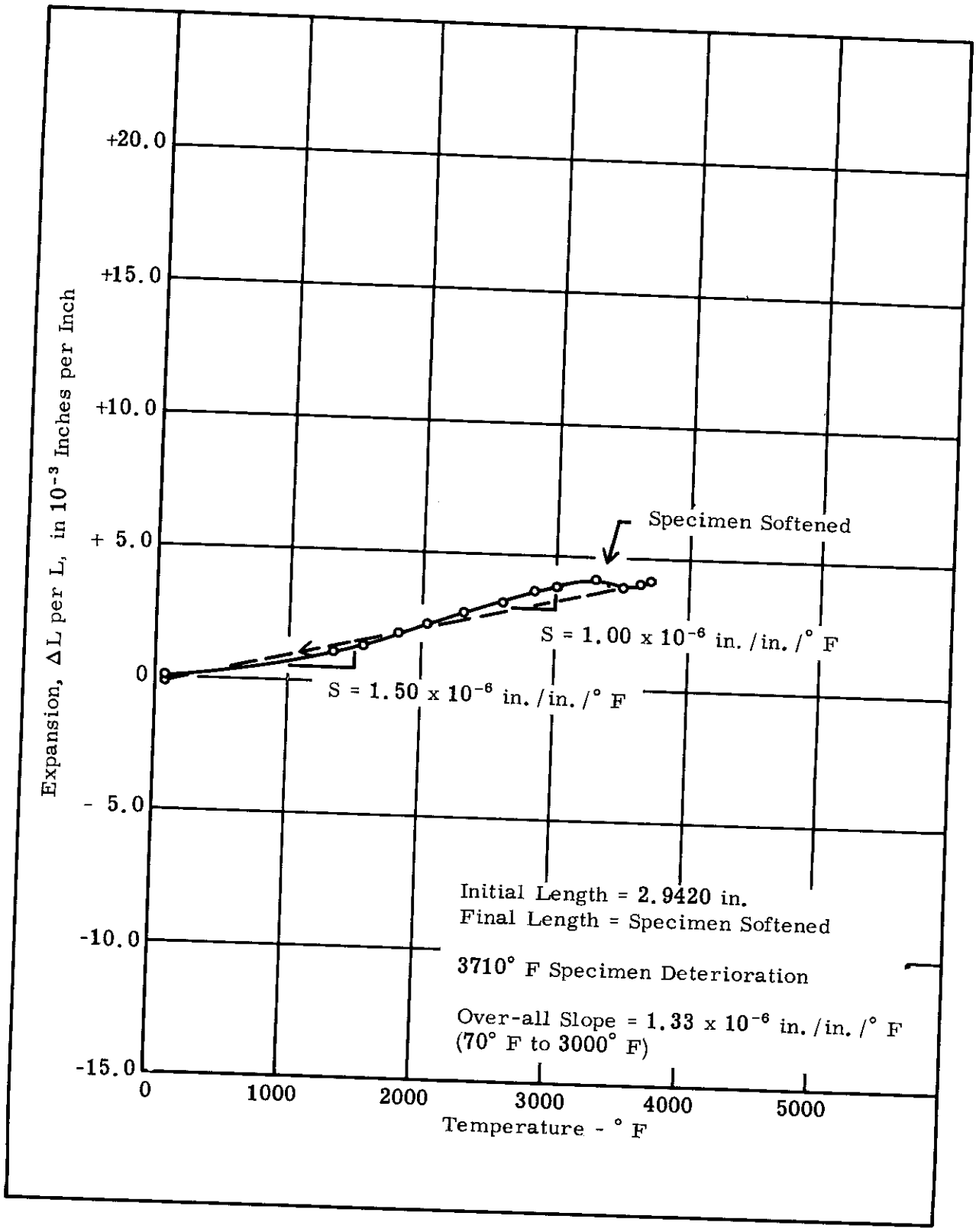

Figure A-30. Thermal Expansion of Zirconium Silicate.

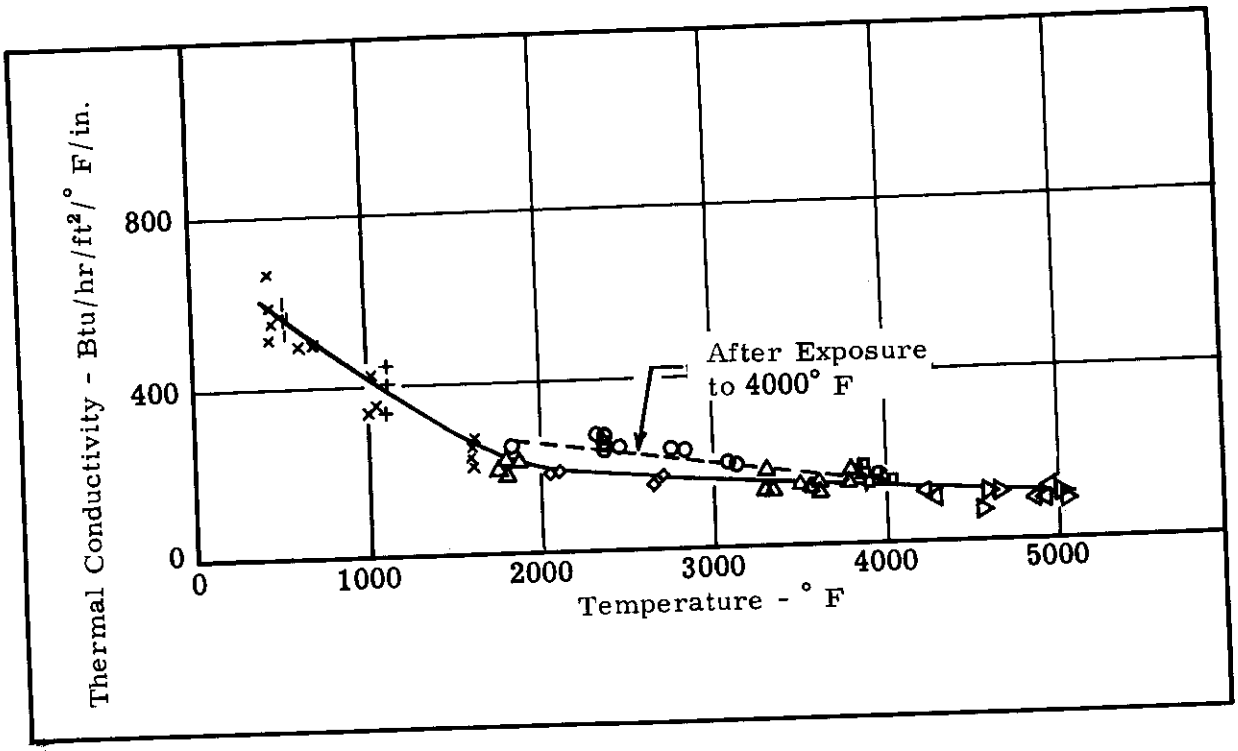

Figure A-31. Thermal Conductivity of ATJ Graphite.

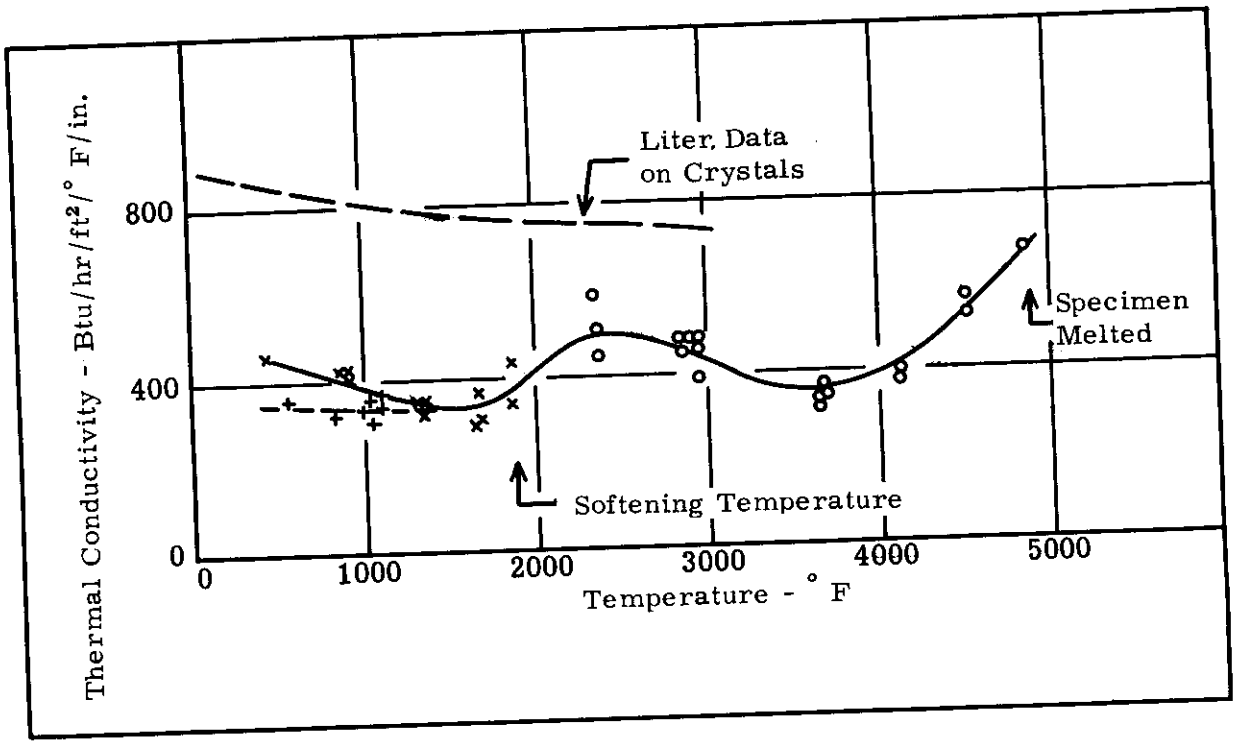

Figure A-32. Thermal Conductivity of Arc-Cast Tungsten.

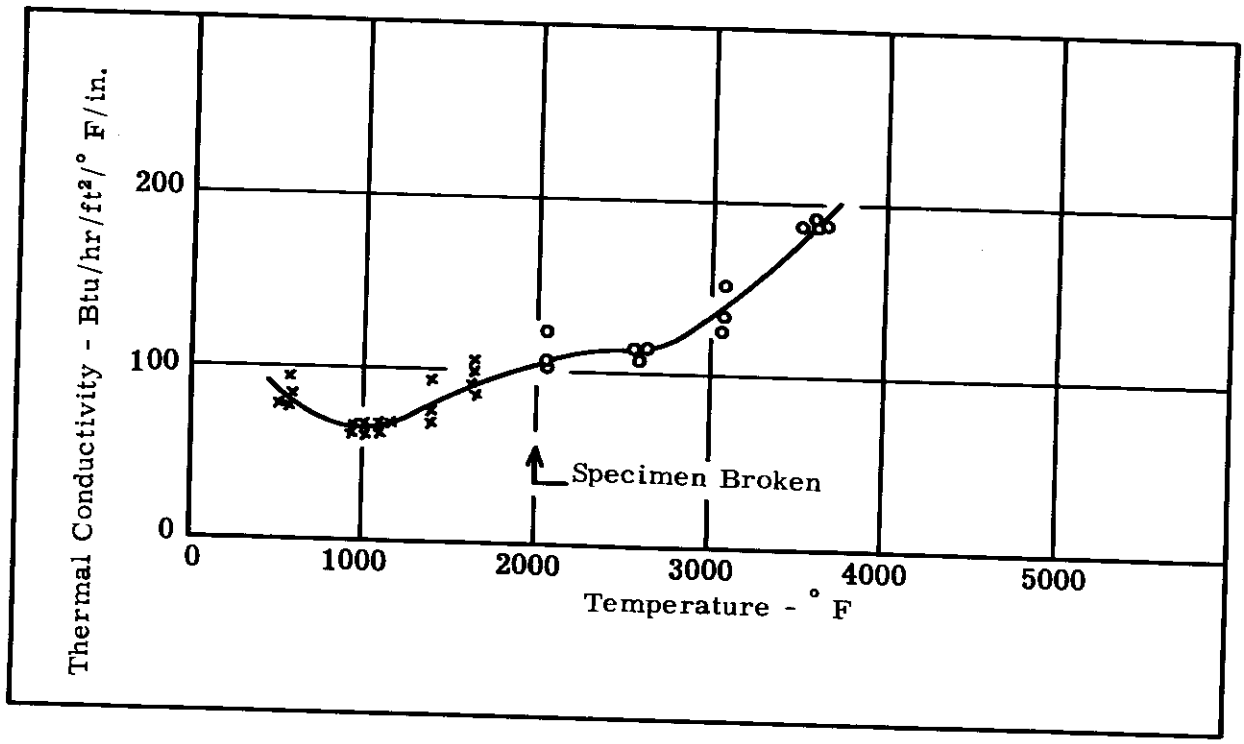

Figure A-33. Thermal Conductivity of Hafnium Nitride.

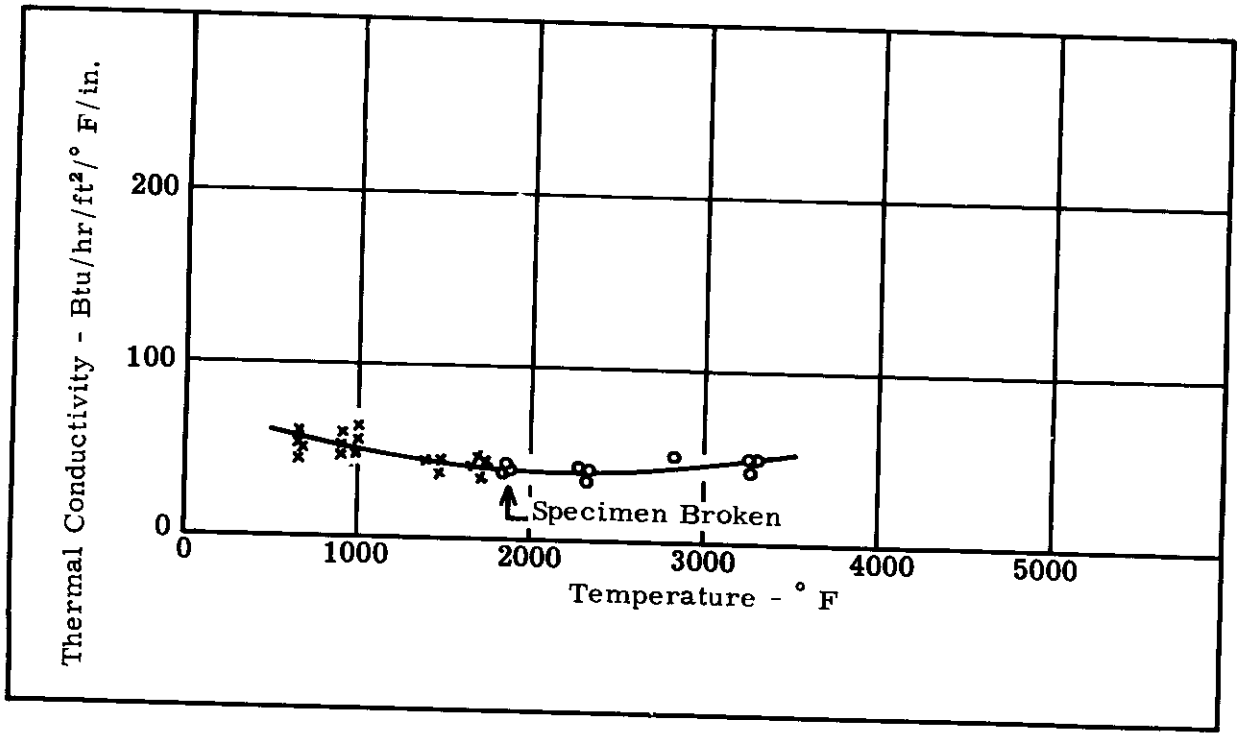

Figure A-34. Thermal Conductivity of Silicon Nitride.

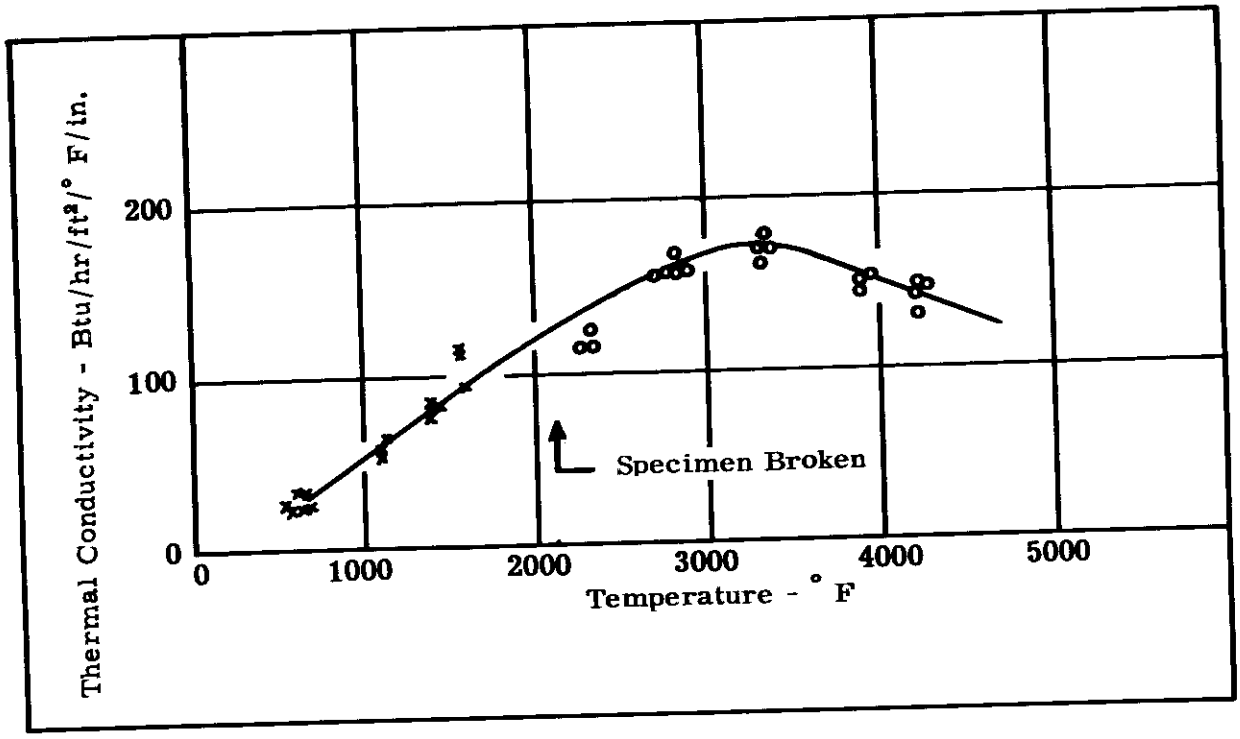

Figure A-35. Thermal Conductivity of Titanium Nitride.

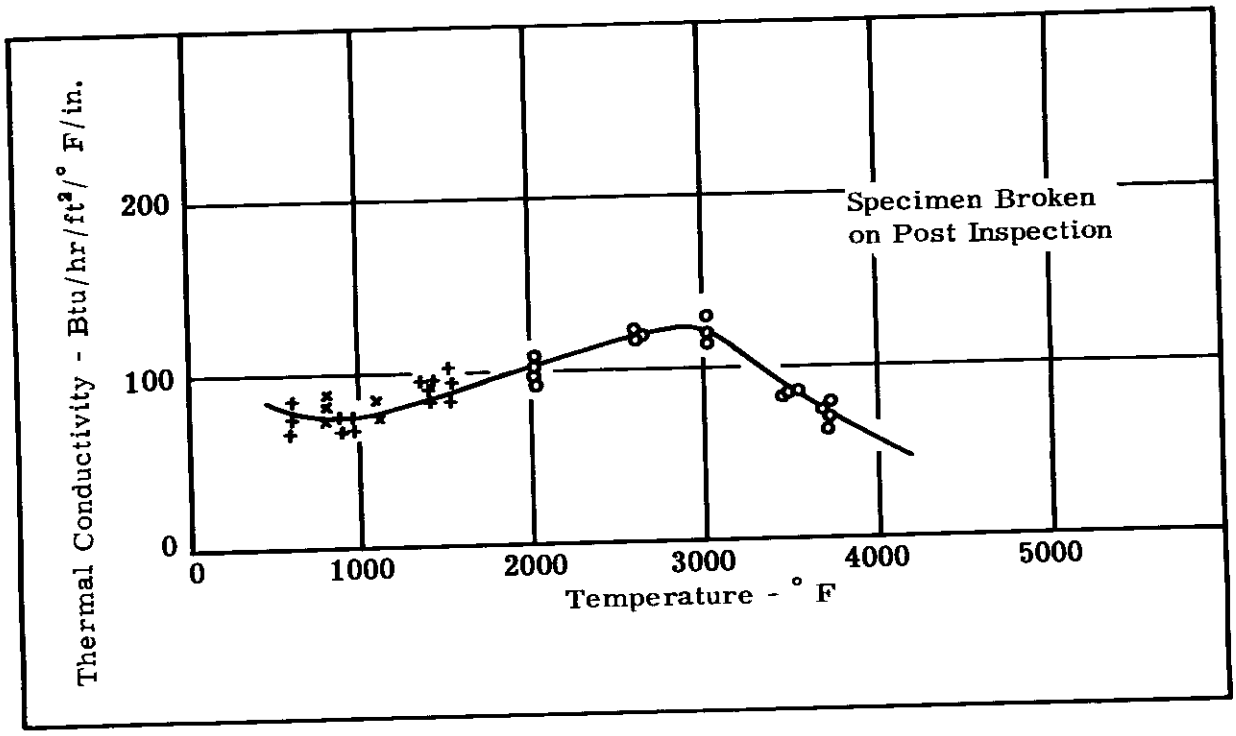

Figure A-36. Thermal Conductivity of Zirconium Nitride.

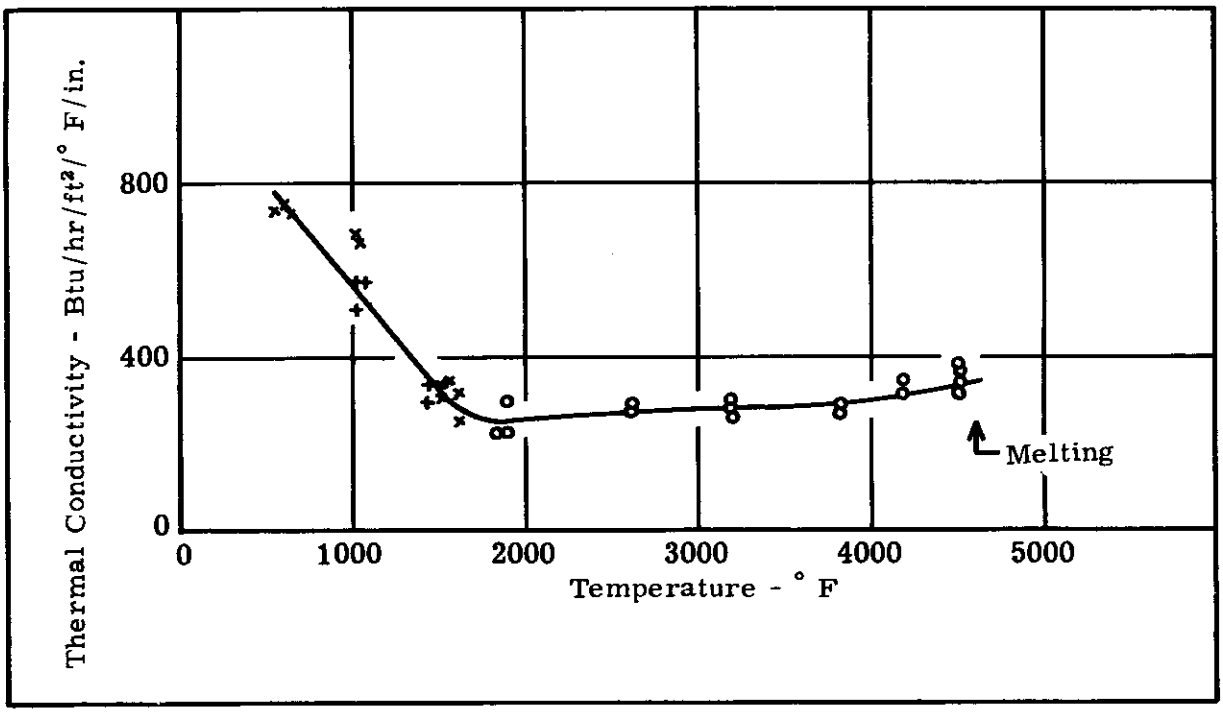

Figure A-37. Thermal Conductivity of Tantalum Boride.

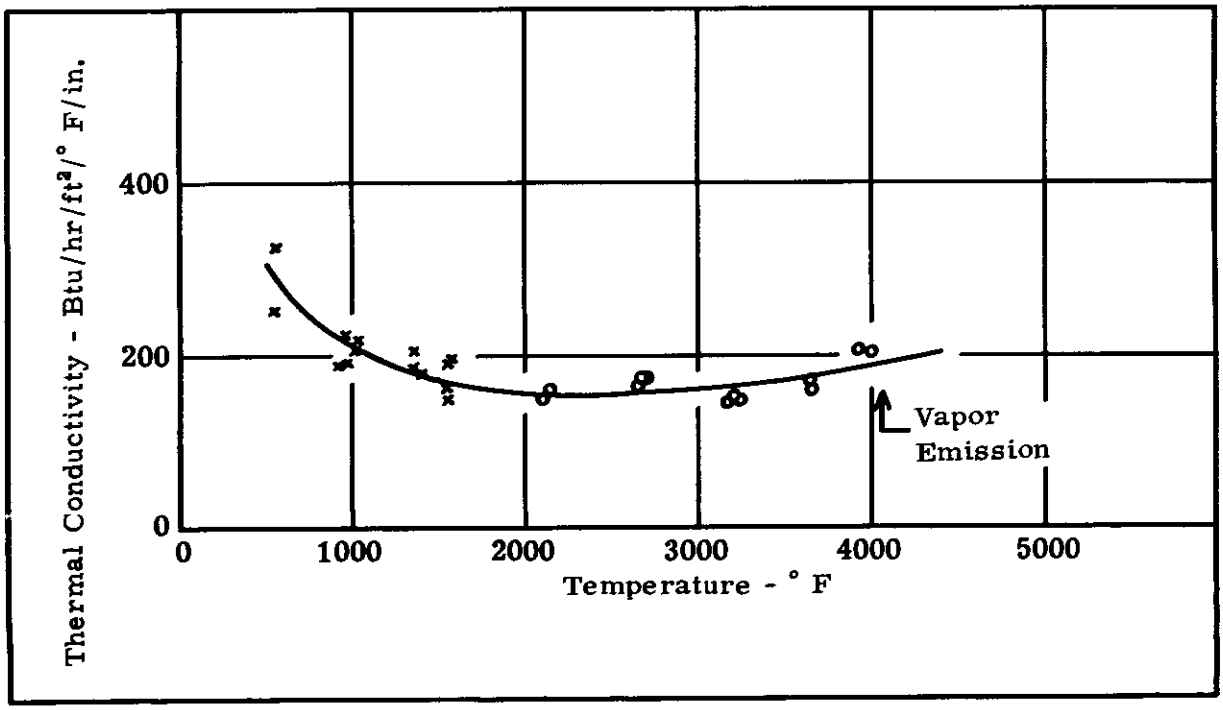

Figure A-38. Thermal Conductivity of Zirconium Boride.

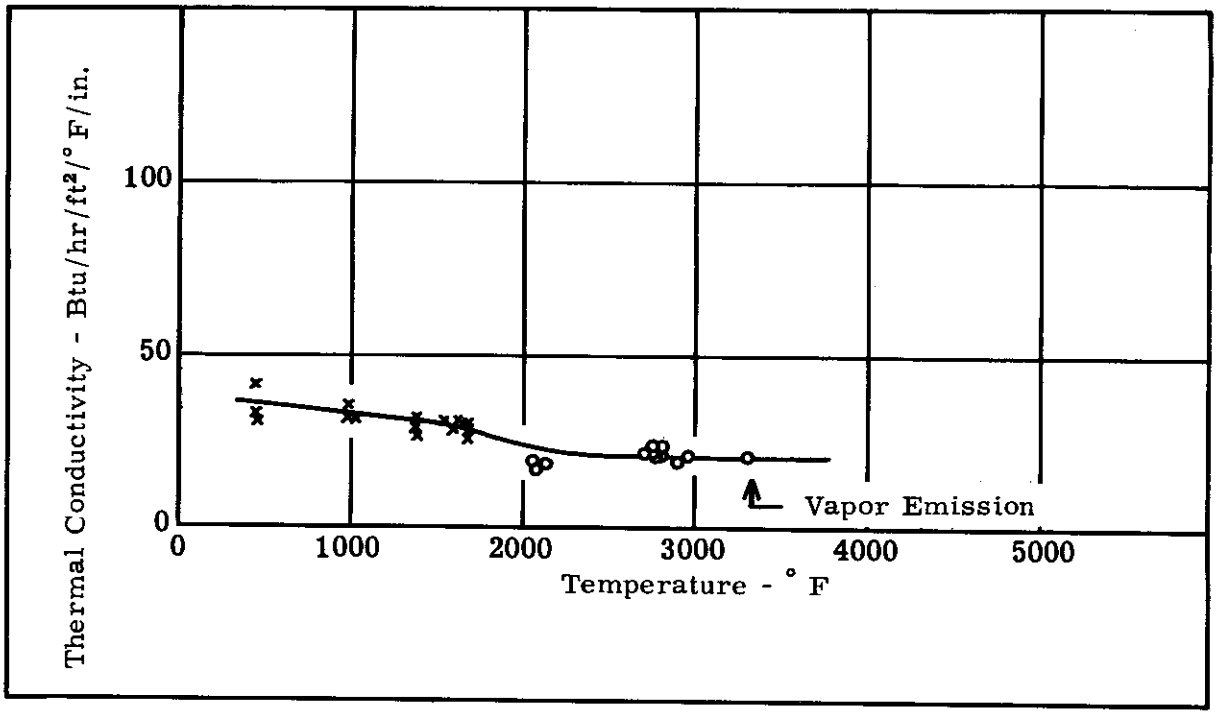

Figure A-39. Thermal Conductivity of Zirconium Silicate.

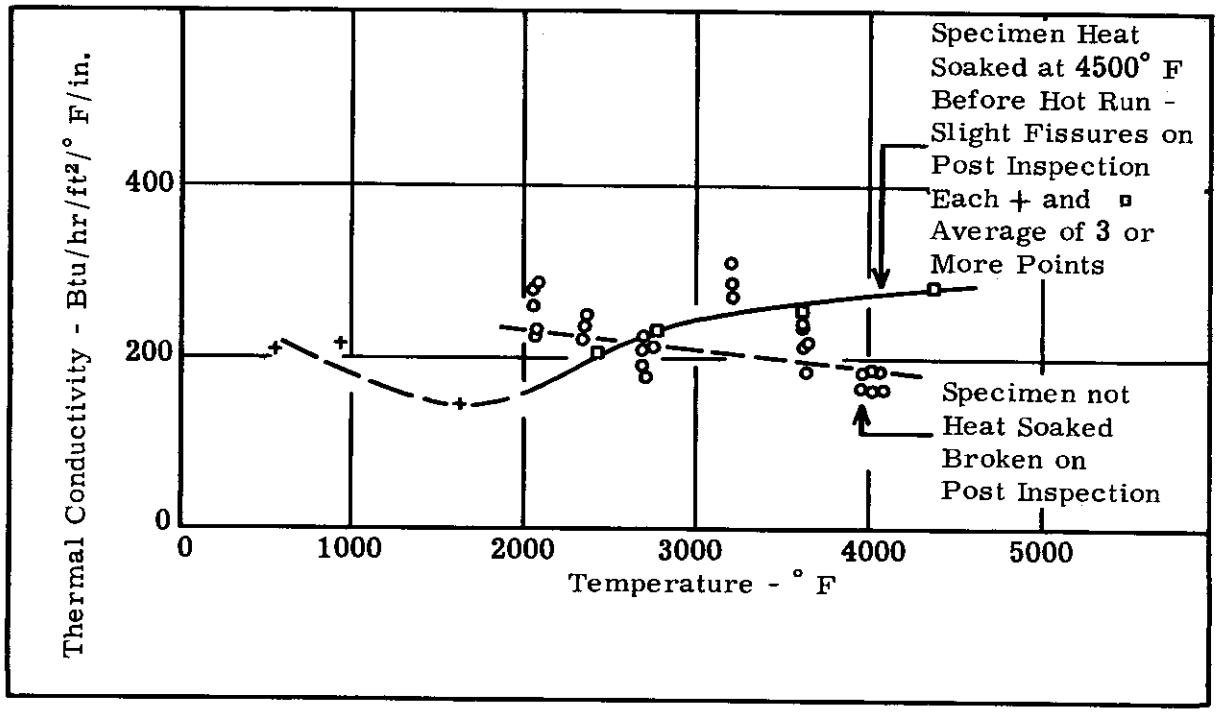

Figure A-40. Thermal Conductivity of Columbium Carbide.

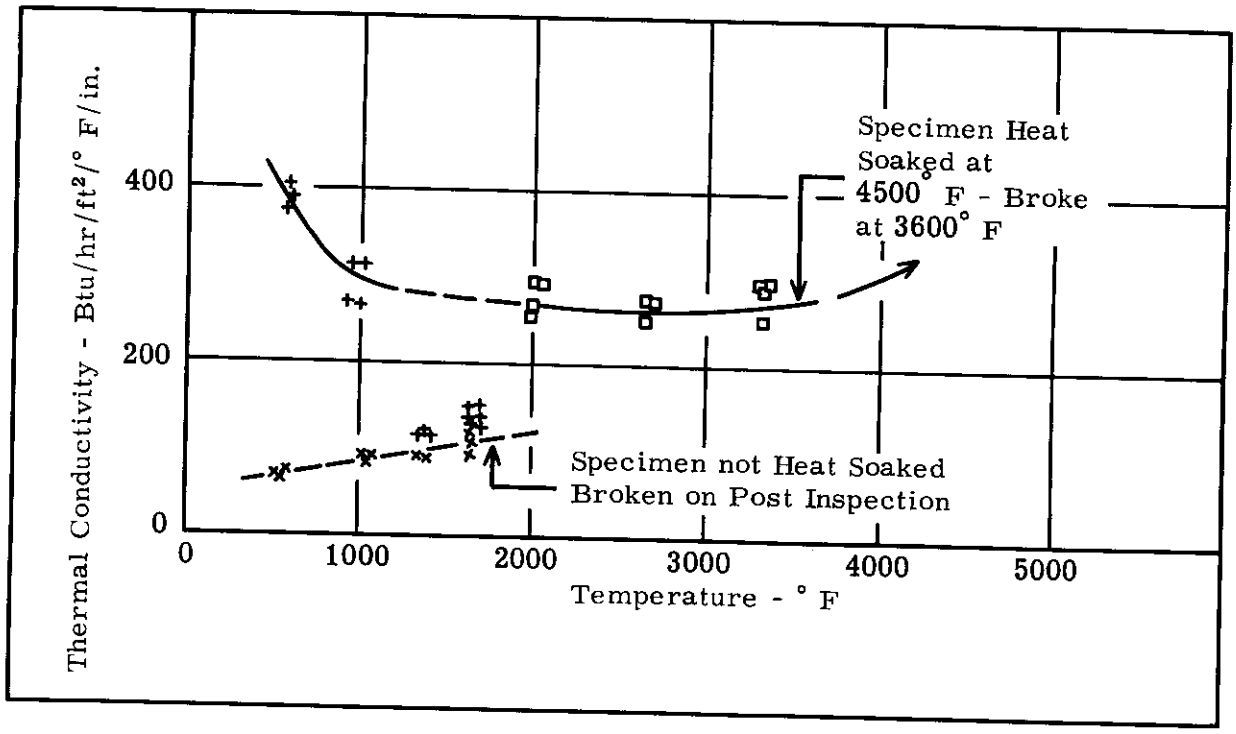

Figure A-41. Thermal Conductivity of Hafnium Carbide.

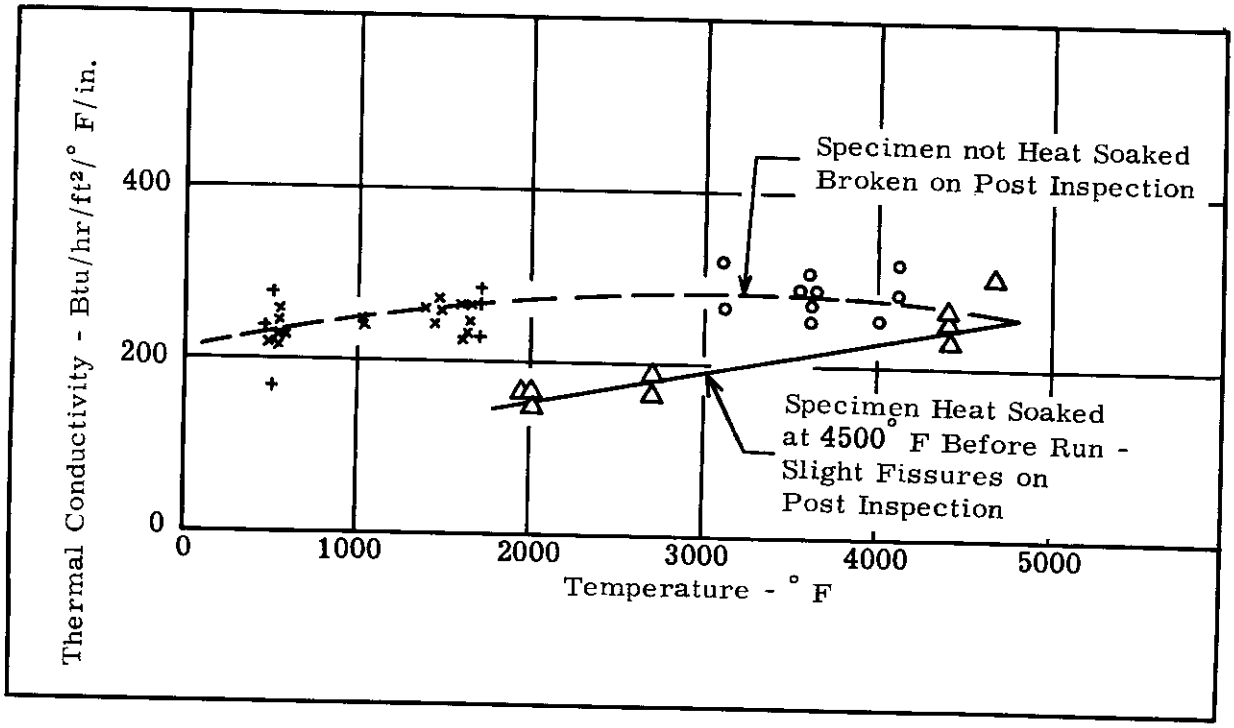

Figure A-42. Thermal Conductivity of Tantalum Carbide.

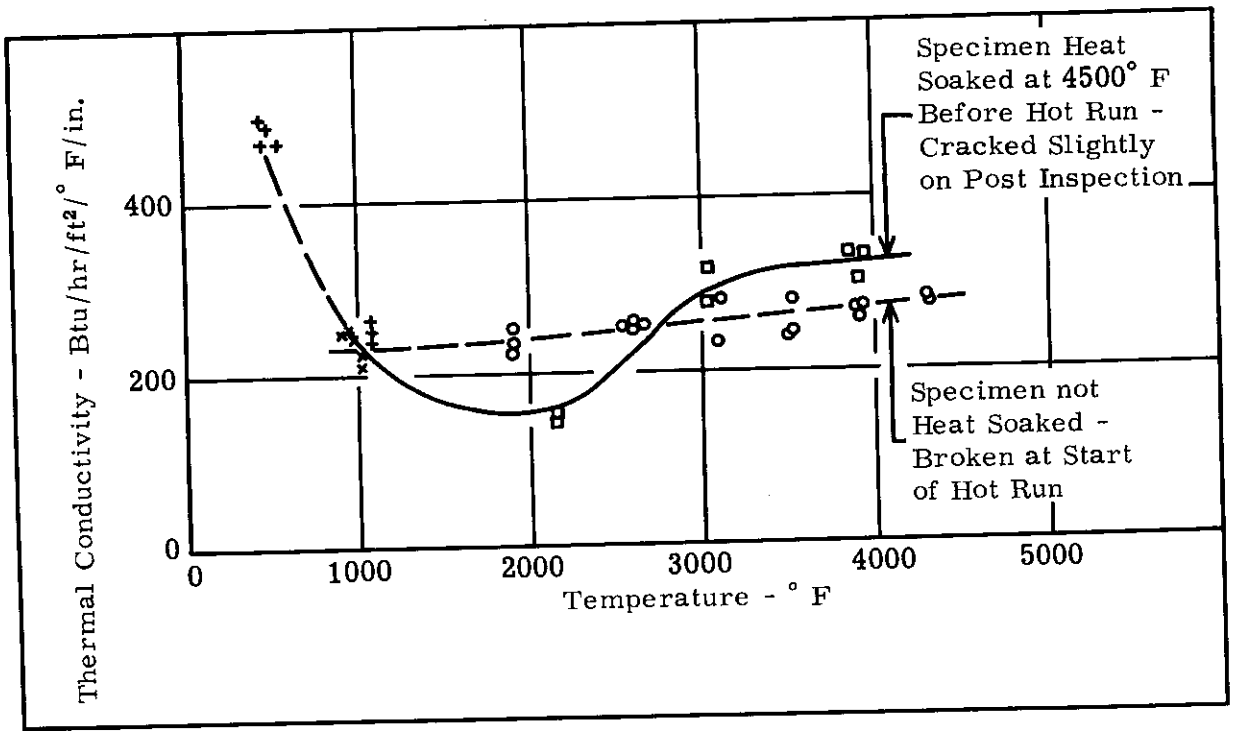

Figure A-43. Thermal Conductivity of Zirconium Carbide.

APPENDIX 2

Data Tables for the Heat Capacity, Thermal Expansion, and Thermal Conductivity Specimens and Calibrators

Table A-1

Enthalpy and Heat Content Data for ATJ Graphite

Recorded Data					Calculated Heat Content	
SRI Run Number	Drop Temperature ° F	Initial Weight Grams	Final Weight Grams	Enthalpy from Drop Temperature to 32° F Btu/lb	Mean Temperature for Calculated Heat Content ° F	Calculated Heat Content from Slope for ± 500° F Around Mean Temperature Btu/lb/° F
HC 16	515	10.695	10.695	93.6	500	0.27
HC 21	517	10.460	10.460	95.5	1000	0.34
HC 15	699	10.695	10.695	194.0	1500	0.42
HC 20	709	10.460	10.460	175.0	2000	0.57
HC 17	1002	10.695	10.645	274.0	2500	0.65
HC 18	1506	10.645	10.550	482.0	3000	0.60
HC 19	1988	10.550	10.460	683.0	3500	0.46
HC 65	2002	10.796	10.790	720.0	4000	0.38
HC 32	2426	10.460	10.375	1030.0	4500	0.46
HC 87	3030	10.790	10.780	1360.0	5000	0.54
HC 126	3400	10.780	10.775	1600.0		
HC 140	4100	10.775	10.775	1840.0		
HC 153	4550	10.775	10.775	2020.0		
HC 185	5150	10.980	10.765	2390.0		

Table A-2

Enthalpy and Heat Content Data for Tungsten

Recorded Data					Calculated Heat Content	
SRI Run Number	Drop Temperature ° F	Initial Weight Grams	Final Weight Grams	Enthalpy from Drop Temperature to 32° F Btu/lb	Mean Temperature for Calculated Heat Content ° F	Calculated Heat Content from Slope for ± 500° F Around Mean Temperature Btu/lb/° F
HC 28	484	96.260	96.260	13.4	500	0.031
HC 22	508	96.260	96.260	12.4	1000	0.034
HC 27	971	96.260	96.260	29.7	1500	0.038
HC 24	994	96.260	96.260	35.0	2000	0.045
HC 25	1498	96.260	96.260	47.6	2500	0.049
HC 26	1970	96.260	96.260	67.8	3000	0.049
HC 33	2411	96.260	96.250	91.8	3500	0.049
HC 92	2959	96.210	96.210	111.0	4000	0.047
HC 128	3400	96.210	96.210	152.0	4500	0.046
HC 142	4130	96.210	96.310	172.0	5000	0.120
HC 149	4530	96.310	96.400	191.0		
HC 186	4975	92.570	92.730	248.0		
	5010 Specimen Melted					

Table A-3

Enthalpy and Heat Content Data for Hafnium Nitride

Recorded Data					Calculated Heat Content	
SRI Run Number	Drop Temperature ° F	Initial Weight Grams	Final Weight Grams	Enthalpy from Drop Temperature to 32° F Btu/lb	Mean Temperature for Calculated Heat Content ° F	Calculated Heat Content from Slope for ± 500° F Around Mean Temperature Btu/lb/° F
HC 156	503	65.635	65.625	24.7	500	[1] (0.062) 0.060 (0.072)
HC 158	1056	65.625	65.625	59.3	1000	0.072 (0.077)
HC 160	1493	65.625	65.625	95.0	1500	0.078 (0.080)
HC 162	1995	65.625	65.688	135.0	2000	0.078 (0.079)
HC 164	2460	61.600	61.515	169.0	2500	0.078 (0.074)
HC 166	3060	61.515	61.410	217.0	3000	0.076 (0.068)
HC 168	3525	61.410	61.300	253.0	3500	0.066 (0.054)
HC 170	4065	61.300	61.220	277.0	4000	0.061 (0.039)
HC 172	4500	61.220	61.130	311.0	4500	0.053
HC 174	4600	61.130	61.110	317.0		
HC 178	4750	61.055	61.025	357.0		
	4750 Specimen Deterioration					

[1] Values in parentheses in this column were calculated from the equation for the enthalpy versus temperature for this material.

Table A-4

Enthalpy and Heat Content Data for Silicon Nitride

Recorded Data					Calculated Heat Content	
SRI Run Number	Drop Temperature ° F	Initial Weight Grams	Final Weight Grams	Enthalpy from Drop Temperature to 32° F Btu/lb	Mean Temperature for Calculated Heat Content ° F	Calculated Heat Content from Slope for ± 500° F Around Mean Temperature Btu/lb/° F
HC 54	495	12.510	12.535	69.4	500	0.21
HC 61	497	12.580	12.585	77.1	1000	0.26
HC 59	1000	12.570	12.580	212.0	1500	0.27
HC 43	1008	12.510	12.510	217.0	2000	0.33
HC 44	1492	12.510	12.530	342.0	2500	0.36
HC 45	1988	12.530	12.510	502.0	3000	0.38
HC 55	2457	12.535	12.570	602.0	3500	0.38
HC 91	2978	12.520	12.350	855.0		
HC 129	3420	12.350	02.780	1010.0		
	3420 Specimen Deterioration					

Table A-5

Enthalpy and Heat Content Data for Titanium Nitride

Recorded Data					Calculated Heat Content	
SRI Run Number	Drop Temperature ° F	Initial Weight Grams	Final Weight Grams	Enthalpy from Drop Temperature to 32° F Btu/lb	Mean Temperature for Calculated Heat Content ° F	Calculated Heat Content from Slope for ± 500° F Around Mean Temperature Btu/lb/° F
HC 106	499	22.865	22.865	72.9	500	0.155
HC 110	1036	22.865	23.005	165.0	1000	0.180
HC 112	1508	23.005	23.092	262.0	1500	0.215
HC 114	2013	23.092	23.245	362.0	2000	0.255
HC 118	2510	23.245	23.440	515.0	2500	0.285
HC 120	2920	23.440	23.235	653.0	3000	0.280
HC 125	3400	23.235	22.950	759.0	3500	0.260
HC 176	3900	22.390	22.385	898.0	4000	0.235
HC 144	4650	22.950	22.685	1050.0	4500	0.220
	4700 Specimen Deterioration					

Table A-6

Enthalpy and Heat Content Data for Zirconium Nitride

Recorded Data					Calculated Heat Content	
SRI Run Number	Drop Temperature ° F	Initial Weight Grams	Final Weight Grams	Enthalpy from Drop Temperature to 32° F Btu/lb	Mean Temperature for Calculated Heat Content ° F	Calculated Heat Content from Slope for ± 500° F Around Mean Temperature Btu/lb/° F
HC 34	501	36.950	36.950	48.1	500	0.081
HC 52	501	37.065	37.085	40.7	1000	0.103
HC 51	1005	37.095	37.065	79.5	1500	0.135
HC 35	1016	36.950	36.950	88.5	2000	0.142
HC 36	1496	36.950	37.050	167.0	2500	0.140
HC 64	1499	36.910	36.920	158.0	3000	0.140
HC 37	1919	37.050	37.095	212.0	3500	0.140
HC 66	2011	36.920	36.590	222.0	4000	0.140
HC 57	2453	37.085	37.050	247.0	4500	0.140
HC 103	3040	35.730	35.730	337.0	5000	0.140
HC 107	3650	35.740	35.710	495.0		
HC 175	3720	35.620	35.615	444.0		
HC 133	4150	35.710	35.680	540.0		
HC 145	4380	35.680	35.635	521.0		
HC 180	4810	35.615	35.525	614.0		
	4810 Specimen Deterioration					

Table A-7

Enthalpy and Heat Content Data for Tantalum Boride

Recorded Data					Calculated Heat Content	
SRI Run Number	Drop Temperature ° F	Initial Weight Grams	Final Weight Grams	Enthalpy from Drop Temperature to 32° F Btu/lb	Mean Temperature for Calculated Heat Content ° F	Calculated Heat Content from Slope for ± 500° F Around Mean Temperature Btu/lb/° F
HC 53	502	64.885	64.890	28.2	500	0.060
HC 38	521	64.850	64.850	33.4	1000	0.087
HC 39	992	64.850	64.850	54.2	1500	0.100
HC 48	1004	64.900	64.885	62.7	2000	0.110
HC 40	1522	64.850	64.915	113.0	2500	0.110
HC 41	2007	64.915	64.900	164.0	3000	0.110
HC 58	2446	64.890	64.825	217.0	3500	0.110
HC 68	2994	64.825	64.795	261.0	4000	0.110
HC 124	3400	64.795	64.785	346.0	4500	0.110
HC 138	4125	64.785	64.780	381.0		
HC 146	4610	64.780	64.815	470.0		
	4610 Specimen Deterioration					

Table A-8

Enthalpy and Heat Content Data for Zirconium Boride

Recorded Data					Calculated Heat Content	
SRI Run Number	Drop Temperature ° F	Initial Weight Grams	Final Weight Grams	Enthalpy from Drop Temperature to 32° F Btu/lb	Mean Temperature for Calculated Heat Content ° F	Calculated Heat Content from Slope for ± 500° F Around Mean Temperature Btu/lb/° F
HC 100	498	22.735	22.735	51.7	500	0.125
HC 101	1023	22.735	22.735	126.0	1000	0.158
HC 102	1522	22.735	22.735	231.0	1500	0.186
HC 104	2041	22.735	22.860	318.0	2000	0.201
HC 105	2600	22.860	22.805	426.0	2500	0.205
HC 115	3010	22.805	22.770	500.0	3000	0.205
HC 127	3400	22.635	22.505	606.0	3500	0.205
HC 141	4130	22.435	22.405	750.0	4000	0.205
	4750 Specimen Deterioration					

Table A-9

Enthalpy and Heat Content Data for Zirconium Silicate

Recorded Data					Calculated Heat Content	
SRI Run Number	Drop Temperature ° F	Initial Weight Grams	Final Weight Grams	Enthalpy from Drop Temperature to 32° F Btu/lb	Mean Temperature for Calculated Heat Content ° F	Calculated Heat Content from Slope for ± 500° F Around Mean Temperature Btu/lb/° F
HC 108	490	20.895	20.895	49.9	500	0.135
HC 109	1069	20.895	20.895	152.0	1000	0.193
HC 111	1510	20.895	20.895	264.0	1500	0.225
HC 113	1998	20.895	20.835	366.0	2000	0.225
HC 116	2510	20.890	20.895	478.0	2500	0.240
HC 119	3020	20.885	20.850	619.0	3000	0.290
HC 121	3400	20.850	19.350	741.0	3500	0.320
	3710 Specimen Deterioration					

Table A-10

Enthalpy and Heat Content Data for Columbium Carbide

Recorded Data					Calculated Heat Content	
SRI Run Number	Drop Temperature ° F	Initial Weight Grams	Final Weight Grams	Enthalpy from Drop Temperature to 32° F Btu/lb	Mean Temperature for Calculated Heat Content ° F	Calculated Heat Content from Slope for ± 500° F Around Mean Temperature Btu/lb/° F
HC 84	495	49.238	49.238	29.6	500	0.090
HC 73	524	49.280	49.280	32.9	1000	0.115
HC 75	1007	49.280	49.280	94.6	1500	0.120
HC 88	1018	49.238	49.205	82.8	2000	0.118
HC 77	1479	49.280	49.280	144.0	2500	0.128
HC 80	2004	49.280	49.245	209.0	3000	0.142
HC 82	2479	49.245	49.238	256.0	3500	0.140
HC 94	2994	49.200	49.180	336.0	4000	0.140
HC 177	3500	49.135	49.135	413.0	4500	0.140
HC 154	4150	49.150	49.150	492.0		
HC 136	4160	49.140	49.250	504.0		
HC 179	4740	49.135	49.135	579.0		
	4740 Specimen Deterioration					

Table A-11

Enthalpy and Heat Content Data for Hafnium Carbide

Recorded Data					Calculated Heat Content	
SRI Run Number	Drop Temperature ° F	Initial Weight Grams	Final Weight Grams	Enthalpy from Drop Temperature to 32° F Btu/lb	Mean Temperature for Calculated Heat Content ° F	Calculated Heat Content from Slope for ± 500° F Around Mean Temperature Btu/lb/° F
HC 157	512	62.565	62.555	24.0	500	0.055
HC 159	1027	62.555	62.585	62.5	1000	0.067
HC 161	1501	62.585	62.685	83.7	1500	0.071
HC 163	1993	62.685	62.825	124.0	2000	0.071
HC 165	2465	58.810	58.800	163.0	2500	0.072
HC 167	3060	58.800	58.770	204.0	3000	0.072
HC 169	3530	58.770	58.750	238.0	3500	0.071
HC 171	4050	58.750	58.710	274.0	4000	0.071
HC 187	4440	58.250	58.220	321.0	4500	0.070
HC 183	4970	58.645	58.360	320.0	5000	0.070

Table A-12

Enthalpy and Heat Content Data for Tantalum Carbide

Recorded Data					Calculated Heat Content	
SRI Run Number	Drop Temperature ° F	Initial Weight Grams	Final Weight Grams	Enthalpy from Drop Temperature to 32° F Btu/lb	Mean Temperature for Calculated Heat Content ° F	Calculated Heat Content from Slope for ± 500° F Around Mean Temperature Btu/lb/° F
HC 74	508	86.920	86.920	20.8	500	0.050
HC 76	1002	86.920	86.920	49.0	1000	0.060
HC 85	1496	86.620	86.620	80.6	1500	0.069
HC 81	2004	86.920	86.910	119.0	2000	0.078
HC 83	2456	86.910	86.902	162.0	2500	0.082
CC 93	2860	86.615	86.590	184.0	3000	0.082
HC 122	3515	86.590	86.545	258.0	3500	0.082
HC 137	4170	86.545	86.530	286.0	4000	0.082
HC 150	4510	86.530	86.140	324.0	4500	0.082
	4660 Specimen Deterioration					

Table A-13

Enthalpy and Heat Content Data for Zirconium Carbide

Recorded Data					Calculated Heat Content	
SRI Run Number	Drop Temperature ° F	Initial Weight Grams	Final Weight Grams	Enthalpy from Drop Temperature to 32° F Btu/lb	Mean Temperature for Calculated Heat Content ° F	Calculated Heat Content from Slope for ± 500° F Around Mean Temperature Btu/lb/° F
HC 46	500	35.110	35.110	38.4	500	0.091
HC 47	995	35.110	35.110	78.1	1000	0.110
HC 60	1011	35.130	35.130	100.0	1500	0.125
HC 49	1483	35.110	35.110	158.0	2000	0.125
HC 50	1997	35.110	35.110	214.0	2500	0.125
HC 56	2438	35.110	35.130	255.0	3000	0.125
HC 95	2975	34.360	34.335	342.0	3500	0.130
HC 96	3800	34.335	34.330	433.0	4000	0.150
HC 98	4200	34.320	34.320	517.0	4500	0.170
HC 99	4420	34.320	34.320	500.0		
HC 147	4700	34.320	34.305	608.0		
	4700 Specimen Deterioration					

Table A-14

Enthalpy and Heat Content Data for Electrolytic Copper

Recorded Data					Calculated Heat Content	
SRI Run Number	Drop Temperature ° F	Initial Weight Grams	Final Weight Grams	Enthalpy from Drop Temperature to 32° F Btu/lb	Mean Temperature for Calculated Heat Content ° F	Calculated Heat Content from Slope for ± 500° F Around Mean Temperature Btu/lb/° F
HC 155	521	29.650	29.650	46.5	500	0.094
	641	66.415	66.415	59.5	1000	0.101
HC 134	1007	29.700	29.660	93.0	1500	0.108
HC 117	1166	29.815	29.700	110.0		
	1532	67.000	67.000	152.0		
	1562	68.000	68.000	152.0		

Table A-15

Enthalpy and Heat Content Data for Sapphire

Recorded Data					Calculated Heat Content	
SRI Run Number	Drop Temperature ° F	Initial Weight Grams	Final Weight Grams	Enthalpy from Drop Temperature to 32° F Btu/lb	Mean Temperature for Calculated Heat Content ° F	Calculated Heat Content from Slope for ± 500° F Around Mean Temperature Btu/lb/° F
HC 3	497	21.765	21.765	97.6	500	0.240
HC 4	1008	21.765	21.765	235.0	1000	0.280
HC 5	1503	21.765	21.765	391.0	1500	0.320
HC 6	2005	21.765	21.765	548.0	2000	0.325
HC 7	2100	21.765	21.765	613.0	2500	0.320
HC 67	2148	21.730	21.690	590.0	3000	0.320
HC 31	2456	21.765	21.730	686.0		
HC 69	3006	21.690	21.685	875.0		

Table A-16

Enthalpy Data for 304 Stainless Steel Basket

Recorded Data				
SRI Run Number	Drop Temperature ° F	Initial Weight Grams	Final Weight Grams	Enthalpy from Drop Temperature to 32° F Btu/lb
HC 10	497	4.855	4.855	81.5
HC 29	673	4.855	4.855	105.0
HC 89	703	4.855	4.855	111.0
HC 90	873	4.855	4.855	134.0
HC 86	1005	4.855	4.855	108.0
HC 72	1006	4.855	4.855	91.6
HC 11	1012	4.855	4.855	160.0
HC 30	1344	4.855	4.855	134.0
HC 63	1496	4.855	4.855	196.0
HC 12	1503	4.855	4.855	196.0
HC 135	1569	4.855	4.855	229.0
HC 13	2005	4.855	4.875	295.0
HC 14	2057	4.875	4.935	306.0

Table A-17

Enthalpy Data for CS Graphite Basket

Recorded Data				
SRI Run Number	Drop Temperature ° F	Initial Weight Grams	Final Weight Grams	Enthalpy from Drop Temperature to 32° F Btu/lb
HC 130	2500	3.215	3.215	1030
HC 71	2524	3.215	3.215	876
HC 70	3001	3.215	3.215	1190
HC 131	3010	3.215	3.215	1040
HC 132	3600	3.215	3.215	1380
HC 143	4150	3.215	3.215	1730

Table A-18

Equations Expressing the Heat Capacity and Enthalpy as Functions of Temperature

Material	Equation for Enthalpy of Material H in Btu/lb and T in ° F	Equation for Heat Content of Material HC in Btu/lb/° F and T in ° F
ATJ Graphite	$H = -37.33 + 207.0 \times 10^{-3}T + 121.8 \times 10^{-6}T^2 - 14.06 \times 10^{-9}T^3$	$HC = 207.0 \times 10^{-3} + 243.6 \times 10^{-6}T - 42.18 \times 10^{-9}T^2$
Tungsten	$H = 5.432 + 11.98 \times 10^{-3}T + 13.76 \times 10^{-6}T^2 - 1.627 \times 10^{-9}T^3$	$HC = 11.98 \times 10^{-3} + 27.52 \times 10^{-6}T - 4.881 \times 10^{-9}T^2$
Hafnium Nitride	$H = -21.08 + 85.70 \times 10^{-3}T - 5.118 \times 10^{-6}T^2 + 0.6422 \times 10^{-9}T^3$	$HC = 85.70 \times 10^{-3} - 10.236 \times 10^{-6}T + 1.9266 \times 10^{-9}T^2$
Silicon Nitride	$H = -72.18 + 311.6 \times 10^{-3}T - 39.93 \times 10^{-6}T^2 + 12.31 \times 10^{-9}T^3$	$HC = 311.6 \times 10^{-3} - 79.86 \times 10^{-6}T + 36.93 \times 10^{-9}T^2$
Titanium Nitride	$H = 43.15 + 24.21 \times 10^{-3}T + 94.23 \times 10^{-6}T^2 - 11.36 \times 10^{-9}T^3$	$HC = 24.21 \times 10^{-3} + 188.46 \times 10^{-6}T - 34.08 \times 10^{-9}T^2$
Zirconium Nitride	* $H = 0.3726 + 71.0 \times 10^{-3}T + 22.30 \times 10^{-6}T^2 - 2.231 \times 10^{-9}T^3$	$HC = 71.0 \times 10^{-3} + 44.60 \times 10^{-6}T - 6.693 \times 10^{-9}T^2$
Tantalum Boride	$H = -1.8063 + 46.49 \times 10^{-3}T + 22.137 \times 10^{-6}T^2 - 2.2874 \times 10^{-9}T^3$	$HC = 46.49 \times 10^{-3} + 44.274 \times 10^{-6}T - 6.8622 \times 10^{-9}T^2$
Zirconium Boride	$H = -0.3478 + 76.24 \times 10^{-3}T + 49.21 \times 10^{-6}T^2 - 5.773 \times 10^{-9}T^3$	$HC = 76.24 \times 10^{-3} + 98.42 \times 10^{-6}T - 17.319 \times 10^{-9}T^2$
Zirconium Silicate	$H = -57.78 + 220.3 \times 10^{-3}T - 18.93 \times 10^{-6}T^2 + 6.776 \times 10^{-9}T^3$	$HC = 220.3 \times 10^{-3} - 37.86 \times 10^{-6}T + 20.328 \times 10^{-9}T^2$
Columbium Carbide	$H = -20.64 + 100.5 \times 10^{-3}T + 6.497 \times 10^{-6}T^2 - 0.1154 \times 10^{-9}T^3$	$HC = 100.5 \times 10^{-3} + 12.994 \times 10^{-6}T - 0.3462 \times 10^{-9}T^2$
Hafnium Carbide	$H = 8.169 + 28.62 \times 10^{-3}T + 19.57 \times 10^{-6}T^2 - 2.494 \times 10^{-9}T^3$	$HC = 28.62 \times 10^{-3} + 39.14 \times 10^{-6}T - 7.482 \times 10^{-9}T^2$
Tantalum Carbide	$H = 2.674 + 26.25 \times 10^{-3}T + 21.36 \times 10^{-6}T^2 - 2.576 \times 10^{-9}T^3$	$HC = 26.25 \times 10^{-3} + 42.72 \times 10^{-6}T - 7.728 \times 10^{-9}T^2$
Zirconium Carbide	$H = -39.41 + 150.3 \times 10^{-3}T - 18.67 \times 10^{-6}T^2 + 3.210 \times 10^{-9}T^3$	$HC = 150.3 \times 10^{-3} - 37.34 \times 10^{-6}T + 9.630 \times 10^{-9}T^2$
Sapphire	$H = -23.34 + 215.6 \times 10^{-3}T + 53.08 \times 10^{-6}T^2 - 8.554 \times 10^{-9}T^3$	$HC = 215.6 \times 10^{-3} + 106.16 \times 10^{-6}T - 25.662 \times 10^{-9}T^2$

* Slight Adjustment from Least Squares

Note: 1 All enthalpy-temperature equations obtained on computer by least squares fit to a cubic.
2 Heat content-temperature equations obtained from derivative of enthalpy-temperature equation.
3 All equations obtained from observed data with zero enthalpy reference at 32° F.

Table A-19

Thermal Expansion of ATJ Graphite

Temperature °F	Observed Total Elongation 10^{-3} inches	Observed Unit Elongation 10^{-3} inches/inch	Unit Elongation Correction for Dilatometer Motion 10^{-3} inches/inch	Corrected Specimen Unit Elongation 10^{-3} inches/inch
70 [1]	0	0	0	0
1430	2.8	0.9	1.1	2.0
1530	3.0	1.0	1.2	2.2
1850	3.8	1.3	1.6	2.9
2270	4.5	1.5	2.1	3.6
2450	4.8	1.6	2.3	3.9
2650	5.3	1.8	2.7	4.5
2850	5.8	1.9	3.0	4.9
3000	6.3	2.1	3.2	5.3
3220	7.2	2.4	3.5	5.9
3540	8.4	2.8	4.0	6.8
3770	9.0	3.0	4.4	7.4
70	5.2	1.7	0	1.7

Table A-19 (Continued)

Thermal Expansion of ATJ Graphite

Temperature °F	Observed Total Elongation 10^{-3} inches	Observed Unit Elongation 10^{-3} inches/inch	Unit Elongation Correction for Dilatometer Motion 10^{-3} inches/inch	Corrected Specimen Unit Elongation 10^{-3} inches/inch
70 [2]	0	0	0	0
1100	2.0	0.7	0.7	1.4
1375	2.9	1.0	1.0	2.0
1820	4.0	1.3	1.5	2.8
2130	4.7	1.6	2.0	3.6
2450	5.4	1.8	2.4	4.2
2680	6.0	2.0	2.7	4.7
3040	6.7	2.2	3.2	5.4
3390	7.4	2.5	3.7	6.2
3800	8.1	2.7	4.5	7.2
4050	9.3	3.1	4.9	8.0
4500	11.2	3.7	5.6	9.3
4770	13.4	4.5	6.2	10.7
4950	13.7	4.6	6.5	11.1
3620	5.9	2.0	4.2	6.2
2350	3.1	1.0	2.2	3.2
70	1.0	0.3	0	0.3

Table A-19 (Continued)

Thermal Expansion of ATJ Graphite

Temperature ° F	Observed Total Elongation 10^{-3} inches	Observed Unit Elongation 10^{-3} inches/inch	Unit Elongation Correction for Dilatometer Motion 10^{-3} inches/inch	Corrected Specimen Unit Elongation 10^{-3} inches/inch
70 [3]	0	0	0	0
600	2.6	0.9	0.4	1.3
600	2.7	0.9	0.4	1.3
1090	4.5	1.5	0.7	2.2
1610	6.7	2.2	1.3	3.5
2100	8.8	2.9	1.9	4.8
2600	10.2	3.4	2.6	6.0
2850	12.3	4.1	3.0	7.1
3260	14.7	4.9	3.5	8.4
3650	16.5	5.5	4.2	9.7
3950	18.1	6.1	4.7	10.8
4310	19.3	6.5	5.3	11.8
4325	20.1	6.7	5.3	12.0
4570	22.3	7.5	5.7	13.2
4860	24.2	8.1	6.3	14.4
5000	25.6	8.6	6.5	15.1
5075	27.6	9.2	6.6	15.8
3800	24.6	8.2	4.5	12.7
2920	24.1	8.1	3.0	11.1
2050	23.8	8.0	1.8	9.8
70	25.8	8.6	0	8.6

Zero return prevented by melted tungsten reflection shield

Table A-19 (Continued)

Thermal Expansion of ATJ Graphite

Temperature ° F	Observed Total Elongation 10^{-3} inches	Observed Unit Elongation 10^{-3} inches/inch	Unit Elongation Correction for Dilatometer Motion 10^{-3} inches/inch	Corrected Specimen Unit Elongation 10^{-3} inches/inch
70 [4]	0	0	0	0
1400	5.3	1.8	1.0	2.8
1500	6.1	2.0	1.1	3.1
1960	8.5	2.8	1.7	4.5
2480	10.7	3.6	2.4	6.0
3075	13.6	4.5	3.3	7.8
3500	15.5	5.2	4.0	9.2
3950	18.1	6.0	4.7	10.7
4500	20.6	6.9	5.6	12.5
3970	17.1	5.7	4.7	10.4
3500	13.6	4.5	4.0	8.5
2640	9.2	3.1	2.7	5.8
1620	4.5	1.5	1.3	2.8
70	- 0.3	-0.1	0	- 0.1

[1] Run SRI - E19
Initial Specimen Length = 2.9920"
Final Specimen Length = 2.9940"

[2] Run SRI - E30
Initial Specimen Length = 2.9909"
Final Specimen Length = 2.9953"

[3] Run SRI - E33
Initial Specimen Length = 2.9960"
Final Specimen Length = 2.9972"

[4] Run SRI - E34
Initial Specimen Length = 2.9970"
Final Specimen Length = 2.9970"

Table A-20

Thermal Expansion of Tungsten

Temperature °F	Observed Total Elongation 10^{-3} inches	Observed Unit Elongation 10^{-3} inches/inch	Unit Elongation Correction for Dilatometer Motion 10^{-3} inches/inch	Corrected Specimen Unit Elongation 10^{-3} inches/inch
70 [1]	0	0	0	0
1280	2.1	0.8	0.9	1.7
1380	2.2	0.8	1.0	1.8
1550	2.5	0.9	1.2	2.1
1730	2.8	1.1	1.5	2.6
2020	3.2	1.2	1.8	3.0
2220	3.5	1.3	2.1	3.4
2430	3.8	1.4	2.3	3.7
2650	4.1	1.5	2.7	4.2
2820	4.4	1.7	3.0	4.7
2930	4.5	1.7	3.1	4.8
2960	4.2	1.6	3.2	4.8
3230	4.5	1.7	3.5	5.2
3440	4.7	1.8	3.8	5.6
3650	4.6	1.7	4.2	5.9
70	-1.3	-0.5	0	-0.5
70 [2]	0	0	0	0
650	0.9	0.3	0.4	0.7
1370	1.5	0.6	1.0	1.6
1495	1.9	0.7	1.2	1.9
2000	2.9	1.1	1.7	2.8
2300	3.4	1.3	2.2	3.5
2510	3.9	1.5	2.5	4.0
2610	4.5	1.7	2.5	4.2
2840	4.8	1.8	3.0	4.8

Table A-20 (Continued)

Thermal Expansion of Tungsten

Temperature ° F	Observed Total Elongation 10^{-3} inches	Observed Unit Elongation 10^{-3} inches/inch	Unit Elongation Correction for Dilatometer Motion 10^{-3} inches/inch	Corrected Specimen Unit Elongation 10^{-3} inches/inch
3160	4.9	1.8	3.4	5.2
3320	5.0	1.9	3.7	5.6
3550	4.5	1.7	4.0	5.7
3660	4.2	1.6	4.2	5.8
3850	3.1	1.2	4.5	5.7
4180	2.9	1.1	5.0	6.1
4450	2.6	1.0	5.5	6.5
4575	2.0	0.8	5.8	6.6
4760	0.8	0.3	6.2	6.5
4860	-1.5	-0.6	6.3	5.7
4900	-3.8	-1.4	6.4	5.0
4920	-5.2	-2.0	6.4	4.4
4985	-7.0	-2.6	6.5	3.9
5010	Specimen Melted			

[1] Run SRI - E27
Initial Specimen Length = 2.6660"
Final Specimen Length = 2.6660"

[2] Run SRI - E31
Initial Specimen Length = 2.6660"
Final Specimen Length = Specimen Melted

Table A-21

Thermal Expansion of Tantalum Boride

Temperature ° F	Observed Total Elongation 10^{-3} inches	Observed Unit Elongation 10^{-3} inches/inch	Unit Elongation Correction for Dilatometer Motion 10^{-3} inches/inch	Corrected Specimen Unit Elongation 10^{-3} inches/inch
70 [1]	0	0	0	0
1100	4.6	1.5	0.7	2.2
1330	6.2	2.0	1.0	3.0
1470	8.7	2.8	1.1	3.9
1725	11.6	3.7	1.5	5.2
2050	13.8	4.4	1.8	6.2
2320	15.7	5.0	2.2	7.2
2510	17.3	5.5	2.5	8.0
2700	18.5	5.9	2.7	8.6
2940	19.3	6.1	3.1	9.2
3150	20.5	6.5	3.4	9.9
3350	22.0	7.0	3.7	10.7
3600	22.9	7.3	4.1	11.4
3700	22.9	7.3	4.3	11.6
3850	24.3	7.7	4.5	12.2
4220	25.2	8.0	5.2	13.2
4330	22.0	7.0	5.3	12.3
4220	-45.0	-14.3	5.2	- 9.1
3320	-55.2	-17.5	3.7	-13.8
3600	-52.9	-16.8	4.1	-12.7
3710	-52.5	-16.7	4.3	-12.4
3900	-51.0	-16.2	4.6	-11.6
3910	-50.7	-16.1	4.6	-11.5
3940	-50.4	-16.0	4.7	-11.3
3975	-50.2	-15.9	4.7	-11.2

Table A-21 (Continued)

Thermal Expansion of Tantalum Boride

Temperature °F	Observed Total Elongation 10^{-3} inches	Observed Unit Elongation 10^{-3} inches/inch	Unit Elongation Correction for Dilatometer Motion 10^{-3} inches/inch	Corrected Specimen Unit Elongation 10^{-3} inches/inch
4120	-49.2	-15.6	5.0	-10.6
4200	-48.9	-15.5	5.1	-10.4
4250	-48.2	-15.3	5.2	-10.1
4400	-47.1	-15.0	5.5	- 9.5
4450	-46.4	-14.7	5.5	- 9.2
4600	-44.8	-14.2	5.8	- 8.4
70	-72.8	-23.1	0	-23.1
Specimen partially melted on post inspection				
4610 Specimen Deterioration				

[1] Run SRI - E25
Initial Specimen Length = 3.1530"
Final Specimen Length = 3.0940" (Incipient Melting)

Table A-22

Thermal Expansion of Zirconium Boride

Temperature °F	Observed Total Elongation 10^{-3} inches	Observed Unit Elongation 10^{-3} inches/inch	Unit Elongation Correction for Dilatometer Motion 10^{-3} inches/inch	Corrected Specimen Unit Elongation 10^{-3} inches/inch
70 [1]	0	0	0	0
441	0.6	0.2	0.2	0.4
551	1.3	0.4	0.3	0.7
741	2.2	0.7	0.5	1.2
774	2.5	0.9	0.5	1.4
737	2.4	0.8	0.5	1.3
997	3.5	1.2	0.6	1.8
1047	3.7	1.3	0.7	2.0
1242	4.7	1.6	0.9	2.5
1574	6.5	2.2	1.2	3.4
1660	7.2	2.4	1.4	3.8
1793	8.0	2.7	1.5	4.2
1998	9.4	3.2	1.7	4.9
2048	9.6	3.3	1.8	5.1
1474	7.1	2.4	1.2	3.6
1708	8.4	2.8	1.4	4.2
1976	9.7	3.3	1.7	5.0
2175	10.8	3.7	2.0	5.7
2515	13.4	4.5	2.5	7.0
2960	14.9	5.1	3.1	8.2
3130	15.6	5.3	3.4	8.7
3320	15.7	5.3	3.7	9.0
3620	14.5	4.9	4.2	9.1
3600	14.4	4.9	4.1	9.0
3750	14.3	4.8	4.4	9.2
70	- 6.5	-2.2	0	-2.2

Table A-22 (Continued)

Thermal Expansion of Zirconium Boride

Temperature °F	Observed Total Elongation 10^{-3} inches	Observed Unit Elongation 10^{-3} inches/inch	Unit Elongation Correction for Dilatometer Motion 10^{-3} inches/inch	Corrected Specimen Unit Elongation 10^{-3} inches/inch
70 [2]	0	0	0	0
1500	6.6	2.2	1.2	3.4
1665	8.7	2.9	1.4	4.3
1860	10.1	3.4	1.6	5.0
1980	10.1	3.4	1.7	5.1
2030	11.2	3.5	1.8	5.3
2190	11.9	3.7	2.0	5.7
2360	13.6	4.6	2.2	6.8
2510	13.9	4.7	2.5	7.2
2670	15.3	5.2	2.7	7.9
2880	16.6	5.6	3.0	8.6
3300	17.6	6.0	3.6	9.6
3280	17.9	6.1	3.6	9.7
3350	18.6	6.3	3.7	10.0
3600	19.3	6.6	4.1	10.7
3880	19.0	6.4	4.5	10.9
3880	17.8	6.0	4.5	10.5
70	- 4.6	-1.6	0	- 1.6

Table A-22 (Continued)

Thermal Expansion of Zirconium Boride

Temperature ° F	Observed Total Elongation 10^{-3} inches	Observed Unit Elongation 10^{-3} inches/inch	Unit Elongation Correction for Dilatometer Motion 10^{-3} inches/inch	Corrected Specimen Unit Elongation 10^{-3} inches/inch
70 [3]	0	0	0	0
1500	8.3	2.8	1.2	4.0
1770	10.0	3.4	1.5	4.9
2220	13.0	4.4	2.1	6.5
2580	15.6	5.3	2.5	7.8
3190	19.2	6.5	3.5	10.0
3550	21.7	7.4	4.0	11.4
3820	23.7	8.0	4.5	12.5
4125	25.0	8.5	5.0	13.5
4330	25.4	8.6	5.3	13.9
4380	24.8	8.4	5.4	13.8
4550	22.5	7.6	5.7	13.3
70	- 7.5	-2.5	0	- 2.5
4750 Specimen Deterioration				

[1] Run SRI - E3
Initial Specimen Length = 2.9470"
Final Specimen Length = 2.9450"

[2] Run SRI - E4
Initial Specimen Length = 2.9450"
Final Specimen Length = 2.9463"

[3] Run SRI - E21
Initial Specimen Length = 2.9463"
Final Specimen Length = 2.9416"

Table A-23

Thermal Expansion of Columbium Carbide

Temperature ° F	Observed Total Elongation 10^{-3} inches	Observed Unit Elongation 10^{-3} inches/inch	Unit Elongation Correction for Dilatometer Motion 10^{-3} inches/inch	Corrected Specimen Unit Elongation 10^{-3} inches/inch
70 [1]	0	0	0	0
1100	5.9	2.0	0.8	2.8
1390	7.7	2.6	1.0	3.6
1610	9.0	3.0	1.3	4.3
1830	10.8	3.6	1.5	5.1
1975	11.8	3.9	1.7	5.6
2340	14.0	4.7	2.2	6.9
2720	16.3	5.4	2.8	8.2
3280	20.6	6.9	3.6	10.5
3560	24.4	8.1	4.0	12.1
3850	32.8	10.9	4.5	15.4
4200	42.6	14.2	5.1	19.3
4450	49.0	16.3	5.5	21.8
4600	53.5	17.8	5.8	23.6
4600	55.5	18.5	5.8	24.3
4600	59.0	19.7	5.8	25.5
4640	60.9	20.3	5.9	26.2
4680	63.5	21.2	6.0	27.2
4730	64.0	21.3	6.1	27.4
4660	63.8	21.3	6.0	27.3
4660	63.7	21.2	6.0	27.2
4660	63.4	21.1	6.0	27.1
70	34.3	11.4	0	11.4
4740 Specimen Deterioration				

[1] Run SRI - E18
Initial Specimen Length = 2.9505"
Final Specimen Length = 2.9874"

Table A-24

Thermal Expansion of Hafnium Carbide

Temperature °F	Observed Total Elongation 10^{-3} inches	Observed Unit Elongation 10^{-3} inches/inch	Unit Elongation Correction for Dilatometer Motion 10^{-3} inches/inch	Corrected Specimen Unit Elongation 10^{-3} inches/inch
70 [1]	0	0	0	0
680	3.3	1.1	0.4	1.5
820	4.2	1.4	0.5	1.9
1000	5.2	1.7	0.7	2.4
1460	7.7	2.6	1.1	3.7
1865	10.2	3.4	1.6	5.0
2270	12.4	4.1	2.1	6.2
2640	14.4	4.8	2.7	7.5
2910	15.7	5.2	3.0	8.2
3180	16.8	5.6	3.5	9.1
3400	17.8	5.9	3.8	9.7
3660	18.8	6.3	4.2	10.5
3930	19.5	6.5	4.7	11.2
4320	19.5	6.5	5.3	11.8
4580	19.3	6.4	5.8	12.2
4810	19.5	6.5	6.2	12.7
2500	8.1	2.7	2.5	5.2
1630	3.8	1.3	1.3	2.6
70	- 4.7	-1.6	0	- 1.6
70 [2]	0	0	0	0
1390	9.1	3.0	1.0	4.0
1620	13.7	4.6	1.3	5.9
2165	17.8	5.9	2.0	7.9
2410	19.7	6.6	2.3	8.9
2650	21.5	7.2	2.7	9.9

Table A-24 (Continued)

Thermal Expansion of Hafnium Carbide

Temperature ° F	Observed Total Elongation 10^{-3} inches	Observed Unit Elongation 10^{-3} inches/inch	Unit Elongation Correction for Dilatometer Motion 10^{-3} inches/inch	Corrected Specimen Unit Elongation 10^{-3} inches/inch
2900	22.5	7.5	3.0	10.5
3100	23.6	7.9	3.3	11.2
3430	25.2	8.4	3.9	12.3
3630	26.7	8.9	4.2	13.1
3750	27.8	9.3	4.4	13.7
3970	29.3	9.8	4.7	14.5
4100	30.6	10.2	5.0	15.2
4270	31.8	10.6	5.2	15.8
4435	32.6	10.9	5.5	16.4
4680	33.4	11.1	6.0	17.1
4810	34.5	11.5	6.2	17.7
4910	35.6	11.9	6.4	18.3
4960	35.6	11.9	6.5	18.4
5000	35.8	11.9	6.5	18.4
5055	36.5	12.2	6.6	18.8
5060	36.6	12.2	6.6	18.8
5080	36.9	12.3	6.7	19.0
5040	36.2	12.1	6.6	18.7
5080	36.7	12.2	6.7	18.9
5140	37.1	12.4	6.8	19.2
5150	37.2	12.4	6.8	19.2
5160	37.5	12.5	6.8	19.3
5175	38.0	12.7	6.8	19.5
5180	38.3	12.8	6.9	19.7
5200	38.4	12.8	6.9	19.7

Table A-24 (Continued)

Thermal Expansion of Hafnium Carbide

Temperature ° F	Observed Total Elongation 10^{-3} inches	Observed Unit Elongation 10^{-3} inches/inch	Unit Elongation Correction for Dilatometer Motion 10^{-3} inches/inch	Corrected Specimen Unit Elongation 10^{-3} inches/inch
5220	38.6	12.9	6.9	19.8
5210	38.8	12.9	6.9	19.8
5200	39.0	13.0	6.9	19.9
5220	39.5	13.2	6.9	20.1
70	0.8	0.3	0	0.3

[1] Run SRI - E28
Initial Specimen Length = 3.0040"
Final Specimen Length = 3.0015"

[2] Run SRI - E32
Initial Specimen Length = 3.0015"
Final Specimen Length = 3.0040"

Table A-25

Thermal Expansion of Tantalum Carbide

Temperature °F	Observed Total Elongation 10^{-3} inches	Observed Unit Elongation 10^{-3} inches/inch	Unit Elongation Correction for Dilatometer Motion 10^{-3} inches/inch	Corrected Specimen Unit Elongation 10^{-3} inches/inch
70 [1]	0	0	0	0
1120	5.1	1.7	0.8	2.5
1590	6.7	2.2	1.3	3.5
1980	8.0	2.7	1.7	4.4
2300	9.2	3.1	2.2	5.3
2390	10.0	3.3	2.3	5.6
2590	10.6	3.5	2.5	6.0
2840	11.8	3.9	3.0	6.9
3200	13.5	4.5	3.5	8.0
3450	14.9	5.0	3.9	8.9
3600	16.7	5.6	4.1	9.7
3720	17.4	5.8	4.3	10.1
3520	16.7	5.6	4.0	9.6
3640	18.5	6.2	4.2	10.4
3340	19.8	6.6	3.7	10.3
3130	20.5	6.8	3.4	10.2
70	5.9	2.0	0	2.0
70 [2]	0	0	0	0
1700	5.4	1.8	1.4	3.2
2070	7.0	2.3	1.8	4.1
2380	8.8	2.9	2.2	5.1
2710	10.3	3.4	2.8	6.2
3230	12.0	4.0	3.5	7.5
3650	13.5	4.5	4.2	8.7
3850	14.6	4.9	4.5	9.4
3870	14.8	4.9	4.5	9.4
3930	16.0	5.3	4.6	9.9
70	14.0	4.7	0	4.7

Table A-25 (Continued)

Thermal Expansion of Tantalum Carbide

Temperature °F	Observed Total Elongation 10^{-3} inches	Observed Unit Elongation 10^{-3} inches/inch	Unit Elongation Correction for Dilatometer Motion 10^{-3} inches/inch	Corrected Specimen Unit Elongation 10^{-3} inches/inch
70 [3]	0	0	0	0
2280	12.2	4.1	2.1	6.2
3035	16.2	5.4	3.2	8.6
3785	20.6	6.9	4.4	11.3
3950	21.2	7.1	4.7	11.8
4125	21.9	7.3	5.0	12.3
4250	22.7	7.6	5.2	12.8
4430	24.5	8.2	5.5	13.7
4575	27.2	9.1	5.8	14.9
4655	29.7	9.9	6.0	15.9
4650	30.8	10.3	6.0	16.3
4660	34.6	11.5	6.0	17.5
4660	35.1	11.7	6.0	17.7
70	14.2	4.7	0	4.7
4660 Specimen Deterioration				

[1] Run SRI - E7
Initial Specimen Length = 3.0010"
Final Specimen Length = 3.0010"

[2] Run SRI - E16
Initial Specimen Length = 3.0020"
Final Specimen Length = 3.0040"

[3] Run SRI - E17
Initial Specimen Length = 3.0040"
Final Specimen Length = 3.0179"

Table A-26

Thermal Expansion of Zirconium Carbide

Temperature °F	Observed Total Elongation 10^{-3} inches	Observed Unit Elongation 10^{-3} inches/inch	Unit Elongation Correction for Dilatometer Motion 10^{-3} inches/inch	Corrected Specimen Unit Elongation 10^{-3} inches/inch
339 [1]	0	0	0	0
630	0.9	0.4	0.2	0.6
901	2.0	0.8	0.4	1.2
1046	2.7	1.1	0.5	1.6
1170	3.6	1.4	0.6	2.0
1470	5.3	2.1	0.9	3.0
1703	8.1	3.2	1.2	4.4
1717	8.7	3.4	1.2	4.6
1900	19.5	7.7	1.5	9.2
1950	31.1	12.3	1.5	13.8
2010	32.4	12.8	1.6	14.4
1550	33.7	13.3	1.0	14.3
1670	34.1	13.5	1.2	14.7
2000	36.0	14.2	1.6	15.8
1525	2.3	0.9	1.0	1.9
2020	2.0	0.8	1.6	2.4
2400	2.0	0.8	2.1	2.9
2560	1.5	0.6	2.3	2.9
2750	1.0	0.4	2.6	3.0
2860	0.1	0.0	2.8	2.8
3240	- 0.8	- 0.3	3.3	3.0
3250	- 1.0	- 0.4	3.3	2.9
2890	- 1.5	- 0.6	2.8	2.2
2900	- 2.8	- 1.1	2.8	1.7

Table A-26 (Continued)

Thermal Expansion of Zirconium Carbide

Temperature °F	Observed Total Elongation 10^{-3} inches	Observed Unit Elongation 10^{-3} inches/inch	Unit Elongation Correction for Dilatometer Motion 10^{-3} inches/inch	Corrected Specimen Unit Elongation 10^{-3} inches/inch
2650	- 3.3	- 1.3	2.5	1.2
2900	- 3.9	- 1.5	2.8	1.3
70	-18.5	- 7.3	-0.2	-7.5
Specimen broken on post inspection				
70 [2]	0	0	0	0
630	2.2	1.0	0.4	1.4
900	3.1	1.4	0.6	2.0
1170	3.9	1.8	0.8	2.6
1520	5.3	2.5	1.2	3.7
1700	6.1	2.8	1.4	4.2
1940	7.0	3.2	1.7	4.9
2150	7.6	3.5	2.0	5.5
2340	8.4	3.9	2.2	6.1
2510	9.1	4.2	2.5	6.7
2660	9.6	4.4	2.7	7.1
2820	10.0	4.6	3.0	7.6
3020	10.2	4.7	3.2	7.9
3275	10.3	4.8	3.6	8.4
3480	10.5	4.9	3.9	8.8
3570	10.6	4.9	4.1	9.0
3725	10.8	5.0	4.3	9.3
3800	10.8	5.0	4.5	9.5
3800	10.5	4.9	4.5	9.4
3810	10.4	4.8	4.5	9.3

Table A-26 (Continued)

Thermal Expansion of Zirconium Carbide

Temperature °F	Observed Total Elongation 10^{-3} inches	Observed Unit Elongation 10^{-3} inches/inch	Unit Elongation Correction for Dilatometer Motion 10^{-3} inches/inch	Corrected Specimen Unit Elongation 10^{-3} inches/inch
3810	10.2	4.7	4.5	9.2
3840	10.2	4.7	4.5	9.2
3800	10.2	4.7	4.5	9.2
3800	9.9	4.6	4.5	9.1
3830	9.8	4.5	4.5	9.0
3300	8.7	4.0	3.6	7.6
3460	9.1	4.2	3.9	8.1
3740	9.6	4.4	4.4	8.8
70	2.8	1.3	0.0	1.3
Specimen broken on post inspection				
4700 Specimen Deterioration				

[1] Run SRI E2
Initial Specimen Length = 2.531"
Final Specimen Length = Specimen Broken

[2] Run SRI - E26
Initial Specimen Length = 2.1630
Final Specimen Length = Specimen Broken

Table A-27

Thermal Expansion of Hafnium Nitride

Temperature °F	Observed Total Elongation 10^{-3} inches	Observed Unit Elongation 10^{-3} inches/inch	Unit Elongation Correction for Dilatometer Motion 10^{-3} inches/inch	Corrected Specimen Unit Elongation 10^{-3} inches/inch
70 [1]	0	0	0	0
1000	8.2	2.7	0.7	3.4
1790	12.1	4.3	1.5	5.8
2030	16.0	5.3	1.8	7.1
2340	22.4	7.5	2.2	9.7
2560	29.1	9.7	2.5	12.2
2760	27.2	9.1	2.8	11.9
2910	18.7	6.2	3.0	9.2
3250	6.0	2.0	3.5	5.5
3410	5.6	1.9	3.8	5.7
3670	4.6	1.5	4.0	5.5
3900	- 0.3	- 0.1	4.6	4.5
4125	- 7.6	- 2.5	5.0	2.5
4530	-26.8	- 8.9	5.6	- 3.3
4710	-40.0	-13.3	6.0	- 7.3
70	-70.0	-23.3	0	-23.3
Specimen broken on post inspection				
4750 Specimen Deterioration				

[1] Run SRI - E29
Initial Specimen Length = 3.0015"
Final Specimen Length = 2.9400" (Broken)

Table A-28

Thermal Expansion of Silicon Nitride

Temperature °F	Observed Total Elongation 10^{-3} inches	Observed Unit Elongation 10^{-3} inches/inch	Unit Elongation Correction for Dilatometer Motion 10^{-3} inches/inch	Corrected Specimen Unit Elongation 10^{-3} inches/inch
70 [1]	0	0	0	0
561	0	0	0.4	0.4
594	-0.1	0	0.4	0.4
743	-0.1	0	0.5	0.5
1302	+0.3	0.1	1.0	1.1
1476	1.3	0.4	1.1	1.5
1776	1.6	0.5	1.5	2.0
1992	2.4	0.8	1.7	2.5
1998	2.9	1.0	1.7	2.7
974	3.1	1.0	0.6	1.6
1497	3.1	1.0	1.1	2.1
1765	3.1	1.0	1.5	2.5
2015	3.1	1.0	1.7	2.7
1665	3.3	1.1	1.4	2.5
1559	3.3	1.1	1.2	2.3
1475	3.3	1.1	1.1	2.2
1401	3.3	1.1	1.0	2.1
1062	3.3	1.1	0.7	1.8
1037	3.4	1.1	0.7	1.8
945	3.5	1.2	0.6	1.8
1336	3.5	1.2	1.0	2.2
1499	3.4	1.1	1.2	2.3
1758	3.4	1.1	1.5	2.6
1995	3.3	1.1	1.7	2.8
2247	3.5	1.2	2.1	3.3

Table A-28 (Continued)

Thermal Expansion of Silicon Nitride

Temperature °F	Observed Total Elongation 10^{-3} inches	Observed Unit Elongation 10^{-3} inches/inch	Unit Elongation Correction for Dilatometer Motion 10^{-3} inches/inch	Corrected Specimen Unit Elongation 10^{-3} inches/inch
2464	4.2	1.4	2.4	3.8
2507	4.7	1.6	2.5	4.1
2794	5.3	1.8	2.8	4.6
2893	5.5	1.8	3.0	4.8
3020	5.5	1.8	3.2	5.0
3100	5.5	1.8	3.3	5.1
3280	5.5	1.8	3.5	5.3
70	6.0	2.0	0	2.0
Specimen broken on post inspection				
3420 Specimen Deterioration				

[1] Run SRI - E1
Initial Specimen Length = 2.9835"
Final Specimen Length = Specimen Broken

Table A-29

Thermal Expansion of Titanium Nitride

Temperature °F	Observed Total Elongation 10^{-3} inches	Observed Unit Elongation 10^{-3} inches/inch	Unit Elongation Correction for Dilatometer Motion 10^{-3} inches/inch	Corrected Specimen Unit Elongation 10^{-3} inches/inch
70 [1]	0	0	0	0
1745	8.8	4.6	1.5	6.1
2500	12.9	6.8	2.5	9.3
2960	14.2	7.5	3.1	10.6
3000	12.3	6.5	3.2	9.7
3200	9.3	4.9	3.5	8.4
3300	3.6	1.9	3.6	5.5
3300	2.5	1.3	3.6	4.9
3700	1.4	0.7	4.3	5.0
3850	- 4.7	- 2.5	4.5	2.0
4300	-10.7	- 5.6	5.3	- 0.3
4530	-15.6	- 8.2	5.7	- 2.5
4630	-20.8	-11.0	5.9	- 5.1
4700	-23.0	-12.1	6.0	- 6.1
70	-49.6	-26.2	0	-26.2
4700 Specimen Deterioration				

[1] Run SRI - E20
Initial Specimen Length = 1.8980"
Final Specimen Length = 1.8440"

Table A-30

Thermal Expansion of Zirconium Nitride

Temperature °F	Observed Total Elongation 10^{-3} inches	Observed Unit Elongation 10^{-3} inches/inch	Unit Elongation Correction for Dilatometer Motion 10^{-3} inches/inch	Corrected Specimen Unit Elongation 10^{-3} inches/inch
70 [1]	0	0	0	0
1350	17.9	6.0	1.0	7.0
1470	19.2	6.4	1.1	7.5
1850	21.6	7.2	1.5	8.7
2260	23.7	7.9	2.1	10.0
2500	24.9	8.3	2.5	10.8
2660	25.3	8.4	2.7	11.1
2860	25.6	8.5	3.0	11.5
3175	30.5	10.2	3.5	13.7
3430	33.3	11.1	3.8	14.9
3640	37.6	12.5	4.2	16.7
3910	40.4	13.5	4.6	18.1
4300	44.9	15.0	5.3	20.3
4500	46.4	15.5	5.6	21.1
4340	44.8	14.9	5.4	20.3
4460	47.6	15.9	5.5	21.4
4560	50.0	16.7	5.7	22.4
4575	52.3	17.4	5.7	23.1
4620	63.8	21.3	5.9	27.2
4330	66.7	22.2	5.3	27.5
4400	70.0	23.3	5.5	28.8
4635	73.6	24.5	5.9	30.4
4645	78.0	26.0	5.9	31.9
3920	71.3	23.8	4.6	28.4
4395	74.3	24.8	5.5	30.3

Table A-30 (Continued)

Thermal Expansion of Zirconium Nitride

Temperature °F	Observed Total Elongation 10^{-3} inches	Observed Unit Elongation 10^{-3} inches/inch	Unit Elongation Correction for Dilatometer Motion 10^{-3} inches/inch	Corrected Specimen Unit Elongation 10^{-3} inches/inch
4550	77.8	25.9	5.7	31.6
4550	80.7	26.9	5.7	32.6
4270	76.0	25.3	5.2	30.5
3380	70.4	23.5	3.7	27.2
70	54.0	18.0	0.0	18.0
Specimen broken on post inspection				
4810 Specimen Deterioration				

[1] Run SRI - E24
Initial Specimen Length = 2.9700"
Final Specimen Length = 3.0333" (Broken)

Table A-31

Thermal Expansion of Zirconium Silicate

Temperature ° F	Observed Total Elongation 10^{-3} inches	Observed Unit Elongation 10^{-3} inches/inch	Unit Elongation Correction for Dilatometer Motion 10^{-3} inches/inch	Corrected Specimen Unit Elongation 10^{-3} inches/inch
70 [1]	0	0	0	0
1340	0.2	0.1	1.0	1.1
1570	0.6	0.2	1.2	1.4
1820	1.0	0.3	1.5	1.8
2045	1.4	0.5	1.8	2.3
2310	1.8	0.6	2.2	2.8
2600	2.0	0.7	2.5	3.2
2840	2.0	0.7	3.0	3.7
3000	2.0	0.7	3.2	3.9
3300	1.9	0.6	3.6	4.2
3500	-0.5	-0.2	4.0	3.8
3650	-0.6	-0.2	4.2	4.0
3710	-0.6	-0.2	4.3	4.1
70	-0.3	-0.1	0	-0.1
Specimen had softened on post inspection				
3710 Specimen Deterioration				

[1] Run SRI - E6
Initial Specimen Length = 2.9420"
Final Specimen Length = Specimen Softened

Table A-32

Thermal Conductivity of ATJ Graphite

SRI Run Number	Specimen Outer Face Temperature ° F	ΔT Across $\frac{1}{8}$" Test Section ° F	Heat Removed by $\frac{1}{4}$" Calorimeter Section Btu/hr	Mean Temperature of Test Section ° F	Thermal Conductivity of Test Section Btu/hr/ft²/° F/in.
C49	-	11	132	470	550
	-	12	156	473	595
	-	11	167	475	695
	-	11	122	484	508
	-	21	236	636	515
	-	22	242	646	505
	-	60	466	1046	356
	-	63	600	1053	436
	-	64	490	1082	350
	-	133	611	1581	210
	-	135	671	1596	228
	-	133	591	1606	204
	-	131	782	1628	274
	-	134	817	1623	280

Table A-32 (Continued)

Thermal Conductivity of ATJ Graphite

SRI Run Number	Specimen Outer Face Temperature ° F	ΔT Across $\frac{1}{8}$" Test Section ° F	Heat Removed by $\frac{1}{4}$" Calorimeter Section Btu/hr	Mean Temperature of Test Section ° F	Thermal Conductivity of Test Section Btu/hr/ft²/° F/in.
C56	1880	85	455	1810	246
	1900	85	425	1830	229
	2465	100	596	2385	273
	2470	100	620	2390	284
	2480	109	600	2395	252
	2510	125	616	2410	226
	2515	115	602	2425	240
	2900	120	625	2805	239
	2900	120	641	2805	245
	2900	125	665	2800	244
	3260	170	711	3125	192
	3260	170	735	3125	198
C57	1865	75	302	1805	185
	1870	65	326	1820	230
	1875	75	325	1815	198
	3440	130	498	3335	175
	3460	170	498	3325	135
	3465	200	534	3305	122
	3740	220	630	3565	131
	3750	205	633	3585	141
	3730	200	610	3570	140
	3760	225	583	3580	119
	3975	210	648	3805	141
	3920	170	696	3785	188

Table A-32 (Continued)

Thermal Conductivity of ATJ Graphite

SRI Run Number	Specimen Outer Face Temperature ° F	ΔT Across $\frac{1}{8}$" Test Section ° F	Heat Removed by $\frac{1}{4}$" Calorimeter Section Btu/hr	Mean Temperature of Test Section ° F	Thermal Conductivity of Test Section Btu/hr/ft²/° F/in.
C61	2200	115	454	2110	181
	2200	120	480	2105	183
	2855	165	659	2725	183
	2855	160	562	2725	161
C64	1800	46	342	1037	340
	1800	42	367	1040	400
	1800	41	400	1046	448
C69	-	8	100	545	573
	-	9	108	548	551
	-	8	103	548	592
	-	8	92	549	528
C92	3980	160	680	3850	195
	3970	175	673	3830	176
	3970	155	558	3845	165
	3980	155	513	3855	152
	4220	210	635	4050	139
C98	4615	80	111	4550	64
	4640	50	104	4600	96
	4640	50	105	4600	96
	5070	80	179	5005	103
	5100	90	174	5030	89

Table A-32 (Continued)

Thermal Conductivity of ATJ Graphite

SRI Run Number	Specimen Outer Face Temperature ° F	ΔT Across 1/8" Test Section ° F	Heat Removed by 1/4" Calorimeter Section Btu/hr	Mean Temperature of Test Section ° F	Thermal Conductivity of Test Section Btu/hr/ft²/° F/in.
C99	4380	150	390	4260	119
	4375	100	242	4295	111
	5050	90	241	4980	123
	4985	120	241	4890	92
	5050	130	242	4945	85

Table A-33

Thermal Conductivity of Tungsten

SRI Run Number	Specimen Outer Face Temperature ° F	ΔT Across $\frac{1}{8}$" Test Section ° F	Heat Removed by $\frac{1}{4}$" Calorimeter Section Btu/hr	Mean Temperature of Test Section ° F	Thermal Conductivity of Test Section Btu/hr/ft²/° F/in.
C54	-	11	85	547	352
	-	31	221	831	326
	-	44	345	1072	360
	-	43	318	1089	340
	-	45	338	1087	344
	-	44	338	1057	352
	-	46	368	1066	367
	-	45	300	1072	306
C55	-	14	142	411	464
	-	41	382	896	427
	-	43	405	899	431
	-	42	376	915	410
	-	86	627	1313	334
	-	86	658	1323	350
	-	87	682	1324	359
	-	99	656	1675	304
	-	99	825	1686	382
	-	98	633	1694	296
	-	81	626	1854	354
	-	82	788	1857	440

Table A-33 (Continued)

Thermal Conductivity of Tungsten

SRI Run Number	Specimen Outer Face Temperature ° F	ΔT Across $\frac{1}{8}$" Test Section ° F	Heat Removed by $\frac{1}{4}$" Calorimeter Section Btu/hr	Mean Temperature of Test Section ° F	Thermal Conductivity of Test Section Btu/hr/ft²/° F/in.
C85	2370	35	455	2340	595
	2370	30	330	2345	503
	2370	40	386	2340	442
	2950	55	569	2905	473
	2950	65	564	2900	397
	2950	50	539	2910	494
C86	2400	45	450	2368	460
	2910	60	646	2860	493
	2910	65	660	2860	455
	3690	85	668	3620	360
	3690	95	774	3615	373
	3690	95	780	3615	375
	3690	95	710	3615	342
	3690	95	675	3615	326
	3690	75	598	3630	365
	4140	80	690	4075	395
	4140	85	733	4070	396
	4170	80	670	4105	384
	4170	90	816	4100	415
	4560	60	742	4510	565
	4560	65	770	4510	542
	4860	40	760	4830	580
	5010 Specimen Melted				

Table A-34

Thermal Conductivity of Hafnium Nitride

SRI Run Number	Specimen Outer Face Temperature ° F	ΔT Across $\frac{1}{8}$" Test Section ° F	Heat Removed by $\frac{1}{4}$" Calorimeter Section Btu/hr	Mean Temperature of Test Section ° F	Thermal Conductivity of Test Section Btu/hr/ft²/° F/in.
C67	-	29	49	543	77.3
	-	28	57	546	93.5
	-	29	55	553	86.2
	-	28	50	553	82.0
	-	29	49	555	77.0
	1490	69	103	996	68.4
	1490	71	98	1001	63.5
	1490	73	105	1004	65.7
	1490	69	100	1011	66.5
	1490	70	102	1011	66.5
	1490	70	98	1015	63.8
	1490	70	95	1019	62.1
	1850	90	151	1368	77.0
	1850	89	136	1371	70.3
	1850	90	188	1370	95.5
	2110	108	232	1601	98.0
	2110	109	217	1602	91.0
	2110	111	260	1609	107.5
	2110	111	201	1609	82.9

Table A-34 (Continued)

Thermal Conductivity of Hafnium Nitride

SRI Run Number	Specimen Outer Face Temperature ° F	ΔT Across $\frac{1}{8}$" Test Section ° F	Heat Removed by $\frac{1}{4}$" Calorimeter Section Btu/hr	Mean Temperature of Test Section ° F	Thermal Conductivity of Test Section Btu/hr/ft²/° F/in.
C78	2060	110	300	1970	125.0
	2060	110	255	1970	106.0
	2060	120	273	1945	104.0
	2680	185	450	2530	111.0
	2680	170	410	2545	111.0
	2680	175	424	2540	111.0
	2680	185	435	2530	108.0
	3225	195	581	3070	137.0
	3225	220	630	3050	131.0
	3180	200	560	3020	128.0
	3180	200	620	3020	142.0
	3700	190	800	3550	193.0
	3700	175	720	3560	189.0
	3700	175	720	3560	189.0
	3700	185	764	3550	189.0
	4750 Specimen Deterioration				

Table A-35

Thermal Conductivity of Silicon Nitride

SRI Run Number	Specimen Outer Face Temperature ° F	ΔT Across $\frac{1}{8}$" Test Section ° F	Heat Removed by $\frac{1}{4}$" Calorimeter Section Btu/hr	Mean Temperature of Test Section ° F	Thermal Conductivity of Test Section Btu/hr/ft²/° F/in.
C53	-	75	89	626	54.5
	-	78	78	641	46.0
	-	77	85	644	50.4
	-	81	108	633	61.5
	-	146	172	915	54.0
	-	146	146	916	45.8
	-	147	167	925	52.0
	-	125	142	896	52.0
	-	128	121	900	43.2
	-	126	148	903	54.0
	-	295	219	1422	34.0
	-	286	228	1438	36.4
	-	293	264	1456	41.2
	-	286	257	1454	41.3
	-	350	277	1687	36.2
	-	334	254	1683	34.9
	-	312	301	1690	44.1
	-	279	295	1691	48.4
	-	263	246	1689	42.8

Table A-35 (Continued)

Thermal Conductivity of Silicon Nitride

SRI Run Number	Specimen Outer Face Temperature ° F	ΔT Across $\frac{1}{8}$" Test Section ° F	Heat Removed by $\frac{1}{4}$" Calorimeter Section Btu/hr	Mean Temperature of Test Section ° F	Thermal Conductivity of Test Section Btu/hr/ft²/° F/in.
C59	2000	225	196	1820	39.9
	2000	215	190	1830	40.5
	2055	230	206	1870	41.0
	2530	335	278	2260	38.0
	2560	335	242	2290	33.0
	2580	320	282	2325	40.5
	2580	300	275	2340	42.0
	3075	290	317	2845	50.0
	3490	330	300	3225	41.6
	3490	300	334	3250	50.9
	3500	350	380	3220	49.6
	3420 Specimen Deterioration				

Table A-36

Thermal Conductivity of Titanium Nitride

SRI Run Number	Specimen Outer Face Temperature ° F	ΔT Across $\frac{1}{8}$" Test Section ° F	Heat Removed by $\frac{1}{4}$" Calorimeter Section Btu/hr	Mean Temperature of Test Section ° F	Thermal Conductivity of Test Section Btu/hr/ft²/° F/in.
C73	-	40	29	610	33.2
	-	43	31	621	32.6
	-	44	24	628	24.9
	-	45	25	643	25.4
	-	115	161	1114	64.0
	-	115	156	1115	62.2
	-	115	135	1115	53.8
	1760	145	245	1432	77.3
	1760	146	273	1434	85.5
	1760	148	253	1434	78.3
	1880	144	368	1555	117.0
	1880	147	371	1552	115.5
	1880	151	306	1552	92.8

Table A-36 (Continued)

Thermal Conductivity of Titanium Nitride

SRI Run Number	Specimen Outer Face Temperature ° F	ΔT Across $\frac{1}{8}$" Test Section ° F	Heat Removed by $\frac{1}{4}$" Calorimeter Section Btu/hr	Mean Temperature of Test Section ° F	Thermal Conductivity of Test Section Btu/hr/ft²/° F/in.
C77	2525	240	499	2335	95.0
	2525	235	580	2335	113.0
	2525	235	621	2335	121.0
	2525	235	570	2335	111.0
	3080	240	809	2890	154.0
	3080	220	805	2905	168.0
	3080	220	743	2905	155.0
	3080	210	726	2910	157.0
	3540	210	758	3370	165.0
	3540	165	733	3410	204.0
	3540	175	704	3400	184.0
	3540	180	700	3395	178.0
	4100	240	770	3910	147.0
	4100	260	788	3890	139.0
	4100	220	755	3925	157.0
	4470	320	976	4215	140.0
	4500	300	970	4260	148.0
	4500	320	900	4245	129.0
	4500	300	950	4260	145.0
	4700	230	920	4515	183.0
	4700	220	948	4525	197.0
	4700 Specimen Deterioration				

Table A-37

Thermal Conductivity of Zirconium Nitride

SRI Run Number	Specimen Outer Face Temperature ° F	ΔT Across $\frac{1}{8}$" Test Section ° F	Heat Removed by $\frac{1}{4}$" Calorimeter Section Btu/hr	Mean Temperature of Test Section ° F	Thermal Conductivity of Test Section Btu/hr/ft²/° F/in.
C65	-	44	81	807	84.0
	-	47	75	818	73.1
	-	85	135	1139	72.7
	-	85	162	1141	87.2
C66	-	29	42	600	65.6
	-	29	50	600	79.0
	-	29	49	608	76.5
	-	30	57	610	87.0
	-	58	94	882	74.1
	-	59	83	899	64.6
	-	60	99	900	75.1
	-	60	88	901	66.8
	1820	87	170	1379	89.5
	1820	88	183	1389	95.3
	1820	90	191	1404	97.0
	1820	92	158	1411	78.5
	1980	92	168	1541	83.5
	1980	98	183	1538	85.5
	1980	92	177	1542	88.5
	1980	94	191	1543	93.5
	1980	94	207	1541	101.0

Table A-37 (Continued)

Thermal Conductivity of Zirconium Nitride

SRI Run Number	Specimen Outer Face Temperature °F	ΔT Across $\frac{1}{8}$" Test Section °F	Heat Removed by $\frac{1}{4}$" Calorimeter Section Btu/hr	Mean Temperature of Test Section °F	Thermal Conductivity of Test Section Btu/hr/ft²/° F/in.
C76	2130	170	380	1995	102.5
	2130	160	350	2000	100.0
	2120	160	376	1990	108.0
	2140	180	353	1995	90.0
	2140	160	328	2010	94.0
	2750	175	466	2610	122.0
	2750	175	448	2610	117.0
	2740	175	440	2600	115.0
	3220	240	677	3030	129.0
	3240	225	555	3060	113.0
	3240	230	561	3055	112.0
	3250	260	662	3040	117.0
	3800	405	748	3475	84.5
	3800	415	748	3470	82.5
	3800	465	868	3430	85.5
	4170	500	690	3770	63.4
	4170	415	655	3840	72.3
	4180	390	688	3870	80.8
	4180	390	672	3870	79.0
	4180	400	672	3860	77.0
	4810 Specimen Deterioration				

Table A-38

Thermal Conductivity of Tantalum Boride

SRI Run Number	Specimen Outer Face Temperature ° F	ΔT Across $\frac{1}{8}$" Test Section ° F	Heat Removed by $\frac{1}{4}$" Calorimeter Section Btu/hr	Mean Temperature of Test Section ° F	Thermal Conductivity of Test Section Btu/hr/ft²/° F/in.
C71	-	8	129	611	738
	-	9	147	626	745
	-	8	131	648	748
	1675	22	314	1012	654
	1675	23	334	1046	666
	1675	21	308	1054	670
	2080	61	425	1492	319
	2080	71	485	1507	312
	2080	65	482	1506	340
	2080	69	532	1503	353
	2160	108	690	1545	293
	2160	66	470	1654	326
C79	-	23	280	999	557
	-	25	272	1005	498
	-	24	293	1004	559
	-	77	568	1446	338
	-	77	485	1439	288

Table A-38 (Continued)

Thermal Conductivity of Tantalum Boride

SRI Run Number	Specimen Outer Face Temperature ° F	ΔT Across $\frac{1}{8}$" Test Section ° F	Heat Removed by $\frac{1}{4}$" Calorimeter Section Btu/hr	Mean Temperature of Test Section ° F	Thermal Conductivity of Test Section Btu/hr/ft²/° F/in.
C81	1930	60	376	1880	287
	1950	70	350	1895	229
	1950	75	371	1890	227
	2650	100	720	2570	330
	2650	90	616	2580	314
	3250	110	742	3160	309
	3250	110	703	3160	292
	3250	110	605	3160	252
	3900	120	684	3805	261
	3900	120	725	3805	277
	3900	110	695	3810	290
	4250	130	872	4145	308
	4250	130	915	4145	322
	4250	120	915	4155	350
	4580	130	985	4475	347
	4580	115	980	4490	390
	4580	140	980	4470	320
	4580	150	1015	4460	310
	4580	120	965	4485	369
	4610 Specimen Deterioration				

Table A-39

Thermal Conductivity of Zirconium Boride

SRI Run Number	Specimen Outer Face Temperature ° F	ΔT Across $\frac{1}{8}$" Test Section ° F	Heat Removed by $\frac{1}{4}$" Calorimeter Section Btu/hr	Mean Temperature of Test Section ° F	Thermal Conductivity of Test Section Btu/hr/ft²/° F/in.
C52	-	17	94	562	253
	-	17	120	576	324
	-	72	309	991	196
	-	70	338	1001	221
	-	73	296	1014	186
	-	78	348	1024	204
	-	75	370	1020	226
	-	125	510	1362	187
	-	117	520	1386	204
	-	121	484	1405	183
	-	155	640	1533	190
	-	142	500	1550	161
	-	133	435	1568	150
	-	135	589	1582	199

Table A-39 (Continued)

Thermal Conductivity of Zirconium Boride

SRI Run Number	Specimen Outer Face Temperature ° F	ΔT Across $\frac{1}{8}$" Test Section ° F	Heat Removed by $\frac{1}{4}$" Calorimeter Section Btu/hr	Mean Temperature of Test Section ° F	Thermal Conductivity of Test Section Btu/hr/ft²/° F/in.
C60	2200	80	266	2135	152
	2200	75	256	2140	156
	2740	105	405	2655	177
	2740	110	428	2650	178
	2800	100	373	2720	171
	3340	160	523	3210	150
	3340	165	530	3210	147
	3340	165	510	3210	142
	3770	170	595	3635	160
	3760	160	617	3630	177
	4110	160	711	3980	204
	4200	160	736	4070	211
	4220	160	715	4090	205
	4750 Specimen Deterioration				

Table A-40

Thermal Conductivity of Zirconium Silicate

SRI Run Number	Specimen Outer Face Temperature ° F	ΔT Across $\frac{1}{8}$" Test Section ° F	Heat Removed by $\frac{1}{4}$" Calorimeter Section Btu/hr	Mean Temperature of Test Section ° F	Thermal Conductivity of Test Section Btu/hr/ft^2/° F/in.
C51	-	81	58	445	32.5
	-	83	54	454	29.7
	-	90	80	463	40.8
	-	317	240	1002	34.7
	-	318	218	991	31.4
	-	321	217	1003	31.0
	-	476	306	1402	29.4
	-	479	278	1414	26.6
	-	477	292	1421	28.0
	-	489	316	1562	29.6
	-	490	321	1578	30.0
	-	484	317	1589	30.0
	-	482	298	1607	28.3
	-	483	334	1604	31.6
	-	522	328	1700	28.7
	-	526	312	1700	27.2
	-	525	346	1717	30.2
	-	550	318	1734	26.4

Table A-40 (Continued)

Thermal Conductivity of Zirconium Silicate

SRI Run Number	Specimen Outer Face Temperature ° F	ΔT Across $\frac{1}{8}$" Test Section ° F	Heat Removed by $\frac{1}{4}$" Calorimeter Section Btu/hr	Mean Temperature of Test Section ° F	Thermal Conductivity of Test Section Btu/hr/ft²/° F/in.
C58	2200	400	146	1880	16.7
	2350	450	163	1990	16.6
	2350	415	150	2020	16.5
	2375	309	161	2065	18.9
	3160	480	219	2775	20.9
	3160	475	225	2780	21.7
	3160	475	228	2780	22.0
	3170	475	218	2790	21.0
	3170	470	247	2790	24.1
	3170	500	220	2770	20.2
	3350	550	244	2910	20.3
	3440	565	222	2990	17.9
	3420	590	260	2950	20.2
	3800	565	245	3350	19.9
	3710 Specimen Deterioration				

Table A-41

Thermal Conductivity of Columbium Carbide

SRI Run Number	Specimen Outer Face Temperature ° F	ΔT Across $\frac{1}{8}$" Test Section ° F	Heat Removed by $\frac{1}{4}$" Calorimeter Section Btu/hr	Mean Temperature of Test Section ° F	Thermal Conductivity of Test Section Btu/hr/ft²/° F/in.
C74	-	16	77	539	220
	-	18	90	552	229
	-	18	66	554	169
	1590	37	216	979	267
	1590	36	217	986	276
	1590	42	140	998	153
	1590	42	194	1000	212
	1590	42	154	1003	168
	1970	111	242	1536	100
	1970	115	274	1529	109
	1970	109	240	1530	102
	-	104	440	1717	194
	-	114	484	1717	194
	-	89	365	1737	188
	-	90	372	1734	189
	-	90	373	1731	189
C80	2125	70	436	2070	286
	2125	65	403	2075	284
	2125	70	358	2070	235
	2125	75	364	2065	222
	2125	70	401	2070	262
	2430	90	495	2360	252

Table A-41 (Continued)

Thermal Conductivity of Columbium Carbide

SRI Run Number	Specimen Outer Face Temperature ° F	ΔT Across $\frac{1}{8}$" Test Section ° F	Heat Removed by $\frac{1}{4}$" Calorimeter Section Btu/hr	Mean Temperature of Test Section ° F	Thermal Conductivity of Test Section Btu/hr/ft²/° F/in.
C80 (Continued)	2430	90	478	2360	244
	2440	100	480	2360	220
	2440	100	520	2360	238
	2820	155	621	2695	184
	2820	135	628	2710	213
	2820	130	540	2715	190
	2820	130	548	2715	193
	2820	110	563	2730	234
	2820	130	610	2715	215
	3300	120	821	3205	314
	3300	110	655	3210	273
	3300	130	765	3195	269
	3300	120	764	3205	291
	3750	180	836	3605	212
	3750	160	848	3620	243
	3750	175	681	3610	178
	3750	170	822	3615	221
	4240	240	975	4050	186
	4240	230	820	4055	163
	4240	220	775	4065	161
	4240	210	762	4070	166
	4240	210	905	4070	197

Table A-41 (Continued)

Thermal Conductivity of Columbium Carbide

SRI Run Number	Specimen Outer Face Temperature ° F	ΔT Across $\frac{1}{8}$" Test Section ° F	Heat Removed by $\frac{1}{4}$" Calorimeter Section Btu/hr	Mean Temperature of Test Section ° F	Thermal Conductivity of Test Section Btu/hr/ft²/° F/in.
C93 (Heat Soaked Specimen)	2460	82	390	2395	218
	2480	90	370	2410	189
	2850	127	541	2750	195
	2825	93	570	2750	280
	3720	100	610	3640	280
	3680	140	705	3570	230
	4470	140	870	4360	286
	4470	150	893	4350	272
	4500	140	890	4390	292
	4550	140	865	4340	282
	4740 Specimen Deterioration				

Table A-42

Thermal Conductivity of Hafnium Carbide

SRI Run Number	Specimen Outer Face Temperature ° F	ΔT Across $\frac{1}{8}$" Test Section ° F	Heat Removed by $\frac{1}{4}$" Calorimeter Section Btu/hr	Mean Temperature of Test Section ° F	Thermal Conductivity of Test Section Btu/hr/ft²/° F/in.
C70	-	39	54	585	63
	-	36	51	592	65
	-	41	57	597	64
	-	84	147	1017	80
	-	86	149	1023	80
	-	89	161	1029	83
	-	90	189	1031	96
	-	92	183	1033	91
	1940	151	291	1393	88
	1940	149	299	1414	92
	1940	149	321	1414	99
	1940	149	325	1414	100
	2140	181	488	1679	124
	2140	186	425	1686	105
	2140	185	386	1686	96

Table A-42 (Continued)

Thermal Conductivity of Hafnium Carbide

SRI Run Number	Specimen Outer Face Temperature ° F	ΔT Across $\frac{1}{8}$" Test Section ° F	Heat Removed by $\frac{1}{4}$" Calorimeter Section Btu/hr	Mean Temperature of Test Section ° F	Thermal Conductivity of Test Section Btu/hr/ft²/° F/in.
C95 (Heat Soaked Specimen)	2050	60	354	2000	270
	2050	60	383	2000	292
	2045	57	366	2000	294
	2022	65	354	1972	249
	2740	85	584	2670	315
	2770	95	577	2695	278
	2775	100	551	2695	252
	2770	100	602	2690	276
	3440	130	707	3335	249
	3440	115	720	3350	287
	3450	115	710	3360	283
	3460	125	760	3360	278

Table A-42 (Continued)

Thermal Conductivity of Hafnium Carbide

SRI Run Number	Specimen Outer Face Temperature ° F	ΔT Across $\frac{1}{8}$" Test Section ° F	Heat Removed by $\frac{1}{4}$" Calorimeter Section Btu/hr	Mean Temperature of Test Section ° F	Thermal Conductivity of Test Section Btu/hr/ft²/° F/in.
C97 (Heat Soaked Specimen)	-	14	115	535	374
	-	13	114	541	401
	-	14	122	546	400
	-	35	244	923	320
	-	36	247	928	314
	-	37	222	930	274
	-	37	216	932	267
	-	154	384	1366	114
	-	154	365	1363	109
	-	154	385	1362	115
	-	154	356	1364	106
	-	182	492	1646	124
	-	176	550	1644	143
	-	175	540	1642	141
	-	165	475	1652	132
	-	163	557	1654	157
	-	154	515	1653	153

Table A-43

Thermal Conductivity of Tantalum Carbide

SRI Run Number	Specimen Outer Face Temperature ° F	ΔT Across $\frac{1}{8}$" Test Section ° F	Heat Removed by $\frac{1}{4}$" Calorimeter Section Btu/hr	Mean Temperature of Test Section ° F	Thermal Conductivity of Test Section Btu/hr/ft²/° F/in.
C72	-	13	80	507	282
	-	15	57	542	174
	-	15	78	547	238
	-	22	258	1015	536
	-	19	283	1016	682
	-	17	208	1034	560
	-	12	208	1039	795
	2160	66	334	1677	231
	2160	57	344	1683	276
	2160	77	484	1690	288

Table A-43 (Continued)

Thermal Conductivity of Tantalum Carbide

SRI Run Number	Specimen Outer Face Temperature ° F	ΔT Across $\frac{1}{8}$" Test Section ° F	Heat Removed by $\frac{1}{4}$" Calorimeter Section Btu/hr	Mean Temperature of Test Section ° F	Thermal Conductivity of Test Section Btu/hr/ft²/° F. in.
C82	-	28	136	533	223
	-	29	141	538	222
	-	27	140	545	237
	-	30	168	558	257
	-	28	156	568	255
	-	30	149	558	228
	1600	46	244	1004	243
	1600	46	278	1005	276
	1600	46	240	1000	239
	1600	46	248	999	247
	1950	61	330	1457	248
	1950	60	356	1456	272
	1950	62	375	1461	277
	1950	63	358	1463	260
	1950	62	348	1464	257
	2060	67	322	1610	220
	2060	67	329	1606	225
	2060	64	380	1612	272
	2060	66	398	1591	277
	2060	63	343	1581	250

Table A-43 (Continued)

Thermal Conductivity of Tantalum Carbide

SRI Run Number	Specimen Outer Face Temperature ° F	ΔT Across $\frac{1}{8}$" Test Section ° F	Heat Removed by $\frac{1}{4}$" Calorimeter Section Btu/hr	Mean Temperature of Test Section ° F	Thermal Conductivity of Test Section Btu/hr/ft²/° F/in.
C83	3250	120	723	3155	276
	3250	90	638	3180	325
	3730	125	845	3630	310
	3730	135	890	3620	303
	3730	125	755	3630	277
	3715	120	760	3620	290
	3715	135	758	3605	258
	3715	125	794	3615	291
	4250	180	1136	4105	289
	4250	135	1125	4140	382
C90 (Heat Soaked Specimen)	2000	55	212	1955	176
	2060	58	195	2015	154
	2030	65	250	1980	176
	2700	80	338	2635	193
	2750	80	290	2685	166
	4060	100	565	3980	258
	4150	110	630	4060	263
	4480	130	674	4375	237
	4450	120	675	4355	258
	4480	110	635	4390	264
	4800	150	990	4680	302
	4660 Specimen Deterioration				

Table A-44

Thermal Conductivity of Zirconium Carbide

SRI Run Number	Specimen Outer Face Temperature ° F	ΔT Across $\frac{1}{8}$" Test Section ° F	Heat Removed by $\frac{1}{4}$" Calorimeter Section Btu/hr	Mean Temperature of Test Section ° F	Thermal Conductivity of Test Section Btu/hr/ft²/° F/in.
C68	-	10	103	491	470
	-	10	107	495	490
	-	9	98	497	495
	-	11	111	504	460
	1560	58	266	1013	210
	1560	57	263	1033	211
	1560	56	274	1035	224
	1560	56	283	1040	232
	1560	54	283	1041	240
	1560	47	293	1064	286
	1560	48	273	1062	261
C75	-	15	69	586	210
	-	18	72	613	184
	-	18	70	615	179
	-	28	189	954	309
	-	28	188	957	307
	-	33	213	968	296
	-	33	225	968	312
	-	163	377	1515	106
	-	164	378	1523	105
	-	163	398	1530	112
	-	161	367	1535	104
	-	162	351	1533	99
	-	157	389	1540	113

Table A-44 (Continued)

Thermal Conductivity of Zirconium Carbide

SRI Run Number	Specimen Outer Face Temperature ° F	ΔT Across $\frac{1}{8}$" Test Section ° F	Heat Removed by $\frac{1}{4}$" Calorimeter Section Btu/hr	Mean Temperature of Test Section ° F	Thermal Conductivity of Test Section Btu/hr/ft²/° F/in.
C84	1970	80	507	1905	290
	1970	95	551	1895	266
	1970	95	500	1895	242
	2700	115	798	2610	318
	2700	120	774	2605	295
	2700	115	785	2610	312
	2700	120	780	2605	298
	3200	110	857	3110	356
	3200	140	806	3090	264
	3610	155	920	3485	272
	3610	115	900	3520	360
	3610	140	856	3500	280
	4030	130	880	3925	310
	4030	130	859	3925	302
	4030	115	841	3940	336
	4400	120	950	4305	364
	4400	115	875	4310	348

Table A-44 (Continued)

Thermal Conductivity of Zirconium Carbide

SRI Run Number	Specimen Outer Face Temperature ° F	ΔT Across $\frac{1}{8}$" Test Section ° F	Heat Removed by $\frac{1}{4}$" Calorimeter Section Btu/hr	Mean Temperature of Test Section ° F	Thermal Conductivity of Test Section Btu/hr/ft²/° F/in.
C94 (Heat Soaked Specimen)	2300	185	618	2150	153
	2320	215	640	2150	136
	3120	125	870	3020	319
	3140	135	815	3030	276
	4030	158	1130	3905	327
	4000	155	1120	3875	332
	4050	180	1175	3905	298
	4050	180	1185	3905	301
	4700 Specimen Deterioration				

APPENDIX 3

Sample Calculation for the Determination of the Thermal Conductivity

Sample Calculation for the Determination of the Thermal Conductivity

Data recorded during run:

H_2O Flow = 15.0 gph

$H_2O\ \Delta T$ = 1.6° F

Specimen ΔT = 70° F (measured by optical pyrometer)

Specimen Outer Face Temperature = 2500° F (measured by optical pyrometer)

Area Computation

$$A = \frac{2\pi (r_2 + r_1)\ l}{2 \qquad 144}$$

where r_2 and r_1 are the $\frac{5}{16}$-inch and $\frac{3}{16}$-inch radii on which the temperature measuring holes are located and l is the $\frac{1}{4}$-inch axial gage length determined by the placement of the thermocouples in the calorimeter.

$$A = \frac{2\pi \left(\frac{5}{16} + \frac{3}{16}\right)}{2} \times \frac{0.250}{144}$$

$$A = 2\pi \times 0.250 \times \frac{0.250}{144}$$

A = 0.00272 square feet

Substituting in the basic heat transfer equation $Q = M\ c\ \Delta T$ where (1) Q is heat flow, Btu/hr, (2) M is weight of water flowing, lb/hr, (3) c is specific heat of water, 1 Btu/lb-° F, and (4) ΔT is temperature difference between the water calorimeter thermocouples, ° F.

$$Q = M\ c\ \Delta T = \frac{15 \text{ gal}}{\text{hr}} \times \frac{8.33 \text{ lb}}{\text{gal}} \times \frac{1 \text{ Btu}}{\text{lb-}^\circ \text{ F}} \times 1.6^\circ \text{ F}$$

Q = 200 Btu/hr

Next, using the heat transfer relation

$$K = \frac{QL}{A\Delta T}$$

where (1) K is the thermal conductivity, Btu/hr-ft^2-$^\circ$ F/in., (2) Q is the heat flow, Btu/hr, (3) L is the radial distance between the two temperature holes in the specimen, $\frac{1}{8}$ inch, (4) A is the arithmetic average cylindrical area, 0.00272 square feet, and (5) ΔT is the temperature drop across the $\frac{1}{8}$-inch radial difference between the two temperature holes, $^\circ$ F.

$$K = \frac{QL}{A\Delta T} = \frac{200 \text{ Btu} \times 0.125 \text{ in.}}{\text{hr} \times 0.00272 \text{ ft}^2 \times 70^\circ \text{ F}}$$

$K = 131$ Btu/hr-ft^2-$^\circ$ F/in.

Finally, to compute the mean temperature, the derived special calculation is used.

Mean Temperature = Outer Face Temperature - 0.80 (specimen ΔT)

Mean Temperature = 2500° F - 0.80 (70° F)

Mean Temperature = 2500 - 56 = 2444° F